UNIVERSITY OF CRETE

DEPARTMENT OF MEDICINE

PhD THESIS

The role of Erf in mouse development

IOANNA PERAKI

HERAKLION, 2017

ΠΑΝΕΠΙΣΤΗΜΙΟ ΚΡΗΤΗΣ

ΤΜΗΜΑ ΙΑΤΡΙΚΗΣ

ΔΙΔΑΚΤΟΡΙΚΗ ΔΙΑΤΡΙΒΗ

Ο ρόλος του Erf στην ανάπτυξη ποντικού

ΙΩΑΝΝΑ ΠΕΡΑΚΗ

ΗΡΑΚΛΕΙΟ, 2017

I dedicate this thesis,

to my husband Thodoris,

and my parents Athena and Emmanouil,

for their constant support, patience and unconditional love.

Thank you very much.

Acknowledgements

I would like to thank Professor George Mavrothalassitis for the assignment of the subject and the opportunity he gave me to prepare this PhD dissertation. I thank him warmly for the trust that he has shown to me, the unlimited help, the willingness to answer every question, the proper observations and the transfer of the knowledge he gave me, allowing me to grow as a research scientist.

I gratefully acknowledge Professor James Palis of the Pediatrics Oncology and Biomedical Genetics of University of Rochester, for his advice and his suggestions in the field of hematopoiesis, which were significant and helped me to continue my research successfully. Many thanks also to Dr. Marieke von Lindern for the support and the hospitality I received through our collaborative work, undertaken at Sanquin Hemopoiesis Research Centre at Netherlands.

I would also like to thank my committee members, Professor George Garinis and Professor George Chalepakis for serving as my committee members and helping me to continue my project.

I also want to thank the members of the lab, Angeliki Vogiatzi (Angela), Kostas Makris (Kavalaris), Aimilia Skafida, Electra Nenedaki as well as the previous members, Elena Vorgia and Andreas Zaragoulias, for the enjoyable moments and for their brilliant comments and suggestions. I really find myself very fortunate to have been able to work alongside such good cooperators. Additionally, I thank all the people in the lab of Pr. Karagogeos for the fun we had and for all the knowledge and equipment we shared all this time.

A special thanks to my husband Thodoris, who was my support in the difficult moments when I was frustrated or irritable, as well as for his patience about the many hours spending in the lab. A big thanks to my parents for their encouragement and for all the sacrifices they have made for me. I would also like to thank all my friends Anna-Maria, Stella, Maria, Sophia, Mary, Emmanouela and Zina, who incented me to strive towards my goal by a pleasant way.

Contents

Περίληψη

Ο Erf είναι ένας μεταγραφικός καταστολέας που εκφράζεται σε όλους τους κυτταρικούς τύπους και ρυθμίζεται από το MAPK μονοπάτι μέσω πυρηνο-κυτταροπλασματικής μετακίνησης. Στη μη φωσφορυλιωμένη μορφή του, ο Erf βρίσκεται στον πυρήνα και είναι ενεργός ως καταστολέας, ενώ η φωσφορυλίωση του από την Erk οδηγεί σε έξοδο στο κυτταρόπλασμα και απενεργοποίηση του. Στην ενεργή πυρηνική του μορφή, ο Erf καταστέλλει τον κυτταρικό πολλαπλασιασμό και μπλοκάρει τα κύτταρα στη φάση G0 / G1. Επιπλέον, ο Erf είναι ικανός να παρεμβαίνει στο TGF-β επαγώμενο EMT μέσω καταστολής της σεμαφορίνης 7α . Ο Erf είναι επίσης ικανός να καταστέλλει την επαγόμενη από ets και ras ογκογονικότητα σε ινοβλάστες και κύτταρα σαρκώματος Ewing.

Ωστόσο, λίγα είναι γνωστά για το ρόλο του Erf στην ανάπτυξη. Η πλήρης απάλειψη του Erf σε ποντίκια οδηγεί σε θνησιμότητα την εμβρυϊκή ημέρα E10.5 λόγω ελαττωμάτων του πλακούντα και τα Erf knockout έμβρυα αποτυγχάνουν να αναπτύξουν χοροαλλαντοϊκή σύντηξη. Για να παρακάμψουμε τα ελαττώματα του πλακούντα και να μελετήσουμε τον ρόλο του Erf στο έμβρυο, χρησιμοποιήσαμε ιστοειδικά ποντίκια στον επιβλάστη. Εδώ, αποδυκνύουμε ότι ο Erf απαιτείται και στα τρία κύματα αιματοποίησης του εμβρύου.

Τα πρώτα αιματοποιητικά κύτταρα σχηματίζονται σε νησίδες αίματος στο λεκιθικό σάκο του εμβρύου την εμβρυϊκή ημέρα 7.5 (E7.5) και αποτελούν το πρωτόγονο κύμα αιμοποίησης (primitive wave). Αυτοί οι πρόδρομοι ερυθροβλάστες είναι τα κυρίαρχα κύτταρα στο αρχικώς κυκλοφορούν αίμα, τα οποία διαφοροποιούνται σε ερυθρά, μακροφάγα και μεγακαρυοκύτταρα. Λίγο μετά, την εμβρυϊκή ημέρα E8.25, παράγεται ένα δεύτερο κύμα αιμοποίησης στο λεκιθικό σάκο, που ονομάζεται οριστικό κύμα (definitive wave) και αποτελείται από τους ερυθρο- μυελοειδείς προγόνους (EMP). Τα EMPs μεταναστεύουν στην κυκλοφορία του αίματος και τελικά αποικίζουν το εμβρυϊκό ήπαρ την εμβρυϊκή ημέρα E10.5. Ένα τρίτο κύμα αιματοποίησης που παράγεται την περιοχή της αορτής - γονάδας - μεσονεφρού (AGM) την E10.5, επίσης μεταναστεύει στην αρχή στο εμβρυϊκό ήπαρ και τέλος στο μυελό των οστών, όπου αποτελεί τα ενήλικα αιματοποιητικά βλαστοκύτταρα (HSC). Παρόλο που

τα HSC μπορούν να βρεθούν στο λεκιθικό σάκο, το AGM φαίνεται να είναι η κύρια πηγή των ενήλικων HSCs.

Τα ποντίκια που έχουν απαλείψει τον Erf στον επιβλάστη, εμφάνισαν σοβαρή αναιμία και πέθαναν στην εμβρυϊκή ημέρα (E) 14,5. Τα έμβρυα Erf $^{-/-}$ είχαν μειωμένα κύτταρα στην περιφέρεια από την E9.5 και μετά, τα οποία μειώθηκαν σημαντικά την E14.5. Η εξάλειψη του Erf είχε ως αποτέλεσμα μειωμένο αριθμό κυττάρων, τα οποία ήταν και τα πιο πρόδρομα κύτταρα του αίματος την E9.5-10.5 με βάση τεχνικών αιματοξυλίνης και ηωσίνης σε λεκιθικούς σάκους, μετρήσεις κυκλοφορούντων κυττάρων αίματος και real-time για τα επίπεδα μεταγραφής των αιμοσφαιρινών στο κυκλοφορούν αίμα. Αυτά τα δεδομένα υποδεικνύουν ένα ελάττωμα στο πρωτόγονο αιματοποιητικό κύμα (primitive wave). Επιπροσθέτως, μειωμένοι ερυθροειδείς-μυελοειδείς (EMP) πρόγονοι και αποικίες ερυθρών ανιχνεύθηκαν στο περιφερικό αίμα την E10.5 με τεχνικές κυτταρομετρίας ροής και δημιουργίας αποικιών προερχόμενων από το λεκιθικό σάκο. Η αιματοποίηση του ήπατος ήταν πρόβληματοκή με επίσης μειωμένους αριθμούς προδρόμων και πιο ώριμων κυττάρων και με ανεπαρκή διαφοροποίηση ερυθροβλαστών. Κυτταρομετρία ροής με ειδικούς δείκτες για διαφοροποίηση ερυθρών και η τεχνική σχηματισμού αποικιών επιβεβαίωσαν την αναποτελεσματική διαφοροποίηση των ερυθροβλαστών. Τέλος, ο Erf φαίνεται να είναι απαραίτητος για τη διατήρηση ή διαφοροποίηση των HSCs, όπως φαίνεται από την μειωμένη ικανότητα επαναπληθυσμού τους μετά από μεταμόσχευση σε ποντίκια (CRU).

Επιπλέον, αποδεικνύουμε ότι τα μειωμένα επίπεδα του Erf προκαλούν κρανιοσυνοστέωση σε ανθρώπους και ποντίκια. Μεταλλάξεις του Erf βρέθηκαν σε ανθρώπους με κρανιοσυνοστέωση και η σπουδαιότητά τους μελετήθηκε με κλωνοποίηση μεταλλάξεων του Erf και προσδιορισμό τους με τη μέθοδο της λουσιφεράσης. Επιπλέον, ο Runx2, ένας πιθανός στόχος του Erf στην οστεογένεση, ο οποίος βρέθηκε από το Chip-seq, μελετήθηκε με συν-επιμόλυνση του Erf και Runx2 και τη μέθοδο λουσιφεράσης. Αποδεικνύουμε ότι η Erf επηρεάζει την αποτελεσματικότητα ολόκληρης της αιματοποίησης και της οστεογένεσης. Σε αυτό το πλαίσιο, ο Erf θα μπορούσε να αποτελέσει έναν ελκυστικό στόχο παρέμβασης.

Abstract

Erf is a ubiquitously expressed transcriptional repressor regulated by MAPK via nucleo-cytoplasmic shuttling. In its non-phosphorylated form, Erf is nuclear and active as a repressor, while phosphorylation by Erks in the nucleus, leads to cytoplasmic export and inactivation. In its active nuclear form, Erf blocks cell proliferation and arrests cells at G0/G1 phase in a cell type-specific manner. Moreover, Erk signaling is essential to “transform” the cell cycle inhibitory and proapoptotic action of TGF on epithelial cells, into a growth promoting and migratory response, rendering it as repressor of epithelial mesenchymal transition. *Erf* is also able to suppress ets- and ras-induced tumorigenicity in fibroblasts and Ewing’s Sarcoma cells.

However, little is known for the role of *Erf* in development. Total elimination of *Erf* in mice leads to lethality at embryonic day E10.5 due to placental defects. *Erf* knockout embryos fail to undergo chorioallantoic fusion and labyrinth development. To bypass placenta defects and study the role of Erf in the embryo proper, we employed epiblast conditional mice. Here, we show that *Erf* is required in all three waves of embryo hematopoiesis.

The first hematopoietic cells are formed in blood islands in the mouse embryo and have arisen from extraembryonic mesoderm at the neural plate stage of development at embryonic day 7.5 (E7.5) and are called the primitive wave. These primitive erythroblasts that come from the yolk sac comprise the predominant cells in the early circulating blood, resulting to erythroid, macrophage and megakaryocyte cell lineage in bloodstream. Shortly after, at embryonic day E8.25, a second wave is produced in the yolk sac, called the definitive wave and is consisted of erythroid and myeloid progenitors (EMPs). It migrates in bloodstream and finally colonize the fetal liver at embryonic day E10.5. A third wave of hematopoiesis that emerges from the aorta – gonad – mesonephros (AGM) region at E10.5, also migrates in the beginning to the fetal liver and finally the bone marrow, where it comprises the adult hematopoietic stem cells (HSC). Even though HSCs can be found in yolk sac, the AGM seems to be the major source of the adult HSCs.

Mice lacking *Erf* in embryo proper exhibited severe anemia and died around embryonic day (E) 14.5. *Erf*$^{-/-}$ embryos had reduced peripheral blood cells from E9.5 onwards that precipitated at E14.5. Elimination of *Erf* resulted in both reduced and more immature blood cells at E9.5-10.5 based on hematoxylin and eosin assays in yolks sacs, counts of circulating blood cells and real-time for transcription levels of globins in circulating blood. These data indicate a defect in the primitive hematopoietic wave. In addition, reduced erythroid-myeloid progenitors and colony forming cells could be detected at peripheral blood at E10.5 based on flow cytometry and colony assays, indicating a defect in the yolk sac derived definitive hematopoietic progenitors. Liver hematopoiesis was also impaired with decreased numbers of precursor and mature cells and inefficient differentiation of immature erythroid precursors. Assays with specific markers for flow cytometry and colony assays confirmed the inefficient differentiation of erythroblasts. Finally, elimination of *Erf* appeared to be necessary for hematopoietic stem cell maintenance or differentiation, as evident by their impaired repopulation ability.

Moreover, we show that reduced levels of Erf cause craniosynostosis in human and mice. Erf mutations were found in humans with craniosynostosis and their significance was studied with cloning of Erf mutations and luciferase assays. Moreover, Runx2, a possible target of Erf in osteogenesis found by Chip-seq, was studied by co-transfection of Erf and Runx2 followed by luciferase assay. It would thus appear that *Erf* affects the efficiency of the entire hematopoiesis and osteogenesis. To that extend, Erf could serve as an appealing intervention target.

1. Introduction

Part I: Hematopoiesis

Hematopoiesis is the formation of blood cells and occurs during embryonic development and adulthood to produce and replenish the blood system. The first blood cells that have been identified in the conceptus are those of the erythroid lineage. Red blood cells (RBCs) comprise the most abundant cell type in the body and function primarily to transport oxygen and carbon dioxide. Examination of the circulating blood cells of developing mammalian embryos at the last century revealed two distinct, temporally overlapping populations of erythroid cells. The earliest population consisted of larger, nucleated cells and the subsequent population consisted of smaller, enucleated RBCs (Palis et al., 1999; Fraser et al., 2007; Palis, 2014). These larger, nucleated erythroblasts throughout early development were called as “primitive” wave of erythropoiesis to distinguish it from the “definitive” wave that occurred not only during fetal life as well as postnatal life and their origin derives from particular anatomical sites in the developing embryo (Palis et al., 1999).

1. Waves of hematopoiesis in the developing embryo

The hematopoietic system proceeds through various developmental programs that lead in the development of different waves of hematopoiesis at different anatomical sites in the fetal embryo. These waves comprise distinct precursors that will give rise to all the differentiated blood cells which enter the circulation (Palis et al., 1999).

The first hematopoietic cells are formed in blood islands in the mouse embryo and have arisen from extraembryonic mesoderm at the neural plate stage of development at embryonic day 7.5 (E7.5) (Haar and Ackerman, 1971) and are called the primitive wave (Haar and Ackerman, 1971; Wong et al., 1986; Rich, 1992) (Figure 1). These primitive erythroblasts that come from the yolk sac comprise the predominant cells in the early circulating blood, resulting to erythroid, macrophage and megakaryocyte cell lineage in bloodstream (Kingsley et al., 2004; Fraser et al., 2007; Palis et al., 2010).

Shortly after, at embryonic day E8.25, a second wave is produced in the yolk sac, called the definitive wave and is consisted of erythroid and myeloid

progenitors (EMPs) (Rich and Kubanek, 1979; Palis et al., 1999; Bertrand et al., 2005; Tober et al., 2007). It migrates in bloodstream and finally colonize the fetal liver at embryonic day E10.5 (Steiner and Vogel, 1973; Houssaint, 1981; Palis et al., 1999; Kina et al., 2000) (Figure 1).

A third wave of hematopoiesis that emerges from the aorta – gonad – mesonephros (AGM) region at E10.5, also migrates in the beginning to the fetal liver and finally the bone marrow (Muller et al., 1994; Godin et al., 1995; Medvinsky and Dzierzak, 1996; de Bruijn et al., 2000) where it comprises the adult hematopoietic stem cells (HSC) (Figure 1). Even though HSCs can be found in yolk sac, the AGM seems to be the major source of the adult HSCs (Medvinsky and Dzierzak, 1996; de Bruijn et al., 2000).

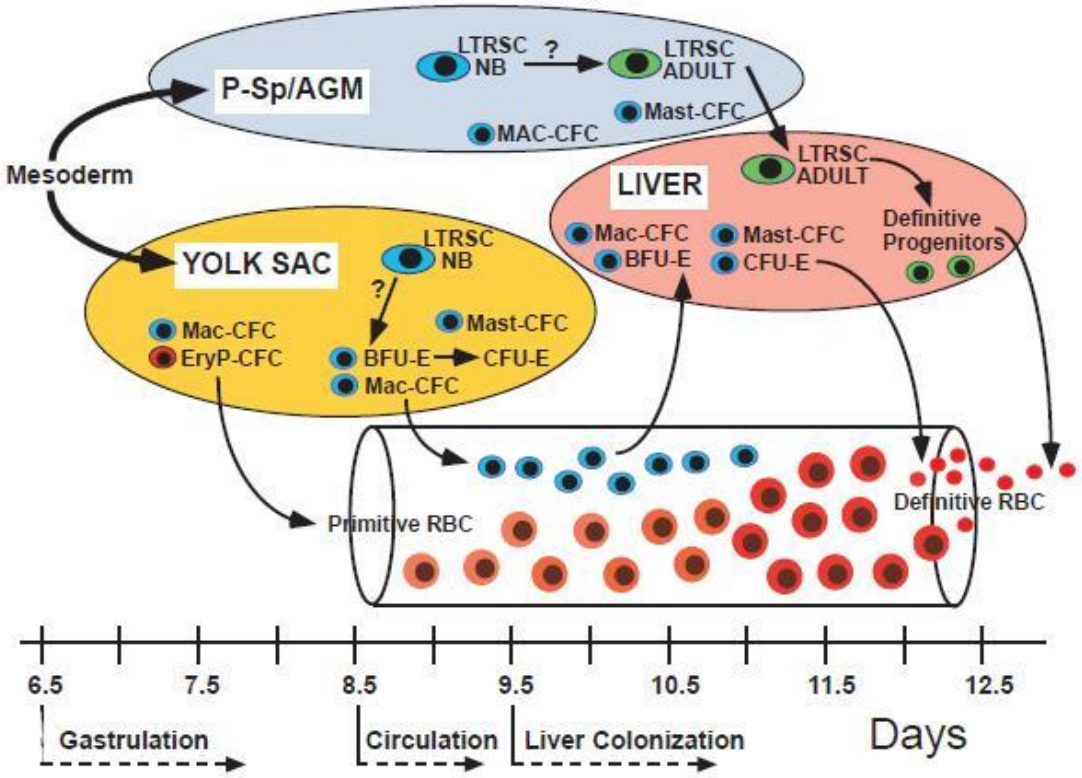

Figure 1. Model of early hematopoietic ontogeny in the mouse embryo. P-Sp/AGM, paraaortic splanchnopleura/aorta-gonad-mesonephros region; RBC, red blood cells; EryPCFC, primitive erythroid progenitors; Mac-CFC, macrophage progenitors; BFU-E, burstformingunit erythroid; CFU-E, colony-forming unit erythroid; Mast-CFC, mast cell progenitors; LTRSC: NB, longterm newborn-repopulating stem cells; LTRSC: ADULT, longterm adult-repopulating stem cells (Palis et al., 1999).

1a. Primitive yolk sac derived wave

Primitive red cells are derived from the yolk sac blood islands shortly after gastrulation, at E7.5 in the mouse (Haar and Ackerman, 1971; Silver and Palis, 1997). Primitive erythroblasts are produced by specific progenitor cells, called primitive erythroid colony-forming cells (EryP-CFC), which generate colonies that can be discriminated from definitive erythroid colonies by their maturation time, morphology of colonies, and the pattern of expression of globin genes (Wong et al., 1986; Palis et al., 1999). EryP-CFC are first located in the murine yolk sac at E7.25, after the start of gastrulation and before the creation of blood islands. Then EryP-CFC rapidly expand in numbers reaching a peak at E8.0, after which they are reduced up to no longer been found by E9.0 (Palis et al., 1999). These progenitors are the predominant red cells in the embryo until the first definitive cells migrate from the fetal liver to the circulation at E12 (Steiner, 1973; Brotherton et al., 1979; Kingsley et al., 2004). Thereafter, anemia is observed before E13 is because of the lack or reduced synthesis of primitive cells (Kingsley et al., 2004; Fraser et al., 2007).

After 24 hrs, primitive proerythroblasts can be detected in a primary vascular plexus. These immature primitive erythroblasts start to circulate at E8.25 coincident with, or soon after, the onset of contractions of the heart (Ji et al., 2003; McGrath et al., 2003; Lucitti et al., 2007). They continue to divide in the periphery until E13, (Bethlenfalvay and Block, 1970) and accumulate increasing amounts of hemoglobin, becoming progressively less basophilic (Steiner, 1973; Sasaki and Matsumura, 1986). Synthesis of hemoglobin continues until replication ceases (Fantoni et al., 1968) and primitive red cells have a steady-state hemoglobin content of about 80–100 pg per cell, ~ six times the amount of hemoglobin was found in adult erythrocytes (Steiner, 1973). This is consistent with the discovery that primitive erythroblasts are almost six times larger than erythrocytes in adulthood (Kingsley et al., 2004).

EryP have not special antigens to be discriminated from definitive cells, so based on a EryP-GFP transgenic mouse system, EryPs were found at a percentage 95% of circulating blood cells at E10.5. From E12.5 onward, circulating EryP decreased rapidly, and by E16.5, only 5% of the cells were GFP. Additionally, primitive can be distinguished from definitive based on their morphology (Figure 2). Primitive erythroblasts are large, nucleated cells

compared to definitive ones (Barker, 1968; Steiner, 1973). However, as they mature they have similar characteristics to the definitive cell, including (1) expansion of erythroblast numbers through a limited set of symmetric divisions of the cell, 2) loss of nucleoli (E9.5-E10.5), 3) reduce in cell size (E10.5 – E11.5), 4) accumulation of hemoglobin, 5) decrease in RNA content, 6) progressive nuclear condensation (E10.5 onward) and enucleation (E12.5 onward) (Fraser et al., 2007; Palis, 2014) (Figure 2). By E12.5, the primitive erythroblasts have matured to an orthochromatic stage and cell division decrease. Moreover, primitive erythroblasts lose the intermediate filament vimentin and nuclear histone proteins, changes that also happen throughout maturation of definitive erythroblasts (Morioka et al., 1998; Fraser et al., 2007). As primitive erythroid cells enucleate between E12.5 and E17.5, the association of their outer membrane bilayer with the underlying cytoskeleton is increased. Primitive erythroid cells lose 35% of their surface area and 50% of their volume between E14.5 and E17.5. The lack of surface area and volume occurs whether or not the cells are enucleated (Waugh et al., 2013). These data suggest that, unlike definitive erythropoiesis, the maturational processes of membrane remodeling and enucleation are uncoupled.

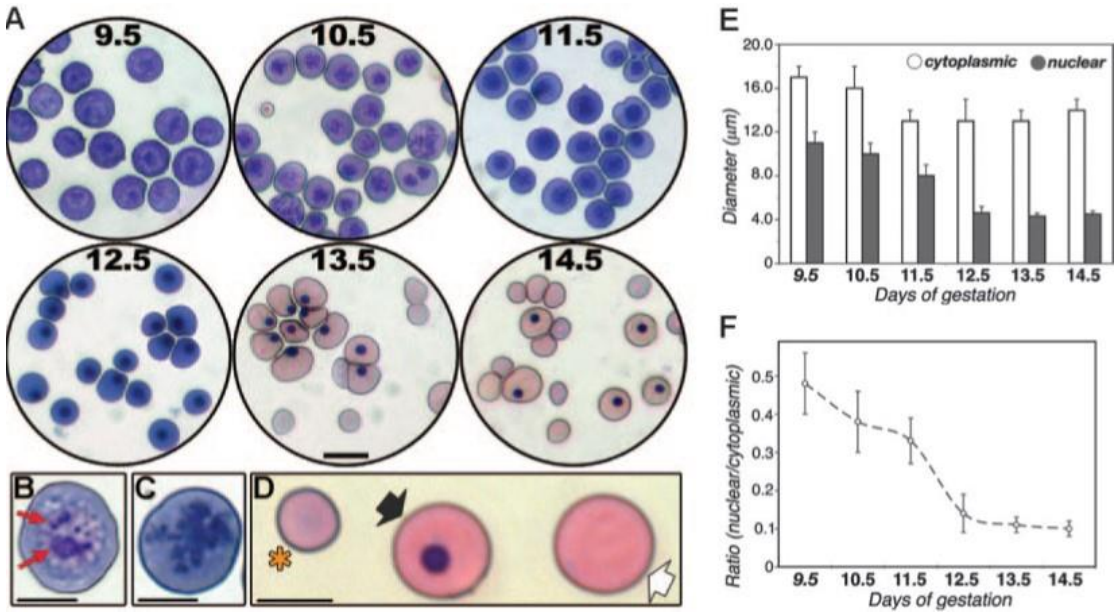

Figure 2. Cytologic changes during primitive erythroid maturation. (A) Giemsa-stained cytospin preparations of blood from wild-type embryos at E9.5 to E14.5. Scale bar, 20 μm. Circulating blood cells from E9.5 **(B)** and E10.5 **(C)** embryos, showing loss of nucleoli (red arrows in B) within the intervening 24 - hour period. Scale bar, 10 μm. **(D)** Enucleated definitive (*), larger nucleated primitive (black arrow) and nucleated primitive (white arrow) erythroid cells in circulation at E14.5. Scale bar, 10 μm. **(E)** Diameters of circulating E9.5 to E14.5 embryonic blood cells and their nuclei, (F) Ratio of mean cross-sectional area of nuclei and cytoplasms of circulating embryonic blood cells. A dramatic decrease in nuclear diameter and cross-sectional area was observed, coincident with nuclear condensation (compare with panel A). Data in panels E and F are expressed as mean ± SD.

1b. Definitive yolk sac derived wave

Shortly after the production of primitive wave, a second wave also starts in the yolk sac at embryonic day E8.25, termed the definitive wave and is consisted of erythroid and myeloid progenitors (EMPs) (Palis et al., 1999; Bertrand et al., 2005; Tober et al., 2007) that start to colonize the fetal liver at embryonic day E9.5, until a third wave takes place of them in the bone marrow.

The most immature cells of this wave are the highly proliferative erythroid progenitor cells, called burst forming unit erythroid cells (BFU-E) (Palis et al., 1999). These progenitors have the ability to create colonies ex vivo and give rise to more mature erythroid cells, the colony forming unit erythroid (CFU-Es) (Rich and Kubanek, 1979). BFU-E-derived colonies require 7 and 14 days in

mouse and human systems, respectively, to form mature colonies containing more than a thousand erythroid cells. On the contrary, the more mature CFU-E progenitors require only 2 and 7 days in mouse and human systems, respectively, to create mature colonies that consist of only 16–32 cells. Thus, CFU-E are only 4–5 cell divisions upstream of the mature RBCs. (Steiner and Vogel, 1973; Houssaint, 1981; Palis et al., 1999; Kina et al., 2000). In vivo, BFU-E were found exclusively in the yolk sac up to the 10- 15 somite pairs by which time circulation has begun (Figure 3). By 20- 25 somite pairs (E9.0), small numbers of these progenitors were in the bloodstream and the embryo proper, even though the majority was located in the yolk sac. Even at the 26-29 somite pairs (E9.5), there were still 10- to 40-fold more BFU-E in the yolk sac than in the embryo proper, consistent with that these definitive erythroid progenitors come from this extraembryonic site (Fig. 3). Subsequently, BFU-E numbers are decreased in the yolk sac and increased in the bloodstream and embryo proper. BFUE were found in the liver rudiment at the earliest stages checked (40-43 somite pairs), and their numbers expanded dramatically in this tissue (approximately 25-fold) for the next 24 hours. This wave of BFU-E progenitors in the yolk sac, bloodstream and liver is followed, both temporally and spatially, by CFU-E. CFU-E display a more advanced stage of development within the definitive erythroid lineage and generate small colonies consisted of enucleate erythrocytes. CFU-E were first detected at 26-29 somite pairs (E9.5) and were found predominantly in the yolk sac although lower numbers were present in the bloodstream and embryo proper. By 40-43 somite pairs (E10.5), high numbers of CFU-E were found in both the bloodstream and the liver. During the next 24 hours, the number of CFU-E increased 18-fold in the liver, and was reduced in the yolk sac and bloodstream. Together, these findings are consistent with the idea that the definitive erythroid lineage develops initially within the yolk sac and mature from BFU-E to CFU-E stages.

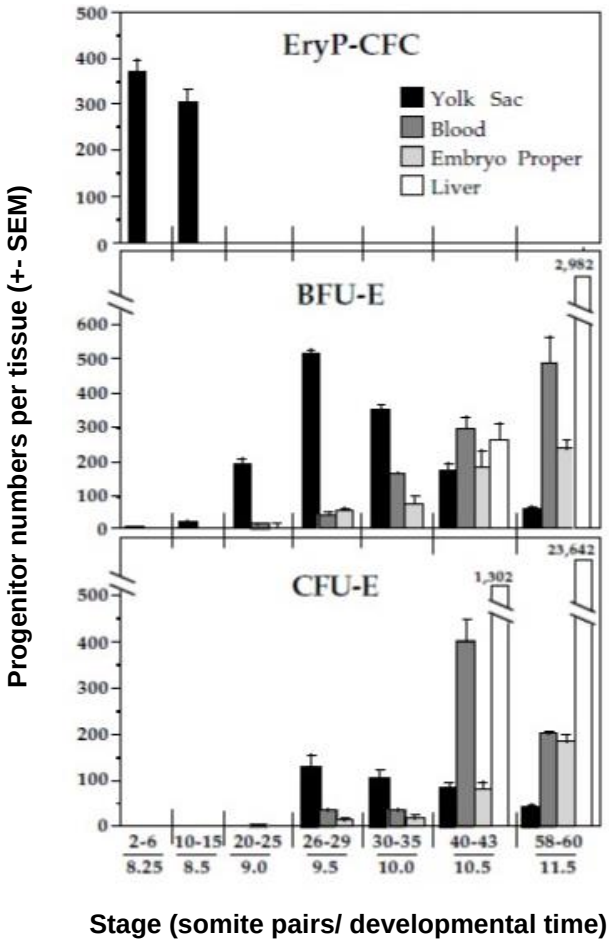

Figure 3. Distribution of primitive erythroid (EryP-CFC), definitive erythroid (BFU-E and CFU-E), within various compartments of the mouse conceptus during somitogenesis (E8.25-E11.5). (Palis et al., 1999)

BFU-E/CFU-E differentiate to enucleated red blood cells through multiple maturational after they migrate to the liver. The fetal erythroid compartment is consisted of morphologically identifiable, which are characterized by progressive (1) erythroblast expansion through a limited set of symmetric cell divisions, (2) accumulation of hemoglobin, (3) decrease in cell size, (4) nuclear pyknosis, and (5) decrease in RNA content, like erythroid primitive cells. These nucleated precursors are at progress from proerythroblast (ProE) to basophilic (BasoE), polychromatophilic (PolyE), and orthochromatic (OrthoE) forms (Figure 4A). They can be discriminated based on the dynamic expression of Ter119 glycophorin A and the CD71 transferrin receptor on the surface of maturing cells populations (Figure 4B). Erythroid cells can be identified in five distinct populations, based on characteristic staining patterns: $CD71^{med}$ $TER119^{-}$ (R1), $CD71^{high}$ $TER119^{-}$ (R2), $CD71^{high}$ $TER119^{high}$ (R3), $CD71^{med}$ $TER119^{high}$ (R4), and $CD71^{low}$ $TER119^{high}$ (R5). R1 cells comprise ≥ 40% CFU-Es, R2 contain only a few CFU-Es and R3 – R5 contain no erythroid

progenitors. The morphologic characteristics are corresponded to primitive progenitor cells and proerythroblasts in the R1 population, proerythroblasts and early basophilic erythroblasts in R2, early and late basophilic erythroblasts in R3, polychromatophilic and orthochromatophilic erythroblasts in R4, and late orthochromatophilic erythroblasts and reticulocytes in the R5 population (Sieff et al., 2010).

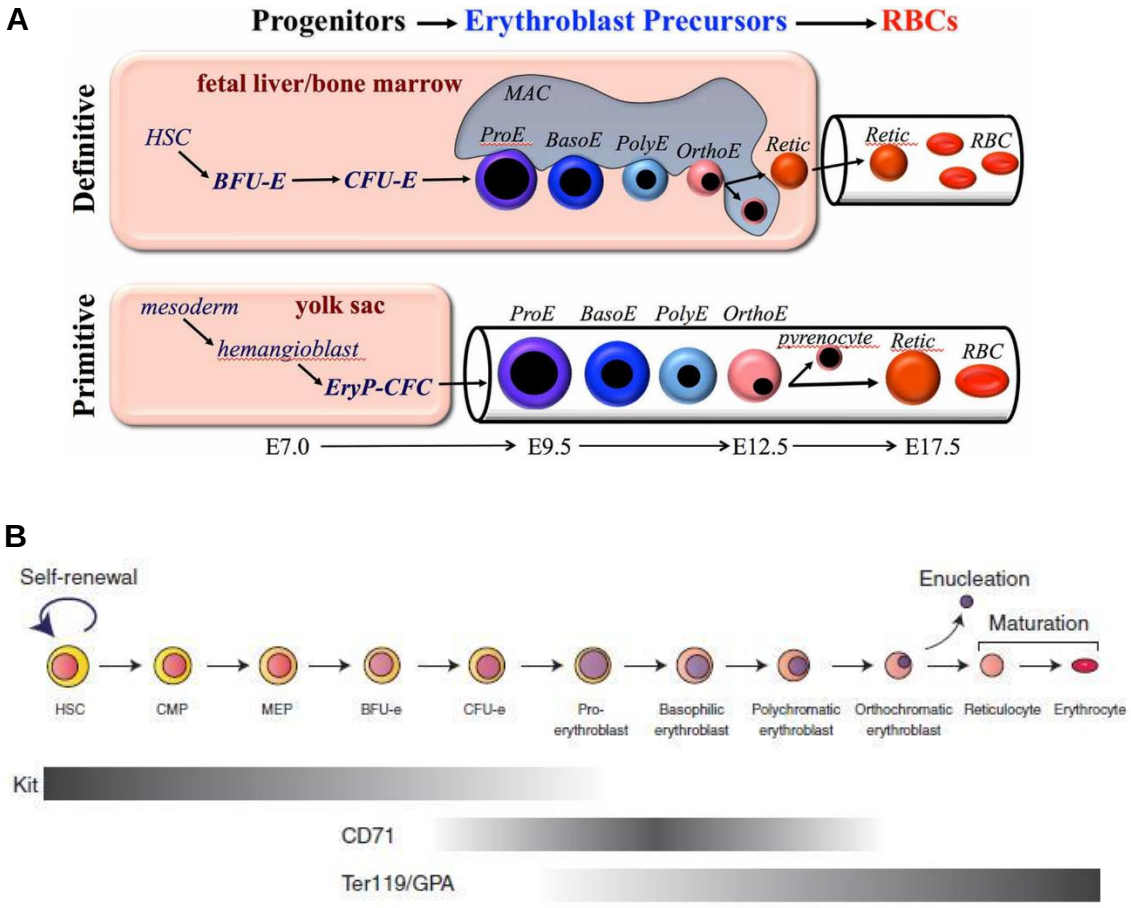

Figure 4. Overview of primitive and definitive erythropoiesis. (A) Both forms of erythroid cell production are characterized from the progressive developmement of cells through three compartments: progenitors, erythroblast precursors, and red blood cells (RBCs). Erythroid progenitors (BFU-E, CFU-E, and EryP-CFC) are defined by their capacity to form colonies of maturing erythroid cells *in vitro*. Erythroid precursors are defined morphologically as proerythroblasts (ProE), basophilic erythroblasts (Baso), polychromatophilic erythroblasts (PolyE), and orthochromatic erythroblasts (OrthoE). OrthoE enucleate to for a pyrenocyte that contains the condensed nucleus,and a reticulocyte (Retic), that goes to mature into a RBC. Definitive erythropoiesis in the adult organism is derived from hematopoietic stem cells (HSC), while primitive erythropoiesis occurs just once from mesoderm cells in the early

embryo (Palis, 2014), (B) Markers of Erythroid differentiation in the mouse. The expression of the c-Kit, CD71 and Ter119 used cell surface markers to identify the various stages is indicated by the bars. Cells at the CFU-e and pro-erythroblast stage are the most sensitive to, and dependent on the presence of EPO. Gray, low expression; black, high expression; HSC, hematopoietic stem cell; CMP, common myeloid progenitor; MEP, megakaryocyte-erythroid progenitor; BFU-e, burst-forming unit, erythroid; CFU-e, colony-forming unit, erythroid (Dzierzak and Philipsen, 2013).

The maturation of erythroblasts in the fetal liver and postnatal bone marrow occurs within erythroblastic islands, consisted of erythroblasts which are attached to central macrophages (reviewed by Chasis and Mohandas, 2008). Macrophages have been shown to be crucial for erythroblast proliferation, particularly in the stress erythropoiesis (Hanspal et al., 1998; Rhodes et al., 2008; Chow et al., 2013; Ramos et al., 2013). In mammals, the end of a precursor maturation is enucleation, which leads to the formation of two cell types. The first population is consisted of reticulocytes that have most of the cytoplasm and hemoglobin, as well as the proteins which are needed to create a unique cytoskeletal network (Gaiduschek and Singer, 1979; Koury et al., 1989; Lee et al., 2004; Liu et al., 2011). The second population is consisted of pyrenocytes (“extruded nuclei”) that have the con-densed nucleus surrounded by a lipid bilayer and thin cytoplasm (McGrath et al., 2008a). Enucleation is a complex process that is consisted of multiple steps, including the establishment of cell polarity throughout microtubule action, the creation of a conractile actomyosin ring, vesicle formation, and lipid crafts between reticulocyte and pyrenocytes (Keerthivasan et al., 2010; Konstantinidis et al., 2012; Wang et al., 2012). Soon after their formation in the fetal liver and bone marrow, pyrenocytes flip phosphotidylserine onto their surface, providing an “eat me” signal, and are digested by macrophages (Yoshida et al., 2005). Enucleated definitive red cells start to emerge from the liver at E12 (Kingsley et al., 2004) and over the next several days, the number of definitive erythroid cells expands exponentially in the circulation with a continued rapid growth of the fetus (Kingsley et al., 2004).

1c. Definitive AGM derived wave

During mouse ontogeny, a third wave of fetal hematopoiesis comprises long-term HSC that are required for continued synthesis of fetal erythrocytes within the liver, and finally adult erythrocytes within the bone marrow. First HSCs appear in the intra-embryonic aorta-gonad-mesonephros (AGM) region at day 10 of gestation (Muller et al., 1994; Medvinsky and Dzierzak, 1996). Then, HSCs are also found in the yolk sac and fetal liver (Moore and Metcalf, 1970; Muller et al., 1994; Medvinsky and Dzierzak, 1996). Moreover, significant numbers of HSCs are found in the mouse placenta (Gekas et al., 2005), nearly coincident with the appearance of HSCs in the AGM region and for several days thereafter. Placental HSCs could arise through de novo generation or colonization upon circulation, or both. The relative contribution of each of the above sites to the final pool of adult HSCs remains largely unknown. However, the AGM region is the most potent source of adult repopulating HSCs (Medvinsky and Dzierzak, 1996), which are thought to colonize the fetal liver at E11.5. HSC do not mature at their site of synthesis (Godin et al., 1999) (Figure 5). Thus, they have insufficient time to generate the mature erythrocytes that emerge from the liver beginning at E12.

The AGM region is an anatomically complex tissue forming several organ systems in addition to hematopoietic cells. The AGM is derived from the mesodermal germ layer and generally extends from the forelimbs to the hindlimbs of the E9.5 - E12.5 mouse embryo. The first discernible tissue formed in the corresponding region of the E8 mouse embryo is the vasculature of the paired dorsal aortas. At E8.5, the aortas are linked to the yolk sac vasculature through the vitelline artery, and at E9 the paired aortas fuse to form a single midline dorsal aorta (Garcia-Porrero et al., 1995). The umbilical artery forms the connection between the dorsal aorta and the placenta. The urogenital system begins to form at E9 (Rugh et al., 1990). Differentiation of the embryonic excretory system begins with the pronephric ducts at E9 and the mesonephric ducts at E10. By late E11, the pro/mesonephric ducts are regressing and by E12 the metanephros (definitive kidney) has become prominent in the caudal aspect of the embryo. The gonads begin to be discernible at E10 and primordial germ cells (PGCs) migrate into them. By E12 the gonads have enlarged significantly and are prominent ventral to the mesonephroi. As hematopoietic

cells have been detected in association with each of the three developing organ systems, it is of great interest to determine where within the actively differentiating AGM region the first HSCs develop.

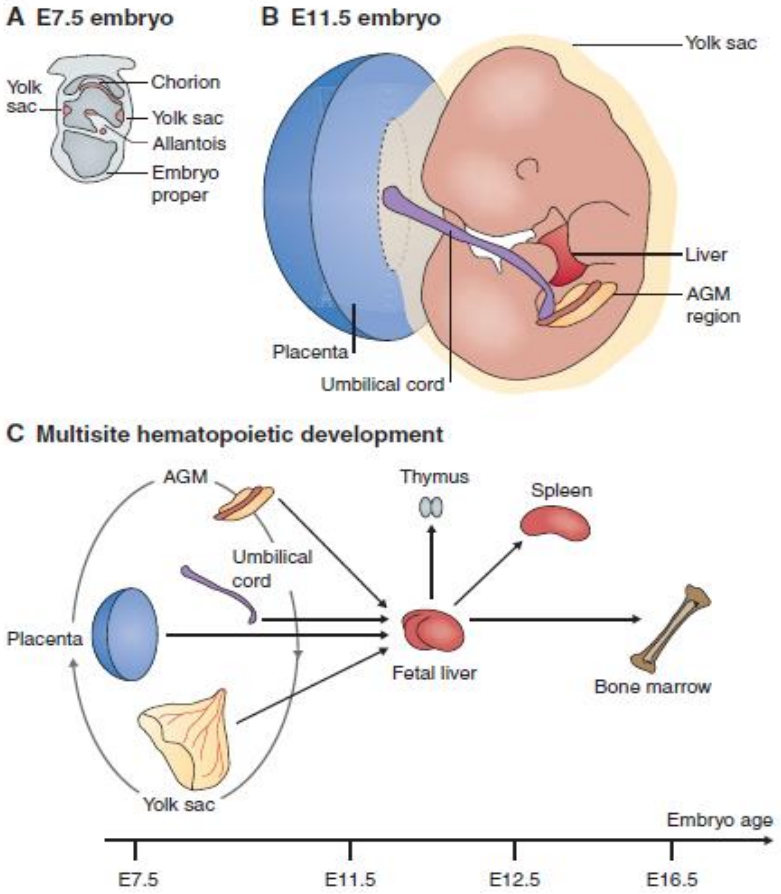

Figure 5. Continuity in embryonic hematopoietic development. (A) A schematic of an E7.5 mouse embryo (anterior to the left), showing extraembryonic hematopoietic sites (yolk sac, chorion, allantois). The liver rudiment starts developing by the end of E9, (B) A schematic of an E11.5 mouse embryo (anterior uppermost), showing tissues that develop into embryonic hematopoietic stem cell (HSC) niches: the chorion contributes to the placenta; the allantois to the umbilical cord and partly to the placenta; the P-Sp develops into the aorta-gonadmesonephros (AGM) region. The yolk sac expands and encompasses the embryo, (C) A model of multisite hematopoietic development, showing hematopoietic progenitors and definitive HSCs (d) from the sites shown in B colonizing the liver rudiment and each other (as shown by the circular arrow). Disagreement exists about which of these sites is the genuine source of dHSCs and the adult hematopoietic system. After expansion in the fetal liver, dHSCs colonize the bone marrow, spleen and thymus. In adulthood, the thymus and spleen are colonized by bone marrow progenitors (not shown) (Medvinsky et al., 2011).

All hematopoietic cells ultimately derive from a small population of hematopoietic stem cells (HSCs), which is separable into at least two subsets: long-term reconstituting HSCs (LT-HSCs) and short-term reconstituting HSCs (ST-HSCs). LT-HSCs maintain self-renewal and multi-lineage differentiation potential throughout life. ST-HSCs derive from LT-HSCs and, although they maintain multipotency, they exhibit more-limited self-renewal potential. Further differentiation of ST-HSCs generates multipotent progenitors (MPPs) (Figure 6). Hematopoietic progenitor cells lose their differentiation potential in a stepwise fashion until they eventually generate all of the mature cells of the blood system. Several potentially distinct subsets of MPPs have been described. In the model proposed by the Weissman group (Akashi et al., 2000), multipotential progenitors (MPPs or short-term HSCs [ST-HSCs]) give rise to either a common lymphocyte progenitor (CLP) or a common myeloid progenitor (CMP), which, in turn, gives rise to either a granulocyte-macrophage progenitor (GMP, equivalent to CFU-GM) or a megakaryocyte-erythroid progenitor (MEP). The alternate model suggested by the Jacobson group (Adolfsson et al., 2005) involves the generation of MEPs directly from the MPPs/ STHSCs, whereas a lymphoid-primed multipotential progenitor (LMPP) has the potential to generate both CLPs and GMPs. LT-HSC, (Dzierzak and Philipsen, 2013). HSC and progenitor populations can be discriminated by flow cytometry, using antibodies that recognize unique combinations of cell surface markers.

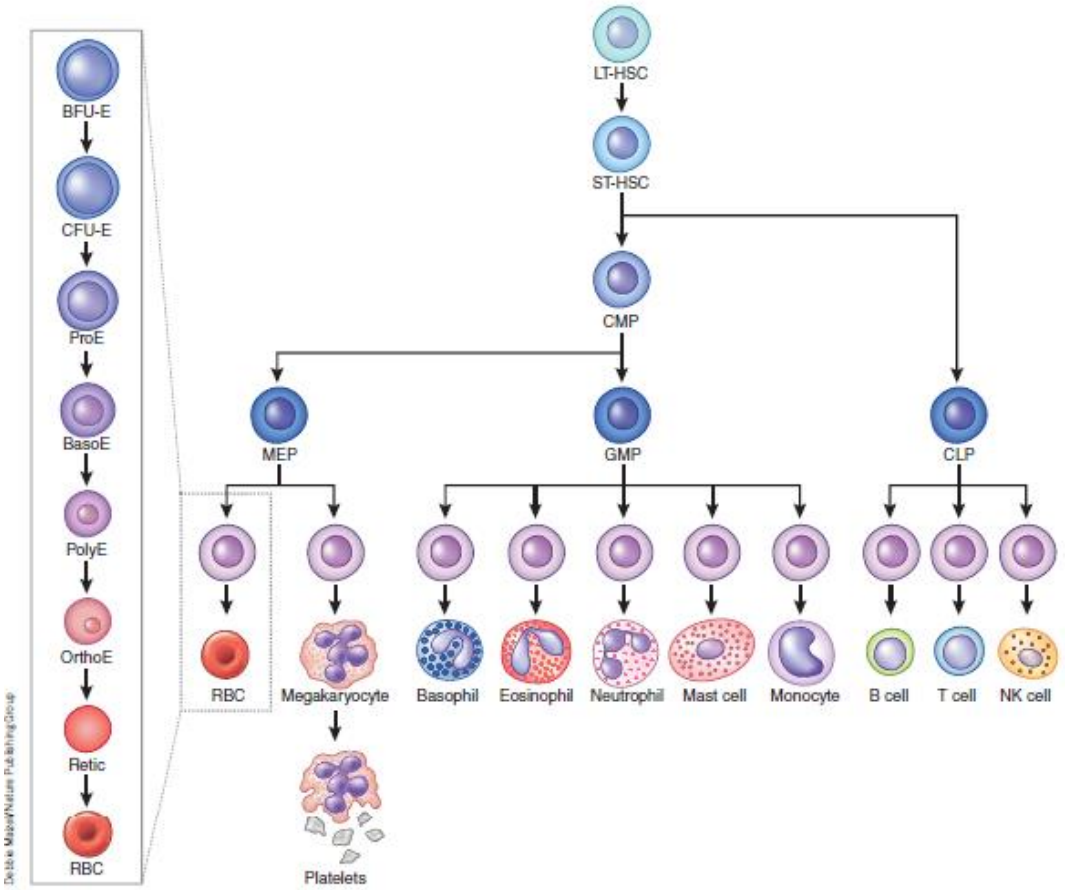

Figure 6. Differentiation of hematopoietic stem cells. (Akashi et al., 2000) (solid arrows), Long Term HSCs (LT-HSCs) has the potential of self-renewal and give rise to to multipotential progenitors (MPPs)\short-term HSCs (ST-HSCs) or ST-HSCs give rise to multipotential progenitors (MPPs) (not shown). Lineage-committed oligopotent progenitors derived from them include the common lymphoid progenitor (CLP), common myeloid progenitor (CMP), which give rise to megakaryocyte-erythrocyte progenitor (MEP) and granulocyte-monocyte progenitor (GMP) populations. The alternate model suggested by the Jacobson group (Adolfsson et al., 2005) (dotted arrows) involves the generation of MEPs directly from the MPPs/ STHSCs, whereas a lymphoid-primed multipotential progenitor (LMPP) has the potential to generate both CLPs and GMPs. LT-HSC, (Dzierzak and Philipsen, 2013).

2. Mouse globins in primitive and definitive erythroblasts

Hemoglobin molecules contain globin chains derived from both the α- and β- globin gene loci. Primitive and definitive erythroid cells have distinct patterns of globin gene expression. While definitive erythroid cells in the mouse express α1-, α2- β1-, and β2-globins, primitive erythroid cells in addition express ζ-,

βH1-, and εy-globins (Trimborn et al., 1999). These latter embryonic globin genes are differentially expressed in primitive erythroid cells (Farace et al., 1984; E. Whitelaw et al., 1990; Kingsley et al., 2006). The initially expressed ζ- and βH1-globin genes are superseded by the α1-, α2-, and εy-globin genes, a process termed ‘‘maturational’’ globin switching since this globin switching occurs as primitive erythroid precursors terminally differentiate (Kingsley et al., 2006). Embryonic βH1-globin transcripts are expressed in yolk sac blood islands as early as E7.5, but expression of εy-globin transcripts has not been investigated before E9.5 (D. A. Whitelaw, 1990). A relative transition in βH1- and εy-globin mRNA levels has been described in fetal blood between E10.5 and E13.5 (Farace et al., 1984; D. A. Whitelaw, 1990). βH1 is the first β-globin mRNA to significantly accumulate in immature primitive erythroid cells from E7.5 through E8.5. As primitive red cells continue to mature in the bloodstream, εy-globin transcripts are up-regulated and supersede βH1-globin mRNA levels. εy remains the predominant β-globin transcript as primitive orthochromatic erythroblasts enucleate between E12.5 and E15.5 and become reticulocytes. These changes in the relative levels of βH1- and εy-globin serve as a striking in vivo example of maturational globin switching (Figure 7). Primitive erythroid cells in human embryos also appear to undergo maturational globin switching. Both ζ- to α-globin and ε- to γ-globin gene switches have been described between 5 and 7 weeks gestation (Peschle et al., 1985). Other, less dramatic, changes occur in the relative levels of β-globin genes as primitive erythroid cells mature in the bloodstream. There is a small increase both in β1- and in gestation. It is likely that these transcripts are responsible for the progressive increase in adult hemoglobin found in primitive erythroblasts between E12.5 and E14.5 (Brotherton et al., 1979).

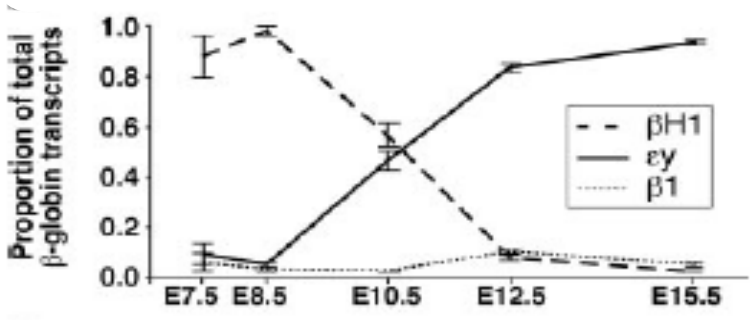

Figure 7. Globin switching as primitive erythroid cells mature at embryonic day 7.5 to 15.5. Relative mRNA levels of εy-, βH1-, and β1-globin transcripts reveal the βH1- to εy-globin switch between E8.5 and E12.5. The E7.5 and E8.5 values are based on dissected yolk sac tissues, E10.5 on whole peripheral blood and E12.5 and E15.5 values on sorted cell populations.

The down-regulation of βH1- and the up-regulation of εy-, β1-, and β2-globin mRNAs between E10.5 and E12.5 are paralleled by changes in RNA Pol II density at their promoters. Furthermore, the βH1- and εy -globin genes in primitive erythroid cells reside in a single large hyperacetylated domain, suggesting that the maturational globin switching is regulated by altered transcription factor presence instead of chromatin accessibility as postulated in the adult (Kingsley et al., 2006). In contrast, the regions containing these genes are not associated with histone hyperacetylation (Bulger et al., 2003) and they are not expressed in definitive erythroid cells (Trimborn et al., 1999; Kingsley et al., 2006). The occurrence of maturational globin switching highlights the importance of cell context when studying globin gene regulation. These results suggest that differential expression of adult versus embryonic globin genes is regulated in part by chromatin modifications.

3. Ontogeny of hematopoiesis

At the earliest stages of blood development, the primitive hematopoietic and endothelial cells that make up a rudimentary circulatory system emerge simultaneously; thus, their origins has long been vigorously debated. One theory suggests that these lineages are generated from a common bipotent progenitor (hemangioblast), (Choi et al., 1998; Fehling et al., 2003) whereas the other suggests that they are independently fated among mesodermal

progenitors during gastrulation (Kinder et al., 1999). To date, this debate has not been resolved at this stage of development. In contrast, at later stages of blood development (definitive hematopoiesis), it has become increasingly clear over the past few years that multilineage HSCs/progenitor cells arise from specialized vascular endothelial cells that acquire blood-forming potential (hemogenic endothelium), at least within the yolk sac, placenta, and AGM (Hirschi, 2012). This is not surprising, given that the possibility had been noted almost 100 years ago. Indeed, the earliest use of the term “hemangioblast” refers to the precursor cells that give rise to blood-forming (hemogenic) endothelial cells (Hirschi, 2012).

3a. The Mesoderm

In mouse blastocyst, the inner cell mass at 3.5 days post coitum comprises a population of cells – which can give rise to a derivative of three germ layers (endoderm, mesoderm and ectoderm) – that eventually develop into both intraembryonic and extraembryonic tissues as embryo develops. The hematopoietic system that derives from the mesodermal germ layer generates distinct hematopoietic precursors (Palis et al., 1999). The early production of erythroid lineage cells in the yolk sac is a transient extraembryonic tissue. They are derived from mesodermal cells that are formed from epiblast cells in agressing through the primitive streak (Kinder et al., 1999). The newly formed mesodermal cells migrate posteriorly, enter the yolk sac, and come in close contact with endoderm cells. It is this interaction between the two cell layers that is required for the initiation of erythropoiesis. Interestingly, the mesodermal cells that migrate into the yolk sac form blood islands containing not only red blood cells, but also endothelial cells (Belaoussoff et al., 1998).

3b. The hemangioblast

The overlapping ontogenic appearance of both erythroid and endothelial cells indicates a common mesodermal precursor - the hemangioblast - with bilineage potential (Murray, 1932). Hemangioblast precursors are found primarily in the primitive streak and not in the yolk sac, it is thought that they rapidly commit to hematopoietic and vascular fates soon after their emergence

during early gastrulation. There is increasing evidence to suggest that many, if not most, yolk sac vascular cells arise from unilineage angioblast precursors and not from hemangioblasts (Weissman, 2006). In contrast, hemangioblast precursors contain primitive erythroid, definitive erythroid, and multilineage myeloid potential (Choi et al., 1998). This is further supported by the overlap in genetic programs for the two lineages (i.e., expression of Flk-1 [KDR], Scl [Tal1], and CD34) and the lack of both lineages in embryos deficient for some of these genes (Tavian et al., 1999). Surprisingly, hemangioblasts in vivo are localized not in the yolk sac but in the posterior primitive streak (Huber et al., 2004). As they migrate to the yolk sac, they begin their commitment to endothelial and hematopoietic progenitors, with several of these cells contributing to the formation of each blood island (Weissman, 2006). These findings support the concept that all primitive erythroid and the first definitive erythroid cells in the embryo are ultimately derived from hemangioblast precursors.

3c. The hemogenic endothelium

Hemogenic endothelium is a specialized subset of developing vascular endothelium that acquires hematopoietic potential and can give rise to multilineage hematopoietic stem and progenitor cells during a narrow developmental window in tissues such as the extraembryonic yolk sac and embryonic aorta-gonad-mesonephros. In vitro studies suggest that mesodermal precursors first generate hemogenic endothelium, which then generate blood cells or vascular endothelial cells in a linear sequence. Even blood cells referred to as “hemangioblast - derived” have recently been proposed to be produced via an endothelial intermediate. Moreover, it has been suggested that this endothelium generates blood cells of definitive wave in the yolk sac or AGM region (L. K. Lee et al., 2016). Therefore, definitive hematopoiesis cannot occur in the absence of endothelial cell development (Shalaby et al., 1995; Shalaby et al., 1997) (Figure 8).

The idea that blood cells developed from a hemogenic endothelium was proposed around 100 years ago and was based on microscopic observations

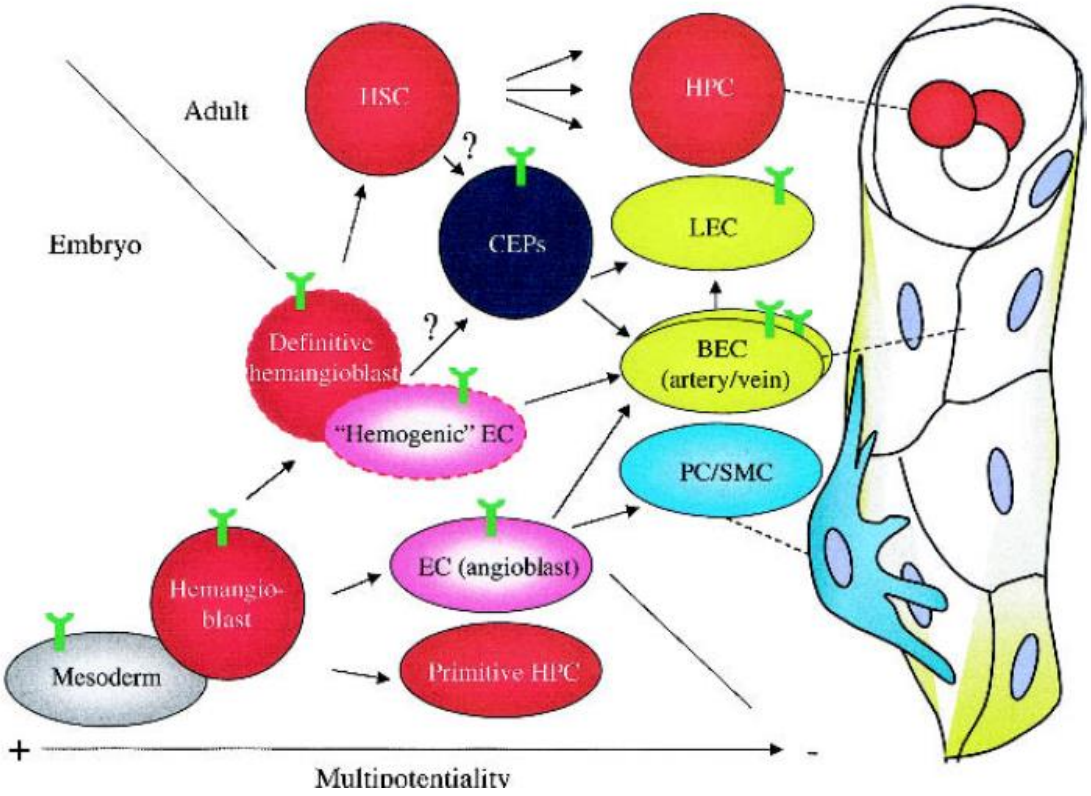

Figure 8. A schematic view of possible developmental lineage relationships of embryonic and adult hematopoietic and endothelial cells. During mbryogenesis, the lateral mesoderm or "hemangioblasts" derived from the mesoderm give rise to both primitive hematopoietic (HPC) and endothelial (EC) cell lineages. Part of the pericytes/ smooth muscle cells (PC/SMCs) are apparently derived from the ECs. The originof the definitive (adult-type) HPCs in embryos is not clear, and different views have been presented ranging between the concepts of "definitive hemangioblast" and "hemogenic EC" (delineated by broken lines). After the embryonic differentiation of the arterial and venous endothelial cells (BEC), lymphatic endothelial cells (LECs) are generated from the latter. In adults, the discovery of circulating EC progenitors (CEP), derived from hemangioblastic cells or the hematopoietic stem cells (HSCs), has suggested that adult angiogenesis may operate in part by similar mechanisms as in the embryos. A blood vessel is shown on the *right*, with an indication of the corresponding constituent cells. The expression of VEGFR-2 (Y) and Tal1 (in red, low-level in pink) in the cells has been marked (Kubo and Alitalo, 2003).

of developing embryos and represented in beautiful drawings (Goldie et al., 2008; Kissa and Herbomel, 2010). The first *in vivo* experimental support came much later, from lineage tracing of endothelium in the chick embryo (Shalaby et al., 1995; Lancrin et al., 2009). More recently, lineage-tracing studies in which

Cre recombinase was expressed under the regulatory control of the endothelial marker VE-Cadherin (VECadh) lent further support to this model (Shalaby et al., 1997; Li et al., 2012). Arguably, the strongest support for an endothelial origin of hematopoietic cells came from the recent time-lapse imaging studies that visualized the transition of endothelium into blood in real-time, both *in vitro* and *in/ex vivo* (Samokhvalov et al., 2007). The process of endothelial cells taking on a hematopoietic fate has been termed the endothelial-to-hematopoietic transition (EHT), and involves the bending out and rounding up of an endothelial cell and its subsequent detachment from the vascular wall and formation of a free-moving hematopoietic cell (Robert-Moreno et al., 2008). These imaging and lineage tracing studies provided compelling support for a large body of *in vitro* and *ex vivo* data that had earlier supported an endothelial origin of blood. In addition, Lee *et al.*, suggested that Lyve1 which is expressed in the hemogenic endothelium can distinguish definitive wave against primitive wave (L. K. Lee et al., 2016), indicating that primitive cells may not arise from the same precursor called hemogenic endothelium.

4. Liver: a major organ of hematopoiesis

In mammals, the liver serves as the main hematopoietic organ during a considerable period of prenatal ontogeny. In murine liver, for example, hematopoietic cells first appear in 10 - day embryos, with hematopoietic function of the organ reaching a peak on embryonic days 13–14 (Sasaki and Sonoda, 2000). Hematopoiesis requires specific microenvironment that produces chemical signals to attract hematopoietic cells and regulates their proliferation and differentiation via contact and humoral interactions.

4a. Liver development

The endoderm germ layer is established during gastrulation and forms a primitive gut tube that is subdivided into foregut, midgut and hindgut regions (Figure 9a). Fate mapping studies in the mouse embryo at embryonic day 8.0 of gestation indicate that the embryonic liver originates from the ventral foregut endoderm (Tremblay and Zaret, 2005). The first morphological sign of the embryonic liver is the formation of the hepatic diverticulum, an out-pocket of

thickened ventral foregut epithelium adjacent to the developing heart at E9.0 (Figure 9b). The anterior portion of the hepatic diverticulum gives rise to the liver and intrahepatic biliary tree, while the posterior portion forms the gall bladder and extrahepatic bile ducts. At E9.5, the hepatic endoderm cells, known as hepatoblasts delaminate from the epithelium and invade the adjacent septum transversum mesenchyme (STM) to form the liver bud (Houssaint, 1981; Medlock and Haar, 1983). The STM contributes fibroblasts and stellate cells of the liver. Between E10 - E15 the liver bud undergoes a period of accelerated growth as it is vascularized and colonized by hematopoietic cells to become the major fetal hematopoietic organ. The hepatoblasts are bi-potential and those residing next to the portal veins become BECs that will line the lumen of the intrahepatic bile ducts (IHBD), while the majority of hepatoblasts in the parenchyma differentiate into hepatocytes (Lemaigre, 2003). The maturation of functional hepatocytes and the formation of a biliary network connected to the extrahepatic bile ducts (EHBD) are gradual. Beginning at E13 this process continues until after birth to generate the characteristic tissue architecture of the liver (Si-Tayeb et al., 2010).

A

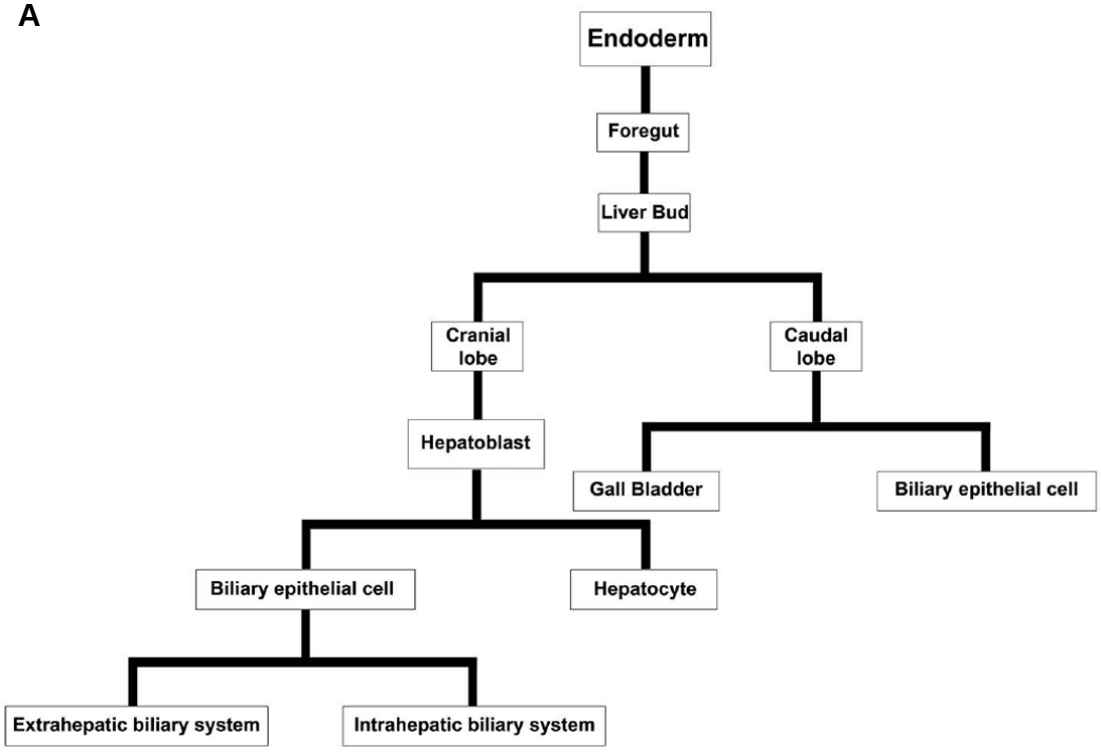

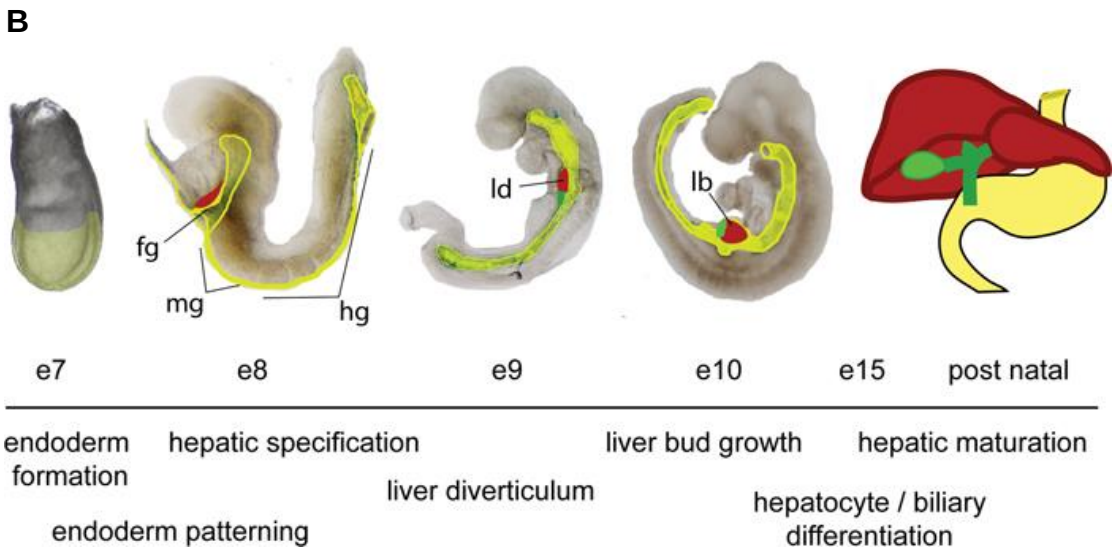

Figure 9. Time line of mouse liver development. (A) Liver cell lineage. The cell lineage steps during hepatic development (red) from uncommitted endoderm to functional adult hepatocytes and biliary epithelium, **(B)** The schematic shows mouse embryos at different stages of development with the endoderm tissue highlighted in yellow, the liver in red and the gall bladder in green. The major developmental events are listed below. The endoderm germ layer is formed during gastrulation (e6.5-e7.5). Throughout gastrulation and early somite stages of development (E7-E8.5) the endoderm is patterned along the A-P axis into foregut (fg) midgut (mg) and hindgut (hg) progenitor domains. Morphogenesis forms foregut and hindgut pockets as the endodermal cup is transformed into a gut tube. By E8.5 hepatic fate specified in a portion of the ventral foregut endoderm adjacent to the heart. As the embryo grows the endoderm forms a gut tube and the liver domain moves to the midgut. The liver diverticulum (ld) forms by E9 and expands into an obvious liver bud (lb) by E10. The liver grows, and by E15 hepatoblasts are differentiating into hepatocyte and biliary cells. Final maturation of the liver is gradual and continues into the postnatal period (Si-Tayeb et al., 2010).

4b. Hematopoietic niche of the liver

The hematopoietic microenvironment of the fetal liver is created by a complex of cell types, including epitheliocytes, resident macrophages, and several stromal cell populations of mesenchymal origin such as hepatic stellate cells, fibroblasts, myofibroblasts, vascular smooth muscle and endothelial cells, and mesenchymal stromal cells (MSCs).

i. Liver Epithelium

At early stages of liver development, its epithelium is represented by bipotent hepatoblasts, which subsequently differentiate into hepatocytes and cholangiocytes. Hepatoblasts can be identified by the simultaneous expression of both hepatic (cytokeratin 18, albumin) and biliary epithelial markers (cytokeratin 19) and also of E-cadherin (Terrace et al., 2007).The morphology and phenotype of liver epithelial cells change in the course of development, and these changes correlate with hematopoietic activity (Ayres-Silva Jde et al., 2011). Cells of the hepatocyte lineage appear to play an important role in the regulation of erythropoiesis: they closely interact with erythroblasts and produce erythropoietic cytokines such as stemcell factor and erythropoietin (Ayres-Silva Jde et al., 2011). Localization of megakaryocyte lineage cells among hepatocytes described in human fetal liver and thrombopoietin production by some lines of murine hepatocytes both suggest a contribution of the hepatic epithelium to the control of megakaryocytopoiesis (Aiuti et al., 1998). The biliary epithelium can also support both long-term proliferation of hematopoietic cells and production of committed erythroid or granulocyte/macrophage progenitors by means of contact interactions via liver regulating protein that is expressed on the surface of the epitheliocytes (Corlu et al., 1998).

ii. Macrophages

In the developing liver, macrophages first appear in sinusoids. At the stage of active liver hematopoiesis, they migrate to the parenchyma to form erythroblastic islands consisting of a central macrophage surrounded by erythroblasts and sparse lymphocytes (Sasaki and Iwatsuki, 1997).The interaction of erythroid cells with macrophages mediated by the erythroblast macrophage protein (Emp) is necessary for their enucleation. Moreover, macrophages express vascular cell adhesion molecule VCAM-1, which also mediates their adhesive interactions with erythroblasts, and jagged-1, a ligand for the Notch signal system involved in regulation of hematopoiesis]. The central macrophages of erythroblastic islands degenerate as hematopoiesis in the liver ceases (Sasaki and Iwatsuki, 1997). Another population of

macrophages in the fetal liver consists of Kupffer cells, which line the sinusoids. Some recent findings suggest that they derive from the yolk sac and are not a progeny of definitive hematopoietic stem cells. Their functions in the maintenance of hematopoiesis consist in phagocytosis of the nuclei extruded from late-stage erythroblasts (Bankston and Pino, 1980) and secretion of erythropoietin. The presence of dividing and maturing erythroblasts in the vacuoles of Kupffer cells, which has been observed in the fetal liver, may also indicate the role of these cells in the regulation of erythropoiesis (Bankston and Pino, 1980).

iii. Hepatic Stellate Cells

The hepatic stellate cells, or Ito cells, are located in the perisinusoidal space of Disse. Quiescent stellate cells contain retinoid lipid droplets. When activated, they lose these droplets and acquire morphological and phenotypic feature characteristics of myofibroblasts, including the expression of smooth muscle actin [20]. Activation of stellate cells occurs upon liver damage (Sato et al., 2003). They also become activated in monolayer cultures but remain quiescent when cultured on collagen gel (Sato et al., 2003). The stellate cells of the fetal liver express desmin, *β*3-integrin, nestin, CRBP-1, N-CAM, and reelin. Some researchers consider that these cells are derived from mesenchymal cells of septum transversum, which form the submesothelial layer under the liver capsule, but their epithelial origin cannot be excluded. The number of hepatic stellate cells increases in the course of development. In the fetal period, they are associated with hematopoietic cells and apparently regulate hematopoiesis by secreting chemoattractants (such as stromal cell-derived factor-1) as well as by means of contact interactions mediated by VCAM-1. Hepatic stellate cells are also known to secrete erythropoietin and stem cell factor. Therefore, these cells can be regarded as an important component of the hematopoietic microenvironment (Friedrich et al., 1996).

iv. Fibroblasts and Myofibroblasts

In either adult or fetal liver, fibroblasts (myofibroblasts) are located in the region of portal triads, around central veins, and in the Glisson capsule or, in

the fetal liver, in the submesothelial layer of mesenchymal cells (Ayres-Silva Jde et al., 2011). Portal myofibroblasts express smooth muscle actin and desmin and aremorphologically similar to activated stellate cells. However, they are not related by origin to hepatic stellate cells; unlike the latter, they express CD90, gremlin, fibulin-2, and interleukin-6 but do not express reeli. Perivascular fibroblasts of the fetal liver are cells of mesodermal origin. All stromal cells of portal triads at early developmental stages express smooth muscle actin, but they are subsequently substituted by fibroblasts characteristically expressing vimentin (but not smooth muscle actin). Thus, myofibroblasts disappear during development and are absent in the normal adult liver. Morphological and immunohistochemical analysis of fetal liver reveals myelopoiesis mainly around the blood vessels, that is, in places where the fibroblasts and myofibroblasts are located. These findings may reflect their important role in the regulation of myeloid differentiation. However, the role of myofibroblasts and fibroblasts in the regulation of hematopoiesis has not been studied sufficiently. Some data suggest their involvement in organizing the hematopoietic microenvironment by producing extracellular matrix components, including fibronectin and collagen. Adhesion to fibronectin appears to stimulate proliferation of both hematopoietic stem/progenitor and erythroid cells, which is confirmed by correlation between the content of this protein in the periportal region and the activity of hematopoiesis in human fetal liver. In murine fetal liver, myeloid cells are associated with perivascular and subcapsular collagen, that may suggest a significance of its production by stromal cells for supporting myelopoiesis (Ayres-Silva Jde et al., 2011).

v. Myoid Cells

Differentiated smooth muscle cells in the human fetal liver have been found only in the tunica media of hepatic artery branches. However, the fetal mouse liver has served as the source of numerous stromal cell lines expressing markers of different stages of smooth muscle cell differentiation (Friedrich et al., 1996). Many of these lines, especially those at early or middle differentiation stages, can maintain hematopoiesis in long term culture and probably correspond to pericytes located around venous capillaries. Immature cells of

this lineage are likely to produce hematopoietic cytokines, as it has been shown for myoid cells of bone marrow stroma, whereas more mature (contractile) cells may control migration of hematopoietic cells by modifying the permeability of intercellular spaces between endotheliocytes. Unexpectedly, the fetal liver in different species has proved to contain precursor cells of skeletal muscles showing spontaneous fusion into myotubes in vitro. These cells may enter the liver and other organs of the embryo when they migrate from the dermomyotome to populate areas where skeletal muscles are to be formed. However, in view of the data that skeletal myoblasts secrete a wide range of regulatory molecules, including stromal cell-derived factor-1 and hematopoietic cytokines such as macrophage colony stimulating factor, their specific role in the maintenance of liver hematopoiesis cannot be excluded (Ayres-Silva Jde et al., 2011).

vi. Vascular Endothelium

The endothelium of blood vessels in different parts of fetal liver acini differs in structure: it forms a continuous layer in portal vessels but is fenestrated in central veins (Ayres-Silva Jde et al., 2011). Regarding the hematopoietic function of the liver, of special interest is the endothelium of sinusoids, which mature blood cells must penetrate to enter the circulation. The sinusoids at early stages of development are lined with a continuous endothelium, but its structure subsequently changes so that it becomes highly permeable to blood cells and regulatory molecules. The basal membrane disappears, composition of the extracellular matrix changes, and diaphragmed or open fenestrae, intercellular fissures, and temporary migration pores are formed. The porosity of the sinusoidal endothelium decreases by the end of prenatal ontogeny, when its structure and phenotype approach those in the adult liver. Due to the expression of cell adhesion molecules such as E-selectin and VCAM-1 and chemoattractants such as stromal cell-derived factor-1, the sinusoidal endothelium in the fetal liver can control the homing of hematopoietic cells, their retention in the niche, and release into the circulation. In the fetal liver, hematopoietic stem cells interact with the sinusoidal endothelium via activated protein C. This interaction facilitates self-renewal of the stem cells and prevents

their apoptosis. Moreover, endothelial cell lines or medium conditioned by them maintain in vitro differentiation of erythroid and granulocyte macrophage lineage cells, which is evidence for the ability of endotheliocytes to regulate hematopoiesis via contact interactions with hematopoietic cells and secretion of cytokines. Fetal liver endothelial cells can also promote lymphopoiesis from primitive hematopoietic cells (Ayres-Silva Jde et al., 2011).

vii. Mesenchymal Stromal Cells (MSCs)

Multipotent MSCs are plastic-adhesive cells with a specific antigenic phenotype and potential for osteogenic, adipogenic, and chondrogenic differentiation (Kozhevnikova et al., 2009). To date, MSCs have been revealed in many organs (including the fetal liver), where they apparently reside in vascular walls. MSCs of the fetal liver have certain distinctive features, compared to such cells from other organs. Thus, they show higher proliferative activity than MSCs from the adult bone marrow, but their osteogenic and adipogenic potential is lower (Kozhevnikova et al., 2009). With respect to osteogenic capacity, they are also inferior to MSCs from other fetal organs. In the course of embryonic development, MSC supposedly migrate to the liver from the aortic-gonad-mesonephros region (X. Y. Wang et al., 2008), although their de novo formation from the septum transversum mesenchyme is also possible. The amount of these cells in the liver changes during development in correlation with hematopoietic activity, which is evidence for their important role in organization of the hematopoietic microenvironment. The cessation of hematopoiesis in the liver is accompanied by a decrease in not only the number of MSCs but also in their proliferative activity and differentiation potential (Dennis and Charbord, 2002). In the fetal liver, MSCs are a probable source of stromal cells similar in their characteristics to smooth muscle cells (Dennis and Charbord, 2002); it is also not excluded that they can differentiate into myofibroblasts and endothelial cells (Paniushina et al., 2004). Apparently, the role of these cells is not limited to their differentiation into more specialized components of the hematopoietic stroma. It has been shown for bone marrow MSCs that they can produce stromal cell-derived factor-1, interact with hematopoietic cells via surface molecules (VCAM-1, cadherins, integrins and,

etc.), and regulate their proliferation and differentiation by secreting wide range of cytokines (Paniushina et al., 2004). Such regulatory functions are also likely for MSCs of the fetal liver, although experimental evidence for their ability to maintain hematopoiesis is as yet scarce (Paniushina et al., 2004).

5. ‘‘Stress’’ erythropoiesis

The relative hypoxia of the fetus is critical for erythropoiesis and is coupled with the need to increase red cell mass due to the expanding blood volume from growth (Alter, 1979). It creates signals and responses similar to those found in the adult where acute hypoxia elicits a ‘‘stress’’ response characterized by the rapid synthesis of large erythrocytes expressing increased amounts of fetal hemoglobin (Alter, 1979). The link between stress and fetal erythropoiesis is further supported by the phenotype of Stat5-null and flexed tail mice that each have normal steady-state adult erythropoiesis but display a transient fetal anemia and a blunted response as adults to acute erythroid stress induced by acute anemia (Lenox et al., 2005). Therefore, adult stress erythropoiesis in adults may represent a reactivation of a fetal erythroid program that is distinct from adult steady state erythropoiesis and is first used to rapidly expand the number of definitive erythrocytes during embryogenesis (Lenox et al., 2005).

6. Anemia

Anemia is defined as a decreased quantity of circulating RBCs (erythrocytes). This is a major source of morbidity and mortality worldwide. Recent epidemiological studies suggest that one-third of the world’s population is affected (Kassebaum et al., 2014).

Anemia, which ensues when homeostatic mechanisms go awry, is caused by three basic problems affecting RBCs: reduced production, increased destruction (hemolysis), or loss (hemorrhage). The associated defects can either be intrinsic or extrinsic to RBCs (or their precursors) (W. C. Wang et al., 2005). Much of this burden is due to nutritional, infectious, and systemic etiologies, including iron deficiency, malaria, schistosomiasis, and chronic kidney disease(Kassebaum et al., 2014). Genetic disorders of hemoglobin (Hb), including sickle cell disease (SCD) and thalassemia, are also common

causes of clinically significant anemia, particularly among children (Allen et al., 2010).

7. The genetic control of hematopoiesis

7a. Genes involved in primitive hematopoiesis

Primitive hematopoiesis is largely regulated by two transcription factors, Gata1 and Pu.1 (now known as Sfpi1 in mouse; Spi1b in zebrafish), that exhibit a cross-inhibitory relationship to regulate primitive erythroid and myeloid fates. Gata1 is a master regulator of erythrocyte development (Cantor and Orkin, 2002); *Gata1*−/− mice die during gestation owing to failed differentiation of proerythroblasts into mature erythrocytes. In zebrafish, *gata1*- expressing cells also express erythrocyte-specific hemoglobin, analyzed by benzidine staining, indicating that genes encoding both alpha and beta embryonic globin (*hbbe3*, *hbbe1.1*, *hbae3* and *hbae1*) are expressed in these cells (Detrich et al., 1995). In addition to promoting erythroid-specific gene regulation, Gata1 suppresses myeloid fate; in Gata1 knockdown experiments in zebrafish, blood cells switch to myeloid cells and express myeloid-specific genes, such as *pu.1*, *mpo* (*myeloperoxidase*, now known as *mpx*; a granulocyte-specific gene) and *l-plastin* (*lcp1*). By contrast, Pu.1 is a master regulator of the myeloid cell fate, which includes macrophages and granulocytes (Scott et al., 1994). Similar to the fate switch observed in Gata1 knockdowns, Pu.1 knockdown leads to an increase in *gata1* expression in the anterior lateral mesoderm (ALM) and later these cells express *hbae1*, demonstrating their erythroid switch (Rhodes et al., 2005). As Gata1 and Pu.1 have been shown to interact physically (Cantor and Orkin, 2002), the switch is hypothesized to occur as a result of direct competition between Gata1 and Pu.1 for target genes.

7b. Genes involved in definitive hematopoiesis

Runx1 is a member of the runt family of transcription factors and plays an important role in hematopoiesis (Q. Wang et al., 1996). *Runx1* knockout mice lose definitive erythroid, myeloid and lymphoid cells, indicating the importance of Runx1 in definitive hematopoiesis. In zebrafish, *runx1* expression begins at the five-somite stage in the posterior lateral mesoderm (PLM) and in neural

tissues. At 30 hpf, *runx1* is expressed in the dorsal aorta. Zebrafish *runx1* seems to be dispensable in primitive hematopoiesis, but is required for definitive hematopoiesis, as highlighted by experiments in which Runx1 knockdown results in decreased lymphopoiesis. Runx1 knockdown also leads to a decrease in the expression of *cmyb*, which belongs to the myb family of proto-oncogenes. In zebrafish, cmyb expression begins at around the 10- to 12-somite stage during the primitive wave of hematopoiesis. At around 36 hpf, *cmyb* is expressed in *runx1*-expressing cells in the ventral wall of the dorsal aorta (Gering and Patient, 2005). *cmyb* is also expressed at 2 dpf in the CHT; these cells then migrate to the thymus and the pronephros (early kidney). Importantly, *Myb* knockout mice die owing to failure of fetal liver erythropoiesis, indicating an essential role for cmyb in definitive hematopoiesis (Mucenski et al., 1991).

7c. Genes associated with hemangioblast

During development, an array of transcription factors coordinates the development of the hemangioblast, the precursor to both primitive erythroid progenitors, definitive and endothelial cells. Within the ventral lateral mesoderm of zebrafish embryos, the ALM is a major site of primitive myelopoiesis. By contrast, cells within the PLM contribute predominantly to development of erythrocytes in addition to some myeloid cells. From the two-somite stage in zebrafish, an early stage of development, cells co-expressing *tal1*, *gata2*, *lmo2*, *fli1* and *etsrp* (*etv2* – Zebrafish Information Network), which encode important transcription factors that control the expression of other genes involved in hemangioblast development, appear in both the ALM and the PLM (Paik and Zon, 2010). These cells are postulated to be hemangioblasts based on evidence indicating the requirement of these transcription factors for both endothelial and hematopoietic differentiation. Gata2, for example, is required for maintenance and proliferation of hematopoietic progenitor cells, as *Gata2−/−* mice are embryonically lethal and die from severe anemia. *Tal1*−/− embryos lose the ability to undergo primitive erythropoiesis and myelopoiesis in both the zebrafish and mouse. Endothelial differentiation is affected by Tal1 knockdown, indicating that Tal1 is also required for endothelial differentiation

(Dooley et al., 2005). Lmo2 acts in parallel with Tal1 and Gata2, and *Lmo2*−/− mice die due to loss in yolk sac erythropoiesis. Furthermore, Fli1 has been hypothesized to work upstream of Tal1 and Lmo2. Finally, *etsrp* is required for the vascular endothelial and primitive myeloid cells in zebrafish (Sumanas and Lin, 2006). It has a functional homolog in both mammals and *Xenopus (Salanga et al., 2010)*. In mouse, knockout of *Etsrp* (*Etv2*) results in complete depletion of endothelium and blood cells, indicating that it plays a role in the induction of bipotent progenitors. These cells co-expressing *tal1*, *gata2*, *lmo2*, *fli1* and *etsrp* in the ALM and PLM of zebrafish have the ability to become either angioblasts (endothelial progenitors) or HSCs, adding further evidence to the hypothesis of the hemangioblast.

7d. Factors regulating HSC emergence from hemogenic endothelium and their self-renewal

The process by which HSC are generated from hemogenic endothelium is referred to as the endothelial to hematopoietic transition. Moreover, there are many genes and pathways that are important for HSC renewal, but owing to space restrictions, there are two important signaling pathways. There is some controversy, but there is general consensus that these pathways are important for the self-renewal of HSCs.

Runx1 (AML1) is a sequence-specific DNA binding protein that is part of a family of transcription factors called core binding factors (CBF), and an essential master regulator of EHT during aortic hematopoiesis (M. J. Chen et al., 2009). Consistent with a role in EHT, Runx1 deficiency in embryonic stem cells prevents the formation of blood cells from hemogenic endothelium (Lancrin et al., 2009). It is expressed in all sites of definitive hematopoiesis in the embryo and pre-cedes emergence of HSPC. This patterned transition from endothelial cell phenotype to a hematopoietic phenotype is in part controlled by binding of multiprotein complexes containing GATA, Ets (PU.1) (Huang et al., 2008), and SCL family factors to Runx1 enhancers known to be involved in HSC emergence (Nottingham et al., 2007) and is also marked by loss of expression of genes associated with arterial identity, such as Sox17 and Notch1

(Lizama et al., 2015), further supporting the idea of temporal transcriptional regulation governing cell fate as a central tenet of EHT.

The regulatory regions of hematopoietic genes are known to be bound by Runx1, as well as a transcription factor complex composed of stem cell leukemia protein (SCL)/T cell acute lymphocytic leukemia protein-1 (TAL-1), LIM domain only 2 (LMO2), GATA1, and GATA2 (Ciau-Uitz et al., 2014), all of which have been implicated in EHT. LMO2 is thought to act as a bridge between SCL/TAL-1 and GATA-binding proteins in a transcriptional activating complex that drives vertebrate hematopoietic specification. Studies of Scl/Tal-1, Lmo2, and Gata1/2 mutant mouse embryos demonstrate that deletion of each gene results in midgestation lethality and impaired definitive hematopoiesis (Robb et al., 1995). SCL is a helix-loop-helix transcription factor that functions upstream of RUNX1, and has been shown to be a critical regulator of hematopoiesis via generation of Tie-2hi c-Kit +CD41- hemogenic endothelium. SCL loss-of-function studies show that hematopoiesis is impaired at both the level of stem cell formation and subsequent differentiation (Zhen et al., 2013). Interestingly, multiple isoforms of SCL [SCLA (full length) and SCLB (N-terminal truncated)] have been identified (Zhen et al., 2013), and may play differential roles in definitive hematopoiesis. In vivo time lapse imaging studies demonstrated selective SCLB isoform expression in the dorsal aorta of hemogenic endothelium just prior to EHT, and this isoform may act upstream of Runx1 to mediate EHT. SCLA, on the other hand, is expressed in HSC after the EHT process, and is critical for maintenance of these newly born cells within the AGM (Zhen et al., 2013).

GATA2 is expressed by the para-aortic splanchnopleura and AGM regions of the mouse embryo (Minegishi et al., 1999). It has been shown to have a role in production and expansion of HSC. the AGM during embryogenesis as well as normal expansion of the adult HSC pool within the bone marrow. Gata2 deficient mice die at E10.5 due to defective primitive erythropoiesis and lack of HSPC generation (Gao et al., 2013). Conditional deletion of a Gata2 cis regulatory element in mouse AGM results in reduced expression of hematopoietic transcription factors SCL and RUNX1, and hemogenic endothelial cells of the mutants fail to generate HSPC, leading to embryonic lethality by E13-14 (Gao et al., 2013).

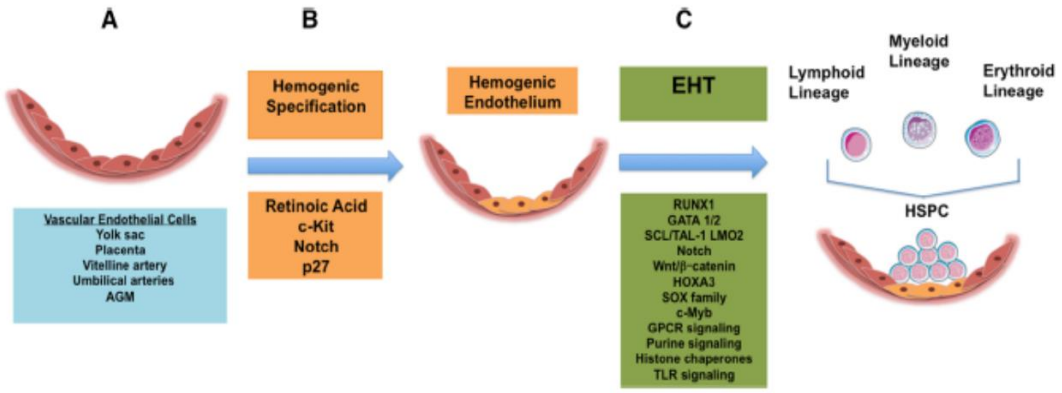

Figure 10. Summary of regulation of hematopoietic specification and generation of hematopoietic stem cells during embryonic development. (A) Schematic representation of endothelial layer of developing vascular wall (pink), listed are intra- and extraembryonic sources of vascular endothelial cells with hemogenic potential (blue box), (B) Schematic representation of progression of events and molecular signals governing hemogenic specification (orange boxes) and (C) endothelial to hematopoietic transition (green boxes), ending with generation of intra-vascular hematopoietic clusters and multilineage hematopoietic stem and progenitor cells (HSPC).

The Wnt family of molecules, which is known to be crucial for embryonic development (Perrimon et al., 2012), is thought to be important for HSC function. However, studies have found contradictory findings with regard to the importance of Wnt signals for normal lymphopoiesis and hematopoiesis, although most studies have found a positive role for Wnt in HSCs during development and regeneration. Recent findings suggest that these opposing conclusions are due to the different levels of Wnt in different experimental conditions, as reviewed by Luis et al (Luis et al., 2011; Luis et al., 2012).

The Notch pathway controls cell fate specification and pattern formation. Activation of Notch signaling has been shown to promote HSC expansion/self-renewal in both mice and humans in adult hematopoiesis (Guruharsha et al., 2012). Loss-of-function mutations, such as inactivation of Notch receptors, ligands or downstream proteins, do not affect HSC function. Populations of human cells expressing CD34 (a cell surface marker for HSCs) can be expanded with exposure to Notch ligands, resulting in >100-fold increase in the

absolute number of cells, which can subsequently enhance the repopulation of immunodeficient mice. Further studies demonstrated that when Notch ligand-expanded cord blood progenitors were used in a clinical setting, there was a rapid recovery of myeloid cells, indicating rapid engraftment of *ex vivo* expanded cells in humans (Delaney et al., 2010). Taken together, these data indicate the importance of Notch-dependent regulation of hematopoietic development and suggest that Notch activation may aid in stimulating the production of hematopoietic cells *in vitro* for use in experimental and clinical applications.

8. MAPK signaling in the regulation of hematopoiesis

The MAPKs are a family of serine/threonine kinases that play an essential role in connecting cell-surface receptors to changes in transcriptional programs (Chang and Karin, 2001). They are expressed ubiquitously and are involved in the regulation of a wide variety of critical cellular functions, including proliferation, differentiation, migration, and apoptosis (C. Dong et al., 2002). There are at least 11 members of the MAPK superfamily, which can be divided into six distinct subgroups based on sequence similarity: (a) ERK1, ERK2; (b) JNK1, JNK2, JNK3; (c)p38MAPKs; (d) ERK5; (e) ERK3; and (f) ERK7 (Schaeffer and Weber, 1999; Davis, 2000) (Figure 11). Each group of MAPKs is activated by a distinct kinase cascade in which a MAP3K or MEKK phosphorylates and activate a downstream dual-specificity MAP2K or MEK, which in turn stimulates MAPK activity through dual phosphorylation on threonine and tyrosine residues within a conserved tripeptide motif (Thr-X-Tyr). Phosphorylation of these threonine and tyrosine residues on MAPKs results in a conformational change that increases substrate accessibility and enhances catalysis. Activation of ERK is through phosphorylation by MEK (MAPK/ERK kinase) 1/2 in response to various cytokines and growth factors and mediates mitogenic and antiapoptotic signals primarily (Chang and Karin, 2001).

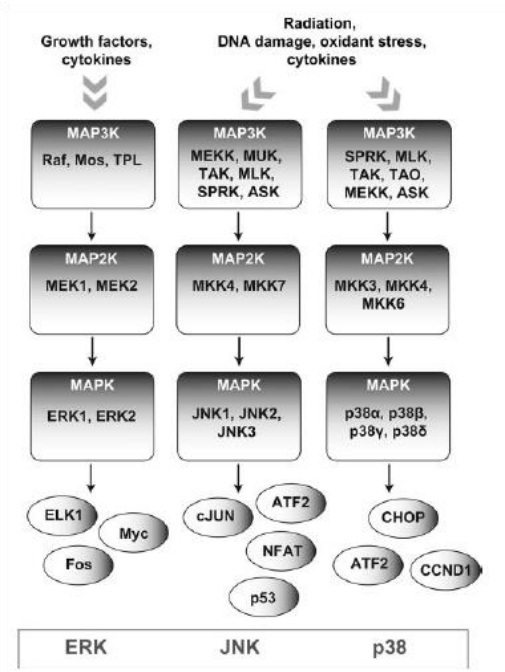

Figure 11. Schematic representation of the three main MAPK signaling cascades: ERK, JNK, p38 family members. MAPKs are part of a three component kinase module consisting of a MAPK, an upstream MEK, and a MEKK that couples the signals from cell-surface cytokine receptors to trigger downstream pathways. Three major groups of MAPKs have been characterized in mammals, including ERKs, JNKs, and p38MAPKs. Each group of MAPK is activated by a distinct kinase cascade in which a MAP3K or MEKK phosphorylates and activates a downstream dual-specificity MAP2K or MEK, which in turn stimulates MAPK activity through dual phosphorylation on threonine and tyrosine residues within a conserved tri-peptide motif (Thr-X-Tyr). Upon activation, MAPK itself can phosphorylate specific target substrates on serine and threonine residues.

8a. The p38 and JNKS MAPKs in hemopoiesis

MAPK signaling is essential in the regulation of multiple processes involved in blood cell production. Extensive work over the last decade has increased our understanding of the mechanisms that are involved in the regulation of normal hematopoiesis. Several studies also support the idea that the ERK MAPK pathway participates in mitogenic responses in various hematological malignancies, whereas the regulatory roles of the JNK and p38MAPK pathways are less well defined and may vary depending on the specific cellular context. The JNK pathway is essential for normal erythropoiesis and lymphopoiesis (C.

Dong et al., 1998; Kim and Ahn, 1998; Sabapathy et al., 2001; Trivedi et al., 2007), whereas p38MAPK pathway is also involved in erythropoiesis, myelopoiesis and the maintenance of HSCs (Nagata et al., 1997; Jacobs-Helber et al., 2000; Jang and Sharkis, 2007). Moreover, p38 and JNK appear to mediate the processes involved in regulating the sensitivity or resistance to various chemotherapeutic agents.

8b. The Erk pathway in hemopoiesis

Erk1 and Erk2, also known as $p44^{MAPK}$ and $p42^{MAPK}$, respectively, were identified as growth factor-stimulated protein kinases phosphorylating MAP-2 and myelin basic protein. They have more than 80% a.a. sequence similarity and can be activated by a wide variety of stimuli, including growth factors, serum, ligands for heterotrimeric G protein-coupled receptors, cytokines, and osmotic and other cell stresses (Lewis et al., 1998). Upon activation, ERK1/2 phosphorylate and regulate the activity of cytoplasmic molecules and nuclear proteins, which in turn can control gene expression (Turjanski et al., 2007). For example, ERK1/2 have been found to phosphorylate p90 RSK, MSK, and MNK, proteins involved in migration, cell attachment, including paxillin and calpain, and transcription factors such as Elk-1, c-Fos, and c-Myc (Raman et al., 2007). Although Erk1 is apparently dispensable during embryonic development, deletion of Erk2 was found to be embryonic-lethal as a result of defects in trophoblast formation, mesoderm differentiation, and placental function, demonstrating distinct biological functions for these related kinases indicating its involvement in these processes (Saba-El-Leil et al., 2003).

In the hematopoietic system, the Erk pathway has been demonstrated to be essential very early in development in vivo and later in vitro. Erk overexpression can inhibit the haemogenic endothelial cell fate in the AGM of zebrafish, maintaining the aortic endothelial identity or enhancing the endothelial cell–cell adhesion (Lan et al., 2014; C. Zhang et al., 2014). An upstream factor of Erk pathway, FGF is required for the induction of mesoderm to hematopoietic tissue in dorsal aorta, while oncogenic H-ras promotes abnormal proliferation early erythroblasts and blocks terminal erythroid differentiation (J. Zhang et al., 2003). Moreover, the PI3K pathway through Raf

/Ras /MAPK affects the differentiation of erythroblasts, but it is not essential for the HSCs (Richmond et al., 2005; Gritsman et al., 2014; Palis, 2014).

Erk also is required for thymocyte differentiation, as mice lacking Erk1 manifest impaired proliferation and maturation of thymocytes, despite expression of Erk2 (Pages et al., 1999). Furthermore, ex vivo studies focusing on ERK1/2 function using differentiation-competent cell lines revealed the importance of the Erk signaling module in regulating myeloid, erythroid, as well as megakaryocyte differentiation (Racke et al., 1997). Experiments using pharmacologic inhibitors have demonstrated that the MEK-ERK pathway is also essential for PMA-induced differentiation of K562 , TF-1, and U937 cells (Herrera et al., 1998; Shelly et al., 1998). Furthermore, ERK1/2-mediated phosphorylation of the C/EBP transcription factor on serine residue 21 was found to regulate negatively the activity of C/EBP and its ability to induce neutrophil differentiation. Similarly, the requirement for MEK-ERK activation has been demonstrated during cytokine-induced differentiation using human hematopoietic progenitors. Modulating the duration and extent of ERK activation was shown to determine the balance between expansion and survival of hematopoietic progenitors during neutrophil differentiation. The underlying molecular mechanism was found to involve regulation of expression of a variety of cell-cycle-modulating proteins, including c-myc, c-fos, p21CIP1, cyclin D1, and cyclin D3. Furthermore, conditional activation of MEK1 also resulted in increased expression of mRNA transcripts, encoding a large number of hematopoietic cytokines that may act as autocrine growth factors to activate signaling pathways implicated in regulating expansion and survival of hematopoietic progenitor cells. Although found to be an essential regulator of expansion and survival of myeloid progenitors, conditional activation of MEK1 did not affect terminal differentiation of neutrophil progenitors. However, a recent study indicates that Erk MAPK signaling may actually be involved in the regulation of early myeloid commitment of HSCs (Hsu et al., 2007). In vitro, GM colony formation of murine HSCs in the presence of MEK-ERK pharmacological inhibitors was inhibited, whereas HSCs ectopically expressing active MEK1 showed increased percentages of macrophage myeloid cells.

In addition, it has been demonstrated recently that ERK1/2- mediated phosphorylation is implicated in the degradation of active GATA-1, a

transcription factor that plays a critical role in regulating erythroid, megakaryocytic, and eosinophil development (Hernandez-Hernandez et al., 2006). Acetylation of GATA-1 was found to stimulate DNA binding and enhance GATA-1-dependent transcription as well as target GATA-1 for degradation by the ubiquitin– proteasome pathway (Hernandez-Hernandez et al., 2006). However, acetylation of GATA-1 alone was not sufficient to cause degradation, but rather, additional phosphorylation on ERK1/2-specific residues was required. Together, this suggests that acetylated, active GATA-1 remains at promoters until its degradation is triggered in response to ERK-mediated phosphorylation. Furthermore, it has been reported that ERK mediates EPO-induced phosphorylation of T cell acute lymphocytic leukemia 1/stem cell leukemia in murine proerythroblasts, a transcription factor belonging to the family of the helix–loop– helix class of transcription factors, which is essential for erythropoiesis (Cheng et al., 1993).

Moreover, murine embryos deficient for MAP3K B-Raf have a quantitative defect in fetal liver hematopoietic progenitor cell development; however, the relative progenitor frequency was not affected in the absence of B-Raf, suggesting that B-Raf plays a critical role in establishing the proper number of myeloid progenitors in the fetal liver (Kamata et al., 2005). Additional data suggest that this phenotype is a result of the loss of associated ERK1/2 activation during hematopoietic progenitor cell formation. In addition to its effect on hematopoietic progenitor development, it has been demonstrated recently that ERK MAPK activity is essential for survival of erythroid CD34 progenitors. Inhibition of ERK1/2 activity completely abolished expansion and subsequent differentiation of CD34 erythrocyte progenitors as a result of induction of apoptosis. Furthermore, recently, it has been reported that UCP2, an inner membrane mitochondrial protein that has been implicated in the regulation of erythropoiesis, modulates expansion of erythrocyte progenitors in a MEK-ERK pathway-dependent manner. Analysis of progenitor cells from bone marrow and fetal liver from UCP2-deficient mice revealed that UCP2 deficiency results in a significant decrease in cell proliferation at the EPO-dependent early phase of erythropoiesis. This was accompanied by reduction in the phosphorylated form of ERK, suggesting that UCP2 is modulating proliferation during erythropoiesis through regulation of Erk activation (Elorza et al., 2008).

All these results suggest that correct activation of the Erk pathway is required for normal hematopoiesis, and modulation of the duration and extent of Erk activation seems to be an important factor in regulating the ultimate balance among expansion, survival, and differentiation of hematopoietic progenitors.

9. Ets genes and hemopoiesis

9a. The Ets family

Ets family proteins can be divided into several subfamilies on the basis of their structural composition and their similarities in the DNA-binding Ets domains. Most of them have the Ets domains in their C-terminal regions. However, several Ets family proteins like the ternary complex factor (TCF) subfamily have the Ets domains in their N-terminal regions. In addition, beside the conserved Ets domain, a subset of Ets family proteins have another evolutionarily-conserved domain called the Pointed (PNT) domain at their N-terminal regions, which forms a helix–loop–helix (HLH) structure for protein-protein interactions (Yordy and Muise-Helmericks, 2000) (Figure 12). NMR-analysis of the structure of the Ets domains revealed that it contains three a-helixes (a1–a3) and four-stranded b-sheets (b1–b4) arranged in the order a1-b1-b2-a2-a3-b3-b4 forming a winged helix–turn–helix (wHTH) topology (Kodandapani et al., 1996). The third a-helix is responsive to contact to the major groove of the DNA. Different members of the Ets family proteins display distinct DNA binding specificities. The Ets domains and the flanking amino acid sequences of the proteins influence the binding affinity, and the alteration of a single amino acid in the Ets domain can change its DNA binding specificities (Mo et al., 2000). Furthermore, DNA sequences flanking the GGAA/T central core also affect the DNA binding affinities of Ets family proteins. For an example, changing sequence of 5’ -GCGGAAGCG-3’ in the MSV enhancer to GCGGATGCG significantly reduces Elf- 1 binding but no effect on Ets-1 binding, while altering this sequence to GCGGAAGAA completely abolishes Ets-1binding but little effect on Elf-1 binding (Thompson et al., 1992). Thus, flanking DNA sequences as well as purine-rich core DNA sequences appear to

be important to determine the preferential binding of individual Ets family proteins.

The function and specificity of ETS proteins is controlled at several levels First, the expression of several ETS genes is either highly tissue-specific or regulated in response to specific extracellular signals. Second, specific intracellular signaling pathways have been shown to directly impinge upon the activity of particular ETS protein by regulating their subcellular compartmentalization (Le Gallic et al., 1999), their DNA binding activity (Rabault and Ghysdael, 1994) or their transactivation (Marais et al., 1993).

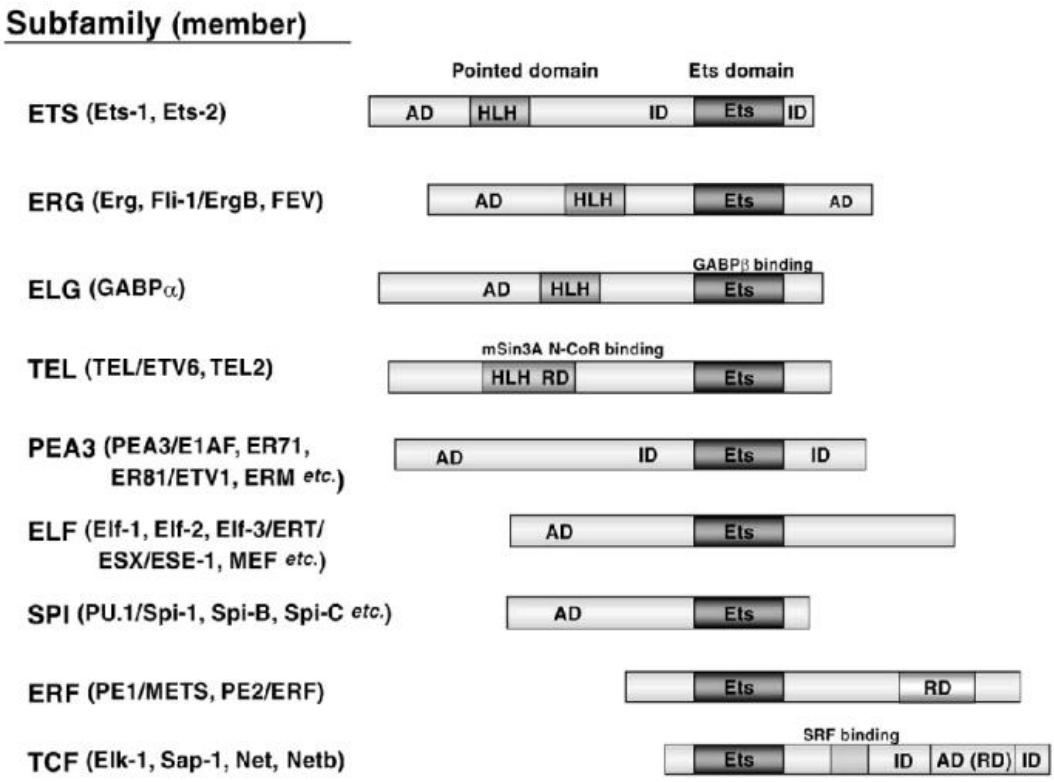

Figure 12. Schematics of the structure of the members of Ets family proteins. Ets, DNA-binding (Ets) domain; HLH, helix–loop–helix domain (Pointed domain); AD, activation domain; ID, auto-inhibitory domain; RD, repression domain.

Finally, regulation of many promoters/enhancers by ETS proteins often critically depend upon their interaction with unrelated transcription factors on composite DNA elements (Goetze et al., 2000). These and other mechanism are presumed to accommodate the multitude of ETS-domain proteins in a cell without apparent conflicts. However, it would be difficult to envision today a

strict gene expression regulation without the presence of transcriptional repressors that ensure transcription blockade of a given gene. To that extent ETS proteins with transcriptional repressor activity may be vital to our understanding of the orchestrated presence and the role of ETS-domain proteins in transcriptional regulation.

A series of signaling pathways, including the MAP kinase (MAPK) pathways ERK1/2, p38 and JNK, as well as the PI3 kinase pathway, among others, are either activated by growth factors or by cellular stress such as UV irradiation (Yordy and Muise-Helmericks, 2000). These signaling pathways transmit external stimuli to the nucleus and activate numerous transcription factors, resulting in both the temporal and spatial changes in gene expression required for cellular growth, differentiation and survival. Cumulative data have revealed that ets family of transcription factors are downstream effectors of this pathways and moreover of the Ras-MAPK signaling cascades (Wasylyk et al., 1998). Phosphorylation of Ets factors by MAPKs controls their subsequent downstream activity, protein partnerships, target specificity and transactivation. Ets family members can also be considered upstream effectors of signal transduction pathways controlling the expression of a number of signaling components including both receptor tyrosine kinases, intermediate signaling molecules (Yordy and Muise-Helmericks, 2000). Moreover, Ets genes are involved in a lot of processes biological processes as vasculogenesis, osteogenesis, neurogenesis and hematopoiesis.

9b. Ets genes involved hemopoiesis

Transcription factors of the ets family have also been shown to regulate hematopoiesis. *Etv2* regulates the emergence of blood and endothelial cells by activating *Flk1* gene that is critical for initiation of hemangioblast formation (D. Lee et al., 2008; F. Liu and Patient, 2008; Sumanas et al., 2008; Kataoka et al., 2011; Okano et al., 2012; Wareing et al., 2012b) and is also required for the formation of hemogenic endothelium at the onset of yolk sac hematopoiesis (Wareing et al., 2012a). *Erg* is a critical regulator for the HSC maintenance during embryonic development (Taoudi et al., 2011). *Fli1* in pluripotent human hematopoietic cells leads to the induction of a megakaryocytic phenotype

(Spyropoulos et al., 2000) and in addition *Fli-1* acts as an inhibitor of erythroid differentiation, by cells having reduced levels of erythroid markers (Athanasiou et al., 2000b). *Fev* regulates the number of *Runx1* expressing cells by transcriptionally activating *Erk2*, to enhance Erk signaling (L. Wang et al., 2013), while PU.1 synergizes with Runx1 and determines its hematopoietic specific expression (Nottingham et al., 2007). PU.1 regulates the HSCs to myeloid committment (Scott et al., 1994; C. Dong et al., 2002).

10. Erf: the transcriptional repressor of the Ets family

Erf (Ets2 repressor factor) is a member of the *ets* family of genes and exhibits strong transcriptional repressor activity in mammals (Sgouras et al., 1995)). Outside the DNA binding domain, it has no significant homology with other ets member, besides PE-1 protein with which they form a new subclass of Ets proteins (Klemsz et al., 1994). Erf was isolated based on its ability to interact in the DNA binding site H1, which is located in the promoter of Ets2 and regulates its transcription (Sgouras et al., 1995). On the contrary, Ets1 and Ets2 have not strong DNA binding affinity for this site. The gene of *Erf* has an homology of 98 % in the coding region and 98 % in the protein level. In addition, the promoters of Erf has an homology 91 % between human and mouse. The gene in both species consists of 4 exons, of which the 2^{nd} and the 3^{rd} translate the DNA binding Ets domain, while the 4^{th} exon translate the suppressor domain (D. Liu et al., 1997). The gene of *Erf* is located on the centromere of chromosome 7 in the mouse and on chromosome 19q13.1 near to centromere. Both chromosomes are connected with translocation that lead to leukemias and cancer of the lung and breast (D. Liu et al., 1997).

Erf protein levels remain constant throughout the cell cycle and embryonic development, in all cell types and tissues tested indicating that has a fundamental cell function. It is a 548 amino acid phosphoprotein, with the DNA binding domain is at the N-terminus and the transcriptional repression domain is at the C-terminus and can antagonize the activity of other ets genes that are known transcriptional activators (Sgouras et al., 1995). However, the phosphorylation level of the protein is altered during cell cycle progression and after mitogenic stimulation (Sgouras et al., 1995). Erf is phosphorylated by Erks

on multiple sites and its phosphorylation determines its subcellular localization. In its non-phosphorylated form is nuclear and active as a repressor, while phosphorylation by Erks in the nucleus, leads to cytoplasmic export and inactivation (Sgouras *et al.,* 1995) (Figure 13). Moreover, Erf has a nuclear localization signal, NLS in the ETS domain, as all the ets proteins. On the contrary, it has not a nuclear export signal. Erf is possibly translocated to the cytoplasm through the mechanism of CRM1 (Le Gallic et al., 2004).

In its active nuclear form, Erf blocks cell proliferation (Le Gallic et al., 1999) and arrests cells at G0/G1 phase (Verykokakis et al., 2007) in a cell type-specific manner. Specifically, nuclear Erf arrests cell cycle progression in G_1 and can suppress *Ras*-dependent tumorigenicity by its ability to repress transcription of c-*Myc*. This is proven by promoter reporter assays that indicate a DNA binding-dependent and repressor domain-dependent *Myc* transcriptional repression. Moreover, chromatin immunoprecipitations in primary cells suggest that ERF specifically binds on the c-*Myc* promoter in an E2F4/5-dependent manner and only under conditions that the physiological c-*Myc* transcription is stopped. Cellular systems overexpressing nuclear ERF exhibit reduced c-*Myc* mRNA and tumorigenic potential. Elimination of *Erf* in animal models results in increased c-*Myc* expression, whereas *Erf*$^{-/-}$ primary fibroblasts fail to down-regulate *Myc* in response to growth factor withdrawal. Finally, elimination of c-*Myc* in primary mouse embryo fibroblasts negates the ability of nuclear ERF to suppress proliferation. Thus, *Erf* provides a direct link between the RAS/ERK signaling and the transcriptional regulation of c-*Myc* and suggests that RAS/ERK attenuation actively regulates cell fate (Verykokakis et al., 2007). Moreover, *Erf* is able to suppress ets- and ras-induced tumorigenicity in fibroblasts (Sgouras et al., 1995) and Ewing's Sarcoma cells (Athanasiou et al., 2000a). In addition, Erk signaling is essential to "transform" the cell cycle inhibitory and proapoptotic action of TGF on epithelial cells, into a growth promoting and migratory response, rendering it as repressor of epithelial mesenchymal transition (Allegra et al., 2012). Specifically, Erf-overexpressing EpRas cells failed to undergo TGF-β-induced EMT, formed three-dimensional tubular structures in collagen gels, and retained expression of epithelial markers.

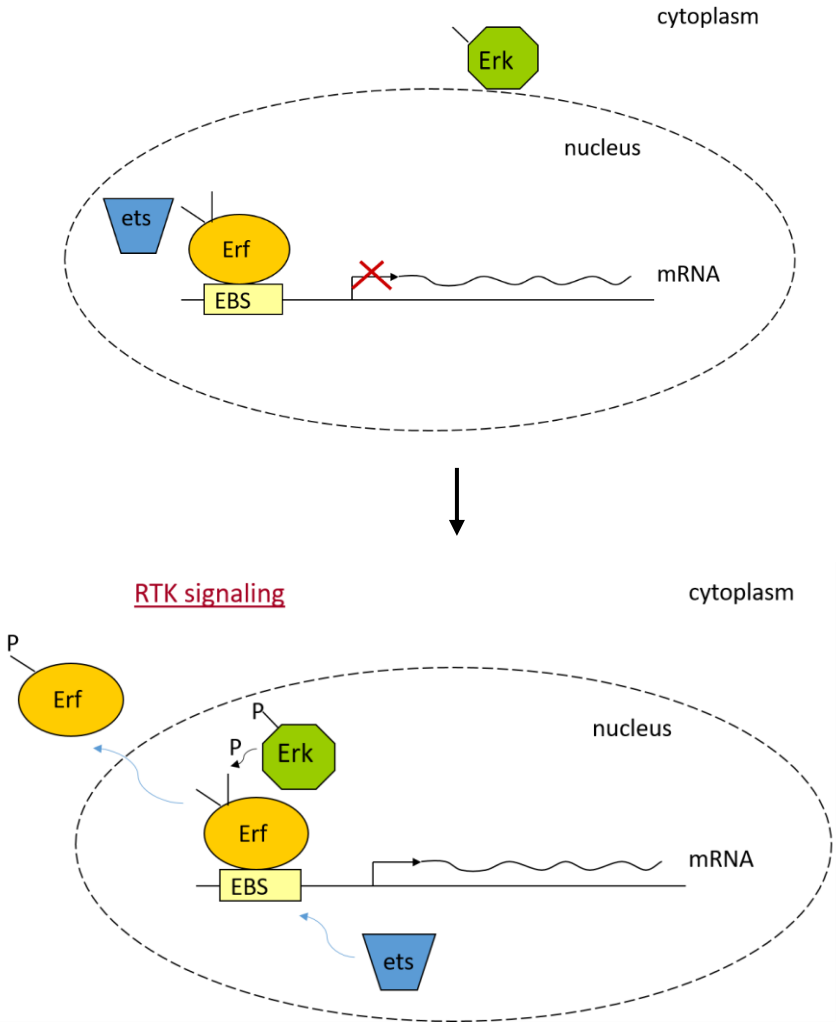

Figure 13. A model for the regulation and function of Erf during Erk-mediated mitogenic stimulation. (Upper) In the absence of Erk activity ERF is nuclear and represses the transcription of genes. (Bottom) Two to 3 min after mitogenic stimulation the activated Erk kinase translocates into the nucleus and phosphorylates Erf. This results in the nuclear export of Erf and another ets gene binds to EBS and leads to transcription of the gene. EB: Ets Binding Domain.

Transcriptome analysis indicated that TGF-β signaling through Smads was mostly unaffected, and Erf suppressed the TGF-β-induced EMT via Semaphorin-7a repression. Forced expression of Semaphorin-7a in ERF-overexpressing EpRas cells reestablished their ability to undergo EMT. In contrast, inhibition of Semaphorin-7a in the parental EpRas cells inhibited their ability to undergo TGF-β-induced EMT. Oncogenic Ras may play an additional

role in EMT via the ERF, regulating Semaphorin-7a and providing a new interconnection between the Ras- and the TGF-β-signaling pathways (Allegra et al., 2012). According to hematopoietic cells, it has been shown that in vitro the MAPK pathway in erythroid differentiation is partially mediated by ERF (Athanasiou et al., 2003). K562 and HEL cells expressing ERF expressed elevated levels of the erythroid-specific markers CD71 and Glycophorin A, as well as hemoglobin and GATA1. Treatment with the Erk kinase inhibitor PD98058 further enhanced the erythroid phenotype in ERF-expressing cells and cells expressing a non-phosphorylatable ERF mutant exhibited an even more enhanced phenotype (Athanasiou et al., 2003).

In its active nuclear form, Erf blocks cell proliferation (Le Gallic et al., 1999) and arrests cells at G0/G1 phase (Verykokakis et al., 2007) in a cell type-specific manner. Specifically, nuclear Erf arrests cell cycle progression in G_1 and can suppress *ras*-dependent tumorigenicity by its ability to repress transcription of c-*Myc*. This is proven by promoter reporter assays that indicate a DNA binding-dependent and repressor domain-dependent *Myc* transcriptional repression. Moreover, chromatin immunoprecipitations in primary cells suggest that ERF specifically binds on the c-*Myc* promoter in an E2F4/5-dependent manner and only under conditions that the physiological c-*Myc* transcription is stopped. Cellular systems overexpressing nuclear ERF exhibit reduced c-*Myc* mRNA and tumorigenic potential. Elimination of *Erf* in animal models results in increased c-*Myc* expression, whereas $Erf^{-/-}$ primary fibroblasts fail to down-regulate *Myc* in response to growth factor withdrawal. Finally, elimination of c-*Myc* in primary mouse embryo fibroblasts negates the ability of nuclear ERF to suppress proliferation. Thus, *Erf* provides a direct link between the RAS/ERK signaling and the transcriptional regulation of c-*Myc* and suggests that RAS/ERK attenuation actively regulates cell fate (Verykokakis et al., 2007). Moreover, *Erf* is able to suppress ets- and ras-induced tumorigenicity in fibroblasts (Sgouras et al., 1995) and Ewing's Sarcoma cells (Athanasiou et al., 2000a). In addition, Erk signaling is essential to "transform" the cell cycle inhibitory and proapoptotic action of TGF on epithelial cells, into a growth promoting and migratory response, rendering it as repressor of epithelial mesenchymal transition (Allegra et al., 2012). Specifically, Erf-overexpressing EpRas cells failed to undergo TGF-β-induced EMT, formed three-dimensional

tubular structures in collagen gels, and retained expression of epithelial markers. Transcriptome analysis indicated that TGF-β signaling through Smads was mostly unaffected, and Erf suppressed the TGF-β-induced EMT via Semaphorin-7a repression. Forced expression of Semaphorin-7a in ERF-overexpressing EpRas cells reestablished their ability to undergo EMT. In contrast, inhibition of Semaphorin-7a in the parental EpRas cells inhibited their ability to undergo TGF-β-induced EMT. Oncogenic Ras may play an additional role in EMT via the ERF, regulating Semaphorin-7a and providing a new interconnection between the Ras- and the TGF-β-signaling pathways (Allegra et al., 2012). According to hematopoietic cells, it has been shown that in vitro the MAPK pathway in erythroid differentiation is partially mediated by ERF (Athanasiou et al., 2003). K562 and HEL cells expressing ERF expressed elevated levels of the erythroid-specific markers CD71 and Glycophorin A, as well as hemoglobin and GATA1. Treatment with the Erk kinase inhibitor PD98058 further enhanced the erythroid phenotype in ERF-expressing cells and cells expressing a non-phosphorylatable ERF mutant exhibited an even more enhanced phenotype (Athanasiou et al., 2003).

However, little is known for the role of *Erf* in development. Total elimination of *Erf* in mice leads to lethality at embryonic day E10.5 due to placental defects (Papadaki et al., 2007). *Erf* knockout embryos fail to undergo chorioallantoic fusion and labyrinth development. *Erf* knockout trophoblast stem cell lines have a delayed differentiation compared to wild-type TSCs and fail to express specific differentiation markers, consistent with the in vivo phenotype. They also fail to close the ectoplacental cone cavity, suggesting that *Erf* may be the first gene identified that regulates this process. Interestingly, the embryo-proper also exhibited some defects that where hard to evaluate however because of the extraembryonic phenotype (Papadaki et al., 2007). In vitro experiments showed that Erf is required for the differentiation of chorionic trophoblasts by suppressing Fgf2 (Vorgia et al., 2017). It is known that lack of Fgf2 promotes TSC differentiation, while Fgf4 or Fgf2 is required for murine TSC maintenance. This expression is repressed via direct interaction of Erf with the Fgf2 transcription unit is increased in the absence of Erf, and is decreased in the presence of an Erf mutant resistant to Erk phosphorylation. Thus, Fgf2 inhibition by Erf appears to be necessary for proper chorionic TSC differentiation, and

may account for the block of chorionic trophoblast differentiation in Erf-knockout animals (Vorgia et al., 2017). Recently, it has also been shown that Erf mutations are involved in prostate cancer (Bose et al., 2017). Erf competes Erg and inactivates its binding which leads to prostate cancer when it is high (Bose et al., 2017).

11. Aim of study

Here, we demonstrate for first time that elimination of *Erf*$^{-}$ in the murine embryo proper at E5 is detrimental to embryonic erythropoiesis and leads to embryonic death around E14.5 due to severe anemia. In order to bypass lethality due to placental defects, we eliminated *Erf* in the epiblast derived cells using the conditional Meox2Cre animals. Employing histological, cellular, molecular and in vivo repopulation assays, we show that *Erf* is required for the timely or quantitative production of both primitive and definitive yolk sac derived hematopoiesis, as well as the production or maintenance of HSCs. In addition, *Erf* is required for the efficient maturation of erythroid precursors into mature erythrocytes. Thus, our data indicate that *Erf* is required throughout hematopoietic development for the homeostasis of this complex system.

Part II. Craniosynostosis

Craniosynostosis is the premature fusion of one or more cranial sutures of the skull, leading to an abnormal head shape (Twigg and Wilkie, 2015). It constitutes a common malformation occurring in 1 of 2,250 live births and usually becomes apparent between the last third of pregnancy and the end of the first year of life. The fusion of a suture abolishes further growth of the abutting bones in a direction perpendicular to the suture. As a consequence, continued enlargement of the brain promotes compensatory overgrowth at other sutures, leading to progressive distortion in the skull shape. Multiple complications can arise because of raised intracranial pressure, facial deformities affecting vision, breathing, and dentition, and other features such as hearing loss or intellectual disability that might be caused by the underlying gene defect or alternatively might occur secondary to craniosynostosis. Surgery to remodel the skull and create extra volume for the brain, with the secondary aim to improve psychosocial adjustment, is currently the mainstay of management (Johnson and Wilkie, 2011; Forrest and Hopper, 2013). No pharmacological interventions are currently validated for prevention of suture fusion.

1. Clinical causes of craniosynostosis

Three interacting factors predispose to the abnormal fusion of a suture (Figure 1A). Least well understood is the effect of mechanical force (strain) transmitted by the growing brain to maintain suture patency. The relationship between brain growth and failure of suture function is complex, because although microcephaly is a recognized risk factor for craniosynostosis, most individuals with microcephaly do not develop this complication. Along similar lines, craniosynostosis has been documented in association with many chromosomal abnormalities, but usually only a minority of those with similar chromosome imbalances actually develop the condition, suggesting non-specific mechanisms through poor brain growth (Wilkie et al., 2010). The second factor, the intrinsic property of the suture itself, is the focus of this review. Finally, extrinsic forces acting on the skull, especially during fetal life,

might frequently precipitate craniosynostosis, especially in the uncomplicated non-syndromic, single-suture-fusion cases. Epidemiological data consistent with a contribution from fetal head constraint include positive associations of craniosynostosis with primiparity, multiple pregnancy, prematurity, and high birth weight (Sanchez-Lara et al., 2010). Compressive strain has been shown experimentally to increase osteogenesis at the suture. In addition, there is some in vivo support for the role of head constraint in craniosynostosis from experimental manipulations performed in mice (Jacob et al., 2007).

2. Classifications of craniosynostosis

As might be anticipated given this plethora of potential causes, craniosynostosis is extremely heterogeneous in its presentation. Three main axes of clinical classification exist (Figure 1B), which enumerate (1) the pattern of suture fusion and consequent skull shape, (2) the occurrence of environmental or genetic predispositions, and (3) the presence of additional clinical features (such as facial dysmorphism, limb anomalies, or learning disability) suggestive of a syndrome (Johnson and Wilkie, 2011; Forrest and Hopper, 2013). Fusion of multiple sutures, positive family history, and additional syndromic features all suggest an underlying genetic predisposition; in some cases, accompanying dysmorphic features are caused by fusion of sutures separating the facial bones. Over the past two decades our understanding of the molecular processes in craniosynostosis, and hence underlying normal suture development, has been transformed by human genetics studies. To date, mutations in 57 genes have been identified as recurrently causing craniosynostosis, and the number of genes is growing rapidly as high-throughput sequencing of exomes (and, increasingly, whole genomes) is applied to the problem. Although further genes, mutations of which are highly penetrant for craniosynostosis, no doubt await discovery, and despite the lag period before animal modeling can be accomplished, distinct modules of pathogenesis are emerging. It is therefore timely to propose a genetic-pathophysiological framework for classifying craniosynostosis, based on integrating knowledge of clinical genetics, suture biology, biochemical studies

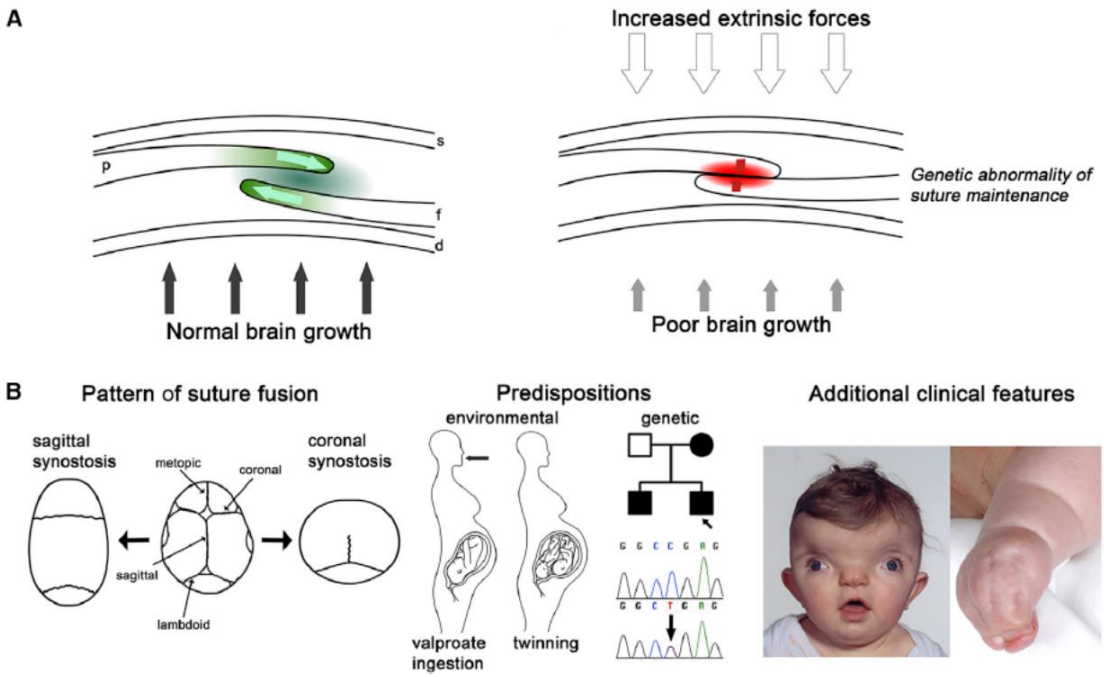

Figure 1. Overview of Clinical Causes and Classification of Craniosynostosis. **(A)** Cross-section of coronal suture showing the developing parietal bone (p) overlying the frontal bone (f). Internally, the dura mater (d) separates the calvaria from the brain; skin (s) is external. Left, normal growth of the skull vault is regulated by a delicate balance of proliferation and differentiation occurring within the suture (green shading) coordinated with enlargement of the underlying brain (black arrows). Right, in craniosynostosis this balance has been disturbed by excessive external force on the skull, usually during pregnancy (unfilled arrows), inefficient transduction of stretch from the growing brain (gray arrows), or intrinsic abnormality of signaling within the suture itself (red shading). **(B)** Approaches to clinical classification. Left: view of skull from above (front at top). Normal skull with major vault sutures central. To either side, the skull shapes resulting from sagittal synostosis (left) and bilateral coronal synostosis (right). The metopic suture closes physiologically at the age of 3–9 months. Center: the clinical history can reveal possible environmental predispositions such as teratogen exposure (most commonly maternal treatment with the anticonvulsant sodium valproate) or twinning (intrauterine constraint); affected relatives with craniosynostosis (filled symbols in pedigree) suggest a likely genetic cause, can be confirmed by diagnostic genetic testing. Right: clinical examination can reveal facial dysmorphic features such as hypertelorism (wide spaced eyes) and grooved nasal tip, suggesting craniofrontonasal syndrome (left), or other physical features such as syndactyly characteristic of Apert syndrome (right) (Twigg and Wilkie, 2015).

of mutant molecules, and cellular and developmental observations of abnormal suture formation in mouse disease models (Twigg and Wilkie, 2015).

To summarize, craniosynostosis can be classified depending on:
- the number of the involved sutures: simple (involving 1 suture) or complex (involving two or more sutures)
- etiology: primary (caused by an intrinsic defect in the suture) or secondary (premature closure of normal sutures because of another medical condition such as deficient brain growth)
- isolated (occurring without other anomalies) or syndromic (accompanied by other dysmorphic features or developmental defects).

All sub-classifications of craniosynostosis can be genetic.
The following are the frequencies of the various sutures involved:

- sagittal: 40% to 58%, etiology unknown;
- coronal: 20% to 29%, estimated one third caused by single-gene mutations
- metopic: 4% to 10%, etiology unknown
- lambdoidal: 2% to 4%, etiology unknown
- multiple: 5% (Ciurea and Toader, 2009)

3. Syndromic Craniosynostosis

The craniosynostosis syndromes are clinically heterogeneous with overlapping features, and, sometimes, an accurate diagnosis is difficult to be made. More than 180 different syndromes involve craniosynostosis (Ciurea and Toader, 2009). The molecular basis of many types of syndromic craniosynostosis is known, and diagnostic testing strategies will often lead to a specific diagnosis. Although the clarification of a genetic lesion does not have a direct impact on the management of the patient in many cases, there is a significant benefit in providing accurate prenatal diagnosis (Chun et al., 2003).

The following clinical descriptions are intended to cover the more common and well-characterized forms of craniosynostosis (Ciurea and Toader, 2009).

- **Appert syndrome**

  coronal craniosynostosis, syndactyly, symphalangism (fusion between the phalanges of the digits), radiohumeral fusion and variable mental retardation
- **Crouzon syndrome**

  variable involvement of other calvarial sutures, brachycephaly, frontal bossing, proptosis, hypertelorism, strabismus, maxillary hypoplasia, mandibular prognathism, atresia of the external auditory canals, premature calcification of stylohyoid ligament,Chiari I malformation, hydrocephalus and mental retardation.
- **Muenke syndrome**

  premature coronal sutural synostosis accompanied by a mild midfacial hypoplasia, hypertelorism, downslanting palpebral fissures, beaking of the nose and brachydactyly
- **Pfeiffer syndrome**

  craniosynostosis, midface deficiency, unusually broad, short, great toes, broad thumbs and variable brachydactyly
- **Saethre–Chotzen syndrome**

  unilateral or bilateral coronal synostosis, facial asymmetry (particularly in individuals with unicoronal synostosis), ptosis, ocular hypertelorism, a low frontal hairline, maxillary hypoplasia, a characteristic appearance of the ear (small pinna with a prominent crus) and short stature.
- **Craniofrontonasal Dysplasia**

  Coronal synostosis with brachycephaly and features of frontonasal dysplasia including hypertelorism, anterior widow’s peak, downslanting palpebral fissures, clefting of the nasal tip, and occasionally cleft lip and palate. Other finger and joint anomalies, abnormal clavicles, and raised scapulae are associated with Sprengel deformity. Longitudinally grooved fingernails are characteristic of this disorder.

4. Genes and processes in suture formation

To formulate the pathophysiological framework, we distinguish five processes in suture formation (Twigg and Wilkie, 2015). These are stem cell specification and migration, lineage commitment, boundary formation and integrity, osteogenic proliferation/differentiation, and resorption/homeostasis. These processes are exquisitely coordinate and overlapping in both time and space, so that the distinctions are to some extent artificial (Figure 3). However, a lot of genes are involved in these processes and a dysfunction of them may lead to craniosynostosis. Specifically, there are presently 57 human genes for which there is reasonable evidence (based on at least two affected individuals with congruent phenotypes) that mutations are causally related to craniosynostosis. Inspection of the complete list suggests that these genes fall into two broad groups.

4a. Stem Cell Specification and Migration

It has long been presumed that sutures contain a population of undifferentiated osteogenic cells with stem cell like properties, cells emanating from the suture populate the periosteum on both surfaces of the growing bones (Zhao et al., 2015). An elegant study pinpoints that the precursors of these cells originate from cephalic paraxial mesoderm, in the region of the rostral mesencephalon/caudal diencephalon and located immediately adjacent to the neural tube, at embryonic day (E)7.5 in response to sonic hedgehog (SHH) accumulation in the adjacent notochord (Figure 2A) (Deckelbaum et al., 2012). Lineage tracing using genetically marked cells shows that this population migrates laterally during E8.5–E9.5 to locate above the developing eye (Deckelbaum et al., 2012).

4b. Lineage Commitment

During a critical period from E9.5 to E11.5, the cells above the developing eye pattern the future coronal suture. It has been proposed the term ‘‘supraorbital regulatory center’’ for this region, in recognition of its role as an organizing center. Put simply, groups of cells with osteogenic potential, originating from neural crest (future frontal bone) and mesoderm (future parietal

bone), are separated by the undifferentiated stem cell population originating from a localized section of paraxial mesoderm (Figure 2B). During E11.5–E13.5, and coordinated with growth of the underlying brain, cells from the supraorbital region extend apically, centered above the diencephalic-telencephalic boundary, to overlay the surface of the rapidly growing brain (Deckelbaum et al., 2012). Descendants of these cells can still be identified in the mid-sutural mesenchyme of the definitive coronal suture at birth (P0), demonstrating that they make a permanent contribution to the population of undifferentiated cells (Deckelbaum et al., 2012). A separate population of descendants becomes integrated into the parietal bone mesenchyme and adopts an osteogenic fate; the future frontal bone originates mostly from cells of neural crest origin (Twigg and Wilkie, 2015).

Key transcription factors involved in orchestrating this early lineage commitment are EN1 (engrailed 1), MSX2, and TWIST1, all of which are present in the supraorbital regulatory center at E11 (Deckelbaum et al., 2012). Recently, individuals with severe bilateral coronal synostosis were described with heterozygous truncations or missense substitution of another transcription factor, ZIC1 (Twigg et al., 2015). A complex and incompletely understood set of positive and negative feedback loops links these transcription factors to the major signaling pathways required to commit cells to an osteogenic fate, including bone morphogenetic proteins (BMPs), wingless-related family members (WNTs), and fibroblast growth factors (FGFs); there is evidence for activity of each of these pathways at this (Mishina and Snider, 2014). However, expression studies do not enable disentanglement of the exact sequence of events or signaling hierarchies involved; neither do classical knockout approaches answer the question, because the multiple roles of these pathways in organogenesis at earlier stages of embryonic development tend to lead to lethality before the cranial sutures are established (Mishina and Snider, 2014). Within the next 24–48 hr of development (E12.0– E13.5), the expression of master regulators of osteogenic differentiation Runx2 and Sp7 is initiated.

4c. Boundary Formation and Integrity

Particular significance for the coronal suture is that it lies at the boundary between tissues with distinct embryological origins: trigeminal neural crest (frontal bone) and cephalic mesoderm (parietal bone) (Morriss-Kay and Wilkie, 2005). Lineage tracing using the Wnt1-Cre/R26R system to label cells of neural crest origin and their progeny shows that the coronal suture itself arises from mesoderm, and this was confirmed using a reciprocal mesodermal driver, Mesp1-Cre (Jiang et al., 2002). The neural crest/mesoderm boundary can be identified from E9.5, and so includes the critical period during which the definitive coronal sutures are forming.

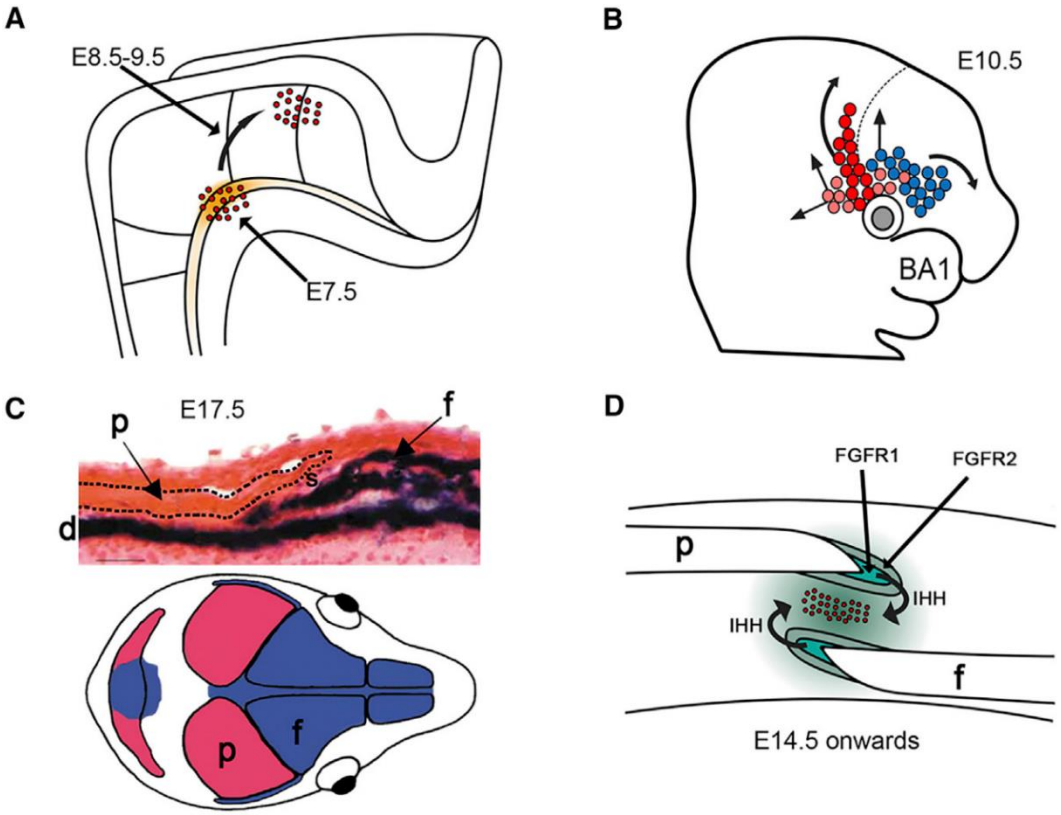

Figure 2. Key Embryological Processes in Coronal Suture Formation. (A) At E7.5, sonic hedgehog secreted by the notochord (orange shading) induces Gli1 expression in adjacent cells of cephalic paraxial mesoderm (red dots). Over the next 48 hr, these cells migrate laterally (curved arrow) to a position above the developing eye, (B) Supraorbital regulatory center at E10.5, showing cells of mesodermal and neural crest origin (pink/red and blue, respectively). Cells migrate to populate the future coronal suture (red), parietal bone (mesodermal cells, pink), and frontal bone (neural crest, with small contribution from mesoderm). Dashed line indicates the diencephalic-

telencephalic boundary. BA1, first branchial arch, (C) Top: cross-section of coronal suture at E17.5, b-galactosidase staining of Wnt1-Cre/R26R mice to demonstrate neuralcrest- derived tissues (dark blue). The frontal bone (f) and underlying dura mater (d) are of neural crest origin, whereas the parietal bone (p; dashed outline) and sutural gap (s) show no blue staining, indicating a mesodermal origin. Bottom: dual origin of the skull bones from neural crest (blue) and cephalic mesoderm (red), (D) View of an established coronal suture (E14 onward). For continued patency, a population of undifferentiated stem cells (red dots) must be maintained in the mid-sutural mesenchyme. The proliferation-differentiation balance between these cells and those in the growing margins of the bones is maintained by a hierarchy of paracrine signaling feedback loops, such as those provided by IHH and FGF receptor signaling (Jiang et al., 2002; Zhao et al., 2015).

The characteristic overlapping of the frontal bone by the parietal bone, forming the oblique cross-section of the coronal suture (Figure 2C), can be understood from the expansion of the underlying cerebral hemispheres toward the hindbrain, taking the neural crest underneath the mesoderm. The dura mater underlying both bones is of neural crest origin (Figure 2C).

Interestingly, the other major sutures have different tissue origins and relationships: the metopic suture uniquely forms within neural crest and the sagittal and lambdoid sutures, like the coronal, have dual neural crest/mesodermal origins, but unlike the coronal, this is not the case along their entire length (Figure 2C). For this reason, in the subset of cases of metopic synostosis that are associated with neurocognitive abnormalities and/or dysmorphic features, a disturbance of neural crest development is the likely mechanism (B. Liu et al., 2014).

Although it was originally thought that the coronal suture boundary did not permit migration of sutural cells either into or from the neural crest, evidence has emerged that the barrier is in fact unidirectional, in that cells of neural crest origin cannot normally cross into the suture, but the reverse does not apply (Deckelbaum et al., 2012). This latter conclusion is consistent with the evidence that the coronal suture contains stem cells; the progeny of these cells can be expected to fuel the growth of both the adjacent bones, parietal and frontal (Figures 2B and 2D). Molecules thought to be important in the maintenance of the suture boundary include the transcription factors EN1, TWIST1, and MSX2

(previous section) and members of the EPHRIN/EPH receptor and JAGGED/NOTCH families; all these molecules have been implicated in tissue boundary formation in multiple other contexts (Ting et al., 2009).

4d. Osteogenic Proliferation and Differentiation

The importance of SHH in the earliest stages of coronal suture development was described above. Gli1, a general marker of HH signaling, is also expressed in the undifferentiated mesenchyme of established postnatal sutures;(Zhao et al., 2015) however, in this context the paralogous molecule Indian hedgehog (IHH) is the instructive ligand. Mice lacking IHH (*Ihh-/-)* have reduced sizes of the developing frontal and parietal bones, reduced Bmp2/Bmp4 expression, and correspondingly widened midline sutures at E15.5; this phenotype is thought to result from a differentiation defect, because proliferation was found to be unaffected (Zhao et al., 2015). Secretion of IHH by differentiating cells is proposed to maintain the recruitment of undifferentiated osteoprogenitors from mid-sutural mesenchyme (Figure 2D) (Zhao et al., 2015).

Notably, the observation that craniosynostosis is frequently associated with defects in certain key cell division genes points to the need for rapid mitotic turnover in the cranial sutures. Twist1, expressed in mid-sutural mesenchyme in the established coronal suture (E16), is directly antagonistic to RUNX2, potentially providing an important mechanism to prevent the midsutural cells from undergoing osteogenesis (Bialek et al., 2004). TWIST1 also has inhibitory activity on levels of bone sialoprotein and osteocalcin, two of the downstream targets of RUNX2: this requires heterodimerization with a type I basic-helix-loop-helix partner (Connerney et al., 2006). In vivo, the strong epistatic genetic interaction between Twist1 and Tcf12 in the murine coronal suture shows that TCF12/HEB is the key partner protein. As is the case for cartilaginous bones, the transcription factor Runx2 represents a well-established positive regulator of commitment to terminal osteogenic differentiation. However, for reasons that remain poorly understood, bones undergoing intramembraneous ossification (such as the skull vault) are dependent on a higher RUNX2 dosage than those undergoing endochondral ossification, so that Runx2/RUNX2 haploinsufficiency is associated with pathologically widened cranial sutures in

both mice and humans (Mundlos et al., 1997). Conversely, craniosynostosis occurs in most individuals with RUNX2 duplication (Mefford et al., 2010).

4e. Resorption/Homeostasis

The steady state in the mature suture represents a balance between osteogenesis and resorption, the latter of which is mediated by osteoclasts of hematopoietic origin (Twigg and Wilkie, 2015). Many of the genes associated with generalized skeletal dysplasias but with only low frequency of craniosynostosis are likely to affect this balance; for example, it is not surprising that osteopetroses, characterized by excessively dense bones and deficient osteoclast function, sometimes feature craniosynostosis in the clinical presentation. A more suture-specific mechanism is likely in the case of interleukin 11 (IL11) signaling, because loss-of-function mutations in the co-receptor IL11RA are predictably associated with craniosynostosis (MIM: 614188) in humans (and fusion of facial sutures in the case of mouse *Il11ra -/-* mutants) (Nieminen et al., 2011).

The role and importance of cartilage intermediates in craniosynostosis is unclear. Although the skull bones are classically described as forming by intramembranous ossification, transient cartilage intermediates are well known to occur (Iseki et al., 1999). The appearance of cartilage is accompanied by downregulation of canonical WNT signaling (revealed, for example, by loss of AXIN2 protein). However, these events were described during postnatal stages, long after the initiating processes leading to craniosynostosis, consistent with the possibility that these represent secondary, downstream consequences of altered signaling arising from earlier events (Twigg and Wilkie, 2015).

5. Erk pathway and Ets genes in osteogenesis

The ERK1/2 isoforms of the MAPK superfamily are known to be involved in the process of osteogenesis. Specifically, ERK1/2 is involved in the process of osteoblasts into mature osteocytes via a Ras-dependent pathway, but it is also essential for the growth and differentiation of osteoblasts and for osteoblast adhesion, spreading, migration, and integrin expression (Lai et al., 2001).

Moreover, ex vivo, ERK controls differentiation of uncommitted hMSC (Wechsler et al., 2015). ERK1/2 target is Runx2/Cbfa1 (Xiao et al., 2000; Xiao et al., 2002), but the role of ERK signaling in the initial activation of the Runx2/Cbfa1 transcription factor and its subsequent contribution to the commitment to osteogenic differentiation in hMSC are entirely unknown.

A key element of cranial vault growth is provided by positive differentiation signals originated from the collagenous non-mineralized matrix produced by osteoblasts along the expanding osteogenic fronts (Morriss-Kay and Wilkie, 2005). Redundant signaling by several fibroblast growth factors (there is evidence to implicate particularly FGF2, FGF9, FGF10, and FGF18) is crucial to orchestrating this process (Iseki et al., 1999). The receptor Fgfr2 is expressed in the rapidly proliferating osteoprogenitor cells, whereas Fgfr1 is associated with a more differentiated state. Increased FGF-signaling flux drives a switch from Fgfr2 to Fgfr1 expression, associated with the onset of osteogenic differentiation (Iseki et al., 1999). The dura mater underlying the sutures also provides a source of growth factors including FGF2 (Levi et al., 2012). However, an increase in the levels of expression of FGF2 by a gain of function mutation leads to overactivation of Erk pathway, resulting to premature mineralization and shortening of the long bones, while a decrease in transcription levels leads to a significant decrease in bone mass and formation (Coffin et al., 1995).

Ets genes are known to be involved in osteogenesis. The erythroblastosis virus E26 oncogene homologue 1 (avian) (Ets1) activates the expression of alkaline phosphatase and osteopontin and it can also up-regulate PthR1 which plays an important role in the control of osteoblast intracellular calcium levels (Qi et al., 2003). Moreover, mice that overexpress transcriptional factor Ets2 have skeletal and cranial defects (Raouf and Seth, 2000). Another Ets family transcriptional activator, PU.1, leads hematopoietic cells to osteoclasts, cells that act like macrophages of osteoblasts in order to exist a balance.

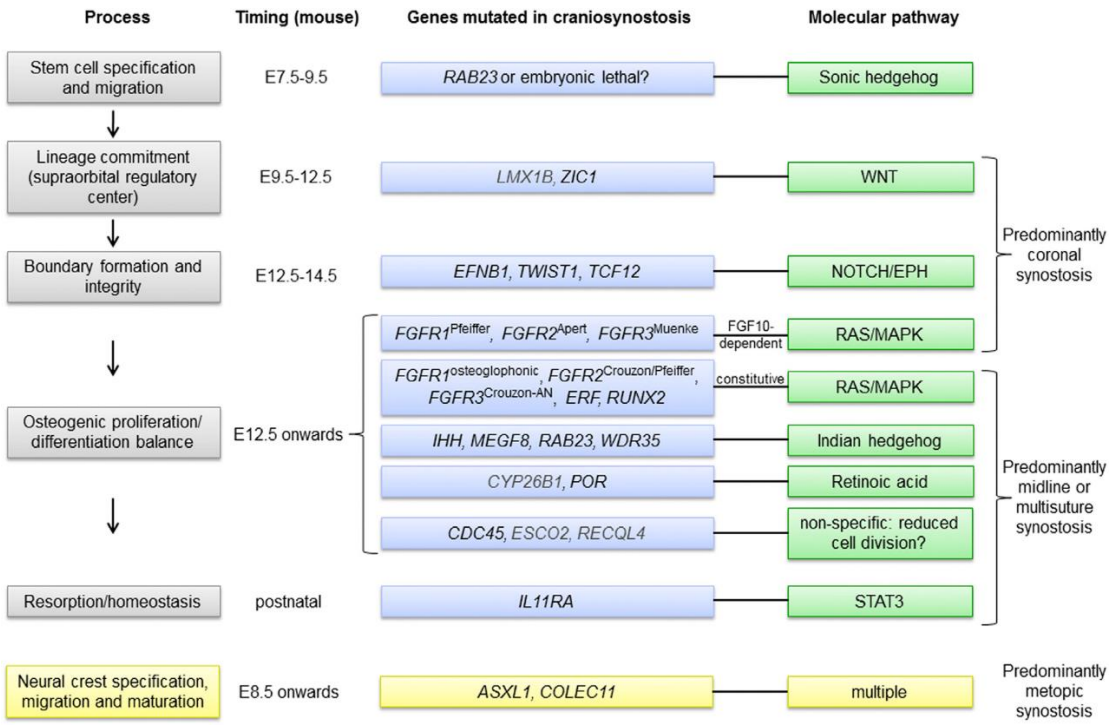

Figure 3. A Genetic-Pathophysiological Framework for Craniosynostosis

Processes in suture formation described in the text are displayed on the left (gray boxes). Other panels show relative timing of events in mouse, genes mutated (blue boxes; black type for core genes and gray type for additional genes), and pathways proposed to be affected (green boxes). Patterning of the supraorbital regulatory center and boundary formation are events particular to coronal suture development; correspondingly, mutations disrupting these processes lead predominantly to coronal craniosynostosis. Later developmental processes (proliferation-differentiation balance, homeostasis) apply to all sutures and correspondingly, pathological suture involvement tends to be more generalized. Mutations involving BMP signaling (MSX2, SKI) are not placed in this framework, pending further information from specific mouse models. Note that the origin of the metopic suture within the neural crest suggests that abnormal maturation of this tissue (through disturbed dynamics of cell identity or migration) might be a common factor predisposing to metopic synostosis, which is not reviewed here (yellow boxes, bottom) (Twigg and Wilkie, 2015).

6. Aim of study

Here we demonstrate for first time that reduced dosage of Erf, which encodes an inhibitory ETS transcription factor directly bound by ERK1/2 (refs. 2–7), causes complex craniosynostosis (premature fusion of the cranial sutures) in mice. Transgenic *Erf* conditional knockout mice created by crosses with *Meox2Cre* mice in order to delete *Erf* in the epiplast stage at embryonic day E5. In this way, mice died at E14.5 because of anemia but what's more is that the $Erf^{loxP/-}$ mice had reduced protein levels of Erf ~ 30% of normal exhibit postnatal multiple-suture synostosis. By contrast, embryonic calvarial development appears mildly delayed. Using chromatin immunoprecipitation in mouse embryonic fibroblasts and high-throughput sequencing, we find that ERF binds preferentially to elements away from promoters that contain RUNX or AP-1 motifs. This work identifies ERF as a novel regulator of osteogenic stimulation by RAS-ERK signaling, potentially by competing with activating ETS factors in multifactor transcriptional complexes.

2. Materials & Methods

Part I. Hematopoiesis

1. Generation of conditional *Erf*$^{-/-}$ mice

To study the role of Erf in different tissues, we crossed strains of mice that express Cre recombinase with *Erf*$^{floxP/loxP}$ mice to eliminate *Erf* in specific tissues as follows:

a. *Meox2*$^{tm1(cre)Sor/J}$ (Jackson Laboratory, stock no 003755) Cre mice were crossed with the *Erf*$^{floxP/loxP}$ mice (32) to generate *Meox2*$^{tm1(cre)Sor/J}$;*Erf*$^{+/-}$ and cross those with *Erf*$^{floxP/loxP}$. Meox2Cre is expressed in the epiblast derived tissues at E5, and as a result we totally eliminate *Erf* in the embryo proper, the allantois of placenta and the mesoderm derived cells of the yolk sac (Tallquist and Soriano, 2000).

b. *Lyve1*$^{tm1.1(EGFP/cre)Cys/J}$ mice (Jackson Laboratory, stock no 012601) were crossed with the *Erf*$^{floxP/loxP}$ to eliminate *Erf* in the hemogenic endothelium (33) and finally in the definitive yolk sac derived wave (34). Its expression starts at E8.5.

c. The liver specific *Alfp-Cre*;*Erf*$^{floxP/loxP}$ mice were used to eliminate *Erf* in hepatic cells (35). Its expression starts at E8.5.

d. ROSA26$^{fl\text{-}STOP\text{-}fl\text{-}YFP}$ mice were employed to detect the tissues that *Erf* is deleted via the Cre recombinase, via fluorescence of yellow fluorescence protein (Srinivas et al., 2001).

2. Blood and tissue collection

To obtain embryonic tissues, timed-pregnant female mice are sacrificed at specified days of gestation by cervical dislocation according to institutional guidelines and the process is performed as follows:

a. Mice are mated with two females in the late afternoon. Females are checked for the presence of a vaginal plug the following morning. If a plug is found, this is considered embryonic d 0 (E0).

b. Pregnant females at the chosen day of gestation are sacrificed, and uteri are isolated from the peritoneum and put into a petri dish containing PBS, penicillin 100 U/mL and streptomycin 100 µg/ml (if tissues are for culture).

c. Employing fine forceps, scissors and stereoscope, remove the muscular wall of uterus out of the individual decidua. Later, with small grasps of the forceps, remove Reichert's membrane, which is the thin tissue layer surrounding the yolk sac. During these manipulations, transfer the embryos to other petri dishes containing PBS to wash maternal blood.
d. Isolate the whole embryo from the placenta by grasping with the fine-tipped forceps the point between the placenta and the whole embryo (see picture below). Keep the forcep very tight and with the other forcep remove the placenta. Keeping tightly in order not to leave the blood and make a wash in PBS. Then, put it in a 12-well plate containing IMDM in 2% FBS (1 ml for E10.5 -E12.5).

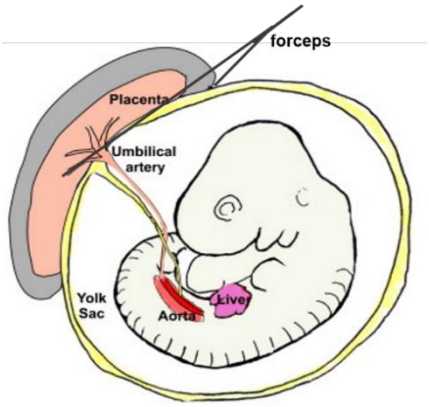

e. Isolate the yolk sac and then the blood vessels (vitelline and umbilical vessels) which connect to the embryo proper will release blood in the well. For bigger quantity of blood, cut the head of the embryo and let it bleed.
f. Count the number of cells in a hematocytometer.
g. For the dissection of fetal liver, under a stereoscope, cut the legs of embryo very carefully (it is easier in that way to isolate the liver).
h. With one forceps touch the embryo in the region near the head, so that being stable and with the other one, try to isolate the very thin membrane (peritoneum) above the liver.
i. Put the fine-tipped forceps as they are open under the liver and grasp the liver very carefully. Be careful so that not isolating the heart.
j. Put the liver in 500 μl IMDM with 2% FBS and dissociate it in single cells by gentle pipetting.
k. Count the number of cells in a hematocytometer.

3. Genotyping

A. DNA extraction

a. Incubate tails, yolk sacs or embryos legs in 300 μl buffer containing 25 mM NaOH and 0.2 mM EDTA, pH 12 for 15 min at 95^{o}C.
b. Add equal volume of a buffer containing 40 mM Tris-HCl, pH 3.5.
c. Spin at 13000 rpm for 2 min.
d. Count DNA in nanodrop.
e. Use 20 – 60 ng in PCRs.

B. PCR for *Erf*, deletion, *Cre* and *Yfp* detection

Detection of each the gene occurs in conditions shown in Table 1.

The exact process is:

a. Make a mix with the corresponding components of the gene, excluding DNA and add Taq polymerase last in the mix.
b. Share the mix (24 μl) in PCR tubes.
c. Perform PCR in the corresponding conditions of gene as shown in Table 2.
d. Load samples with 1 x Orange G buffer (0.1 M EDTA, 80% glycerol, 0.1% OrangeG) in 1.5 – 2.5 % agarose gel.

For the detection of loxP and/or the wt band of Erf, we employed the PCR A, but in transplantation experiments and afterwards we employed a more efficient PCR referred as PCR B.

In addition, for detection of cre recombinasewe can use a PCR for all cre mice except Lyve1cre which is referred as general cre PCR.

Table 1. PCR conditions for Erf, deletion of Erf, Meox2Cre, Lyve1Cre, general cre and Yfp-Rosa.

PCR for Erf A
30 – 60 ng DNA
2.5 µl 10 x buffer E Invitrogen
0.5 µl dNTPs (C_{stock}:10 mM each)
0.5 µl StopF2 primer (C_{stock}: 25 µM)
0.5 µl 5578R (C_{stock}: 25 µM)
0.5 µl DMSO
0.5 µl Taq (C_{stock}: 5u/µl)

PCR for Erf B
30 – 60 ng DNA
2.5 µl 10 x buffer E Invitrogen
0.5 µl dNTPs (C_{stock}:10 mM each)
0.5 µl m11671F (C_{stock}: 25 µM)
0.5 µl 11771R (C_{stock}:25 µM)
0.5 µl DMSO
0.5 µl Taq (C_{stock}: 5u/µl)

PCR for Erf deletion
DNA 20-60 ng
2.5 µl 10 x buffer F Invitrogen
0.5 µl dNTPs (C_{stock}: 10 mM each)
0.5 µl 4021 F (C_{stock}:25 µM)
0.5 µl 11771R (C_{stock}:25 µM)
0.5 µl Taq (C_{stock}: 5u/µl)
dH_2O up to 25 µl

PCR for Meox2Cre
DNA 20-60 ng
2.5 µl 10 x buffer Minotech
0.5 µl dNTPs (C_{stock}: 10 mM each)
0.5 µl oIMR1542 (C_{stock}: 25µM)
0.5 µl oIMR1871 (C_{stock}: 25 µM)
0.5 µl oIMR3671 (C_{stock}: 25 µM)

PCR for General Cre

DNA 20-60 ng

2.5 µl 10 x buffer Minotech

0.5 µl dNTPs (C_{stock}: 10 mM each)

0.5 µl gencre F2 (C_{stock}: 25 µM)

0.5 µl gencre R2 (C_{stock}: 25 µM)

0.5 µl mmtv pos.c R (GRC ctrl)

(C_{stock}: 25 µM)

0.5 µl mmtv pos.c F (GRC ctrl)

PCR for Lyve1Cre

DNA 20-60 ng

2.5 µl 10 x buffer Minotech (-$MgCl_2$)

2 µl $MgCl_2$ Minotech (C_{stock}: 25 mM)

0.5 µl dNTPs (C_{stock}: 10 mM each)

0.5 µl Lyve1Cre 1 (wt) (C_{stock}: 25µM)

0.5 µl Lyve1Cre 2(Lyve) (C_{stock}:25µM)

0.5 µl Lyve1Cre 3 (cre) (C_{stock}:25µM)

0.5 µl Taq (C_{stock}: 5u/ µl)

PCR for YFP-Rosa

DNA 20-60 ng

2.5 λ 10 x buffer Minotech (with $MgCl_2$)

0.5 λ dNTPs (C_{stock}: 10 mM each)

1 λ YFP-LC (C_{stock}: 25 ng/µl)

0.5 λ YFP-R2 (C_{stock}: 25 ng/µl)

2 λ YFP-R3 (C_{stock}: 25 ng/µl)

0.5 µl Taq (C_{stock}: 5u/ µl)

All 10 x buffers of Invitrogen contain 600 mM Tris-HCl and 150 mM Ammonium sulfate, in addition to $MgCl_2$ at the concentrations listed below:

- 10 x Buffer E: 15 mM $MgCl_2$, pH 9
- 10 x Buffer F: 20 mM $MgCl_2$, pH 9

All 10 x buffers from Minotech contain 500 mM KCl, 100 mM Tris-HCl, pH 8.5, 1% Triton X-100,15 mM $MgCl_2$ or w/o.

The programme for PCRs (left), except Lyve1Cre (Rrght), is the following and only the annealing temperature and time change.

PCR programme

1. 93 ºC, 2 min
2. 93 ºC, 30 sec
3. - ºC - sec (Table 2)
4. 72 ºC, 30 sec
5. GoTo 2, 34 cycles
6. 72 ºC, 3 min
7. 4 ºC, for ever

PCR programme for Lyve1Cre

1. 93 ºC, 2 min
2. 93 ºC, 15 sec
3. 65ºC, 15sec, - 0.5 ºC per cycle
4. 68 ºC, 20 sec
5. GoTo 2, 10 cycles
6. 93 ºC, 15 sec
7. 60ºC, 15 sec
8. 72 ºC, 35 sec
9. GoTo 6, 28 cycles
10. 72 ºC, 3 min
11. 4 ºC, for ever

Table 2. Primers, annealing conditions and product size for each PCR.

	Primers for PCR	Annealing	Product
Erf 1st	**StopF2:** 5' - ACC GAG ATT CCT GAG AGC TAT- 3' **5578R:** 5' -AGA GAC TAA AGA GAG CTG TCC- 3'	56°C, 20 sec	loxP ~ 200 bp wt ~ 160 bp
Erf 2nd	**m11671F:** 5'-ACG CCA CAG CCC AAC TCT CC - 3' **11771R primer :** 5'-CAG CAA AAG CTC AGG GAG TG- 3'	56°C, 20 sec	loxP ~ 170 bp wt ~ 101 bp
Erf deletion	**4021F primer :** 5' –GCA CTG CTA GCT CTG AAT GG- 3' **11771R primer :** 5'-CAG CAA AAG CTC AGG GAG TG- 3'	58°C, 10 sec	Deletion 178 bp
Meox2Cre	**oIMR1542 (common):** 5' -GGG ACC ACC TTC TTT TGG CTT C-3' **oIMR1871 (wt):** 5'-AAG ATG TGG AGA GTT CGG GGT AG - 3' **oIMR3671 (mut):** 5'-CCA GAT CCT CCT CAG AAA TCA GC- 3'	64°C, 20 sec	no Cre ~ 410 bp Cre ~ 300 bp
Lyve1Cre	**Lyve1 (wt):** 5' -TGC CAC CTG AAG TCT CTC CT-3' **Lyve2 (Lyve):** 5' -TGA GCC ACA GAA GGG TTA GG-3' **Lyve3 (cre):** 5' -GAG GAT GGG GAC TGA AAC TG-3'	Gradient Tm	no Cre ~ 425 bp Cre ~ 210 bp
General Cre **GRC**	**GenCre F2:** 5' -AAA ATT GCC CTG CAT TAC CG-3' **GenCre R2:** 5' -AT GTT TAG CTG GCC CAA ATG-3' **mmtv pos.c F (GRC):** 5' -CAA ATG TTG CTT GTC TGG TG-3' **mmtv pos.c R (GRC):** 5' -GT CAG TCG AGT GCA CAG TTT-3'	60°C, 20 sec	Cre ~ 250 bp no Cre ~ 210 bp
YFP-ROSA	**YFP LC**: 5'-GCT CTG AGT TGT TAT CAG TAA GG-3' **YFPR2:** 5'-GCG AAG AGT TTG TCC TCA ACC-3' **YFPR3:** 5'-GGA GCG GGA GAA ATG GAT ATG- 3'	, 55°C, 30 sec 72°C, 45 sec	no YFP ~ 500 bp YFP ~ 250 bp

4. Cryosections of placentas and embryos

a. Fix tissues in 4% PFA in 1 x PBS, overnight, at 4^{o}C.
b. Wash with 1x PBS three times.
c. Cryoprotect tissues in 30% w/v sucrose, 0.1% NaN_3 in 1x PBS until it sinks (~24 hrs) at 4^{o}C, on purpose to avoid water crystals and tissue damage.
d. Cover embryos in 7.5% w/v gelatine, 1.5% w/v sucrose in 1x PBS and avoid bubbles (have added gelatine on plates, let it freeze at 4^{o}C, add embryos with the right orientation and add again gelatin to cover them and cool) (you can keep them at 4^{o}C for some days).
e. Cut tissues from gelatin in a shape trapeze as shown below in order to remember how to employ sagittal sections. The wider area of the trapeze will be stuck on the cryostat.
f. Put them on a surface with a drop of OCT and sink it in 2-methylbutane at - 30°C. adjusting it by dry ice. Keep it until bubbles stop.
g. Cut 7 μM sections at -25^{o}C in cryostat.
h. Collect sections on poly-L-lysine-coated superfrost slides.
i. Keep tissues/sections at -80^{o}C.

Note: Prepare 7.5% w/v gelatine, 1.5% w/v sucrose in 1x PBS, gelatin solution must be heated at 50^{o}C to be diluted and after sucrose is added.

Note: Do not heat gelatin more than 50^{o}C.

Note: Gelatine solution is stored at -20^{o}C and it can used 3 times

Note: To de-freeze gelatine incubate some hrs at 37^{o}C.

<u>4% Paraformaldehyde (PFA) Fixative</u>

a. Place 450 ml of dH_2O in a glass beaker
b. Heat to 56°C using a hot plate with stirring.

While stirring, add 20 g of paraformaldehyde powder (Sigma, cat. no. P6148) to the heated water. Cover and maintain at 56°C.

c. Add 5 drops of 2N NaOH (1 drop per 100 ml).
d. The solution should clear within a couple of minutes (There will be some fine particles that will not go away).

Do not heat solution above 60°C. PFA will breakdown at temperatures above 60°C.

e. Remove from heat and add 50 ml of 10 x PBS. Final volume will be 500 ml.
f. Use immediately, or aliquots may be frozen at -20°C and thawed as needed.
g. You can keep PFA at 4ºC for 1 month.
h. Do not male freeze-thaw.

5. Paraffin embedding of yolk sacs

A. Dehydration & Embedding

a. Fix in 4% PFA in 1x PBS, pH 7.4 for 30 min RT (not more than 30 min to avoid blocking Ag activity).
b. Rinse in PBS and store in the same buffer at 4 ºC until embedding.
c. Dehydrate with gradual steps of ethanol:
    - 70 % 1x 15 min (RT, stirring)
    - 90 % 2x 15 min (RT, stirring)
    - 100 % 2x 15 min (RT, stirring)
d. Clear specimens in xylol, 1x 30 min.
e. Impregnate with paraffin at 58º C 2x 30 min each (do not exceed temperature - proteins may denaturate).
f. Orientate samples in embedding moulds (not higher than 65 ºC).
g. Leave O/N for paraffin moulds to become hard.

B. Sectioning

h. Cut 5 µm sections with normal sliding or rotary microtome
i. Place sections in warm water tank (42 ºC) in order to un-fold.
j. “Fish” sections with a glass slide and dry the glass O/N at 40 ºC.

C. Deparaffinize and re-hydrate

k. Deparaffinize sections: 2x 10 min in xylol.
l. Rehydrate sections:

- Ethanol 100%: 2x 5min
- Ethanol 90%: 2x 5min
- Ethanol 70%: 2x 5min
- ddH2O: 1x 5min

6. Smear of Embryonic Blood

a. Collect blood in IMDM containing 2% FBS.
b. Quantitate 2 x 10^5 cells.
c. Centrifuge at 200 g for 5 min.
d. Resuspend in 10 µl IMDM with 2% FBS.
e. Smear a 10 microliter drop on one edge of plain glass slides (no 1 below).
f. Immediately push the drop with another slide forward to the middle of the slide as shown below. Use gentle pressure and a quick push (no 2. 3 below).

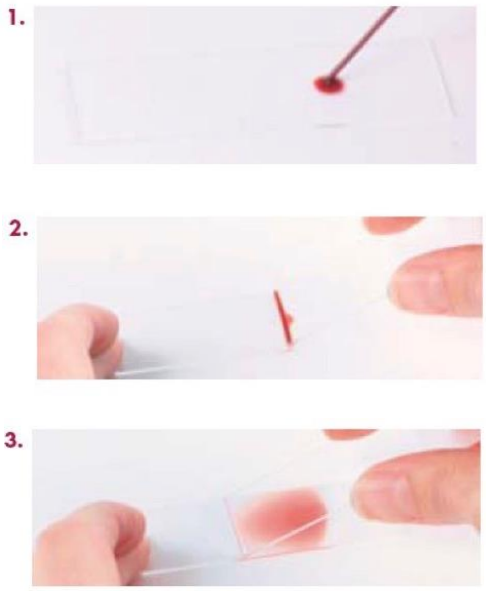

g. Air dry about 10 minutes.
h. Store at -80^{o}C without fixation for morphology staining

7. Giemsa staining

a. Let blood, collected on slides, to dry.
b. Fix with methanol for 10 min.

c. Air-dry.
d. Dilute Giemsa (Merck, cat. No. 9204) 1:20 (always fresh)**.**
e. Place slides in Giemsa solution for 20 minutes.
f. Rinse in deionized water**.**
g. Air dry and evaluate.

8. Benzidine staining

Benzidine staining is a highly selective and efficient method to

demonstrate the presence of hemoglobin deposits in histologic sections.

a. Make blood smears.
b. Incubate ad follows:

- methanol 4'
- 9 v benzidin solution: 1 v 37 % H_2O_2, 5' or until it stains

Make mix always fresh!! Use immidiately.

- Water rinse until shear lines disappear
- Difco red 4' (gift from Dr. Marieke Von Lindern)
- Difco blue 40" (it stains with Difco red as Giemsa)
- H2O rinse about 20" under flowing water;

Not too long → destaining

c. Dry
d. Mount slides with coverslips with entellan mounting medium.

<u>Benzidine solution</u>

0.2% w/v O-Dianisidine in 1.6 % v/v acetic acid

Store at -20^{o}C or -4^{o}C for short term

Protect from light!

Warm before redissolving after 'freezing'

9. Hematoxylin & Eosin Staining

a. Place slides in Hematoxylin - Harris (Sigma, cat. no. HHS128) for 2 min.
b. Wash gently in distilled water until excess stain stops leaching from tissue (approximately 3 changes).
c. Differentiate in 0.38% HCl in 70% Ethanol for 3 sec.
d. Rinse gently in distilled water with 3 changes.
e. Place in 1% w/v Eosin Y in 80% ethanol for 1 min.
f. Rinse in 95% ethanol.
g. Rinse in 100% ethanol for 3 min twice.
h. Clear with 2 changes in xylene.
i. Mount in Entellan and evaluate.

10. Fluorescence staining and confocal microscopy

A. Immunostaining for erythroblasts, hepatocytes, macrophages, yfp and proliferating cells

a. Air dry cryosections.
b. Incubate with a blocking solution containing 5 % fetal bovine serum, 2% BSA, 0.5 % Triton in PBS for 1 hr, RT.
c. Rinse in 1x PBS.
d. Make dilutions of the following antibodies in 1 % fetal bovine serum, 0.4 % BSA in PBS :
    - rat anti-Ter119 (Biolegend, cat. no.116203) for detection of all maturing to enucleated erythroblasts (R3-R5). Dilution 1:200.
    - rat anti-CD71-FITC (Biolegend, cat. no.113805) for detection of all proerythroblasts to maturing enucleated erythroblasts. Dilution 1:200.
    - rabbit anti-HNF4a (Prof. Talianids' gift) for hepatocytes. Dilution 1:500.
    - rabbit anti - pH3 (Merck Millipore, cat. no, 07-424) for proliferating cells. Dilution 1:200.

- rat anti - F4/80 (Biolegend, cat. no,123109) for the macrophages. Dilution 1:200.
- rabbit anti-GFP (Minotech) for yfp cells. Dilution 1:500.

e. Incubate O/N, at 4ºC.
f. Washed 3 times in PBS.
g. Incubate with anti-rat CF555 (Sigma, cat. no. SAB4600060), anti-rabbit FITC (Sigma, cat. no. F0382) and anti-rabbit CF555 (Sigma, cat. no. SAB4600068), in 1:1000, 1:50 and 1:1000 dilution, respectively for 1 hr, RT.
h. Stain nuclei with TO-PRO-3 iodide (Invitrogen cat. no. T3605) for 5 min at RT.
i. Mount slides with mowiol solution (Sigma, cat. no. 81381).
j. Analyze samples by confocal microscope and process them with Leica 2.6.0 confocal imaging software.

B. BrdU immunostaining for proliferating erythroblasts

a. Inject pregnant mice with 50 μg Brdu (Sigma, cat. no. B5002) per gr animal, 2 hrs before sacrificing.
b. Isolate embryos, fix in 4% PFA O/N and make cryosections.
c. Before you start to stain, air dry cryosections.
d. Incubate with a blocking solution containing 5 % fetal bovine serum, 2% BSA, 0.5 % Triton in PBS for 1 hr, RT.
e. Incubate with rat anti-CD71-FITC (Biolegend, cat. no.113805) for detection of all proerythroblasts to maturing enucleated erythroblasts, in dilution 1:200 in 1 % fetal bovine serum, 0.4 % BSA in PBS, O/N, at 4ºC.
f. Wash three times in 1x PBS for 5 min.
g. Then, fix in 4% PFA for 10 min, RT.
h. Wash two times in 1x PBS for 5 min.
i. Incubated slides in a solution containing HCl 2N and Triton 0.5% in 1xPBS for 30 min, at 37ºC in glass bottle.
j. Wash with a neutralization buffer containing sodium tetraborate 0.1M, pH 8.5, three times for 5 min.

k. Incubated with rat anti-Brdu (Bio-rad, cat. no. OBT0030G) in dilution 1:800, 2 hrs, RT.
l. Wash three times for 5 min.
m. Incubated with anti-rat CF555 (Sigma, cat. no. SAB4600060) for 1 hr, RT.
n. Wash three times for 5 min.
o. Stain nuclei with TO-PRO-3 iodide (Invitrogen cat. no. T3605) for 5 min at RT.
p. Mount slides with mowiol (Sigma, cat. no. 81381).
q. Analyze samples by confocal microscope and process them with Leica 2.6.0 confocal imaging software.

C. Tunel staining for apoptotic cells

a. Air dry slides.
b. Fix in 4% PFA for 10 min, RT.
c. Wash in 1 x PBS twice for 5 min.
d. Incubate with 0.1% sodium citrate and 0.5 Triton for 2 min, on ice.
e. Then incubate with the In Situ cell dead kit TMR Red (Roche, cat. no. 12156792910). According to manual instructions, mix 5 µl buffer 1 (enzyme) with 45 µl buffer2 per slide.
f. Incubate 1 hr at dark, 37^{o}C.
g. Wash in 1 x PBS three times for 5 min.
h. Incubate with a blocking solution containing 5 % fetal bovine serum, 2% BSA, 0.5 % Triton in PBS for 1 hr, RT.
i. Incubate with rat anti-CD71-FITC (Biolegend, cat. no.113805) for detection of all proerythroblasts to maturing enucleated erythroblasts, in dilution 1:200 in 1 % fetal bovine serum, 0.4 % BSA in PBS, 1.5 hr, at RT.
j. Wash three times for 5 min.
k. Do not stain nuclei with TO-PRO-3 iodide (Invitrogen cat. no. T3605) for because they have same excitation and emission.
l. Mount slides with mowiol (Sigma, cat. no. 81381).

m. Analyze samples by confocal microscope and process them with Leica 2.6.0 confocal imaging software.

D. Immunostaining for angiogenesis in whole yolk sacs

a. Fix yolk sacs with 4% PFA for 1 hr at room temperature.
b. Wash extensively with PBS.
c. Stain with rat anti – PECAM1 (Pharmingen, cat. no. 553370), O/N, at 4ºC.
d. Incubate with anti-rat FITC conjugated antibody (Sigma, cat. no. F0382) in 1:50 dilution for 1 hour at RT.
e. Place yolk sacs on slides.
f. Add mowiol and try to make them as more open as you can under a stereoscope.
g. Then cover slides.
h. Observe in epifluorescence microscope.

11. Whole Embryo staining for angiogenesis by HRP

a. Dehydrate E10.5 embryos, placed in 6 well plates with:

- 1 x PBS, 2 x 5 min
- 50 % methanol, 2 x 5 min
- 75 % methanol, 2 x 5 min
- 100 % methanol, 2 x 5 min

b. Then, you can keep them at -80ºC for 1 month or continue as following.
c. Incubate with 5% H_2O_2 in methanol on a shaker for 4 hrs, RT. In this way, you inactivate endogenous peroxidase.
d. Wash several times in methanol.
e. Rehydrate in:

- 100 % methanol, 2 x 5 min
- 75 % methanol, 2 x 5 min
- 50 % methanol, 2 x 5 min
- 25 % methanol, 2 x 5 min
- 1 x PBS, 2 x 5 min

f. Incubate in PBMST (3% milk, 0.1 % Triton, 1 xPBS) twice for 1 hr.

g. Incubate rat anti – PECAM1 (Pharmingen, cat. no. 553370) in PBMST, for 48 hrs, at 4ºC.
h. Wash with PBMST five times, 1 hr each.
i. Incubate with anti – rat – Biotin (Sigma, cat. no. B7139) at dilution 1:100 in PBMST, O/N, at 4ºC.
j. Wash with PBMST five times, 1 hr each.
k. Incubate with streptavidin-HRP (Jackson) at dilution 1:50 in PBMST, O/N, at 4ºC.
l. Wash with PBMST five times, 1 hr each.
m. Incubate with PBT (0.2 % BSA, 0.1 % Triton) for 20 min, RT.
n. Incubate with HRP substrate DAP (Sigma, cat. no. D4259). Substrate is made fresh by mixing the two tablets according Sigma' instructions.
o. Check staining on stereoscope not to be overstained (~ 5 min).

12. In situ-hybridization in placenta

A. DNA template for RNA Probes synthesis

a. Linerize plasmid DNA with enzymes that give 5' overhang ends as shown in Table 3.
b. Purify DNA with equal volume phenol.
c. Spin at 16000 g, for 5 min.
d. Keep supernatant and add equal volume phenol/$CHCl_3$.
e. Spin at 16000 g, for 5 min.
f. Keep supernatant and precipitate with 2 volumes 100% ethanol and 1/10 acetic sodium 3 M at -80 ºC.
g. Spin at 16000 g, for 15 min, at 4ºC.
h. Wash with 70% ethanol.
i. Spin at 16000 g, for 15 min, at 4ºC .
j. Resuspend with RNase free water.

B. Transcriptional reaction

a. Make the following <u>transcription reaction</u>:
    - 1 µg linear plasmid DNA
    - 4 µl 5 x transcription buffer (Promega, cat. no. P118B)

- 2 µl DTT 100 mM (Promega)
- 1 µl rATP 10 mM (Promega)
- 1 µl rGTP 10 mM (Promega)
- 1 µl rCTP 10 mM (Promega)
- 0.35 µl rUTP 10 mM (Promega)
- 0.65 µl Dig-UTP 10 mM (Roche, cat. no. 13014721)
- Rnase inhibitor 0.5 units/µl ~ 20 units
- 1 µl T7 (Promega old), or T3 (Roche, cat. no. 11031163001) or SP6 RNA polymerase 20 u/µl
- Water up to 20 µl

b. Incubate for 2 hrs, at 37ºC.
c. Inactivate with 2 units DNAse Turbo (Invitrogen, cat.no. 2238G).
d. Keep 1 µl to confirm DNAse activity. Add 4 µl RNA loading buffer (1x MOPS, 2.2 M formaldehyde, 50% formamide (stabilizes RNA), EthBr 1 µg/µl, 0.4 % Orange G) and make electrophoresis in 2% agarose in TBE w/o ethidium.
e. Add 100 µl TE (1 mM EDTA, 10 mM Tris pH 7.5), 12 µl LiCl 4M and 240 µl 100% ethanol in the transcription mix.
f. Incubate at -80 ºC until to freeze.
g. Spin at 16000 g for 10 min, at 4ºC.
h. Wash with 70% ethanol.
i. Dilute in ~60 µl RNAse free water.
j. Keep 1 µl for electrophoresis to confirm that you have RNA probe.

C. Hydrolysis of RNA probes

Provided that you have synthesized the RNA probe, then you must make hydrolysis of them in order to be smaller than 100 bp.

a. Take half of your sample (30 µl) and add equal volume of 2 x hydrolysis buffer (80mM NaHCO3, 120mM Na2CO3 pH 10.2).
b. Incubate at 60ºC for the corresponding seconds shown in Table 3. Time of hydrolysis is calculated as t = (Lo-L)/kLoL, in which k= 0.11, Lo the initial length of probe and L is the final length of the probe.

c. Add three volumes 100% ethanol (240 µl), 1/10 of volume LiCl 4M (6 µl) and 1/10 acetic acid 10% (6 µl).
d. Incubate at -80 ºC until to freeze.
e. Spin at 16000 g for 10 min, at 4ºC.
f. Wash with 70% ethanol.
g. Dilute in ~50 µl RNAse free water.
h. Keep 1 µl for electrophoresis to confirm that you have RNA probe.

Table 3. Conditions of synthesis of RNA probes Tef5, 4311, Pl1.

Plasmid	Restriction enzyme	RNA polymerase	Type of RNA probe	Hydrolysis 60ºC
pBSK - Tef5	EcoR1	T7	Antisense	19 min
	Xho1	T3	Sense	19 min
pGEM – 4311	EcoR1	SP6	Antisense	-
	HindIII	T7	Sense	-
pGEM - Pl1	HindIII	SP6	Antisense	19 min
	NheI	T7	Sense	19 min

D. RNA in situ hybridization

a. Let slides to dry for 30 min.
b. Fix in 4 % PFA in 1 x PBS for 10 min, RT.
c. Wash with 1x PBS for 5 min (x3).
d. Incubate with proteinase K 20 µg/ml severe for 5 min, RT.
e. Stop reaction with 0.2 % glycine in 1x PBS.
f. Fix in 4 % PFA in 1 x PBS for 5 min, RT.
g. Wash with 1x PBS for 5 min (x3).
h. Incubate with acetylation mix in glass bottles for 10 min, RT.
(It's made fresh every time – last added acetic anhydrite, 196.5 ml nanopure, 2.67 ml triethenolamine 7.5 M (Merck, cat. no. 8379), Cf= 0.1

M, 450 µl NaOH 10N, drops of 0.5 ml acetic anydrate (Merck, cat. no. A6404) cf=0.25%. Mix by adding slides with the bottle).

i. Wash with 1x PBS for 5 min (x2).

RNA Hybridization

j. Denature 100 ng RNA probe in 100 µl Hybridization buffer at 65°C for 5 min.
k. Let then on ice for 2 min. (Optionally pre-hybridization with hybr. Buffer at 55°C for2 hrs).
l. Place slides on humiffied bottle with 5xSSC in 50% formamide.
m. Then add the 100 µl of each probe/ slide
n. Cover with parafilm and let at 55°C for 16-18 hrs.

Washes of excess RNA

o. Wash with 4x SSC preheated at 55°C to remove parafilm.
p. Wash with 2x SSC for 20 min at 55°C.
q. Equilibrate with TNE for 10 min at 37°C.
r. Incubate with RNAse 20 µg/ml in TNE for 30 min at 37°C.
s. Wash with TNE for 5 min at 37°C.
t. Wash with 2x SSC 50% formamide for 20 min at 55°C.
u. Wash with 0. 2x SSC for 20 min at 55°C (x2).

Antibody Incubation and staining

v. Wash with B1 for 5 min, RT.
w. Incubate with B1 with 10% FBS for 1hr.
x. Incubate with alkaline phosphatase (AP)-conjugated anti-digoxigenin (Roche cat.no. 11093274910) 1:2000 in B1 with 1% FBS O/N at 4°C (or 1.5 hr, RT) (100 µl/slide).
y. Wash with B1 for 5 min, RT (x3).
z. Wash in B3 and equilibrate in same buffer for 5 min.
aa. Examine the hybridization with NBT/BCIP solution (Roche, cat. no. 11681451001) (20 µl /ml B3).
bb. Incubate at 37 °C (or RT) until to see staining.

cc. Mount with gelatin mounting (9% w/v gelatin, 50% v/v glycerol, some drops phenol to preserve).

dd. Samples were photographed with 63x lens on a Zeis Axio Scope microscope fitted with ProgRess Jenoptik camera.

Hybridization Buffer

50 % formamide (2.5 ml)
5 x Denhardts (500 µl 50x)
5x SSC (1.25 ml 20x)
Yeast tRNA 200 µg/ml (100 µl 10 mg/ml)
Herring sperm DNA 0.5 mg/ml (310µl 8mg/ml)
340 µl nanopure water
Store aliquots at -20^{o}C

50 x Denhardts

Ficoll 0.5 g
Polyvinylryrrolidone 0.5 g
BSA fraction V 0.5 g
Vf = 50 ml
Filter in 0.45 µm filter
Store aliquots at -20^{o}C

B1

100 mM Tris- HCl pH 7.5
(10 ml 1M)
150 mM NaCl (3 ml 5M)
0.1 % Tween-20
Vf= 100 ml

TNE

Tris 10 mM pH 7.5 (1 ml 1M)
NaCl 0.5 M (10 ml 5M)
EDTA 1 mM (200 µl 0.5 M)
Vf= 100 ml

20 x SSC

NaCl 3 M (87,66 g)
0.3 M $C_6H_5Na_3O_7$ (44,115 g)
V= 500 ml

B3

0.1 M Tris – HCl pH 9.5
(10 ml 1 M)
0.1 M NaCl (2 ml 5 M)
5 mM $MgCl_2$ (0.1 g)
Vf = 100 ml

13. Hematopoietic colony assay

a. Collect peripheral blood / fetal livers in IMDM with 2% FBS (200 μl for E10.5 blood and 500 μl for fetal livers).
b. Make single cells of fetal livers by gentle pipetting.
c. Count cells in hematocytometer.
d. Thaw the required number of aliquots of Methylcellulose mixture at room temperature for approximately 30 minutes without disturbance. Methylocellulose mix contains 1.3 % Serum-free methylcellulose (Stem Cell Technologies, cat. no. H4100), 37% FBS, 1.25 % w/v BSA, 0.25 μM β-mercaptoethanol, 0.1 % Sodium Bicarbonate, 2 mM L-glutamine, 100 units/mL penicillin and 100 μg/mL of streptomycin.
   Note that methylocellulose is viscous, in order cells not to be attached on plate and to form colonies. See recipe below.
e. Dilute $7x10^4$ cells in 100-200 μl IMDM with 2% FBS.
f. Add cells to 1 ml of the methylocellulose mix.
g. Mix cells in methylocellulose in a rotator for some minutes.
h. Let the tube stand for at least 5 minutes to allow the bubbles to rise to the top.
   Add a mix of growth factors in the surface of a 35 mm plate by distributing them with the tip as more as you can in all the plate.
   Note: Be quick, not to dry enough.

- 2 u/ ml erythropoietin (gift from Dr. Marieke von Lindern)
- 10 ng/ml IL-3 (Peprotech, cat. no.213-13)
- 10 ng/ml IL-6 (Peprotech, cat. no.216-16)
- 1 ng/ml GM-CSF (gift from Pr. Papadaki's lab)
- 100 ng/ml SCF (gift from Dr. Marieke von Lindern, produced by supernatant of CHO producer cells) (added only in E10.5 blood).

i. Dispense the methylocellulose mixture containing cells into culture dishes, by attaching a sterile 18 gauge needle to a sterile 1 ml syringe.
   Note: For each tube plated, use a new sterile disposable syringe fitted with a new 16 gauge needle to prevent contamination between samples.
   Note: Do not use pipettes to dispense methylcellulose as the volume

dispensed will not be accurate.

Syringes and large bore blunt-end needles should be used for accurate dispensing of viscous methylcellulose medium and to prevent needle-stick injuries.

j. While holding the syringe containing the Methylocellulose and cells in one hand, remove the lid of a 35 mm dish with the opposite hand. Position the syringe over the center of the dish without touching the dish witht he syringe. Dispense 1.3 ml and replace the lid.

k. Repeat the dispensing procedure for the next 35 mm dish.

l. Distribute the medium evenly across the surface of each 35 mm dish by gently tilting and rotating the dish to allow the medium to attach to the wall of the dish on all sides.

Note: If any medium contacts the lid of the 35 mm dish while distributing the medium across the surface of the dish, replace the lid to minimize the risk of contamination.

m. Place the culture dishes into the outer dish (100 mm petri dish). Add approximately 3 mL of sterile water to the uncovered 35 mm dish. See below.

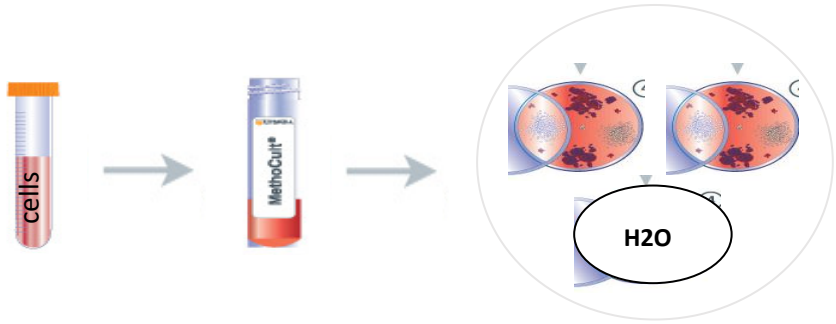

Note: Use of a 100 mm Petri dish with lid and water dish helps maintain humidity and minimize contamination during culture and handling.

n. Incubate at 37°C, in 5% CO2 with ≥ 95% humidity.

o. Score the numbers of colonies after 3 days for CFU-E and 7 days for BFU-E.

Note: Incubation times are dependent on the MethoCult medium formulation.

Methylocellulose mixture for BFU-E / CFU-Es colonies

a. Thaw MethoCult medium (Stem Cell Technologies, cat. no. H4100) at room temperature (15 - 25°C) or overnight at 2 - 8°C.
   Note: Do not thaw MethoCult™ medium at 37°C.
b. Make a mix of the below components:
   - 30 ml FBS (heat inactivated at 56^{o}c for 30 min- use fresh aliquot).
   - 1 ml 200 mM L-Glutamine
   - 1 ml 7.5% sodium bicarbonate
   - 10 ml 10 % BSA (diluted BSA in IMDM)
   - 100 µl 0.2 M β-mercaptoethanol (dilute 1M to 0.2 M with IMDM)
   - 1 ml 10,000 units/mL penicillin and 10,000 µg/mL of streptomycin mixture.

     Note: Filter components before adding to methylocellulose.
c. Add the mix to the 40 ml MethoCult medium (2.6% Methylcellulose in Iscove's MDM).
d. Shake vigorously for 1 - 2 minutes and then let stand for at least 5 minutes to allow bubbles to rise to the top before aliquoting.
e. Use a 5 mL luer lock syringe attached to a 18 gauge needle to dispense MethoCult medium into 3 mL sterile FACs tubes for duplicates.
   Note: It is preferable to dispense the entire contents of the bottle into tubes in order to avoid repeated freezing and thawing of the bottle.
f. Vortex tubes to mix well. Tubes of complete medium can be used immediately or stored at -20°C.
g. After thawing tubes of MethoCult™, mix well, and use immediately. Do not re-freeze.

14. Flow cytometric analysis

A. Detection of EMPs in E10.5 bloodstream

a. Collect peripheral blood from yolk sacs in IMDM with 2% FBS. (Optionally, treat yolk sac with collagenase in order to isolate earlier EMPs, but collagenase damaged CD41^{high} cells in my experiment).
b. Count cells on hematocytometer and put the same number of cells for all genotypes (100000 -500000).
c. Add 1x PBS and centrifuge at 200 g for 5min.
d. Resuspend pellet in PBS/1% fetal bovine, containing the antibodies:
    - FITC-coupled anti - CD16/32 (Biolegend, cat. no. 101305)
    - PE-coupled anti - c-Kit (Biolegend, cat. no. 105807)
    - APC-coupled anti - CD41 (Biolegend, cat. no. 133913)

    Note that you must keep controls with single staining and unstained sample to perform the compensation at flow cytometry machine.
e. Incubate for 15 min at 4°C.
f. Centrifuge at 200 g for 5min at 4°C.
g. Resuspend in 300 µl 1 x PBS.
h. Place samples in FACs tubes.
i. Analyze them in a MoFloT High-Performance Cell Sorter (or another flow cytometry machine).
j. Make your analysis in FlowJo V10 software, by detecting the douple positive CD16/32^{+}CD41^{+} gated on c-Kit^{high} cells.
k. The total number of EMPs arises from multiplying the percentage of CD16/32^{+}CD41^{+} gated on c-Kit^{high} x the percentage of c-Kit^{high} x the total number of blood cells per sample.

B. Detection of erythroblasts R1-R5 in fetal liver

a. Collect fetal livers and make single cells suspension by gentle pipetting.
b. Continue as in 12 A b, c.
c. Incubate fetal liver cells in PBS/1% fetal bovine with the following antibodies:
    - FITC-coupled rat anti-CD71, a marker for all erythroblasts except mature erythrocytes (Biolegend, cat. no.113805).

- biotinylated rat anti-Ter119 antibody (Biolegend, cat. no.116203), a marker for all stages of differentiation from early proerythroblasts to mature erythrocytes.
- streptavidin-PerCP (Biolegend, cat. no.405213)

d. Continue as 12 e - i.
e. Make your analysis in FlowJo V10 software, by detecting the populations in the order they mature: R1: $CD71^{low}$ $Ter119^{-}$, R2: $CD71^{high}$ $Ter119^{-}$, R3: $CD71^{high}$ $Ter119^{+}$, R4: $CD71^{low}$ $Ter119^{+}$, R5: $CD71^{-}$ $Ter119^{+}$.
f. The total number of of each population arises from multiplying the percentage x the total number of blood cells per sample.

C. Cell cycle analysis

a. Isolate fetal livers from E12.5 and E13.5 embryos.
b. Make single cells by gentle pipetting.
c. Count cells in hematocytometer.
d. Place 5 x 10^5 cells in tubes.
e. Add 1 x PBS and centrifuge at 200 g for 5min.
f. Resuspend pellet in 0.25% Triton, 1% BSA in 1xPBS blocking solution.
g. Incubate for 15 min at 4°C.
h. Centrifuge at 300 g for 5 min at 4°C (you need increased g as the pellet is not so compact).
i. Resuspend pellet in 300 μl of propidium iodide 20 μg/ml and RNAse A (Qiagen, cat. no. 19101) 250 μg/ml in PBS solution.
j. Place them in FACs tubes.
k. Incubate for 20 minutes, at 4°C.
l. Analyze samples by BD FACSCalibur Flow cytometer.
   Attention: FACs machine must be suitable for detecting the size of cell. (etc FL2-H, FL2-W).
m. Make your analysis in Flowing software 2-5-1 with histogram analysis of G0/G1, S, G2/M phase.

15. Embryonic Stem cells culture (ESCs)

a. Propagate ES cell lines PC3 (*Erf*$^{+/+}$) and 130/9 (*Erf*$^{-/-}$) in ES cell proliferation medium, on gelatinized 60 mm plates to prevent differentiation of ESC.
b. Feed every day the cells by taking off the medium and adding new (~4 ml).
c. Split about every 2-3 days with trypsin, but 3 hrs before trypsinise you must change medium.
d. Do not split more than 1/10000 and not let medium to become yellow.
   Note: Colonies must be spherical and bright.
   Note: Plate should not be more than 80% confluent.

ES cell proliferation medium

a. Knockout DMEM (Life Technologies, cat. no. 10829018)
b. 2 mM L-Glutamine (100 x Life Technologies, cat. no. 250030-024)
c. 100 u/ml Penicillin, 100 μg/ml Streptomycin (100 x Life Technologies, cat. no. 15140-122)
d. 15% Hyclone Fetal Bovine Serum (GE Healthcare Life Sciences, cat. no. SV30160.03)
e. 1% non-essential amino acids (MEM NEAA Life Technologies, cat. no. 11140)
f. 0.1 mM β-mercaptoethanol (2 μl/ml from 50 mM) (Sigma, cat. no. M3148)
g. 10^3 M ESGRO-Lif
   Note: Add fresh Lif every time from stock 10^6 M (1000 x) always fresh. Lif retains cells in undifferentiated state.

Gelatinized plates

a. Prepare 1% gelatin (Fluka, cat. no. 48723) in np water.
b. Autoclave.
c. Mix gently to dilute gelatin (It is not diluted in low temperature).
d. Store at 4^o C and heat every time in microwave before use.
e. Make 0.1% gelatin every time.

f. Add 3 ml in 60 mm plate.
g. Incubate for 15 min, RT.
h. Take off gelatin and let them dry for 15 min in a hood.

Freeze ES cells

a. Take off medium and rinse in 1x PBS.
b. Trypsinize for 1 to 2 min at 37^{o}C, until cells are detached (0.5 ml for 60 mm plate).
c. Add equal volume of culture medium with FBS to inactivate trypsin.
d. Spin at 200 g for 5 min, RT.
e. Resuspend pellet in 95% Hyclone and 5% DMSO (3 ml for 3 aliquots from a 80% confluent 60 mm plate).
f. Freeze in isopropanol box.

16. Generation of ES cell–derived erythroid cells

EBs are three-dimensional structures in which blood differentiation can be grossly visualized by the formation of hemoglobinized “blood islands” after 6 days, using hematopoietic media.

a. Harvest a 60 mm plate of murine ESCs by washing once with 5 ml PBS followed and trypsinize with 0.5 ml of 0.25% (w/v) trypsin for 1 to 2 min at 37◦C.
b. Add 1 ml IMDM differentiation medium and spin at 200 g for 5 min.
c. Count cells in order to have 500 cells in 20 µl (25 cells/µl or 2.5 x 10^4 cells/ml).
d. Using a multichannel micropipettor, densely plate 20-µl drops of cell suspension onto the bottoms of two to five 10-cm petri dishes.
e. Gently flip the plates to invert the drops.
f. Incubate 48 hrs.

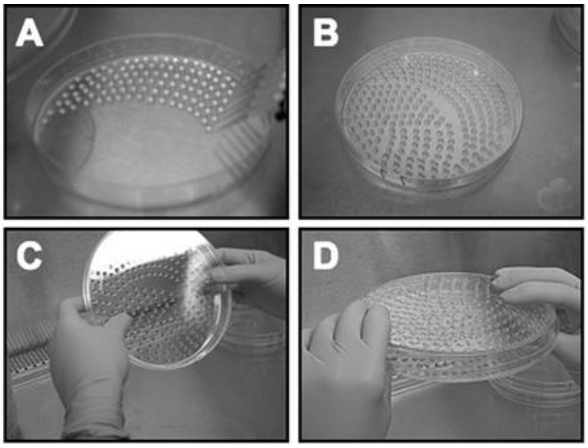

g. At day 2, collect EBs by gently adding medium in the top of drops, while you swirl the plates.
h. Transfer the medium with a 5 ml pipette from all five plates to a single 50 ml conical tube.
i. Rinse the plates with 4 to 6 ml PBS and add to same tube.
j. Allow the pooled day 2 EBs to settle by gravity (~10 min).
k. Aspirate the supernatant without disturbing the EBs.
l. Gently resuspend in 8 ml differentiation medium and transfer to 10-cm nonadherent petri dish (Sterilin, cat. no. BS611).

Note: use petri dish from this company. In others, cells are attached.

m. Incubate for 2 days (better on a shaker set to 50 rpm – unfortunately we didn't have).
n. On day 4 of differentiation, swirl the plate to concentrate the EBs in the edge of the dish. Carefully remove 50% (4 ml) of the medium without disturbing the day 4 EBs.
o. Add 4 ml fresh differentiation medium and return the plate to the incubator (with shaking) for 2 or until 5 more days.

Note: DO NOT pool more than five 10-cm2 petri dishes/50-ml tube. The EBs will grow as they continue to differentiate, and if they are too dense, they may form clumps.

p. Feed cells every 2 days.
q. Dissociate the cells within the day 6 or to 9 EBs by incubation (30 min at 37°C) in a solution of 0.25% collagenase (Gibco) in phosphate-buffered

saline supplemented with 20% Hyclone. Following this incubation, gently pass the cells through a syringe with a 20-gauge needle.

r. Resuspend the cells in 3 ml differentiation medium and count viable cells in an aliquot using 0.4% trypan blue.

   Note: Between day 4 and day 6 of differentiation, EB cavitation results in a large amount of apoptosis and cell death. (20% of EB-derived cells may stain with trypan blue).

s. Spin and wash with PBS.

t. Perform flow cytometry with anti - CD71, c-Kit and Ter119 antibodies to examine the differentiation of erythroblasts in each genotype.

IMDM Differentiation medium

Iscove's IMDM Glutamax (Life Technologies cat. no.31980022) containing:

200 µg/ml holo-transferrin (Sigma, cat. no. T0665)

0.1 mM β-mercaptoethanol (Sigma, cat. no. M3148)

1% v/v 100× penicillin/streptomycin/glutamine (Invitrogen, cat. no. 10378-016)

15% v/v Hyclone Fetal Bovine Serum (GE Healthcare Life Sciences, cat. no. SV30160.03)

50 µg/ml ascorbic acid, cell culture tested (Sigma, cat. no. A4403).

17. Expansion and differentiation of erythroblasts *ex vivo*

To study the expansion and differentiation of erythroblasts, we performed the following experiments in E12.5 and E13.5 fetal livers in Dr. Marieke von Lindern's lab, at Sanquin Research centre, at Netherlands.

A. Expansion of fetal liver erythroblasts

a. Seed fetal liver cells at a concentration of 1 x 10^6/ml into serum-free medium StemPro34 SFM (Life Technologies cat. no. 10639-011) supplemented with:

- 1 unit/ml human recombinant erythropoietin (gift from Dr. Marieke von Lindern), essential for survival at low concentrations.
- 100 ng/ml Stem cell factor (SCF) (gift from Dr. Marieke von Lindern)
- 10^{-6} M dexamethasone (gift from Dr. Marieke von Lindern).

  Note: erythropoietin is essential for survival at low concentrations, but increasing leads to differentiation.

  Note: SCF and dexamethasone are important for proliferation.

  Note: E12.5 livers were placed in a 24 well plate (0.5 ml), while E13.5 livers in a 12 well plate (1ml), after a travel of 6 hrs on ice.

b. Incubate at 37oC, in 5% CO2 with humidity.

c. At day 1 to 5 of cultivation, count cells both in the morning and at night, because they grow very much. Pipette cells up and down, count into casy machine and transfer to another dish in a concentration 1 x 10^6/ml.

   Note: Do not throw cells until you transfer them in a 10 cm culture plate, necause they will be very few for employing different techniques.

   Note: By transferring cells to other dishes you throw away the attached non hematopoietic cells.

d. At day 5 – 11 of expansion, keep a quantity of cells for benzidin staining (hemoglobin content), protein extraction and RNA extraction.

e. Feed cells daily for 40 days for detecting possible small differences in the expansion and maintain cell density at ~ 1 x 10^6 cells/ml.

   Do not forget to note the dilution every time in order to make a graph of how total cells grow every day.

B. Differentiation of fetal liver erythroblasts

a. At day 5 of expansion, place cells from a 60 mm plate (4 ml) in a 50 ml falcon.
b. Wash twice in 40 ml 1 x PBS.
c. Centrifuge at 100 g for 7 min.

   Note: 50 ml falcon helps small cells to adhere at the well, while centrifugation in low g leads only big more immature erythroblasts to precipitate. In this way, you leave out small differentiated erythroblasts.

f. Seed cells at a concentration of 1 x 10^6/ml into serum-free medium StemPro34 SFM (Life Technologies cat. no. 10639-011) supplemented with differentiation factors in a 6 well plate:

- 2 unit/ml human recombinant erythropoietin (gift from Dr. Marieke von Lindern).
- 0.5 mg/ml holo transferrin (gift from Dr. Marieke von Lindern).

g. Incubate for 12, 24, 36 and 48 hrs at 37^{o}C, in 5% CO2 with humidity.
h. Take sample for cell size detection by casy machine, benzidine staining, RNA and flow cytometry analysis in each time point.

C. Gradient concentrations of SCF and Epo

To study the effect of Erf in expansion and differentiation of erythroblasts without pressing the cells to expand or differentiate, we cultivated erythroblasts with gradient concentrations of stem cell factor and erythropoietin.

- Culture with gradient concentrations of SCF

a. Harvest cell as indicated at section 17 B, a-c.
b. Seed cells at a concentration of 1 x 10^6/ml in a 6 well plate (or a 12 well, depending the analysis you want to do).
c. Resuspend cells into serum-free medium StemPro34 SFM (Life Technologies cat. no. 10639-011) supplemented with 0.1 unit/ml epo and SCF gradient concentrations of 30, 10, 3, 1, 0.3, 0.1, 0.03, 0.01 ng/ml.

   Note, that epo is crucial for survival at low concentrations.

d. Incubate for 24 and 48 hrs at 37^{o}C, in 5% CO2 with humidity.

e. Take sample for cell size detection by casy machine, for benzidine staining, RNA and flow cytometry at all time points.

- **Culture with gradient concentrations of Epo**

a. Harvest cell as indicated at section 17 B, a-c.
b. Seed cells at a concentration of 1 x 10^6/ml in a 24 well.
c. Resuspend cells into serum-free medium StemPro34 SFM (Life Technologies cat. no. 10639-011) supplemented with epo gradient concentrations of 3, 1, 0.3, 0.1, 0.03, 0.01 ng/ml.
d. Incubate for 12 hrs at 37^{o}C, in 5% CO2 with humidity.
   Note: Sometimes you may need differentiation until 24 hrs.
e. Take sample for cell size detection by casy machine, for benzidine staining, RNA and flow cytometry.

18. Mouse (Competitive) Repopulating Unit (CRU) assay

A. Prepare recipient mice

a. Irradiate the required number of recipients by exposure 950 cGy γ-irradiation (Gamma cell 220 Nordion irradiator, 2004).

- *Irradiation time (min)= (t_0 x $t_{1/2}$)/ rad, where t_0 = 8600 rad/min and $t_{1/2}$ estimated from the number of hears from 2004, rad = 950.*
- *The irradiation dosage should be predetermined such that one nontreated mice die within 10 to 21 days and transplantation of 5 × 10^5 normal B6(CD45.2) cells ensures survival of >95%.*
- *Radiation-induced mortality can be reduced with neomycin 1 mg/ml for 3 days prior to irradiation and for 4 weeks after transplantation.*
- *It is important to use healthy animals 2 – 3 months that are maintained under standardized pathogen free conditions.*

B. Prepare test cells

b. Harvest liver cells from E12.5 / E13.5 embryos with a mixed C57B6/SV129 background.
c. Prepare a single cell suspension in IMDM with 2% FBS.

d. For the no competitive repopulation studies, dilute 5×10^5 cells fetal liver cells in 0.250 ml IMDM with 2% FBS.
e. For the competitive repopulation studies, dilute 4×10^5 fetal liver cells with 2×10^5 spleen from a wt mouse of the same background.
   Note: Cells must have same MHC class II, in order not to be recognized as antigens.
f. Place them on ice, until to genotyping results.

C. Inject test cells into recipient mice

g. Gently warm the irradiated mice using a heat lamp above the cage from a distance ~ 30 cm for about 3 min. Stop heating, when you see that mice are irritable and have humidity under their mouth. Take care not to expose animals to excessive heat and die.
h. Place the mice in the restraining device (Hliopoulos' lab).
i. Mix the cell suspension well and draw it into a 1 ml syringe with 27-G needle. Remove all air.
j. Inject 0.25 ml into the lateral tail vein of each recipient.
   Note: The same syringe and needle can be used for two to four mice.
   Note: To have a successful injection, you must see the vein to become white as cells get inside. If you feel any resistance do not continue. The needle has injected a tissue and not the vein.
k. Maintain recipient animals with neomycin 1 mg/ml for 4 weeks and monitor mice twice a week for viability and general health.

D. Assess hematopoietic reconstitution in recipient mice

l. Collect peripheral blood from each recipient, plus positive and negative control mice after 1 and 5 months of irradiation.
   Note: Short term-HSCs will differentiate to enucleated cells in the first three months and will lead to the survival of mice, while Long term-HSCs are responsible for survival after 4 months of transplantation.
m. Gently warm the mice using a heat lamp as decribed before to isolate much blood.
n. Make a cut in end of the tail.

o. Collect ~200 µl of blood into 100 µl 0.5 % citrate. Leave on ice.
Note: Avoid heparin (25 units for 100 µl blood) because it inhibits PCR.
Note: Do not collect fewer than 200 µl blood cells, as you will have very few DNA (no red cells are very few) and PCR will not work.

p. Isolate DNA from blood with FlexiGene DNA kit (cat. no. 51204) according its instructions.
Note: DNA extraction from blood cells w/o kit with was inefficient. Kit permits you to throw away erythrocytes and avoid inhibition of PCR by globins. Methods of ficol and red cell lysis were not efficient for PCR.

q. Make PCR for the detection of the loxP allele in loxP/+ transplantaded cell with the m11671, 11771R primers or the deletion of *Erf* in knockouts with the 4021F, 11771R (referred in section genotyping).

19. Ficol density centrifugation

Ficol is a neutral, highly branched, high-mass, hydrophilic polysaccharide which dissolves readily in aqueous solutions.

a. Add ficol equal volume with cells in an eppendorf.
b. Then, add blood cells.
c. Do not mix!
d. Centrifuge at 400 g for 30 min, RT in swinging bucket rotor without brake.
e. Isolate mesophase, which includes white blood or red blood cells in the bottom.

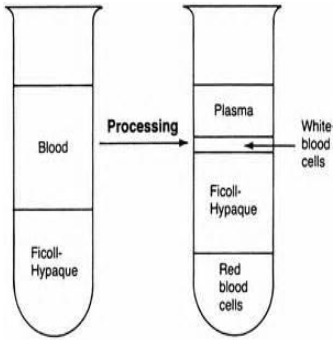

20. Red cell lysis

a. Centrifuge blood cells at 200 g for 5min.
b. Incubate with 1 ml H_2O per 20000 cells for 25 sec.
c. Add equal volume of 1.8% NaCl buffer.
d. Add 1 x PBS.
e. Centrifuge at 200 g for 5min.
f. Make washes with PBS until pellet gets white.

21. RNA extraction from eukaryotic cells

a. Homogenize tissue samples in 1 ml Trizol (Invitrogen, cat. no. 15596018) per 50-100 mg tissue, using homogenizer. For single cells resuspend 1 x 10^6 cells in 1 ml Trizol. The sample volume should not exceed 10% of total volume.
b. Incubate 5 min, RT to permit complete dissociation of nucleoprotein complexes. Wear always gloves to avoid RNAses.
c. Add 0.2 ml chloroform per ml Trizol.
d. Shake tubes vigorously by hand for 15 sec.
e. Incubate 2-3 min, RT.
f. Centrifuge at no more than 12,000 g for 15 min 4ºC.
   The resulting pellet contains extracellular membranes, polysaccharides, and high molecular weight DNA, while the supernatant contains RNA. DNA also is in interphase and organic phase.
g. Transfer aqueous phase to a new tube and add 0.5 ml isopropanol per ml Trizol.
h. Incubate 10 min, RT.
i. Centrifuge no more than 12,000 g, 5 min, 4ºC.
j. Remove supernatant and wash with 1 ml 75 % ethanol per ml Trizol.
k. Centrifuge no more than 7,500 g, 5 min, 4ºC.
l. Dissolve in RNAse free water.
m. Store at – 80 ºC.
n. Not leave RNA at RT much time. RNAaSes will destroy it!!!
o. Load in 1.5 % agarose in 1x TBE (all very well washed!!) with RNA Loading Buffer (1x MOPS, 2.2 M formaldehyde, 50% formamide (stabilizes RNA), EthBr 1 µg/µl, 0.4 % Orange G).

22. cDNA synthesis

A. Dnase Treatment

a. Incubate at 37 ºC for 30 min the following mix:

   0.5 µl 10 x buffer DNase (Invitrogen, cat. no. 81676)

   0.25 µl DNase Turbo 1u/µl (Invitrogen, cat. no. 2238G)

   1 µg RNA

   ddH_2O

   V_F: 5 µl

b. Inactivate Dnase with 1 µl retin (Ambion cat. no. 81746) for 2 min.

c. Spin shortly 1 min and keep supernatant.

B. cDNA synthesis

a. Incubate at 65 ºC for 5 min:

   1 µg RNA

   0.5 µl primer oligo dTT (15 nt) (binds mRNA) (Minotech)

   0.5 µl dNTPs 100 mM (Invitrogen, cat. no. 200820-55)

   ddH_2O

   V_F: 5 µl

b. Let them RT for 2 min to cool.

c. Add the following mix in the first:

   2 µl 5 X RT buffer (Minotech)

   0.5 µl DTT 100 mM (Invitrogen)

   0.5 µl RNase Block 40 U/µl (Invitrogen, cat. no. 10777-0192))

   0.5 µl Affinity RT 10x enzyme, 200 units/ µl (Minotech)

   1.5 µl H_2O

   V_F: 5 µl

d. Incubate at 55 ^{o}C for 1 hr. Be careful incubation temperature depends on RT enzyme and company.
e. Inactivate enzyme at 70^{o}C for 15 min.

Above reagents are from Minotech and performed for Lyve1cre quantifications. Previous cDNA synthesis was performed with Agilent Technologis Affinity Script Multi Temperature cDNA synthesis Kit cat. no. 200436.

23. Real-time quantitative PCR for globins, Erf, Runx1 and Cre recombinase

- Expression levels of βH1 and εy globin were detected in primitive erythroid cells in E10.5 – E11.5 peripheral blood.
- *β*major globin was detected mainly in definitive blood cells in E10.5 – E12.5 peripheral blood and fetal livers.
- Erf quantification was examined in E12.5 - E13.5 fetal livers of *Lyve1Cre* mice.
- Cre quantification was performed in DNA of Alfp-Cre mice to distinguish homozygous grom heterozygous cre mice.
- RunX1 quantification examined in E10.5 peripheral blood with 3 different sets of primers (RunX1, RunX1P1, RunX1P2), which derive from 2 promoters that give 2 variants each one, with P1-derived isoform being predominantly expressed in hematopoietic stem cell, megakaryocytes and T lymphocytes present in thymus and spleen. Runx1 primers involve all the variants.
- All expression levels were normalized to Gapdh levels in the same cDNA.

a. Make a mix with:
   2.5 μl primer (stock 2 μM both)
   5 μl 2 x BrilliantIII SYBRGREEN QPCR mastermix (STRATAGENE cat. no. 600882-51).
b. Share 7.5 μl in each QPCR tube.
c. Add 2.5 μl cDNA that contains:

1. 5 ng for detection of globins
2. 50 – 100 ng for detection of Erf

Or add 2.5 μl DNA that contains:

3. 1 ng for detection of Erf
4. 10 ng for detection of Cre

d. Make a short spin.

e. Run at QPCR machine (STEP ONE Plus Real-time PCR system, Applied Biosystems) with the following Programme.

Note: Internal control was the Gapdh gene.

Table 4. Real – time PCR conditions for globins, Erf, Cre, Runx1 and Gapdh.

Step	T °C	Time	βH1	εy	β_{major}	Erf	Cre	RunX	Gapdh
1	95	3 min							
2	95	30 sec							
3	X	x sec	56°C 20 sec	56°C 20 sec	56°C 45 sec	58°C 15 sec	60°C 20 sec	56°C 20 sec	56°C +-1 15 sec
4	repeat steps 2-3 for 40 cycles								
5 6 7 8	95 55 + 0,3 95	30 sec 45 sec 15 sec							
Product size (bp)			263	150	525	230 cdna	101	X1: 102 P1: 103 P2: 92	153

Table 5. Primers sequences for Real – time PCR conditions.

Primer	Sequence 5' --> 3'	template
βH1-F βH1-R	CTCAAGGAGACCTTTGCTCA AGTCCCCATGGAGTCAAAGA	cDNA
ey- F ey- R	GGAGAGTCCATTAAGAACCTAGACAA CTGTGAATTCATTGCCGAAGTAC	cDNA
β_{major}-F β_{major}-R	CACAAACCCCAGAAACAGACA CTGACAGATGCTCTCTTGGG	cDNA
Erf 9701 F Erf m10268R	TGTGGCACTTTATCCTGGAG CTTGTAGGTGAACCGTTTCC	cDNA
Erf bGH-PA Erf 4021-F	TCGAGATCCACTAGTTCTAGC GCACTGCTAGCTCTGAATGG	DNA
Cre1-F Cre2-R	GCG GTC TGG CAG TAA AAA CTA TC GTG AAA CAG CAT TGC TGT CAC TT	DNA
Runx1-R Runx1-R	CTC CGT GCT ACC CAC TCA CT ATG ACG GTG ACC AGA GTG C	cDNA
Runx1P1-F Runx1P1-R	GAA GTG TAA GCC CAG CAC AGT GGC GGG GGA TTC TAT AAT TT	cDNA
Runx1P2-F Runx1P2-R	TGA ACT TGT ATG TTG GTC TCC CGA TTG AGT AAG GAC CCT G	cDNA
GAPDH-F GAPDH-R	CCAGTATGACTCCACTCACG GACTCCACGACATACTCAGC	cDNA DNA

24. Statistical analysis

Statistical analysis was carried out using the 2 tailed unpaired *t*-test equipped with Excel 2016. For all graphs, data are presented as means ± standard error. The Pearson's chi-square test was used to evaluate the actual over the expected frequency of the genotypes. A * *P* value < 0.05, ** *P* value < 0.005 and *** *P* value < 0.0005 denoted statistical significance.

Part II. Craniosynostosis

1. Caesium Chloride density gradient centrifugation

a. Lightly scratch the surface of frozen *E. coli* glycerol stock with a sterile inoculating loop.
b. Inoculating bacteria into 250 ml LB with antibiotic.
c. Incubate in 37°C shaker, O/N.
d. Spin at 5000 rpm, 10 min, 20 ºC (Sorvall RC 5 C plus centrifuge).
e. Add 5 ml P1 buffer in pellet (have added lysozyme solid).
f. Add 5 ml buffer P2, mix gently and incubate, RT for5 min.
g. Add 7.5 ml P3, on ice for 10 min.
h. Spin at 10000 rpm, 15 min, 4 ºC (Sorvall RC 5 C Plus rotor).
i. Filter supernatant and add 0.6 volumes isopropanol, 10 min, RT.
j. Spin at 1100 g, 10 min, RT.
k. Resuspend pellet in 70% EthOH.
l. Spin at 1100 g, 10 min, RT.
m. Dry pellet and resuspend in 10 ml TE.
n. Add 1 gr CsCl/ ml TE.
o. Add 300 µl EthBr 10 mg/ml in the syringe to pass through the specific tube without pressure. See below.

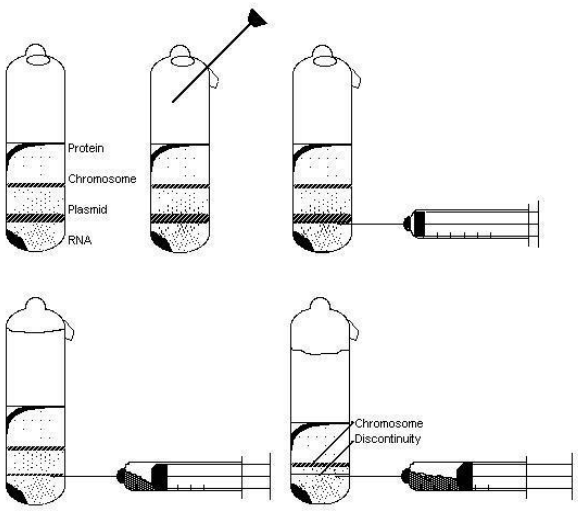

p. Add the sample.
q. Seal the tube and freeze.
r. Spin at 45000 rpm for 40 hrs at 20 ^{o}C.
s. Isolate plasmid by 1 ml syringe 19 G, as image shows.
t. Add isopropanol saturated in CsCl as much as you can.
u. Wash 4-5 times to take off EthBr.
v. Add until 1.5 ml 70% EthOH.
w. Freeze at - 80 ^{o}C.
x. Leave at RT to precipitate Cs and mix.
y. Spin at 13000 rpm for 10 min.
z. Discard supernatant and wash pellet twice with 70% EthOH.
aa. Air dry and resuspend in TE.

P1 buffer

50 mM glucose

25 mM Tris-HCl pH 8

10 mM EDTA

P2 buffer

1% SDS (w/v)

200 mM NaOH

P3 solution

Acetic potassium

3M pH 5.5

TE buffer

1 mM EDTA

10 mM Tris pH 7.5 - 8

LB medium

5 gr NaCl

5 gr Tryptone

2.5 gr Yeast Extract

dH_2O up to 500 ml

autoclave

2. Miniprep

a. Incubate one colony in 3 ml LB with antibiotic, O/N, 37^{o}C.
b. Spin at 16000 g and resuspend in 200 µl P1 with RNase 100 µg/ml and vortex.
c. Add 200 µl P2, mix well and incubate, RT, 4 min.
d. Add 200 µl P3 (ice cold) on ice, 5 min.
e. Spin at 16000 g, RT, 10 min.
f. Add equal volume phenol/chloroform and vortex.

g. Spin at 16000 g for 10 min, RT.
h. Add 0.6 volumes isopropanol and incubate 10 min, RT.
i. Spin at 16000 g for 10 min, RT.
j. Wash pellet with 70% EtOH
k. Spin at 16000 g for 5 min, RT
l. Resuspend in 30 - 50 µl TE.

Note: See recipes for LB media, P1, P2, P3 at protocol 1.

3. Electrocompetent cells

a. Inoculate DH10b cells from a glycerol stub in 50 ml pre-culture with LB* medium

Recipe for LB media is made like LB media with 2 gr NaCl .*

b. Incubate, O/N, at 37^{o}C.
c. Next day, inoculate 5 ml of culture in 500 ml LB* medium.
d. Incubate until OD_{600}= 0.5 - 0.6 (~3 hrs) at 37^{o}C.

Note: Have all the equipmet cold before begine (pippetes, tips, falcons, H_2O).

e. Next, incubate culture on ice in a shaker for 15 – 30 min.
f. Place the 500 ml culture into two chilled Corning bottles.
g. Spin in Sorval 5 RC plus rotor at 4000 rpm, for 15 min at 4°C.
h. Place bottles on ice. Remove supernatant immediately as cell pellet begins to lift off quickly.
i. Gently resuspend each pellet in 500 ml ice-cold dH_20.
j. Spin at 4000 rpm for 15 min at 4°C.
k. Place bottles on ice. Remove supernate. Gently resuspend each pellet in 250 ml of ice-cold dH20.
l. Spin at 4000 rpm, 15 min at 4°C.
m. Gently resuspend each pellet in 50 ml ice-cold dH20.
n. Spin in 50 ml falcons at 1100 g, 10 min at 4°C.
o. Gently resuspend each pellet in 10 ml ice-cold dH20.
p. Spin at 1100 g, 10 min at 4°C.
q. Resuspend in 1 ml 10% glycerol in ice-cold dH20.

r. With cell suspensions on ice, prepare aliquots of 1.5 ml eppendorf tubes on dry ice.
s. Share 50 μl cells in each aliquot.
t. Store frozen cells at -80°C.

4. Gel Extraction

After digestion of the DNA sequence and electrophoresis in 1% agarose (to avoid the big quantity of agarose), isolate the proper band as follows:

a. Cut the DNA band into small slices and spin at 16000 g for 1 min.
b. Add equal volume phenol, vortex and freeze on -80 ^{o}C.
c. Spin at 16000 g for 20 min, RT.
d. Check that agarose has melted. If not, add more phenol and freeze and spin again.
e. Add equal volume phenol/chloroform.
f. Spin at 16000 g for 10 min, RT.
g. Add 2 volumes 100% EthOH and 1/10 3M CH_3COONa of the intitial volume and freeze at -80 ^{o}C.
h. Spin at 16000 g for 10 min, 4 ^{o}C.
i. Wash with 70 % EthOH and spin at 16000 g for 5 min, RT.
j. Resuspend pellet in 5-10 μl TE.

5. Ligation

For cloning a DNA sequence in a plasmid, after digestion with the suitable enzymes and gel extraction of the proper band perform as follows:

a. Make a ligation mix with:

- 50 – 100 ng vector
- ω ng insert, x is estimated as:
  ω ng $_{insert}$= kb_{insert}/kb_{vector} x y x ng vector,
  y= 10 or 5 (10 or 5 ng_{insert}: 1 ng_{vector}), <u>in case we have sticky ends</u>
  y= 2 (2 ng_{insert}: 1 ng_{vector}), <u>in case we have blund ends</u>
- 1 μl 10 x ligase buffer (Minotech w/o ATP)
- 1 μl 1 mM ATP

- 2.5 u/μl ligase (Minotech)
- nanopore H_20 up to 10 μl

b. Incubate at 16^oC for 1 – 6 hrs for sticky ends
   or at 25^oC overnight for blund ends.
c. Ckeck in 2% agarose gel in that ligation is successful.
d. Continue the transformation assay.

6. Transformation by Electroporation

a. Irradiate cuvettes specific for electroporation under UV for 20 min to be sterile.
b. Place them on ice.
   Note: Everything must be at 4^oC, without humidity in cuvettes and DNAs without a lot of salts for efficient electroporation.
c. Add 1 μl of ligation mix with 50 μl DH10b electrocompetent cells.
d. Transfer in cuvettes in sterile conditions.
e. Electroporate at 1800 V for 5 msec.
f. Add 1 ml LB medium without antibiotic and incubate in bacterial tube for 1 hr at 37^oC, in order cells have the time express the resistance to antibiotic.
g. Centifuge at 16000 g for 30 sec.
h. Resuspend pellet in 50 μl LB.
i. Plate cells in LB plates with antibiotic (usual 100 μg/ml ampicillin), O/N at 37^oC.

Bacterial culture plates Recipe

500mL of LB agar (makes about 25 LB agar plates):

a. Weigh out the following into a 1L Erlenmeyer flask:

- 5 gr NaCl
- 5 gr Tryptone
- 2.5 gr Yeast Extract
- 7.5 gr Agar
- add dH_2O to 500 mL

b. Swirl to mix and cover the top of the flask with aluminum foil and label with autoclave tape.
c. Autoclave on the liquid setting for 20 minutes or according to your autoclave's specifications.
d. After removing the solution from the autoclave, allow the agar solution to cool until 55°C. You can have the flask swirling in ice. Be carefull, if you let much time it will not be liquid any more.
e. When pouring plates, keep your bench area sterile by working near a flame or bunsen burner.
f. Add the appropriate amount of desired antibiotic to the solution (500µL if you are using a 1,000x antibiotic stock) and swirl to mix.
g. Pour ~20mL of LB agar per 10cm polystyrene Petri dish.

   Note: Pour slowly from the flask into the center of the petri dish. When the agar has spread to cover about 2/3 of the dish stop pouring and the agar should spread to cover the entire plate. You may need to tilt the plate slightly to get the agar to spread out completely. If you pour in too much, the plate will be fine, but it will reduce the number of plates you can make per batch.

   Note: If bubbles are introduced during the pouring, these can be removed by quickly passing the flame of an inverted bunsen burner over the surface of the plate. Be careful, if you leave the flame too long it will melt the petri dish. Also be careful not to burn yourself.

h. Place the lids on the plates and allow them to cool for 30-60 minutes (until solidified), then invert the plates. Let sit for several more hours or overnight.
i. Label the bottom of plates with antibiotic and date and store in plastic bags or sealed with parafilm at 4°C.

7. Cloning of Erf mutations 256C>T, 194G>A and d1512T

To study activity of mutations 256C>T, and 194G>A in the binding domain or d1512T in the repressor domain of Erf, we performed series of cloning for testing them with a luciferase or β-gal assay.

A. Cloning of mutation 256C>T in pSG5-Erf plasmid

To study the Erf mutations dependent on the DNA binding activity, we employed the vector pSG5-Erf (Mavrothalassitis and Papas, 1991). Co-transfection with pGL3 basic Gata1 or pGL3 enhancer Gata1 in HeLa cells lead to binding of Erf in Gata1 sequence and luciferase is expressed.

a. pSG5-Erf was digested with Kpn1 and EcoR1.
b. pKS Bluescript was digested with Kpn1 and EcoR1.
c. After gel extraction, the 600 bp sequence of Erf ligated to pKS for a better mutagenesis reaction due to its smaller size.
d. Mutagenesis assay was employed (see next).
e. Sequencing at IMBB confirmed mutation.
f. Both pKS+ Bluescript with mutation 256C>T and pSG5-Erf were digested with Kpn1 and EcoR1 enzymes.
g. The 600 bp mutation 256C>T was ligated back to pSG5-Erf vector, as it has SV40 promoter and can express Erf in eukaryotic cells.
h. After transformation, digests confirmed the colony with the ligated insert.
i. Co-transfection in HeLa cells with pGL3 basic Gata1 or pGL3 enhancer Gata1, vectors that have a luciferace gene after promoter, confirmed activity of mutations. The pGL333 control (with three copies of the GATA1 ets-binding site (ebs) and a minimal TK1 promoter), generated by transferring the corresponding promoter fragment from pBLCAT333 (D. K. Watson et al., 1992) into the pGL3-Basic vector (Promega).

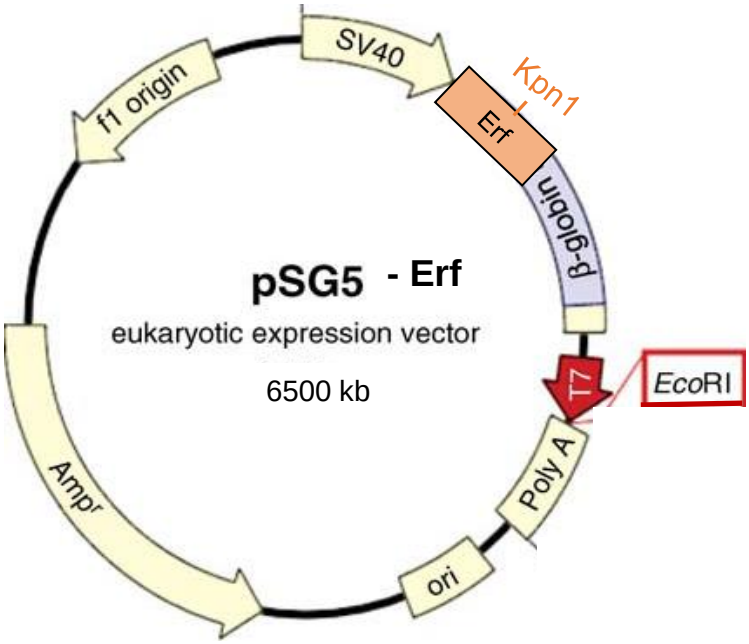

pSG5-Erf vector. Employed for cloning of mutagenesis 256C>T from pKS with EcoR1 and Kpn1.

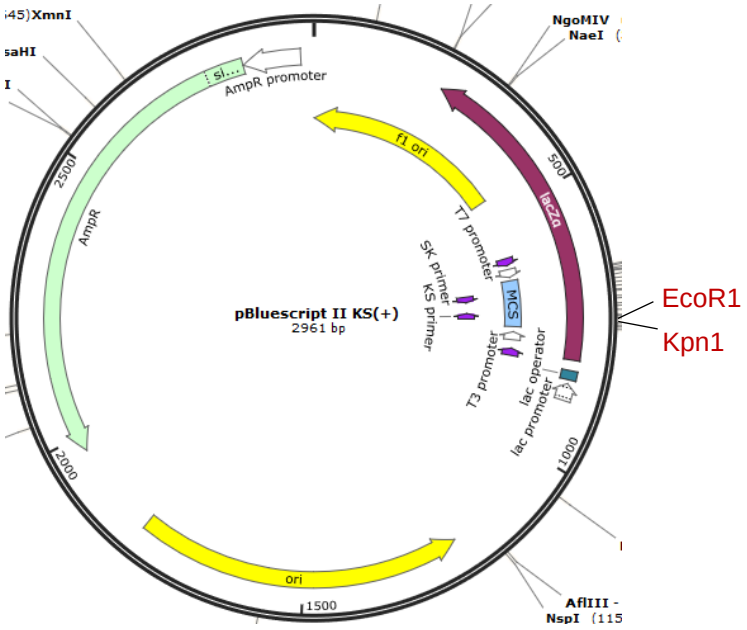

pKS+ Bluescript vector. Employed for cloning Erf with EcoR1 and Kpn1 enzymes for mutagenesis 256C>T.

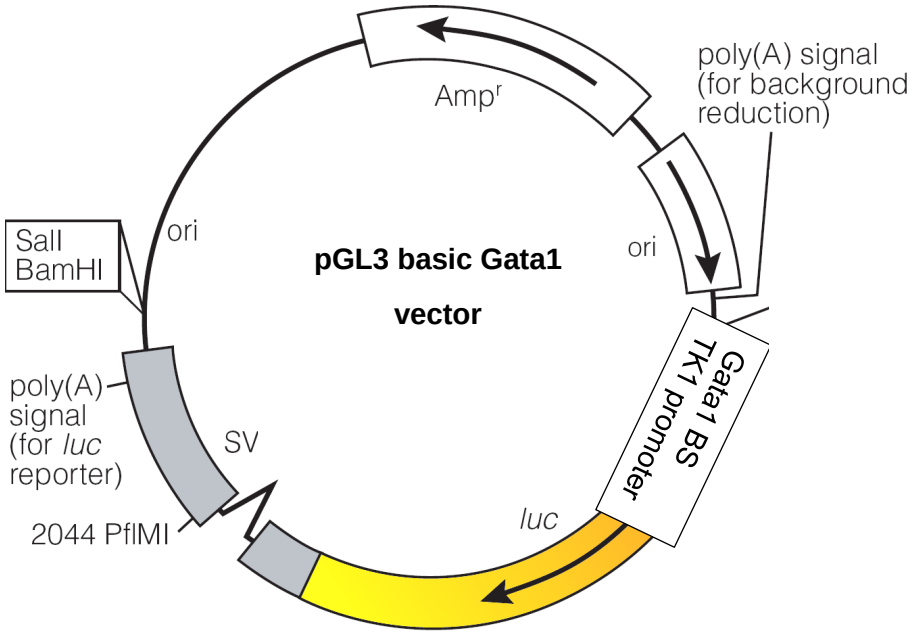

pGL3 basic vector with Gata1 binding sites before TK1 promoter. It was employed for co-transfection with plasmids with Erf mutations and based on bindinf to Gata1 sites, luciferase expression is measured. The same plasmid with an enhancer was also used.

B. Cloning of mutation 256C>T in pSG424-Erf plasmid

For detection of activity of 256C>T mutation, independently of DNA binding activity, we employed pSG424-Erf vector. pSG424-Erf contains a Gal4 DNA binding domain fused with Erf. Co-transfection with pGL3 control GaL4 binding sequence or pGL3 enhancer GaL4 binding sequence leads to binding of fused protein in Gal4 sequence and luciferase is expressed. The pGL3 control Gal4 (gal4 DNA-binding site and the SV40 promoter), generated by transferring the corresponding promoter fragment from SV40/GAL4 (Mavrothalassitis and Papas, 1991) into the pGL3-Basic vector.

a. pSG424-Erf was digested with Bpu1102I.
b. pKS Bluescript with mutation 256C>T was digested with Bpu1102I.
c. After gel extraction the 600 bp mutation 256C>T was ligated back to pSG4-Erf vector.
d. Sequencing at at IMBB confirmed the mutation.
e. After transformation, digests confirmed the colony with the ligated insert.

f. Mutation 256C>T in pSG424-Erf vector was also performed for sequencing after digestion with BamH1/EcoR1 and cloning in pKS Bluescript vector but pSG4-Erf sent to Larissa was mutated finally.

a. Co-transfection in HeLa cells with pGLGal4 reporter (gal4 DNA-binding site and the SV40 promoter) or enhancer, generated by transferring the corresponding promoter fragment from SV40/GAL4 into the pGL3-Basic vector, was used to assess ebs-independent repression.

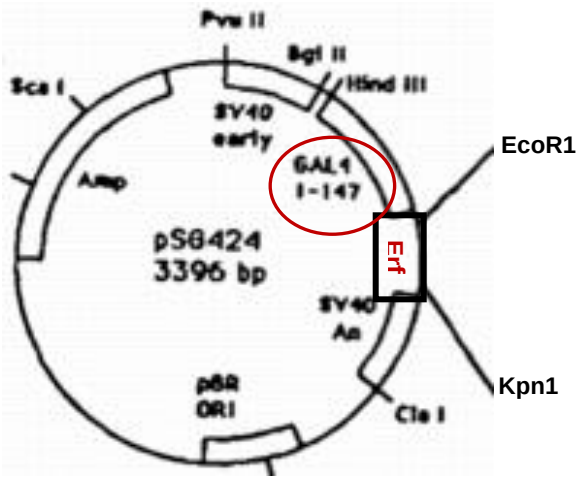

pSG424-Erf vector. Employed for cloning of mutagenesis 256C>T from pKS with EcoR1 and Kpn1.

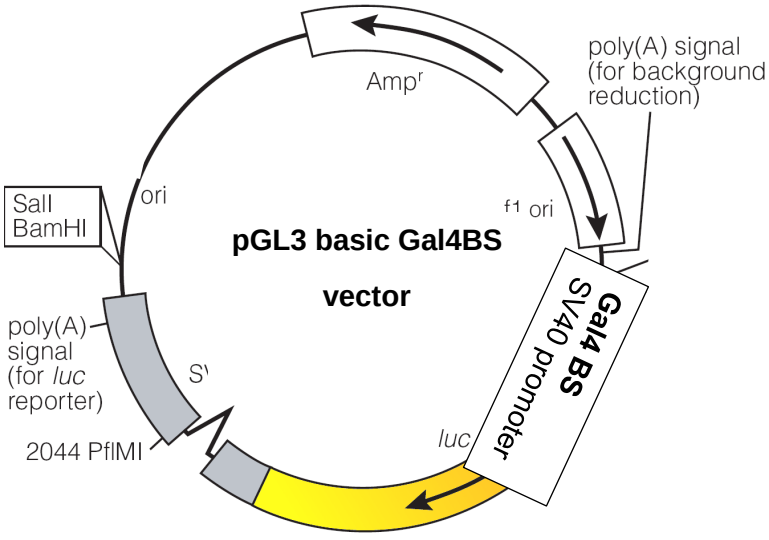

pGL3 basic vector with Gal4 binding sites before SV40 promoter. Employed for co-transfection with plasmid that express fused Gal4 BD-Erf for examination of Erf mutations based on luciferase expression. The same plasmid with a enhancer was also used.

C. Cloning of mutation 194G>A in pSG424-Erf plasmid

The mutation 194G>A in DNA binding domain of Erf was cloned in pSG424-Erf plasmid for reasons mentioned in 7B with the following digestions, but colonies did not grow.

b. pSG5-Erf vector with 194G>A mutation, mutated from M. Avgoulea, was digested with EcoR1 and MspC1.
c. pSG424-Erf vector 2 μg digested partially with 10 units EcoR1 for 5, 10, 15, 20, 25, 30 min.
d. After gel extraction the mutation 194G>A was ligated to pSG424-Erf vector.
e. After transformation, no colonies exist.
f. Next from the beginning, we made the mutation assay (see next) on the pSG424Erf plasmid and the mutation was sent to Larissa, where they had the proper primers. Mutation was confirmed!
g. Cotransfection with pGLGal4 reporter (gal4 DNA-binding site and the SV40 promoter), generated by transferring the corresponding promoter fragment from SV40/GAL4 into the pGL3-Basic vector, was used to assess ebs-independent repression.

D. Cloning of d1512T in pSG5-Erf plasmid

The mutation d1512T in the repressor domain of Erf was cloned in pSG5-Erf plasmid for reason mentioned at 7A, but sequencing showed no mutation.

a. pSG5-Erf was digested with Sst1 and Pst1.
b. pKS Bluescript, cloned with d1512T from M. Avgoulea, was digested with Sst1 and Pst1.
c. After gel extraction, the d1512T sequence ligated to pSG5-Erf.
d. After transformation, digests confirmed the colony with the ligated insert.

Next from the beginning, we made the mutation assay (see next) on the pSG5Erf plasmid and the mutation was sent to Larissa, where they had the proper primers. Mutation was confirmed!

E. Cloning of d1512T in pSG424-Erf plasmid

The mutation d1512T in repressor domain of Erf was cloned in pSG424-Erf plasmid for reasons mentioned at 7B.

a. pSG424-Erf was digested with partially with NheI and then Mspc1.
b. pSG5 Erf with d1512T made from no mutated finally pKSd1512T from M. Avgoulea, was digested with the same enzymes.
e. After gel extraction, the d1512T sequence ligated to pSG4-Erf.
f. Finally there was no mutation.

Next from the beginning, we made the mutation assay (see next) on the pSG424-Erf plasmid and the mutation was sent to Larissa, where they had the proper primers. Mutation was confirmed!

8. Site Directed Mutagenesis for Erf - 256C>T, 194G>A and del1512T

The mutagenesis for the following mutations in specific plasmids was performed by Quick Change Kit.

- Mutation 256C>T on pKS+ Bluescript plasmid
- Mutation 194G>A on pSG424-Erf plasmid
- Mutation del1512T on pSG5-Erf plasmid
- Mutation del1512T on pSG424-Erf plasmid

The process is the following:

a. Extract DNA by miniprep column
b. Make PCR mix:

5 μl 10 x Reaction Buffer

50 ng x vector

125 ng forward primer (refered next for each mutation)

125 reverse primer

1 μl dNTPs 40 mM stock

ddH_2O up to 50 μl

c. Perform the following PCR Programme:

1. Hot start, 95 ^{o}C, 5 min
2. Pause and add 2.5 U Pfu Turbo DNA polymerase
3. 95 ^{o}C, 30 sec
4. 55 ^{o}C, 1 min
5. 68 ^{o}C, 7 min
6. Repeat 3 – 5 for 17 cycles
7. 4 ^{o}C for ever

d. Add 1 µl Dpn1 for 1 hr at 37 ^{o}C to digest methylated parential DNA.
e. Do transformation in XL1 competent cells with 1 µl DNA and send for sequencing.

Primers for 256C>T in pKS+ Bluescript

401-429 Forward: GAGCCGGGCCCTGTGCTATTACTATAAC

401-429 Reverse: CTTATAGTATTAGCACAGGGCCCGGCTC

Primers for 194G>A in pSG424-Erf

339-364 Forward: GATGAGGTGGCCCAGCTGTGGGGC

339-364 Reverse: GCCCCACAGCTGGGCCACCTCATC

Primers for del1512T in pSG5-Erf and pSG424-Erf

1656-1687 Forward: CCCGCTGGGGGCTTGAGGATGAGG

1656-1687 Reverse: CCTCACCCTCAAGCCCCCAGCGGG

9. Cloning of RunX2 and Runx2-Erf binding sites

To confirm that Erf and Runx2 bind at the same motif, discovered from Chip-seq, we performed the following constructs for a luciferase assay.

A. Cloning of Runx2 in pSG5 vector

Runx2 was cloned to pSG5 vector because it has SV40 promoter for expression in eukaryotic cells.

a. pENTP223.1 vector that had already cloned with Runx2 cDNA, was digested with SfiI to isolate Runx2 sequence.
b. pSG5 vector was digested with BamH1.
c. After gel extraction, the Runx2 sequence ligated to pSG5.
a. After transformation, digests confirmed the colony with insert.

B. Cloning of Erf/Runx2 DNA binding motif

Chip-seq of Erf and Runx2 discovered a motif that conceivably is bound by both factors. To confirm that, we designed 3 set of oligonucleotides RxErf d1, RxErf d5, RxErf d10 with small differences, we dimerized and cloned them in a pGL3 promoter vector. Erf and Runx2 binding was confirmed after transfection and luciferase assay.

Dimerization of oligonucleotides of Runx2

a. Make 3 different mixes of RxErf d1, RxErf d5, RxErf d10 containing:
   - 2 µl oligo forward 100 µM
   - 2 µl oligo forward 100 µM
   - 16 µl 50 mM NaCl and 1 mM EDTA
   - H_2O up to 20 µl
b. Incubate for:
   - 5 min, 90^oC
   - 5 min, 72 ^oC
   - 2 hrs, 62 ^oC stop RxErf d10 oligos (18 bp), on ice
   - 5 min, 58 ^oC
   - 2 hrs, 48 ^oC stop RxErf d5 oligos (24 bp), on ice
   - 5 min, 40 ^oC
   - 2 hrs, 30 ^oC stop RxErf d1 oligos (29 bp), on ice
   - 5 ML 45 H2O
c. Dilute each oligo 1:10.
d. Have digested pGL3 promoter with NheI and BglII
e. Ligate 1 µl oligos with 50 ng pGL3 promoter, at 16^oC, O/N.

f. Perform transformations and contrasfect with pSG5-Runx2, pSG5-Erf and pGL3 promoter oligos in HeLa cells. **GGATGTGG.**

	RxErf d1	RxErf d5	RxErf d10
Forward	CTAGAGA**GGATGTGG**TTT	CTAGAGA**GGATGATCG**TGTGGTTT	CTAGAGA**GGATG**AT CGATCGATGTGGTTT
Reverse	GATCAAACCACATCCTCT	ATCAAACCACACGATCATCCTCT	GATGAAACCACATCGATC GATCCATCCTCT

10. Transfection with $CaCl_2$

a. Grow 1.5 – 2 x 10^5 cells/ well with 3 ml medium in 6 well plate at 37ºC, 5% CO_2.

b. Next day cells (80 – 90 % confluency), discard medium and incubate with new one with 10 mM Hepes.

c. Prepare DNA samples:

- 3 µg DNA in 75 µl ddH_2O containing:

  2.25 µg effector (etc pSG5-Erf),

  0.25 µg reporter (etc pGL3-promoter),

  µg plasmids for efficiency (e.t.c. pGFP or RSVGal4)

- 75 µl 0.5 M $CaCl_2$

d. Add 150 µl Solution H/ well <u>in the centre</u> in a 24 well plate (must be cold) (from a relative height by dropping).

e. Add DNA/$CaCl_2$ (from a relative height by dropping). Pipette 2-3 times and let for 15-25 min, RT (check precipitation occurs in microscope).

f. Add the previous mix from a relative height in the cells in all the surface of well. Do not mix!!

g. Incubate at 37ºC, 5% CO_2.

h. Next day, add new medium and this day or after one more day check GFP for transfection efficiency.

Optionally

After 4 hrs incubation:

a. Discard medium and add 1 ml glycerol solution/ well.
b. Incubate 100 sec.
c. Discard glycerol solution and add immediately 1 ml growth media.
d. Discard and add 3 ml growth media.

Transfection Media

10 x HBS	Solution H	Glycerol solution 15%
1.37 M NaCl	10 ml 10xHBS	5 ml Solution H
0.05 M KCl	2 ml 1 M Hepes	1.5 ml sterile glycerol
0.007 M $Na_2HPO_4.7H_2O$	38 ml H2O	3.5 ml sterile ddH2O
0.06 M Dextrose (or glycose)		
Filter in 0.22 nm		

11. Luciferase assay

a. Discard medium of cell culture.
b. Wash twice with 1x PBS.
c. Add 1ml PBS with 1mM EDTA and transfer cells in eppendorfs.
d. Spin at 200 g, 5min, RT.
e. Resuspend pellet in 100 µl 1x RLB lysis buffer /well and freeze at – 80 ^oC for 10 min.
f. Place at 37 ^oC for 2 min.
g. Spin at 200 g for 2 min at 4 ^oC.
h. Transfer the supernatant in new eppendorfs on ice.
i. Add 10 µl luciferin with buffer in 10 µl sample.
j. Mix and count photons at luciferase machine (10 sec).

12. β - galactosidase assay

a. Wash cells with 1 x PBS.
b. Harvest with PBS with 1 mM EDTA.
c. Spin at 300 g for 1 min.

d. Dilute with 100 µl 1 x RLB cell lysis buffer.
e. Freeze at -80ºC.
f. Defreeze and spin at 16000 g for 2 min.
g. Add the following mix in 50 µl cell extract:
    - 550 µl Reaction buffer
    - 1.25 µl b-mercaptoethanol (14.3 M)
    - 100 µl ONPG (4 mg/ml)
    - ddH_2O up to 700 µl
h. Incubate at 37 ºC until become yellow.
i. Add 200 µl 1M Na_2CO_3 to stop the reaction.
j. Count absorption at 410 nm (0.1-1)

Reaction buffer (60 mM Na_2HPO_4, 40 mM NaH_2PO_4,10 mM KCl,1 mM $MgSO_4$)

13. Staining of cartilage and bone in adult mice

a. Remove all the tissues of the sacrificed mouse and let only skull land skeletal as more clear as possible.
b. Fix mice in 90% EtOH for ~ 3 days.
c. Rehydrate in 96% EtOH for ~ 3 days.
d. Place in acetone for 2 days to remove any residual fat.
e. All the following steps are done in the dark:
f. Stain ~ 10 days in filtered staining solution, RT
- 1 vol 0.1% Alizarian red S (in chemical drawer), in 70% EtOH (filtered)
- 1 vol 0.1% Alcian blue 8GS (in chemical drawer), in 70% EtOH (filtered)
- 1 vol acetic acid
- 17 vol 95 % EtOH

g. Rehydrate in 90%, 70%, 40%, 15% ethanol and H_2O.
h. Wait until samplesto sink.
i. Clear in 1% aqueous K-OH for ~ 3 days.
j. Clear in for 30 min:
- (20% glycerol) 1 vol glycerol/4 vol 1% KOH
- (50% glycerol) 1 vol glycerol/1 vol 1% KOH
- (80% glycerol) 4 vol glycerol/1 vol 1% KOH

- Standard glycerol from general stores was used.

k. Store skeletal preparations in 100% glycerol in the dark.

3. Results

Part I: Hematopoiesis

1. *Erf*$^{ed/ed}$ embryos die in utero due to severe anemia.

We have previously shown that elimination of *Erf* in mice leads to lethality at E10.5 because of failed chorioallantoic fusion and labyrinth development (31). To investigate other developmental processes that *Erf* may regulate bypassing the placental defect, we eliminated *Erf* in the epiblast at E5 crossing *Erf*$^{loxP/loxP}$ mice with mice expressing the cre recombinase under the control of the *Meox2* gene (Tallquist and Soriano, 2000). The exact breeding was between males *Meox2*$^{Cre/+}$*;Erf*$^{+/-}$ and females *Erf*$^{loxP/loxP}$ with expected genotypes *Erf*$^{loxP/+}$, *Erf*$^{loxP/-}$, *Meox2*$^{Cre/+}$*;Erf*$^{loxP/+}$ *(Meox2*$^{Cre/+}$*;Erf*$^{+/-}$*)*, *Meox2*$^{Cre/+}$*;Erf*$^{loxP/-}$ *(Meox2*$^{Cre/+}$*;Erf*$^{-/-}$*)* in a Mendel frequency 25% for each one. *Erf* conditional knockout will be named as *Erf*$^{ed/ed}$ for both brevity reasons and discrimination from full *Erf* knockout. After birth, mice were genotyped for detection of *Meox2Cre* and *loxP* site. Genotyping resulted in no band for Meox2cre and loxP (or none) in the same sample, indicating that *Erf*$^{ed/ed}$ die before birth. In order to confirm the critical day of lethality, embryos were isolated at E11.5 – E16.5 and genotyped for *Meox2Cre* gene and *loxP* site. Our results indicate that elimination of *Erf* in the epiblast leads to embryonic death after E14.5 (Figure 1A). However, there was a variation in survival as we could find a few alive embryos at E15.5 and only 1 out of 23 at E16.5. The exact number of litters that was employed for calculation of Mendelian sequences is presented in Table 1. Chi square test showed the statistical important decrease with the expected Mendelian distribution.

Another point is that embryos were pale indicative of anemia (Figure 1B). To confirm the anemia as the main reason of lethality, the blood circulating cells of E14.5 embryos were counted. Our results indicated that *Erf*$^{ed/ed}$ fetuses dropped to less than 5% of the normal *Erf*$^{ed/ed}$ embryos, confirming that *Erf*$^{ed/ed}$ embryos die because of anemia. A few *Erf* knockout fetuses exhibited a few higher levels of circulating blood at E14.5, consistent with the occasional survival until E15.5 or E16.5. On the contrary, *Erf*$^{ed/ed}$ embryos contained approximately 50% of normal circulating blood cells between E9.5 through

E13.5 (Table 2), days in which the primitive wave constitutes the predominant wave (95%) (Figure 1C), indicating that the defect has begun very early in hemopoiesis, already from the production of primitive wave. Provided that EMPs begin to migrate from the liver to the periphery at E14.5, comprising ~ 40% of the total circulating blood (Fraser et al., 2007), the main drop of number of cells to 5% at this day is due to defects both in primitive and definitive wave.

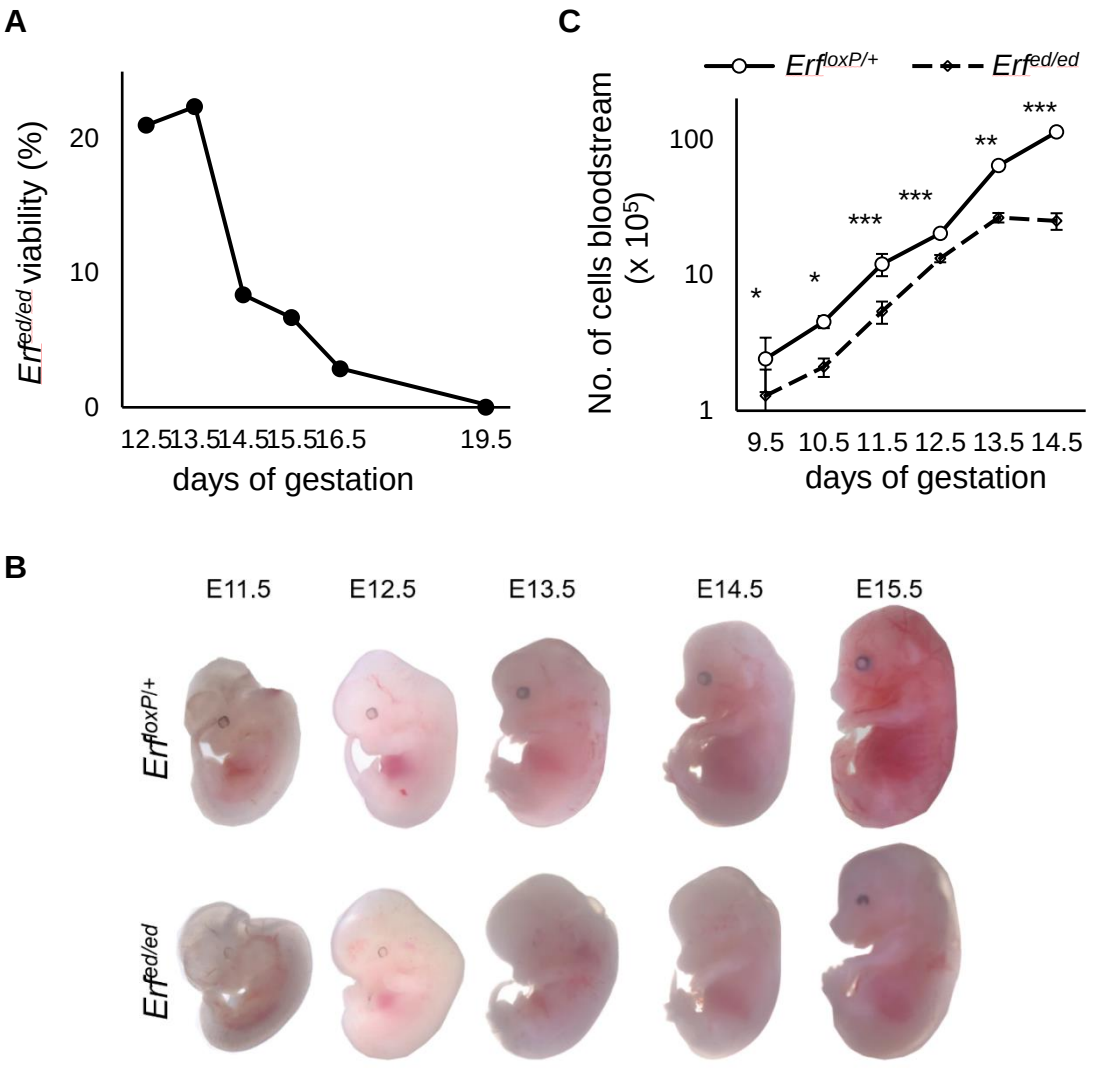

Figure 1. *Erf*$^{ed/ed}$ mice are embryonic lethal and appear anemic. (A) Pregnant mice were sacrificed at the indicated day of gestation and the genotype of the embryos was analyzed. The graph indicates the percentages of alive *Erf*$^{ed/ed}$ embryos. The data are from 160 litters with at least 5 litters for each gestation stage (Table 1). Chi square test showed statistical important decrease with the expected mendelian distribution, after E13.5. **(B)** Representative microphotographs of embryos at E11.5 – E15.5 showing an

apparent anemia and lack of other gross morphology differences of *Erf*$^{ed/ed}$ embryos compared to their *Erf*$^{floxP/+}$ littermates. **(C)** Number of blood cells from the yolk sac and embryo proper at the indicated day of gestation. *Erf*$^{ed/ed}$ embryos exhibit statistically significant decrease throughout E9.5 – E13.5 exacerbated at E14.5. Samples are represented in a logarithmic scale. All values are means ± SE from 35 litters with at least 7 litters for each gestation stage Table 2). Statistical analysis performed using the unpaired t-test with two-tailed distribution. *, $P < 0.05$, **, $P < 0.005$, ***, $P < 0.0005$ for *Erf*$^{floxP/+}$ vs *Erf*$^{ed/ed}$.

Table 1. Number of *Erf*$^{ed/ed}$ embryos in each gestation day, whose lethality was measured as shown in Figure 1A.

Embryonic day	**No. of litters**	**No. of *Erf*$^{ed/ed}$ *embryos***	**No. of total embryos**
9.5	5	6	48
10.5	12	12	86
11.5	12	17	91
12.5	39	45	219
13.5	27	32	152
14.5	15	9	102
15.5	5	2	26
16.5	5	1	23
adult	38	0	248

Table 2. Number of embryos, whose number of cells in bloodstream was counted in each gestation day (epiblast derived conditional mice) as shown in Figure 1C.

		No. of embryos for peripheral blood counts	
Embryonic day	**Litters**	***Erf*$^{floxP/+}$**	***Erf*$^{ed/ed}$**
9.5	3	9	4
10.5	9	24	15
11.5	9	15	11
12.5	5	13	7
13.5	3	3	4
14.5	6	13	7

2. *Erf* elimination in epiblast does not affect placenta development

It has been previously shown that elimination of *Erf* in mice leads to lethality at E10.5 because of failed chorioallantoic fusion and therefore labyrinth development (Papadaki et al., 2007). Here, we used an epiblast derived *Erf* conditional deleted mouse in order to study the role of Erf in the embryo proper. To confirm that conditional *Erf* knockout mice do not die because of placenta defects, we isolated placentas at E12.5 – E13.5 and tested the proper formation of its three layers: labyrinth, spongiotrophoblast and giant cells (E. D. Watson and Cross, 2005). The labyrinth is consisted by a bilayer of syncytiotrophoblasts, which surrounds the fetal blood vessel endothelium and the layer of mononuclear cells which lines the maternal blood sinuses. At E8.5 labyrinth has formed by the process of chorioallantoic attachment, where the allantois and the chorion join together. Specifically, the chorion begins to fold to form the villi, creating a space into which the fetal blood vessels grow from the allantois. The labyrinth is supported structurally by an ectoplacental cone-

derived layer called the spongiotrophoblast. Spongiotrophoblast is a compact layer of cells sandwiched between the labyrinth and the outer giant cell layer (E. D. Watson and Cross, 2005).

In order to investigate possible defect in the three layers of placenta, we performed RNA In Situ Hybridization with the RNA probes Tef-5 for syncytiotrophoblast, 4311 for spongiotrophoblasts and Pl1 for giant cells (Figure 2A, B) in E12.5 -E13.5 placenta sections. Our results indicate no defect in all the three layers. Moreover, the morphology of hematopoietic cells looked normal with maternal and embryonic blood to be in proximity in order nutrients to be exchanged (Figure 2C).

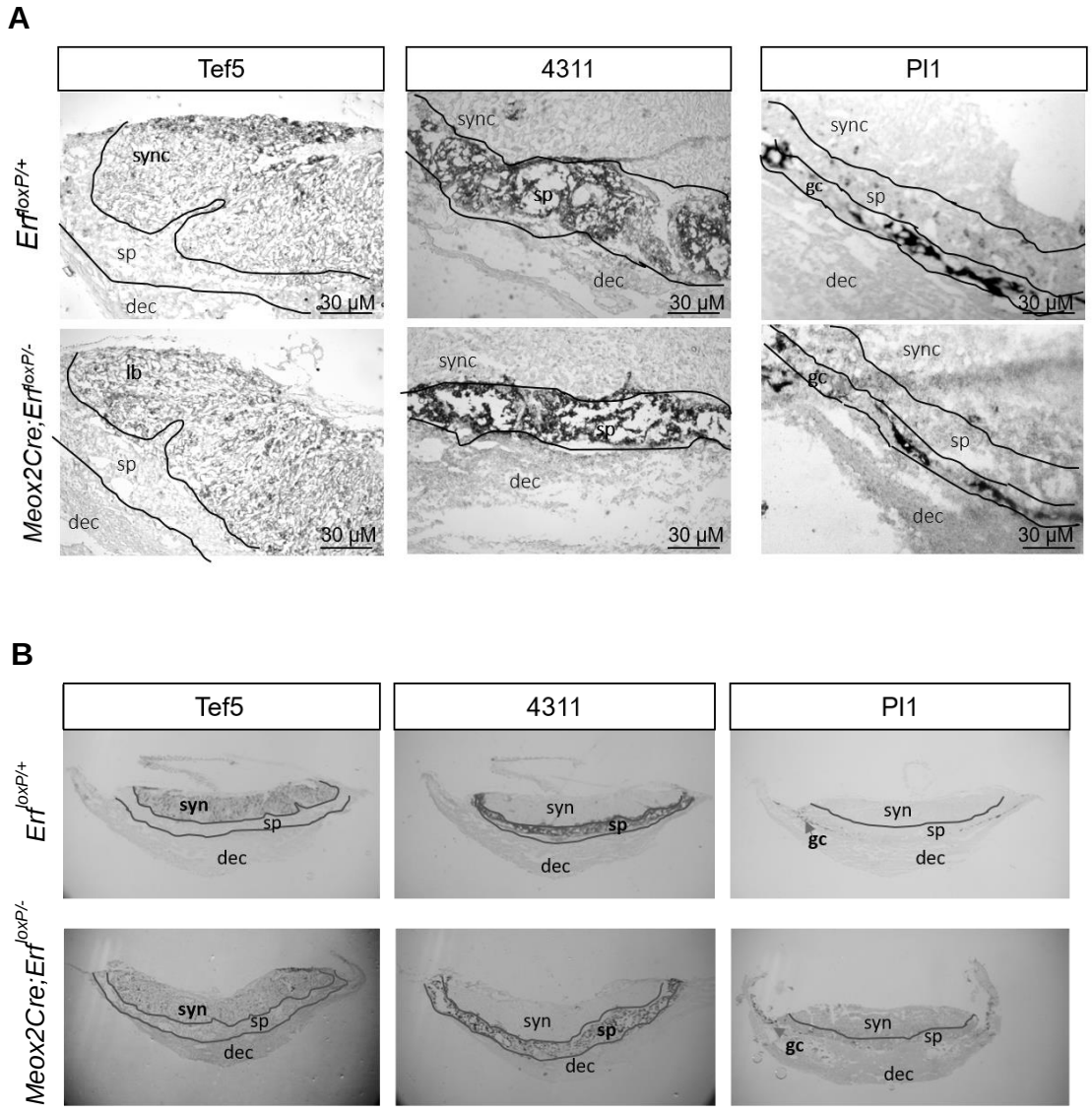

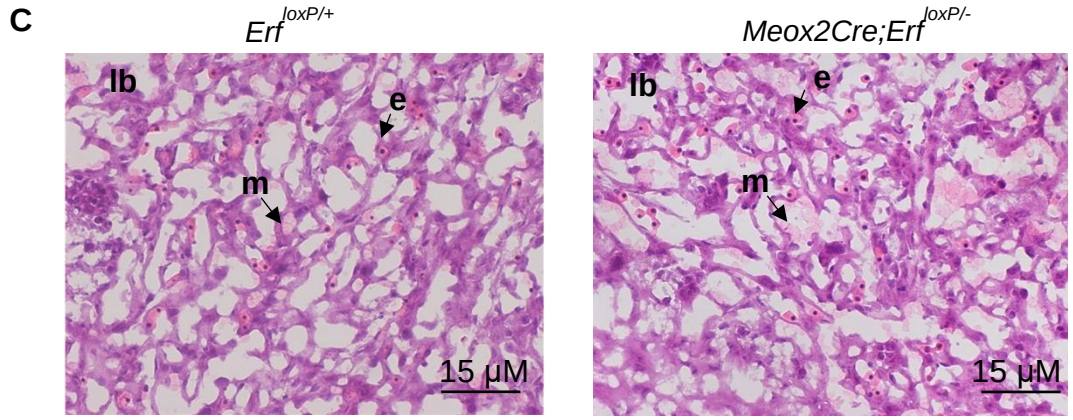

Figure 2. *Erf*$^{ed/ed}$ embryos have no placenta defects and normal erythroblasts. (A) RNA in Situ hybridization on cryosections from E13.5 placentas with the cell type specific markers *Tef5, 4311* that label the syncytiotrophoblast and the spongiotrophoblast respectively and from E12.5 placenta with the marker *Pl1* that labels giant cells layer. **(B)** as (A) but samples were photographed by a stereoscope in order to be visible all the section. Placentas of *Meox2cre; Erf*$^{loxP/-}$ concepti that nurture *Erf*$^{ed/ed}$ embryos appear comparable to their *Erf*$^{loxP/+}$ counterparts. sync: synciotrophoblast, sp: spongiotrophoblast, dec: decidua, gc: giant cells. **(C)** Hematoxylin & Eosin staining fro E13.5 placentas. The nucleated embryonic erythroblasts € and the enucleated maternal erythrocytes (m) are there.

Additional experiments were performed to detect *Erf* elimination in the different cell types of placenta. We crossed *Yfp;Erf*$^{loxP/loxP}$ (Srinivas et al., 2001) mice with *Meox2*$^{Cre/+}$*;Erf*$^{+/-}$ mice. Yfp is a yellow fluorescent protein, which has been inserted after the promoter of a ubiquitously expressed gene, Rosa. A transcriptional stop codon is flanked between loxP sites and this region has been inserted between Rosa promoter and Yfp gene. When cre recombinase is expressed, recognizes the loxP sites, the stop codon is deleted and as a result Yfp is expressed (Figure 3A). To that extend, we studied the *Meox2cre* expression employing immunostaining against YFP in cryosections of placenta, as indicative of Erf elimination. Our results demonstrate that only the vasculature system, which has arisen from allantois, is YFP positive (green) as expected (Figure 3B). This indication is based on the morphology of vasculature, and without employing specific markers for vasculogenesis.

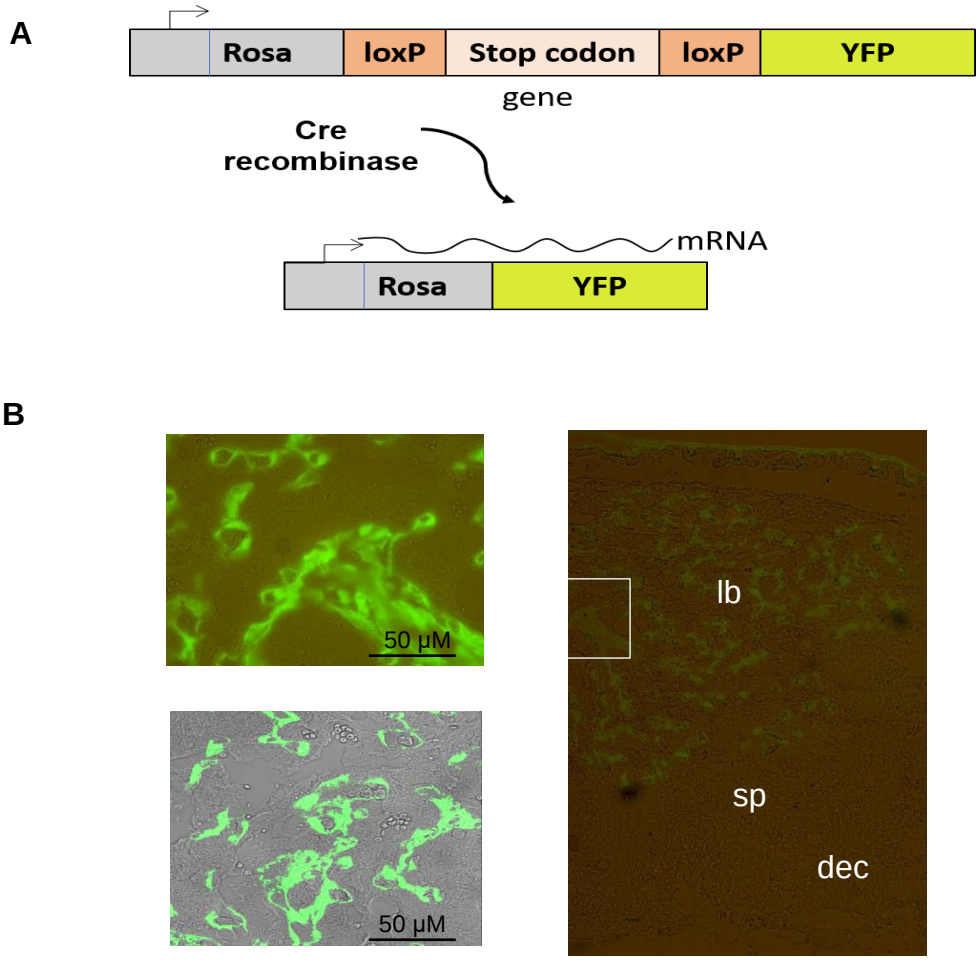

Figure 3. YFP expression in *Meox2*$^{Cre/+;}$ *Erf*$^{loxP/-}$ placentas. (A) YFP constuct. YFP is inserted under the Rosa promoter. When Cre recombinase recognizes the loxP sites deletes the stop codon and then YFP is expressed. **(B)** Expression of YFP protein in *Meox2*$^{Cre/+;}$*Erf*$^{loxP/-}$ placentas. Immunofluorescence against YFP indicates the expression of YFP only in allantois. Magnification 40x on the left and a collapse of 2 pictures magnified 10x on the right. Down left photo is a visible fluorescent photo to see the morphology of all cell types. lb: labyrinth, sp: spongiotrophoblast, dec: decidua.

3. *Erf* does not affect vasculogenesis of yolk sac and embryo

The vasculature system is essential for the circulation of hematopoietic cells. It arises from mesoderm (Samokhvalov, 2012) and there are indications that it comes from hemogenic endothelium. Hemogenic endothelium gives rise to both endodermal cells of vasculature system and hematopoietic cells. When

vascular system is fully formed at E8.25 in yolk sac, endothelial hematopoietic transition (EHT) occurs and the first hematopoietic cells are produced (C. Zhang et al., 2014)

To exclude the fact that the reduced number of hematopoietic cells is result of defects in vascular system, we studied vasculogenesis in both yolk sacs and embryos. To that extend, we stained *Erf*$^{ed/ed}$ yolk sacs and embryos with the marker PECAM1 at E10.5. Our results indicate that the vasculature of yolk sacs and embryos appeared normal with vascular networks proper in width and in branching (Figure 4A and B, respectively). According to that, *Erf*$^{ed/ed}$ mice have normal vasculature of the yolk sac and the embryo, indicating vasculogenesis not being the reason of lethality.

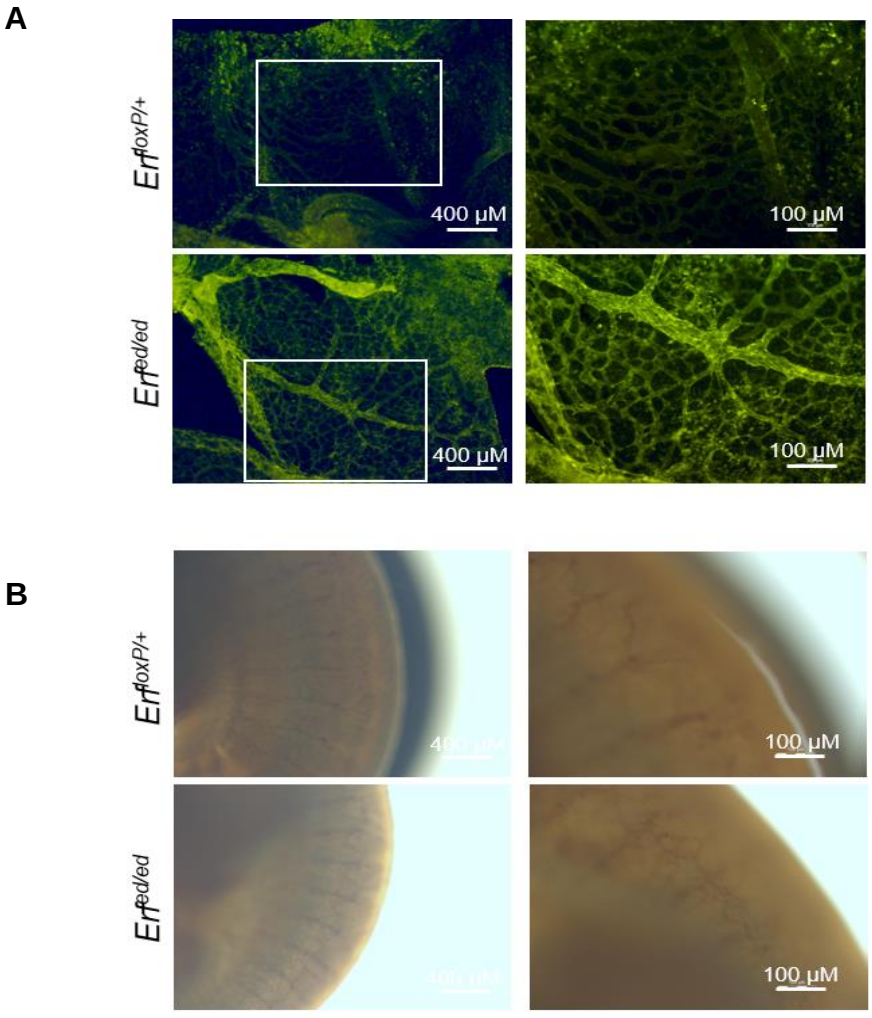

Figure 4. *Erf*$^{ed/ed}$ yolk sacs and embryos exhibit normal vasculogenesis. (A) Fluorescent microphotographs of yolk sac and **(B)** HRP- staining with of embryos from *Erf*$^{loxP/+}$ and *Meox2cre;Erf*$^{ed/ed}$ (*Erf*$^{ed/ed}$) at E10.5, with the angiogenesis marker PECAM-

1. The white boxes on the images on the left indicate the magnified area of the image on the right. In embryos it was difficult to be found the same site for magnification

4. *Erf*$^{ed/ed}$ mice have normal mesothelium and visceral endoderm junctions, but immature primitive progenitors

To confirm that the reduced number of hematopoietic cells at E9.5 yolk sacs is not because of no proper junctions between mesothelium and visceral endoderm as was previously found in *Erf* full knockout by Papadaki *et al.* and moreover to confirm right blood islands formation, we performed hematoxylin and eosin staining in E9.5 yolk sacs.

Our results indicate that at E9.5, the *Erf*$^{ed/ed}$ yolk sac revealed normal mesothelium and visceral endoderm junctions but the blood islands contained fewer and larger primitive erythroblasts (Figure 5A). It is known that more than 95 % of the circulating erythroid cells from E9.5 to E12.5 derive from the primitive wave of hematopoietic progenitors in the yolk sac (Fraser et al., 2007). Thus, the reduced numbers of circulating blood cells would suggest an emergence or a maturation defect in primitive erythropoiesis.

Moreover, photos of whole mounts at E12.5 show that *Erf*$^{ed/ed}$ yolk sacs are pale, confirming the reduced numbers of primitive cells (Figure 5B).

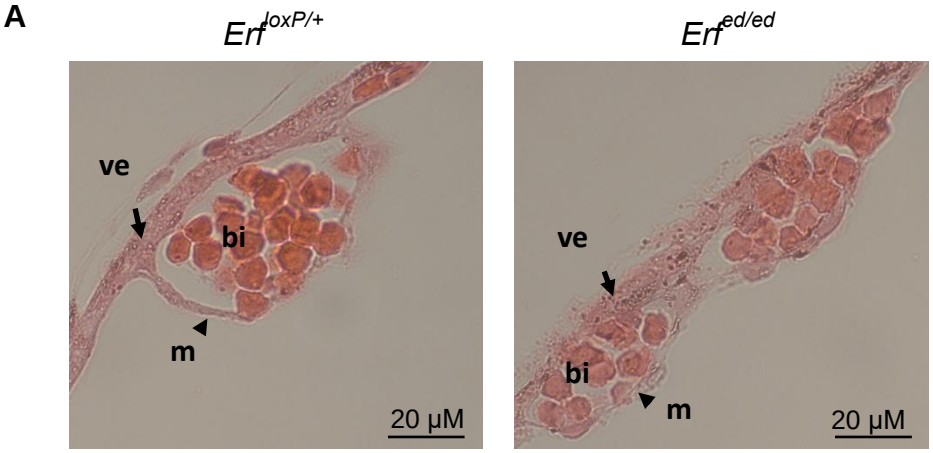

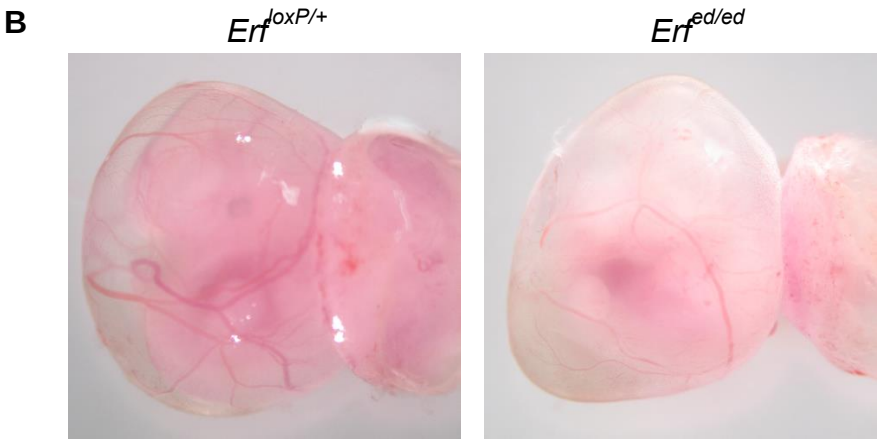

Figure 5. *Erf*$^{ed/ed}$ yolk sacs have normal mesothelium and visceral endoderm junctions but exhibit immature primitive erythroid progenitors. **(A)** Sagittal sections of paraffin-embedded yolk sacs from E9.5 *Erf*$^{ed/ed}$ and *Erf*$^{loxP/+}$ embryos stained with H&E. ve: visceral endoderm, m: mesothelium, bi: blood islands. **(B)** Whole mounts of yolk sacs with embryos and placenta at E12.5.

5. *Erf* elimination impairs primitive erythropoiesis.

Because of the onset of anemia as early as E9.5, we initially examined erythropoiesis at E9.5 and E10.5, when erythroblasts mature semi-synchronously. As it is known, more than 95 % of the circulating erythroid cells from E9.5 to E12.5 derive from the primitive wave of hematopoietic progenitors in the yolk sac (Fraser et al., 2007). Thus, both the reduced numbers of circulating blood cells, shown in figure 1C, and the more immature primitive progenitors shown in figure 5A would suggest a defect in primitive erythropoiesis. To confirm the more immature phenotype of primitive cells observed in the previous staining of H&E in yolk sac, staining of blood smears of E10.5 peripheral blood was performed with Giemsa. Our results confirmed that in the absence of *Erf*, primitive erythroblasts are larger and contain enlarged nuclei with less condensed chromatin (Figure 6).

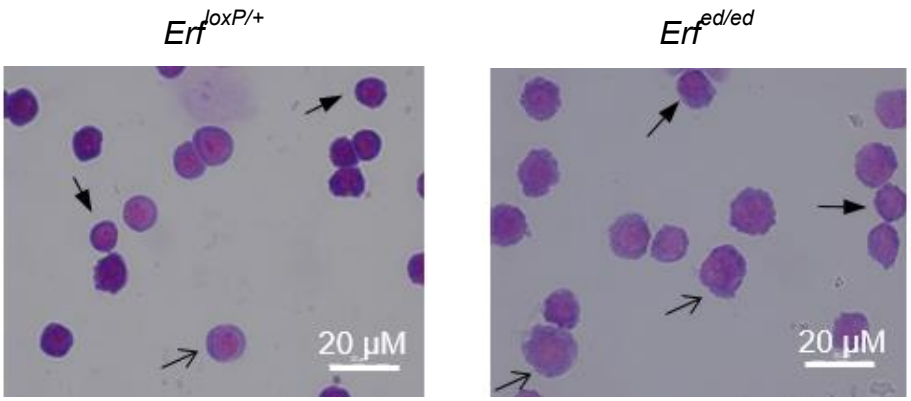

Figure 6. *Erf*$^{ed/ed}$ yolk sacs exhibit immature primitive erythroid progenitors. Representative microphotographs of giemsa stained peripheral blood cells from E10.5 embryos. *Erf*$^{ed/ed}$ cells exhibit larger primitive precursor cells with less condensed chromatin and larger nuclei than their Erf-expressing littermates. Arrow indicates the most immature, larger, progenitors while filled arrow indicates the most mature, smaller, progenitors in each genotype.

Moreover, we analyzed globin mRNA levels by real-time PCR at E10.5 – E11.5 peripheral blood. We used βH1 and εy globin, expressed in immature, and in the more mature primitive cells, respectively, and βmajor globin expressed in the definitive hematopoietic cells (Kingsley et al., 2006). Our results indicate that mRNA levels of *εy*-globin of *Erf*$^{ed/ed}$ embryo after normalization to Gapdh was significantly lower than their *Erf*-expressing littermates at both E10.5 and E11.5, consistent with delayed maturation (Figure 7A). mRNA levels of βH1 did not show any difference (not shown). This happens probably because some definitive cells express βH1 globin. In addition, mRNA levels of βmajor globin were reduced in *Erf*$^{ed/ed}$ embryos at E11.5, indicating an additional defect in EMPs (Figure 7B). In conclusion, these data indicate that elimination of *Erf* results both in decreased numbers and in delayed maturation of primitive erythroid precursors.

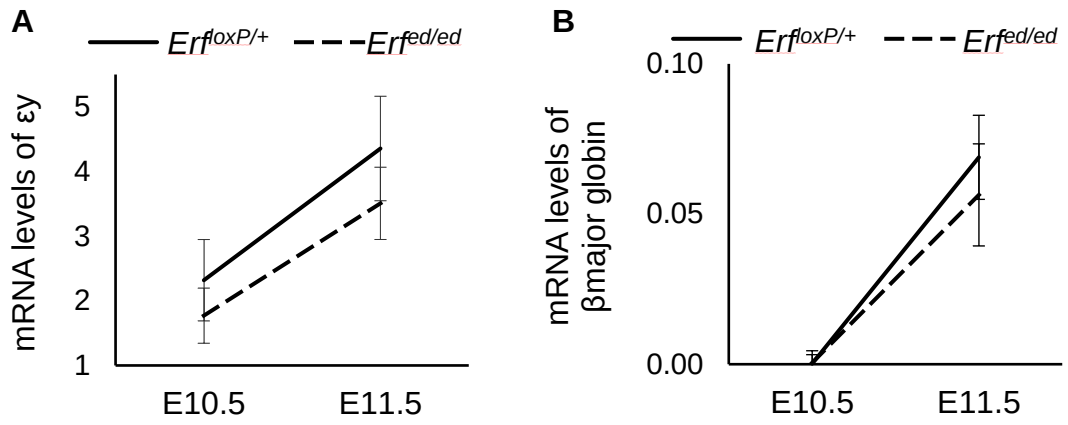

Figure 7. εy globin is reduced in primitive erythrocytes and βmajor in EMPs. (A) εy globin and **(B)** βmajor mRNA levels normalized to Gapdh mRNA levels, were determined by qPCR in blood cells from E10.5 and E11.5 in *Erf*$^{ed/ed}$ and *Erf*$^{floxp/+}$ embryos. βH1did not show any difference probably because of some expression also in EMPs (not shown). All values are means ± SE of at least 6 biological samples of each genotype from 6 litters at E10.5 and of at least 11 biological samples of each genotype from 7 litters at E11.5.

6. *Erf* elimination impairs yolk sac-derived definitive erythroblasts.

The first circulating definitive erythroid cells that emerge at E11.5 - E12.5 are derived from EMP / BFU-E that have seeded the fetal liver (Palis et al., 1999). The profound anemia at E13.5 – 14.5 suggested a defect in EMP. To explore the effect of *Erf* elimination on the progenitors of the definitive hematopoietic wave that emerges in the yolk sac, peripheral blood was isolated at E10.5 and the c-Kit ^{high}, CD41^{+}, CD16/32^{+} erythroid-myeloid progenitor cells (EMP) cells were quantitated by flow cytometry (McGrath et al., 2015). Cells expressing high levels of c-Kit (left panel) that were positive for CD41 and CD16/32 (right panel) were considered the EMP fraction (Figure 8A). As shown in figure 8B, *Erf*$^{ed/ed}$ embryos have half phenotypic EMPs compared to their *Erf*-expressing littermates. Moreover, number of colonies per plate was reduced (data not shown). Consistent with the loss of phenotypic EMP, the number of definitive erythroid progenitors BFU-E and CFU-E, defined by their ability to form colonies in semisolid media, was also significantly reduced at E10.5 (Figure 8C). BFU-E (Burst forming untit erythroid cells) are containing >200 erythroblasts, usually present in >2 clusters and differentiate to CFU-E (colony forming erythroid cells)

containing 1 - 2 clusters with a total of 8 - 200 erythroblasts, differentiating to erythrocytes after 5 divisions. To note that colonies are formed only in semisolid media and in vivo. Number of colonies were counted in each plate and the total number was estimated based the total cell counts in E10.5 peripheral blood of each sample. Numbers were compared to the average number of the *Erf*$^{floxP/+}$ BFU-E / CFU-E colonies of the litter, because the timing of the plug changes the number of cells dramatically at the same day. Taken together both flow cytometry and colony forming assay, these data confirm that the yolk sac-derived EMP wave of hematopoietic potential is also decreased by the loss of *Erf*.

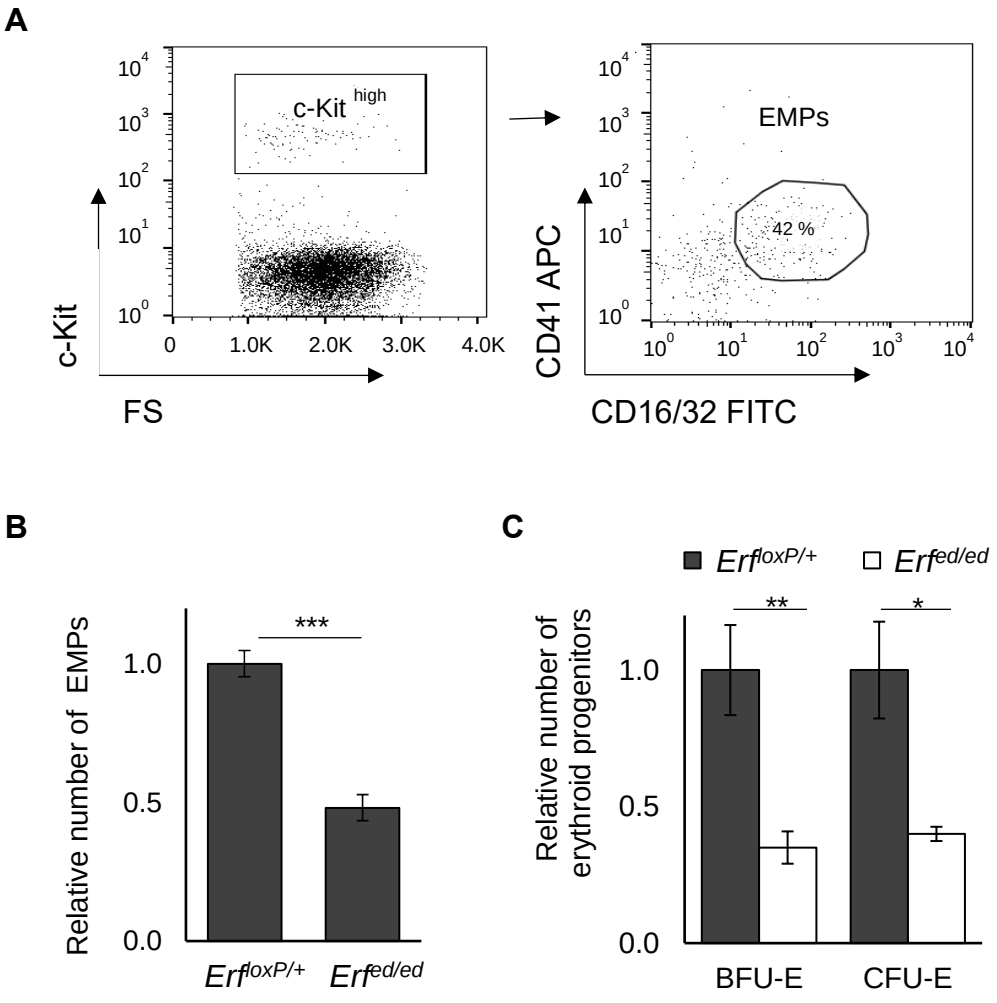

Figure 8. *Erf*$^{ed/ed}$ have decreased definitive progenitors in bloodstream. (A) Representative flow cytometry analysis of blood from E10.5 embryos stained with anti-c-Kit, anti-CD41 and anti CD16/32 antibodies. Cells expressing high levels of c-Kit (left panel) that were positive for CD41 and CD16/32 (right panel were considered the EMP fraction). **(B)** EMP (c-Kit ^{high}, CD41^{+}, CD16/32^{+}) cells from E10.5 *Erf*$^{ed/ed}$ and *Erf*$^{floxP/+}$

embryonic blood were compared to the average number of the Erf $^{loxP/+}$ EMP cells of the litter. All values are means ± SE of 4 biological samples of each genotype from 3 litters. Statistical analysis performed using the unpaired t-test with two-tailed distribution. ***, P < 0.0005. **(C)** Number of BFU-E and CFU-E colonies derived from E10.5 *Erf*$^{ed/ed}$ and *Erf*$^{loxP/+}$ embryo blood were compared to the average number of the *Erf*$^{loxP/+}$ BFU-E / CFU-E colonies of the litter. All values are means ± SE of 6 biological samples of each genotype from 3 litters. Statistical analysis performed using the unpaired t-test with two-tailed distribution. *, P < 0.05, **, P < 0.005, ***, P < 0.0005.

7. Elimination of *Erf* in hemogenic endothelium recapitulates the *Erf*$^{ed/ed}$ hematopoietic phenotype in definitive hematopoiesis.

To determine if Erf exerts a cell autonomous effect on hematopoietic development, we deleted *Erf* in the hemogenic endothelium, utilizing the *Lyve1*$^{tm1.1(EGFP/cre)Cys}$ mice, which express the cre recombinase under the control of the *Lyve1* gene. Recently, it has been shown that *Lyve1* is expressed in hemogenic endothelium and specifically marks EMP but not the primitive hematopoietic wave that emerges in the yolk sac (L. K. Lee et al., 2016). In addition, *Lyve1* is expressed later in blood and lymphatic vessels, lymph nodes, liver, spleen sinuses and lung and endocardial endothelial cells (Okuda et al., 2012; Schlereth et al., 2014; L. K. Lee et al., 2016). *Lyve1*$^{tm1.1(EGFP/cre)Cys/tm1.1(EGFP/cre)Cys}$*Erf*$^{loxP/loxP}$ (*Lyve1*$^{Cre/Cre}$ *Erf*$^{loxP/loxP}$) mice died in utero and appeared anemic, a phenotype analogous to the epiblast-specific *Erf*$^{ed/ed}$ embryos. They were pale (Figure 9A), and at E10.5 showed reduced BFU-Es / CFU-E (Figure 9B), indicating a defect in EMPs before their migration to the liver. At E13.5 they exhibited decreased liver cell numbers and at E14.5 severely reduced blood cells in the bloodstream (Figure 4C and D, respectively). Immunofluorescence in cryosections of E12.5 livers showed decreased percentage of Ter119 cells and no difference in CD71 (data not shown) indicating a consistent phenotype with *Erf*$^{ed/ed}$ embryos in liver definitive wave (see below). Both the small liver size and the reduced number of circulating blood cells suggest impaired EMP-derived hematopoiesis, similar to that observed in epiblast *Erf*-null embryos (see below). This would be indicative of a cell-autonomous defect of *Erf* elimination, specifically in the definitive

hematopoietic wave of the yolk sac. Moreover, yolk sacs and embryos had no vasculogenesis defects. However, a strange phenomenon is that total counts of blood cells at E10.5 – E13.5 peripheral blood was reduced at 50 % in *Lyve1*$^{Cre/Cre}$ *Erf*$^{loxP/loxP}$compared to *Erf*$^{+/+}$ mice, indicating an additional defect in primitive wave, while Lyve1 is not expressed neither in primitive cells nor the microenvironment of yolk sac.

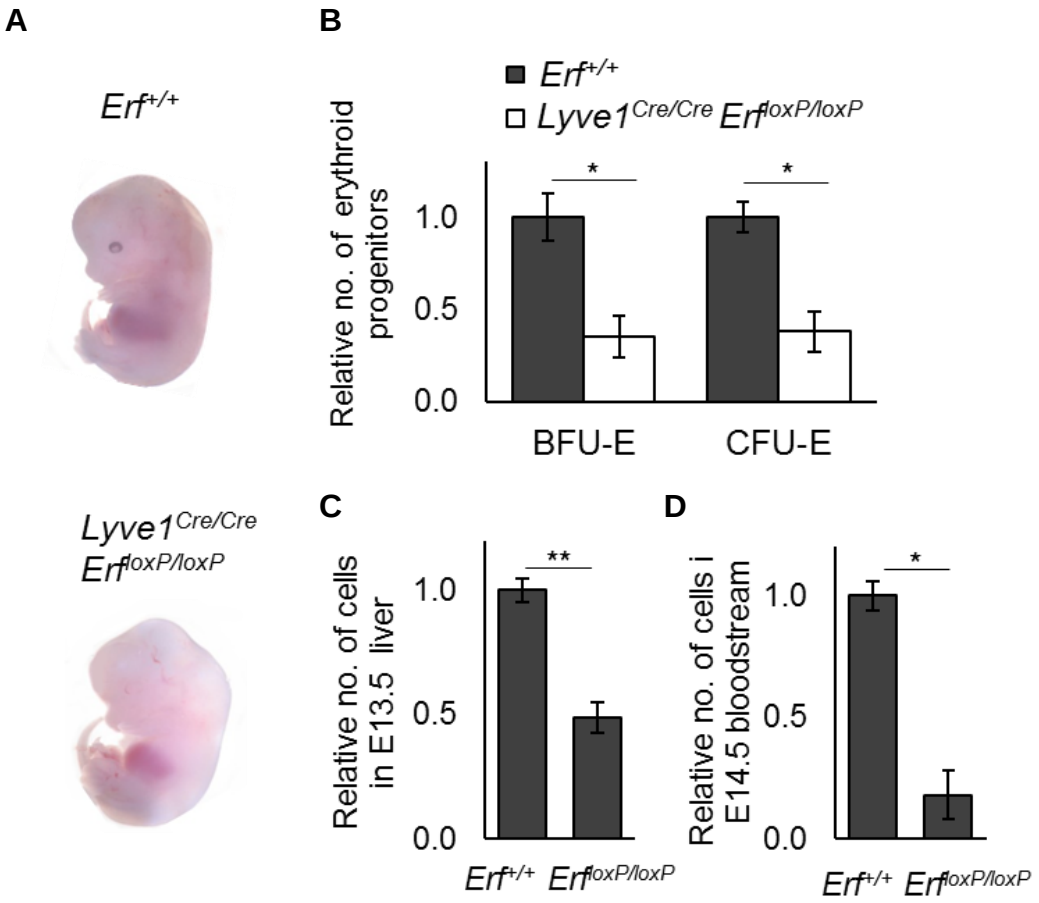

Figure 9. Elimination of *Erf* in definitive yolk sac wave leads to anemia. **(A**) Representative microphotographs of embryos at E13.5 showing an apparent anemia of *Lyve1*$^{tm1.1(EGFP/cre)Cys/tm1.1(EGFP/cre)Cys}$ *; Erf*$^{loxP/loxP}$ *(Lyve1*$^{Cre/Cre}$ *Erf*$^{loxP/loxP}$*)* embryos compared to their *Erf*$^{+/+}$ littermates. **(B)** Number of BFU-E and CFU-E colonies derived from E10.5 *Lyve1*$^{Cre/Cre}$ *Erf*$^{loxP/loxP}$ and *Erf*$^{+/+}$ embryo blood were compared to the average number of the Erf $^{+/+}$ BFU-E / CFU-E colonies of the litter. All values are means ± SE of 4 biological samples from 2 litters. Statistical analysis performed using the unpaired t-test with two-tailed distribution. *, P < 0.05. **(C)** Total liver cell counts of *Lyve1*$^{Cre/Cre}$ *Erf*$^{loxP/loxP}$ embryos compared to the *Erf*$^{+/+}$ littermates at E13.5. All values are means ± SE

of 2 biological samples of each genotype from 2 litters. Statistical analysis performed using the unpaired t-test with two-tailed distribution. *, P < 0.05, **, P < 0.005. **(D)** Total cell counts of *Lyve1*$^{Cre/Cre}$ *Erf*$^{loxP/loxP}$ embryos compared to the *Erf*$^{+/+}$ littermates at E14.5 bloodstream. All values are means ± SE of 2 biological samples of each genotype from 2 litters. Statistical analysis performed using the unpaired t-test with two-tailed distribution. *, P < 0.05.

Table 3. Number of embryos isolated in each gestation day (hemogenic endothelium derived mice).

		No. of embryos for peripheral blood counts	
Embryonic day	**litters**	***Erf*$^{+/+}$**	***Lyve1*$^{Cre/Cre}$ *Erf*$^{loxP/loxP}$**
10.5	6	25	7
11.5	2	6	3
12.5	2	7	2
13.5	2	5	2
14.5	2	8	2

Surprisingly, in contrast to the *Lyve1*$^{Cre/Cre}$ *Erf*$^{loxP/loxP}$ embryos, *Lyve1*$^{Cre/+}$ *Erf*$^{loxP/loxP}$ mice were viable albeit with sub-mendelian frequencies (Figure 10D). Analysis, of the *Erf* expression in fetal livers showed that heterozygous *Lyve1*-cre embryos have significantly higher expression than the homozygous *Lyve1*-cre as well as the *Meox2*-cre embryos (Figure 10C). This would suggest that the frequency of *Erf* elimination and/or the level of expression of *Erf* in EMPs may be critical for the severity of the defect and thus survival.

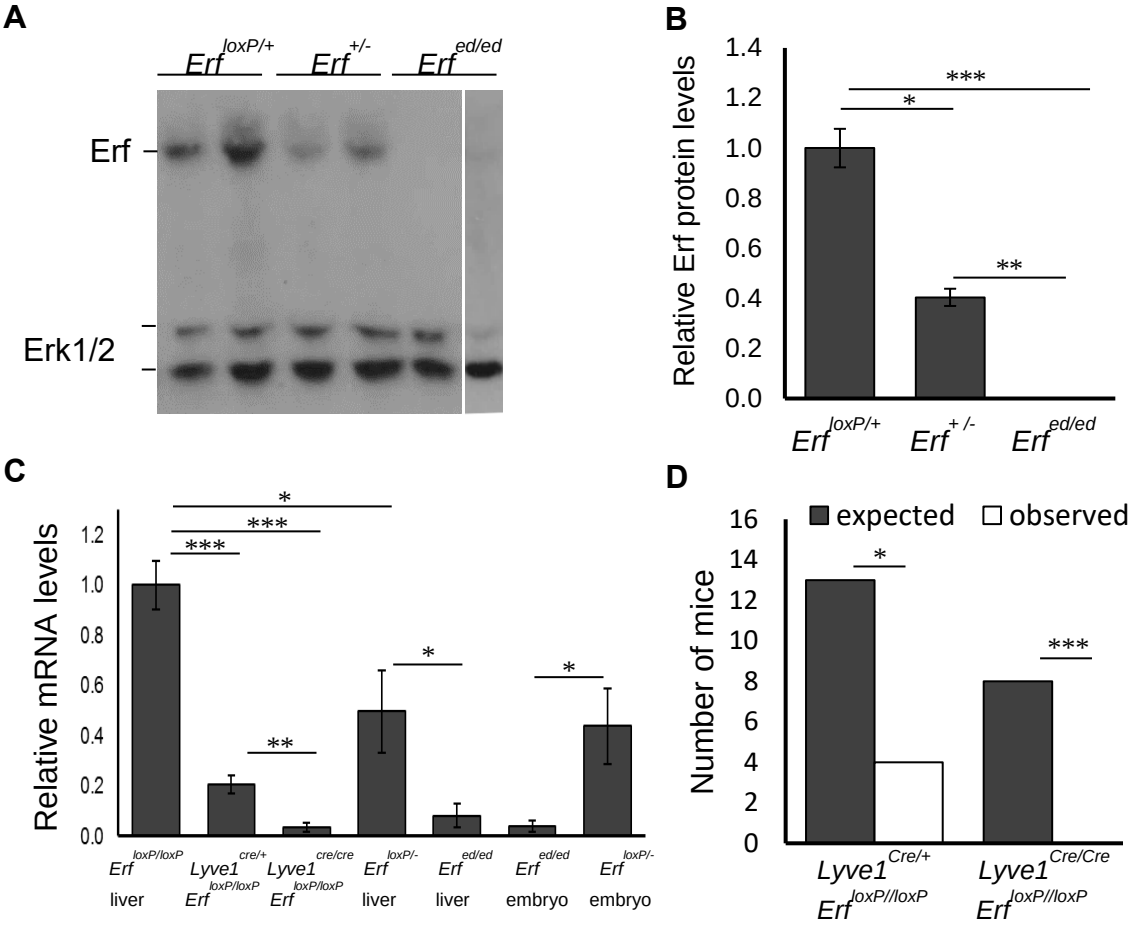

Figure 10. Quantity differences in Erf expression. (A) Protein levels of Erf were determined by western blot from *Erf*$^{loxP/+}$, *Erf*$^{+/-}$ and *Erf*$^{ed/ed}$ E12.5 embryos. Erk1/2 antibody was used for normalization. All samples except for the last one were loaded in the same blot. **(B)** Quantification of Erf protein levels from *Erf*$^{loxP/+}$, *Erf*$^{+/-}$ and *Erf*$^{ed/ed}$ E12.5 embryos. Samples are represented as ratio to *Erf*$^{loxp/+}$ littermates after normalization with Erk1/2 quantities. **(C)** mRNA levels of Erf were determined in fetal livers of *Erf*$^{loxP/loxP}$, *Lyve1*$^{Cre/+}$ *Erf*$^{loxP/loxP}$ and *Lyve1*$^{Cre/Cre}$ *Erf*$^{loxP/loxP}$ E12.5 embryos as well in both livers and whole embryos of *Erf*$^{loxP/-}$ and *Erf*$^{ed/ed}$ at E12.5, employing the qPCR method. Samples were normalized to Gapdh mRNA levels and were quantified corresponding to the 2 loxP alleles. **(D)** Number of animals born with the *Lyve1*$^{Cre/+}$ *Erf*$^{loxP/loxP}$ or the *Lyve1*$^{Cre/+}$ *Erf*$^{loxP/loxP}$ genotype. Chi square test showed statistical important differences of the actual over expected numbers of total 100 mice from 16 different litters. All values are means ± SE of at least 5 samples from 5 litters. Statistical analysis was performed using the unpaired t-test with two-tailed distribution. *, $P < 0.05$, $P < 0.05$, ***, $P < 0.0005$.

8. *Erf* elimination compromises fetal liver erythropoiesis

The increased anemia at E13.5 – E14.5 indicated a profound lack of definitive erythroid cells which are produced at this time in the fetal liver and make up a majority of the circulating cells at these time points (Fraser et al., 2007). Analysis of E11.5 – E13.5 $Erf^{ed/ed}$ embryos revealed significantly reduced liver size (Figure 11A) and liver cell numbers compared to their $Erf^{floxP/+}$ littermates (Figure 11B), while the other organs and the weight of embryos were comparable. The number of samples per liter are shown in Table 4.

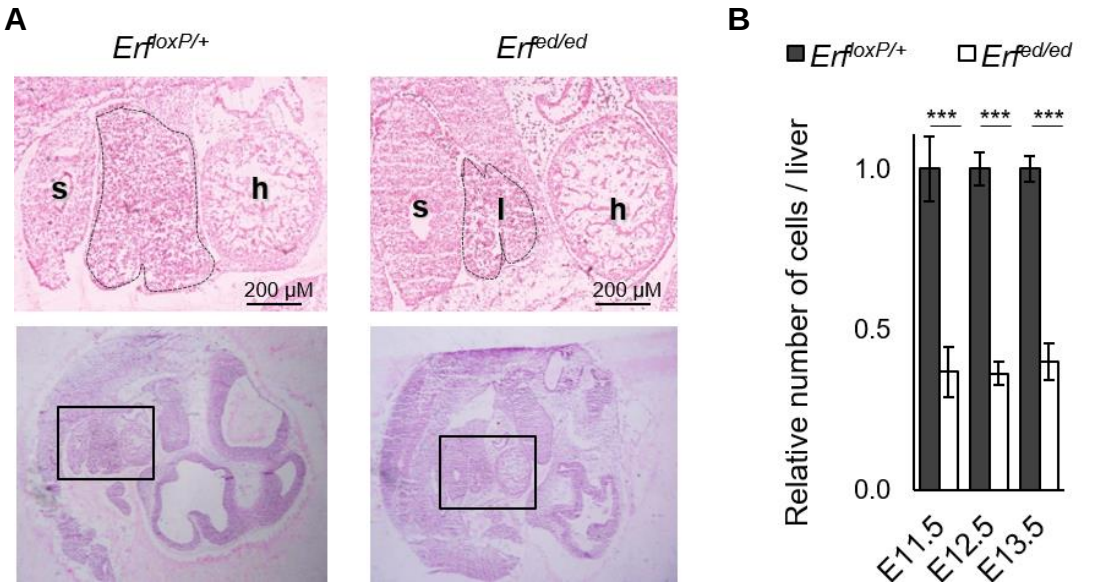

Figure 11. $Erf^{ed/ed}$ livers have decreased size and total cell counts. (A) Sagittal sections from E11.5 $Erf^{ed/ed}$ and $Erf^{floxP/+}$ embryos stained with Hematoxylin and Eosin. Boxes show the magnified picture on the top. s: stomach, l: liver, h: heart. **(B)** Total number of liver cells per liver at E11.5 – E13.5. All values are means ± SE of samples from at least from 6 litters per gestation day. Statistical analysis was performed using the unpaired t-test with two-tailed distribution. *, $P < 0.05$, ***, $P < 0.0005$.

Table 4. Number of liver samples in each gestation day and genotype that were used for counting total cells in liver as shown in Figure11B.

		No. of liver samples	
Embryonic day	**Litters**	***Erf*$^{loxP/+}$**	***Erf*$^{ed/ed}$**
11.5	6	17	8
12.5	9	22	15
13.5	13	28	24

To examine if this reduction is due to the colonization of the liver and/or the expansion of the erythroid progenitors in the liver, we analyzed BFU-E and CFU-E numbers at E11.5 – E13.5. The colonies that were counted had the morphology shown in Figure 12A. GEMM colonies that give rise to BFU-E and CFU-GM. GM colonies were very few and no differences could be found. Consistent with the reduced EMP in the yolk sac and in the bloodstream, *Erf*$^{ed/ed}$ embryos contained fewer BFU-E and CFU-E in the liver compared to their *Erf*$^{loxP/+}$ littermates (Figure 12B,C). Interestingly, BFU-E abundance in *Erf*$^{ed/ed}$ embryo livers at E11.5 was comparable to their *Erf*$^{loxP/+}$ littermates, whereas at E12.5 - E13.5 it was increased (Figure 12D). The abundance of CFU-Es in the *Erf*$^{ed/ed}$ embryo livers was increased compared to *Erf*$^{loxP/+}$ littermates throughout E11.5 – E13.5 (Figure 12E). The number of samples in each litter are shown in Table 5.

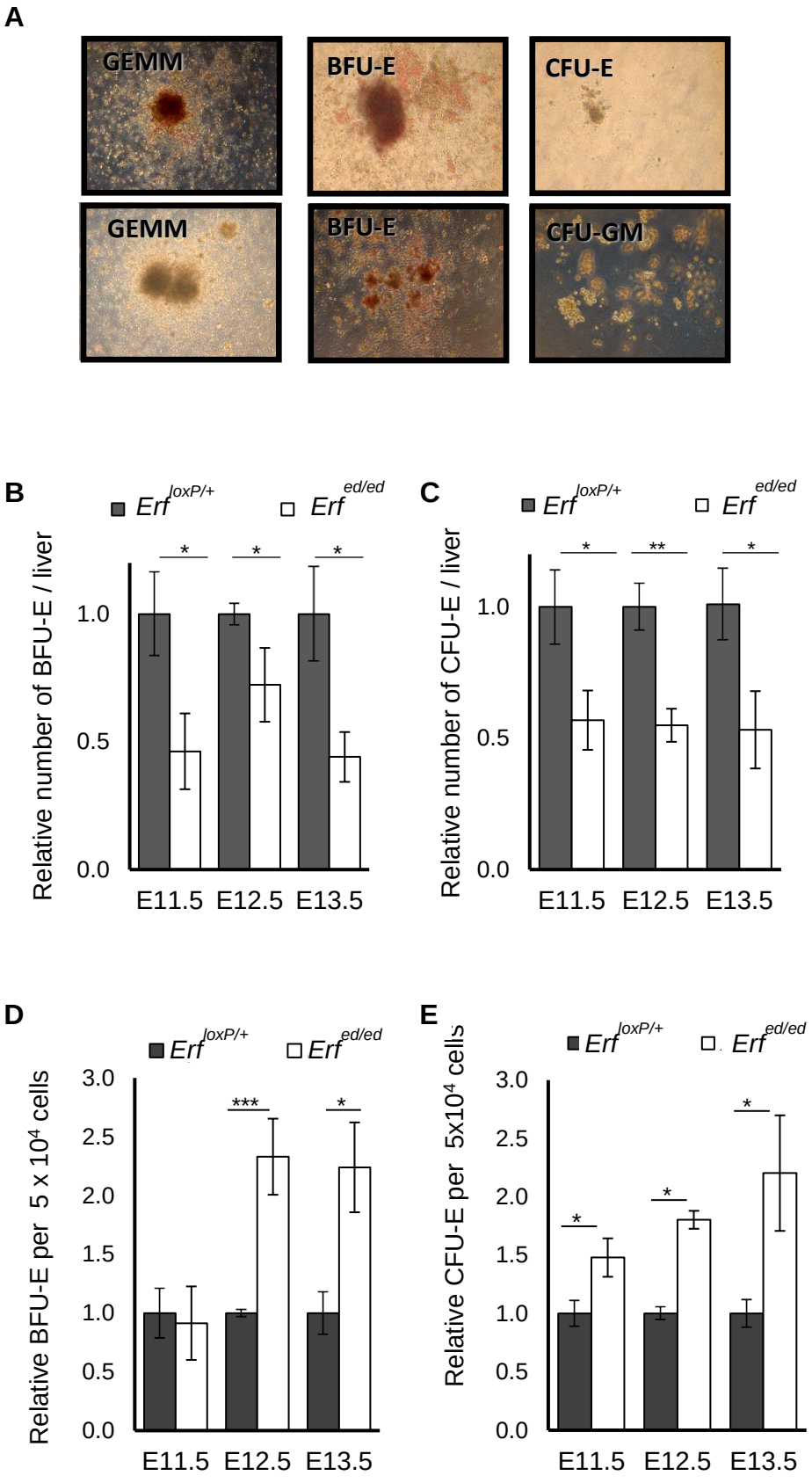

Figure 12. *Erf*$^{ed/ed}$ livers have decreased numbers but increased proportion of BFU-Es and CFU-Es. (A) Morphology of colonies that both ***Erf***$^{loxP/+}$ and *Erf*$^{ed/ed}$ livers form in semi-solid media. CFU-GEMM: Colony-forming unit-granulocyte, erythroid,

macrophage, megakaryocyte contain a colony - erythroid cells as well as 20 or more granulocyte, macrophage and megakaryocyte cells forming 1 or two clusters, BFU-E: Burst-forming unit-erythroid - a colony containing >200 erythroblasts, usually present in >2 clusters, CFU-E: Colony-forming unit-erythroid, a colony containing 1 - 2 clusters with a total of 8 - 200 erythroblasts, CFU-GM: Colony-forming unit-granulocyte, macrophage - a colony containing >40 granulocyte and macrophage cells. **(B)** number of BFU-Es and **(C)** number of CFU-Es per liver at E11.5 – E13.5. **(D)** Proportion of BFU-E and **(E)** CFU-E at 11.5 – 13.5 d.p.c. Samples are represented as ratio to $Erf^{loxp/+}$ littermates. All values are means ± SE of samples from at least from 6 litters per gestation day (Supplemental Table 5). Statistical analysis was performed using the unpaired t-test with two-tailed distribution. *, $P < 0.05$, ***, $P < 0.0005$.

Table 5. Number of samples used in each gestation day and genotype for counting proportion and numbers of BFU-E / CFU-E per liver as shown in Figure 12.

		No. of samples for BFU-E / CFU-E analysis	
Embryonic day	**litters**	***Erf*$^{floxP/+}$**	***Erf*$^{ed/ed}$**
11.5	3	6	5
12.5	5	10	9
13.5	4	9	8

Our results indicate that the reduced numbers of EMPs, which were already reduced from the yolk sac lead to the reduced liver cell count at E11.5 onwards. Moreover, the increased proportion of BFU-E and CFU-E demonstrate a probable additional defect. To that extend, we tested the differentiation of definitive yolk sac derived cells in the liver. We examined erythroid maturation by analyzing the abundance of the R1-R4 populations in E11.5 – E12.5 fetal liver with CD71 and Ter119 staining and flow cytometry. Based on the dynamic expression of these markers, we can discriminate the differentiation of erythroblasts in the following sequence: the early precursor cells and the

proerythroblasts R1 (CD71^{low}Ter119^{-}), which differentiate to the proerythroblasts and the early basophilic proerythroblasts R2 (CD71^{high}Ter119), then the early and late basophilic erythroblasts R3 (CD71^{high}Ter119^{+}), the polychromatophilic and orthochromatic erythroblast R4 (CD71^{low}Ter119^{+}) and the enucleated mature erythrocytes R5 (CD71^{-}Ter119^{+}), which are not shown because of their few proportion (Sieff et al., 2010). This analysis suggested that at E12.5 livers the population R1, as well as R2 are more abundant in *Erf*$^{ed/ed}$ embryo livers, while R3 and R4 populations are less abundant (Figure 13A, B). On the contrary, total cell counts of each population are reduced (Figure 13C). To note here that R1 cells comprise ≥ 40% CFU-Es whereas R2 contain only a few CFU-Es and R3 – R5 contain no erythroid progenitors. According to BFU-Es, R1 accounts for a very small proportion of them (Figure 13C). The increased proportion of R1, R2 population is consistent with the increased proportion of BFU-E and CFU-E that we had found before in colony assays. At E11.5 livers, proportions of R1 – R4 populations is similar while total cell counts of each population is reduced to 50%, indicative of the reduced cells that migrate of the yolk sac to the liver at E11.5 (Figure 13D, E). Probably difference in the proportion of R1-R2 population was not found because the differentiation of erythroblast has not fully started at this day in the liver. Consistent with the colony assays, these data indicate that in addition to the initial colonization there is also a delay and not a block in the maturation of the erythroid precursors in the fetal liver from the R2 population to the following R3-R5.

A

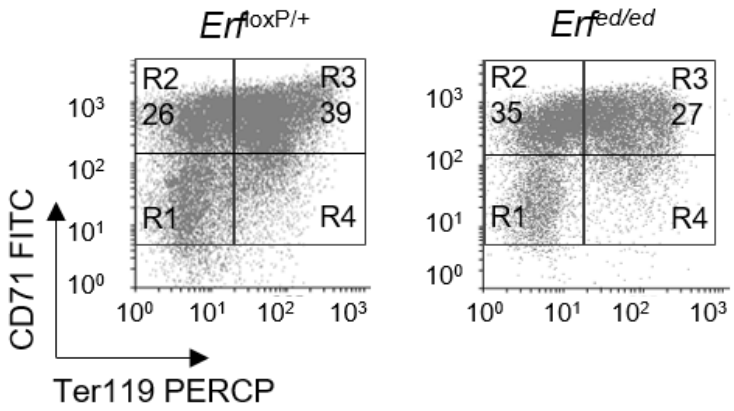

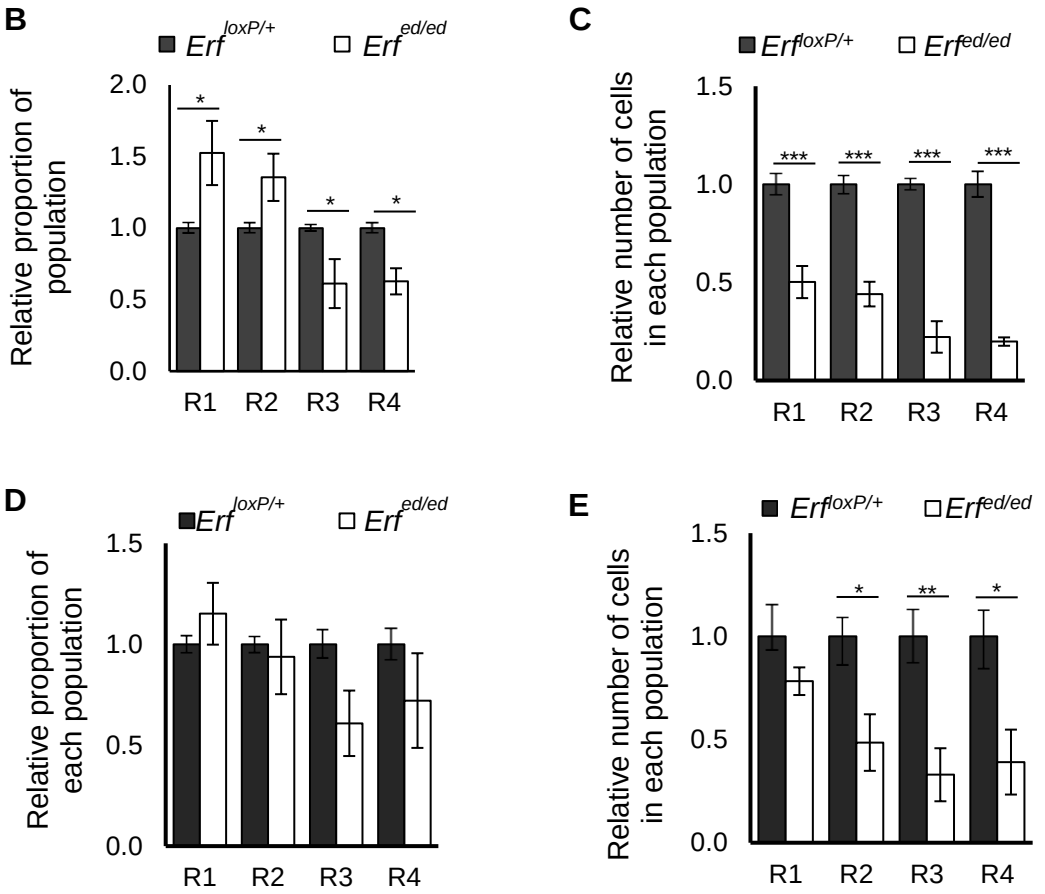

Figure 13. *Erf*$^{ed/ed}$ have decreased differentiation rate in the fetal liver. (A) Representative flow cytometry of *Erf*$^{ed/ed}$ E12.5 liver cells stained for Ter119, a marker for early proerythroblasts to mature erythrocytes (R3 – R5), and CD71, a marker for all proerythroblasts except mature erythrocytes (R1-R4). **(B)** Comparison of R1-R4 proportions and **(C)** total cells of E12.5 embryonic liver analyzed by flow cytometry as in (A). **(D)** Proportions and **(E)** total cells of R1-4 populations from E11.5 embryonic liver cells. The graphs show the values for *Erf*$^{ed/ed}$ and *Erf*$^{floxP/+}$ embryos compared to the average value of the *Erf*$^{floxP/+}$ littermates. All values are means ± SE of at least 6 biological samples of each genotype of at least 4 litters. Statistical analysis was performed using the unpaired t-test with two-tailed distribution. *, $P < 0.05$, **, $P < 0.005$, ***, $P < 0.0005$.

9. *Erf*$^{ed/ed}$ have normal macrophages – erythroblasts contacts

Macrophages form contacts with erythroblasts and form the blood islands in the liver. One macrophage is attached to many erythroblasts and this is important for the differentiation of erythroblasts. To that extend, sagittal sections of embryos and immunofluorescence against the marker of macrophages

F4/80 and the marker of maturing erythroblasts, Ter119 indicated that the contacts between macrophages and erythroblasts in blood islands of the liver were proper so that erythroblasts to differentiate. It would thus appear that the apparent reduced rate of maturation was not due to the lack of erythroblast contacts with macrophages, as they were evident in E12.5 livers (Figure 14) and the maturational defect of the *Erf*$^{ed/ed}$ liver erythroblasts is cell autonomous.

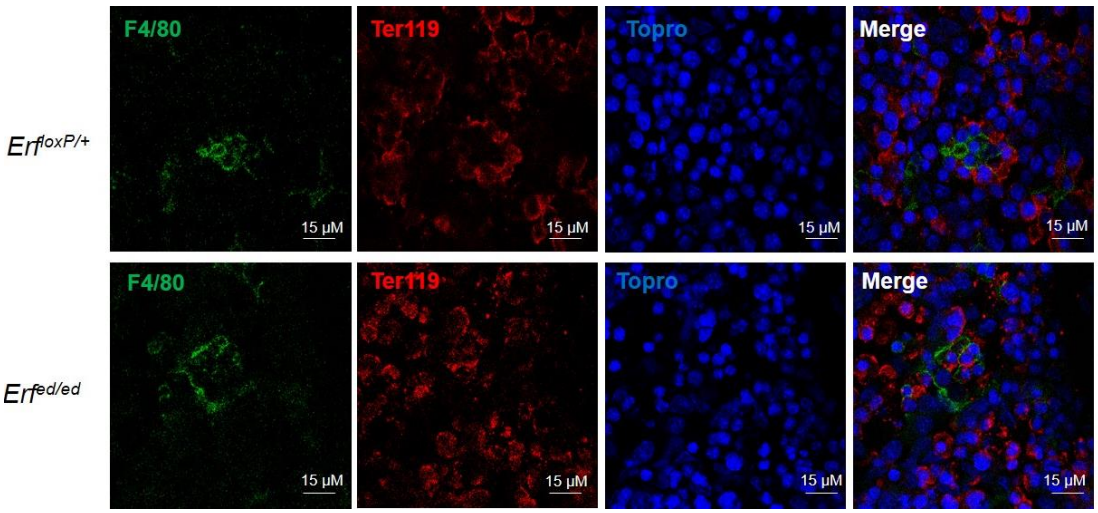

Figure 14. *Erf*$^{ed/ed}$ have normal macrophages – erythroblasts contacts. Confocal microscopy images of sagittal sections of livers from E12.5 *Erf*$^{ed/ed}$ and *Erf*$^{floxP/+}$ embryos stained with anti-F4/80 antibody, a marker for macrophages (green) and Ter119, a marker for maturing erythroblasts (red). Nuclei were stained with TOPRO-3 (blue).

10. *Erf*$^{ed/ed}$ erythroblasts have normal cell cycle and no apoptotic defects in liver

In order to confirm that the increased number of CFU-Es is not a defect in proliferation we performed BrdU staining simultaneously with CD71 cell in order to detect erythroblasts in E12.5 livers (Figure 15 A, B). We analyzed the proportion of CD71 cells that proliferate and the values for *Erf*$^{ed/ed}$ and *Erf*$^{floxP/+}$ embryos were compared to the average value of the *Erf*$^{floxP/+}$ littermates. Our results indicate that *Erf*$^{ed/ed}$ CD71 cells have the same proliferation rate with *Erf*$^{floxP/+}$ littermates. Livers at E11.5 and E13.5 also showed normal proliferation. Additionally, we performed flow cytometry with propidium iodide in E12.5 livers to check cell cycle of the cells. Finally, we did not observe any cell cycle defect

of erythroblasts so, *Erf* does not block any phase of cell cycle of erythroblasts (Figure 15 C).

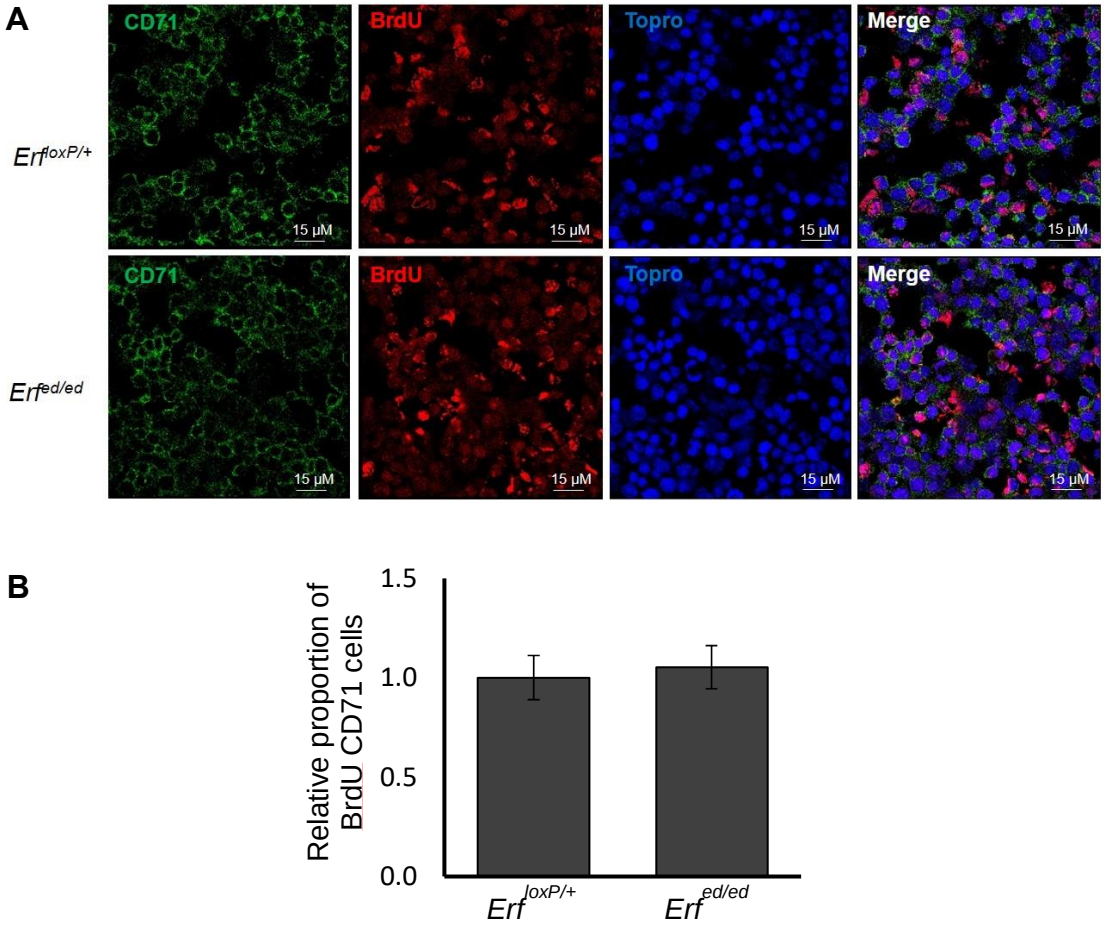

Figure 15. *Erf*$^{ed/ed}$ erythroblasts have normal proliferation. (A) Confocal microscopy images of sagittal sections of livers from E12.5 *Erf*$^{ed/ed}$ and *Erf*$^{loxP/+}$ embryos stained with anti-CD71 antibody, a marker for for maturing erythroblasts (green) and BrdU, a marker proliferating cells(red). Nuclei were stained with TOPRO-3 (blue). **(B)** Proportions of CD71 cells are positive for BrdU at E12.5 livers. The values for *Erf*$^{ed/ed}$ and *Erf*$^{loxP/+}$ embryos were compared to the average value of the *Erf*$^{loxP/+}$ littermates. All values are means ± SE of 4 biological samples of each genotype from 3 litters.

To examine any defect in cell cycle, as we have a differentiation delay, we employed cell cycle analysis at both E12.5 and E13.5 fetal livers. The results were the same in all days, indicating no cycle defect. Samples from 3 *Erf*$^{ed/ed}$ and 3 *Erf*$^{loxP/+}$ from each day were used from 2 litters (Figure 16). However, given that we do not observe any differentiation blockage but severe

quantitative differences, the lack of differences is not surprising. For example, if a progenitor cell had failed to proliferate/differentiate effectively, considering its small proportion in the total liver population and the lack of any unique cell type specific gene markers, it would not have produced any detectable difference.

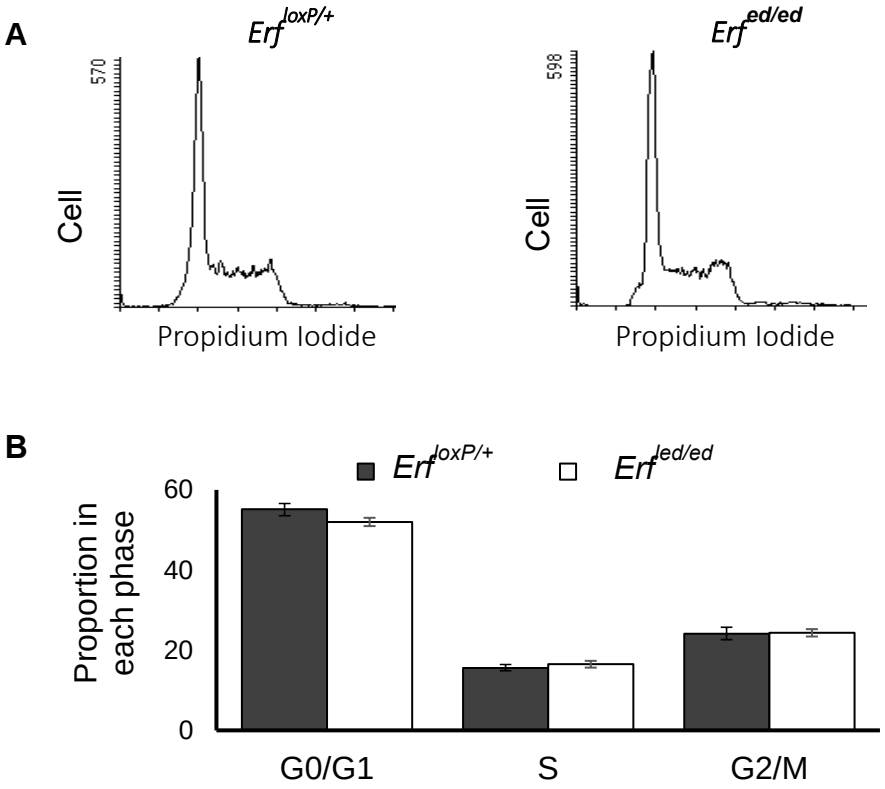

Figure 16. ***Erf*$^{ed/ed}$ erythroblasts have normal cell cycle progression. (A)** Representative flow cytometry profiles of cell cycle of E13.5 *Erf*$^{ed/ed}$ and *Erf*$^{loxP/+}$ fetal livers stained with propidium iodide. **(B)** Proportions of phases G0/G1, S and G2/M of cell cycle at E13.5 livers. All values are means ± SE of 6 biological samples of each genotype from 2 litters.

Additionally, apoptosis tested for a possible reason of the reduced erythroblasts in the fetal liver. To that extend, we performed Tunel in E12.5 livers (Figure 17), as well E11.5 and E13.5 and moreover, we stained with CD71, a marker of erythroblasts. Unfortunately, we were not able to stain nucleus because of the same emission of Tunel with our nucleus staining. Our

results indicate that very few apoptotic cells were found in *Erf*$^{ed/ed}$ and *Erf*$^{floxP/+}$ littermates.

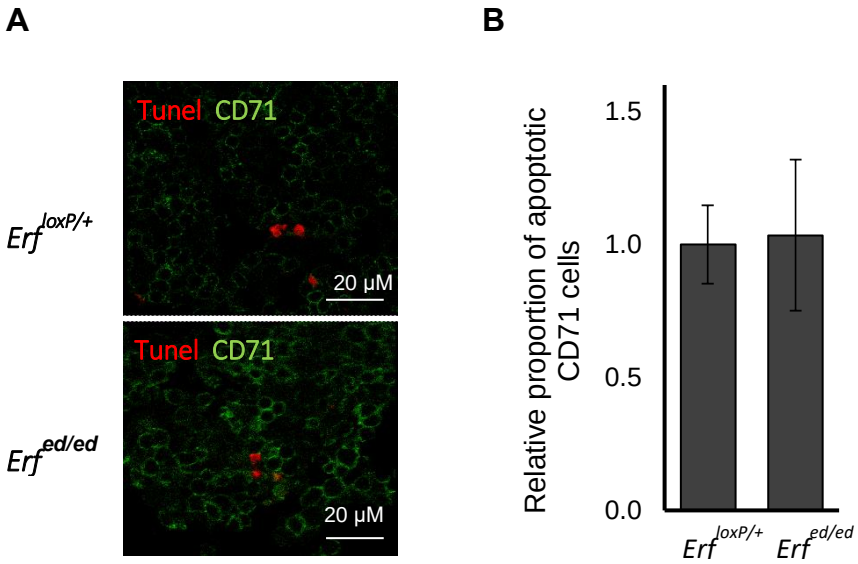

Figure 17. *Erf*$^{ed/ed}$ does not affect apoptosis. (A) Confocal microscopy images of sagittal sections of livers from E12.5 *Erf*$^{ed/ed}$ and *Erf*$^{floxP/+}$ embryos stained with the anti-CD71 antibody for the erythroblasts R1 – R4 and with In Situ cell dead kit TMR (Tunel) for detection of apoptotic cells. **(B)** Proportion of apoptotic cells (Tunel positive) at E12.5 livers. The values for *Erf*$^{ed/ed}$ and *Erf*$^{floxP/+}$ embryos are compared to the average value of the *Erf*$^{floxP/+}$ littermates. All values are means ± SE of at least 2 biological samples of each genotype from 2 litters. Statistical analysis was performed using the unpaired t-test with two-tailed distribution.

11. *Erf* does not affect hepatocytes

To confirm that the reduced fetal liver size is not due to decreased proportion of hepatocytes, we performed immunofluorescence against Hnf4, a marker of hepatoblasts and Ter119, a marker of R3-R4 maturing erythroblasts in E12.5 fetal livers (Figure 18A). Moreover, staining against CD71, a marker of R1 -R4 erythroblasts was performed (Figure 18A). Our data indicate, that proportion of Ter119 cells is decreased, as expected, but proportion of Hnf4 hepatocytes is increased (Figure 18B). This means that the reduced liver size is not because of reduced proportion of Hnf4 cells. As we can see CD71 cells remain the same as expected by the increased proportion of R1, R2 population and the decreased proportion of R3-R4 that come to balance (Figure 18). So, the

increased proportion is a result of the reduced erythroblasts that migrate in the liver.

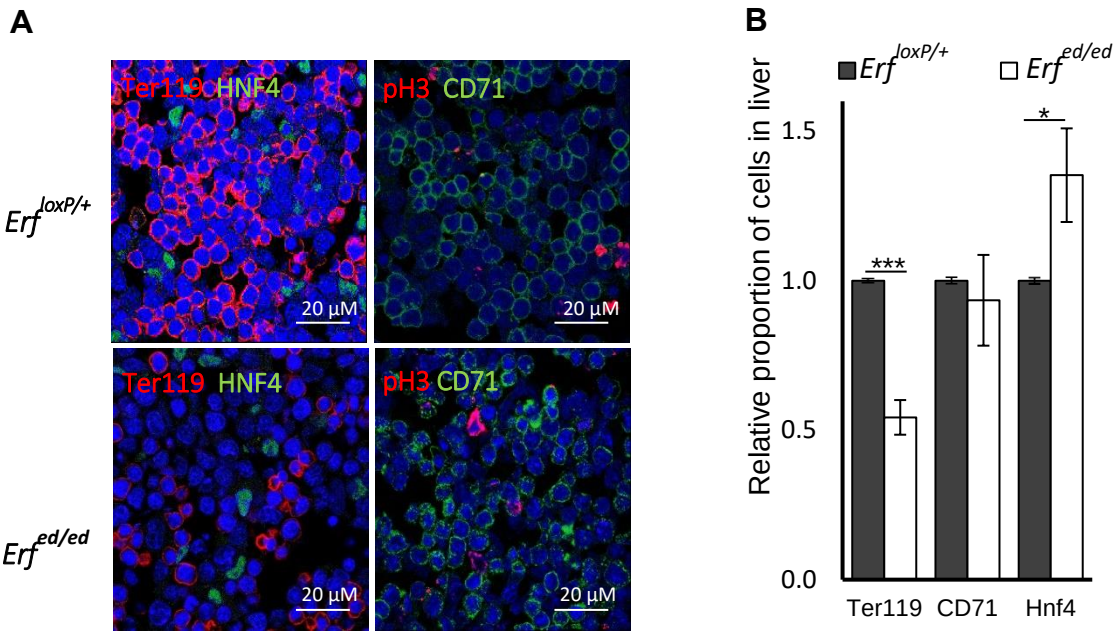

Figure 18. *Erf*$^{ed/ed}$ does not affect hepatic cells. (A) Confocal microscopy images of sagittal sections of livers from E12.5 *Erf*$^{ed/ed}$ and *Erf*$^{loxP/+}$ embryos stained with the anti-Ter119 antibody for detection of the mature erythroblasts R3 – R5, anti-HNF4 antibody for hepatocytes (left panels), anti-CD71 antibody for the erythroblasts R1 – R4 and anti-pH3 antibody for proliferating cells (middle panels). Nuclei were stained with TOPRO-3 (blue). **(B)** Proportion of Ter119, HNF4 and CD71 cells in E12.5 livers. The graph shows the values for *Erf*$^{ed/ed}$ and *Erf*$^{loxP/+}$ embryos, compared to the average value of the *Erf*$^{loxP/+}$ littermates. All values are means ± SE of at least 10 biological samples of each genotype from 8 litters. Statistical analysis was performed using the unpaired t-test with two-tailed distribution. ***, $P < 0.0005$.

We further tested the possible contribution of hepatic cells, eliminating *Erf* specifically in the hepatocytes after crossing the *Erf*$^{loxP/loxP}$ mice with the *Alfp-Cre* mice (Kellendonk et al., 2000). Our results show that *Alfp - cre;Erf*$^{loxP/loxP}$ mice are born Mendelial, indicating that *Erf*$^{ed/ed}$ mice do not die due to defects in hepatocytes and defects in erythroblasts is a cell autonomous defect. We confirmed that Alfp-Cre is expressed by crossing the *Alfp-Cre* mice *with YFP/+* mice (ROSA26 $^{fl\text{-}STOP\text{-}fl\text{-}YFP}$) (Srinivas et al., 2001). Alfp-cre is known that begins to be expressed at E8.5 in a region of hepatic specification and continues until liver is formed. We isolated embryos from E8.5 and E10.5 (and we detected

YFP expression with anti-GFP antibody in sagittal sections (Figure 19). Finally, YFP was detected from E8.5 – E10.5 in the hepatic specification region and in a structure that looks with liver, respectively.

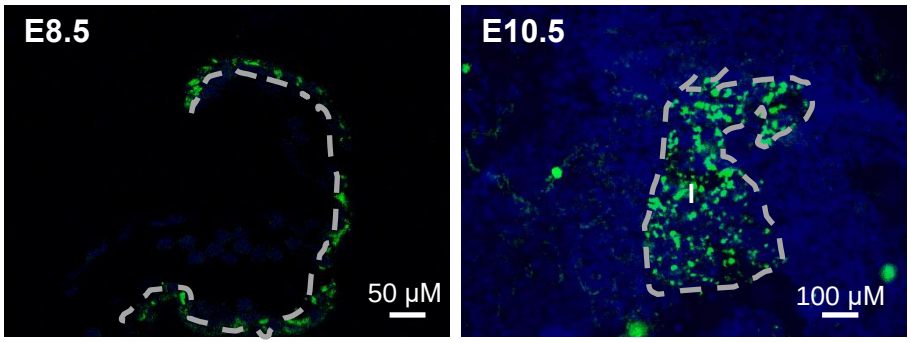

Figure 19. Elimination of Erf in conditional mice in hepatic cells. Immunochemistry for YFP indicates deletion of *Erf* in hepatic cells very early in the liver formation at E8.5 until embryonic day 10.5 that the majority of hepatic cells are produced. The liver specific *Alfp-Cre*;*Erf*$^{loxP/loxP}$; ROSA26 $^{fl\text{-}STOP\text{-}fl\text{-}YFP}$;*Erf*$^{loxP/loxP}$ mice were used to indicate that hepatic cells have no effect on embryo hematopoiesis. YFP: Green, Topro: Blue. Hs: hepatic specification, l: liver. Scale bar on left is 50 μM and on right is 100 μM.

12. *Erf* is required for HSC development

The dramatic decrease in peripheral blood at E14.5 (3%) raised the possibility that not only the EMPs but also the HSCs may be affected by the *Erf* loss. Moreover, the liver total cell counts fell dramatically to 5% at E14.5, confirming the previous consideration. HSCs come from AGM at E10.5 and migrate to the liver reaching a considerable percentage at E14.5, then they migrate to bloodstream where EMPs consist half of the circulating cells.

Therefore, we examined the role of *Erf* in hematopoietic stem cell maintenance and differentiation via both non-competitive and competitive repopulation experiments to evaluate short-term and long-term HSCs. Fifteen to 23 days after the transplantation of E13.5 liver cells in irradiated mice of the same haplotype, 3 of 4 mice repopulated with *Erf*$^{ed/ed}$ cells died in contrast to the mice transplanted with *Erf*-competent spleen cells, indicating a defect in short-term HSCs (Figure 20A). For the competitive repopulation assays, E12.5 fetal liver cells were co-injected with spleen cells from *wt* animals in irradiated *wt* host mice of the same genetic background (Figure 20A).

Donor HSC engraftment was estimated with semiquantitive PCR from blood from tail 5 months after the injection. At this time the majority of the erythrocytes have arisen from the long-term HSCs. PCR for detection of loxP site was performed in *Erf*$^{ed/ed}$ transplantated mice (170 bp band loxP, left panel), while PCR for deletion of *Erf* was performed in *Erf*$^{ed/ed}$ transplantated mice (178 bp band del, right panel). The 101 bp wt *Erf* band (wt) and the 206 bp band from the GRCm38.p4 locus (GRC) are used as PCR controls (Figure 20B). For the quantification controls containing 100 %, 50 %, 10 %, 1 % *Erf*$^{loxP/+}$ or *Erf*$^{ed/ed}$ DNA mixed with *Erf* $^{+/+}$ DNA were used.

Our data suggest that in contrast to the *Erf*$^{loxP/+}$ cells that contributed to almost all the hematopoietic cells of the irradiated animals, the *Erf*$^{ed/ed}$ cells had marginally detectable contribution (Figure 20B), suggesting that the long-term HSCs may also be affected by the elimination of *Erf*.

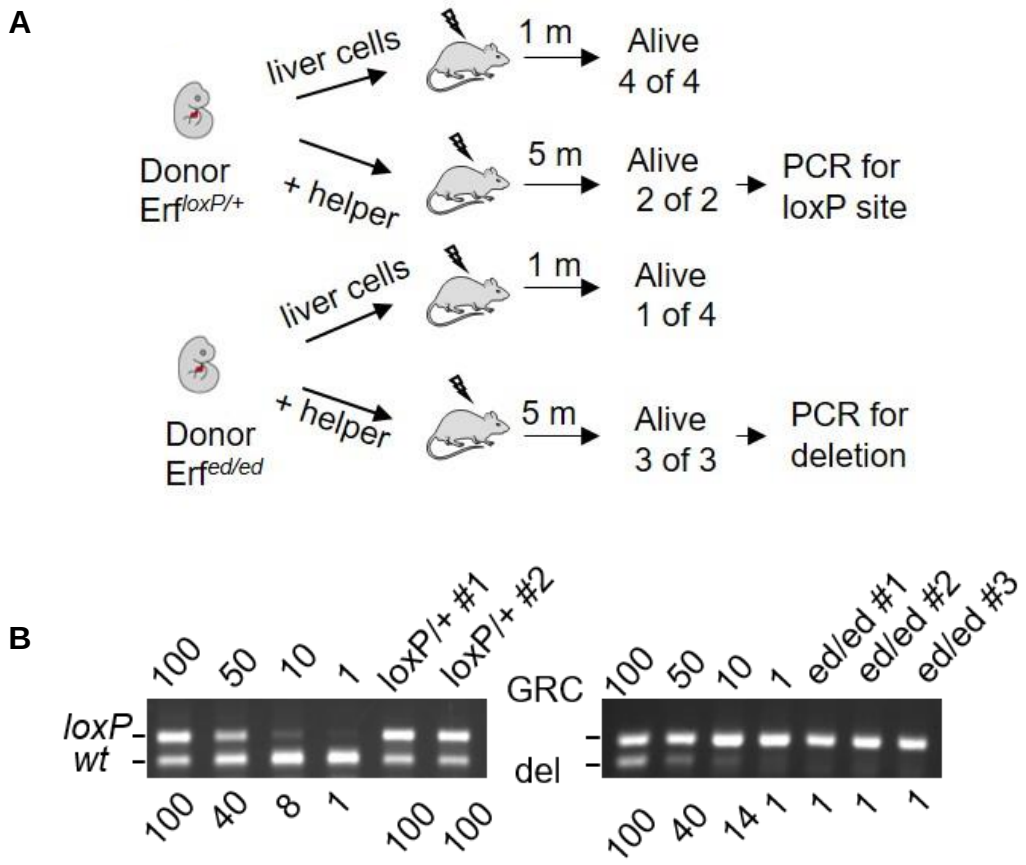

Figure 20. *Erf*$^{ed/ed}$ have reduced HSCs in liver transplant recipients. (A) Outline of repopulation experiments of sublethally irradiated mice with E13.5 liver cells (liver cells) or competitive repopulation experiments with E12.5 liver donor cells (+ helper)

from *Erf*$^{ed/ed\ -}$ and *Erf*$^{loxP/+}$ embryos assayed 1 (1m) or 5 (5m) months after irradiation. **(B)** Detection of the repopulating cells in the competitive repopulation experiment 5 months after irradiation by semiquantitive PCR. Transplanted Erf-expressing cells are detected by the presence of the 170 bp band (loxP, left panel) while *Erf*$^{ed/ed}$ cells by the expression of the 178 bp band (del, right panel) generated after the excision of the *Erf* gene. The 101 bp wt *Erf* band (wt) and the 206 bp band from the GRCm38.p4 locus (GRC) are used as PCR controls. Lanes 100, 50, 10, 1 are quantitation controls containing 100 %, 50 %, 10 %, 1 % *Erf*$^{loxP/+}$ or *Erf*$^{ed/ed}$ DNA mixed with *Erf* $^{+/+}$ DNA. The numbers below indicate the percentage of the test band compared to the 100% sample.

13. Embryonic stem cell induction towards erythroblasts ex vivo

In order to examine the specific stage of erythropoiesis that *Erf* may be involved and the cell autonomous character of the effect, we utilized the *Erf*$^{-/-}$ embryonic stem cells that we had already developed in the lab and induced them towards hematopoietic cell lineage.

Murine ESCs are pluripotent cells that come from the early embryo. When ESCs are cultivated in media with anti-differentiation factors as Lif, they can proliferate while they have the capacity to differentiate into any cell type of the three germ layers by forming embryonic bodies (EBs) (Dang et al., 2002). EBs increase in size and they form the three germ layers at day 2, endoderm, mesoderm and ectoderm. Removing the anti-differentiation agents, the cells can differentiate in any lineage by adding specific differentiation factors. Each day of differentiation reflects the production of specific progenitors during differentiation and each population can be detected and compared with the right combination of antibodies (Carotta et al., 2004).

There are many ways of generation of embryoid bodies like the methylocellulose culture or the liquid suspension culture of ESCs (Dang et al., 2002). In our protocol, we used the hanging drop culture, in which ESCs form aggregates and form a hanging drop. To that extend, we directed ES cell differentiation into the erythroid lineage, using an established 3-step protocol combining the embryoid body (EB) differentiation technique with erythroid culture conditions. To fulfil this, we used defined culture conditions to direct differentiation into the erythroid lineage. Initially, we cultured EBs in the

presence of differentiation media to hematopoietic cells comparing to the formation of EBs without induction. The outer surface of the developing EBs give rise to primitive endoderm which will regulate the cell fate to the three layers of gastrulation (W. S. Chen et al., 1994). In the presence of differentiation factors, mesoderm will be more induced compared to no induction in order to give rise to hemangioblast which will differentiate to both hematopoietic and endodermic lineage at day 4 (Choi et al., 1998). To identify the early stage that the defect begins, we compared the size of EBs with and without induction at day 2 (Figure 21). We created hanging drops with different numbers of cells ranging from 100 to 1000 cells with the aim of not leading the system towards differentiation because of the large number of cells. However, the number of 100 cells was not effective to make a well-formed EB but above 250 cells, embryoid bodies were formed properly. Four experiments were performed and the two of four showed reduced size of EBs in *Erf*$^{-/-}$ (Figure 21A, B compared to 20C, D). Unfortunately, there was a variation from experiment to experiment and we could not make a conclusion. Moreover, this variation may be due to transferrin, as we used aliquots of holo one or not. However, comparing *Erf*$^{-/-}$ to *Erf*$^{+/+}$ without induction, the result was similar with that from hematopoiesis induced ESCs.

A

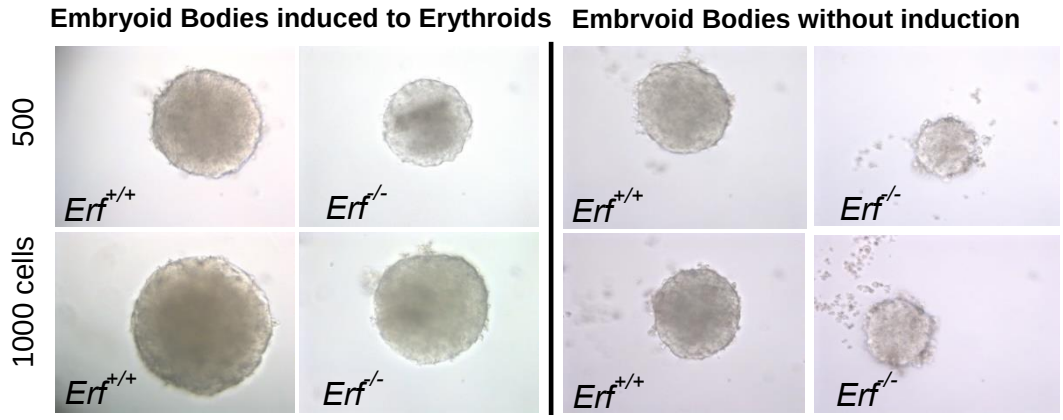

B

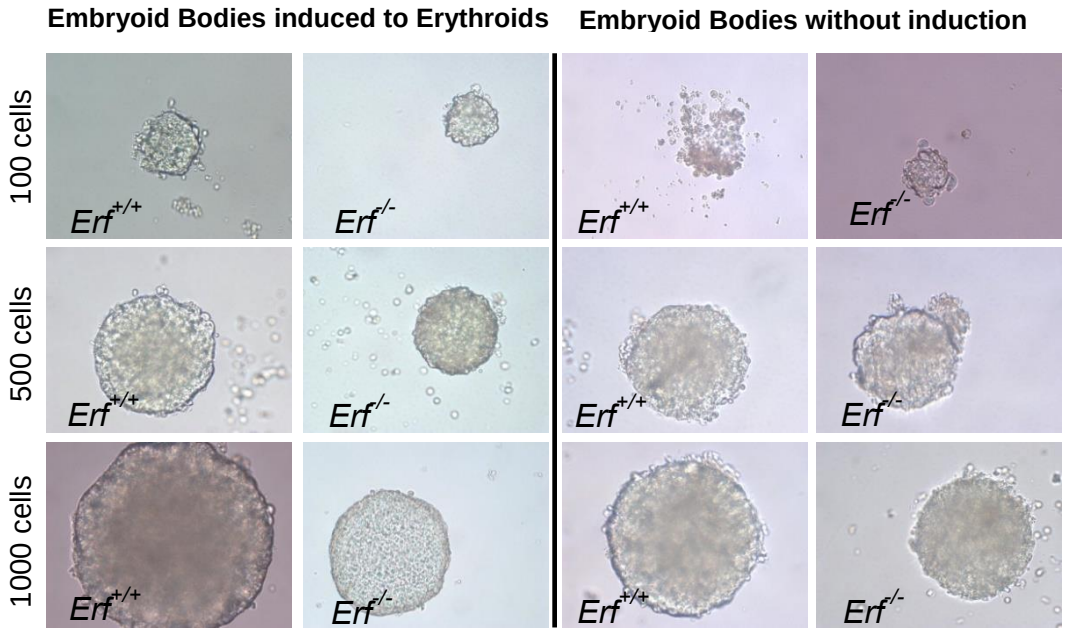
Embryoid Bodies induced to Erythroids
Embryoid Bodies without induction
100 cells
500 cells
1000 cells
Erf+/+
Erf-/-
Erf+/+
Erf-/-
Erf+/+
Erf-/-
Erf+/+
Erf-/-
Erf+/+
Erf-/-
Erf+/+
Erf-/-

C

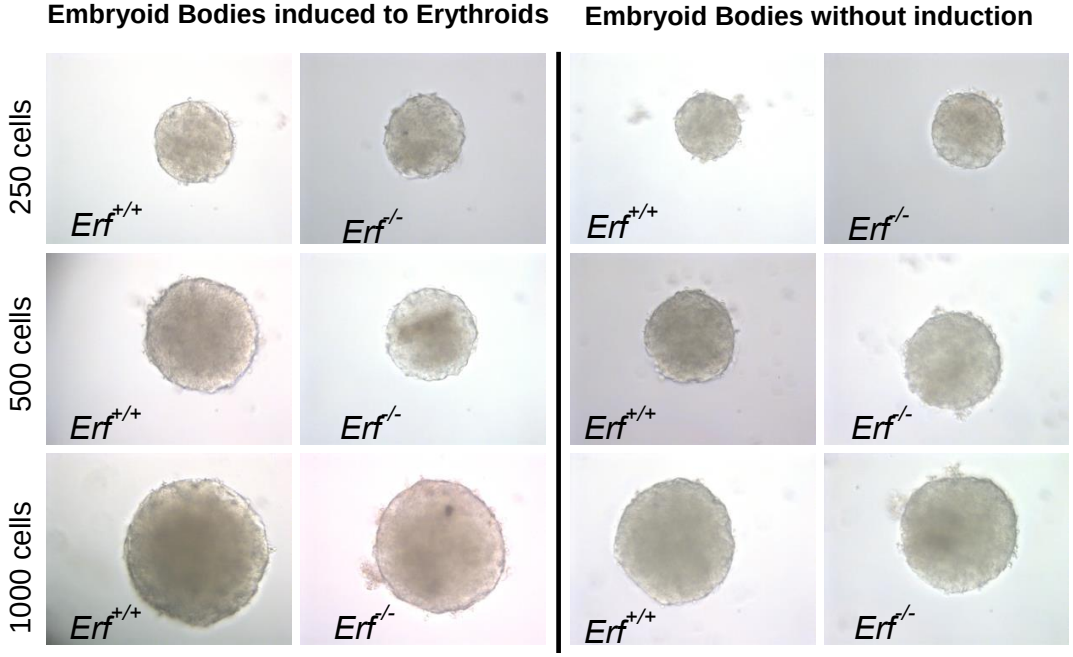
Embryoid Bodies induced to Erythroids
Embryoid Bodies without induction
250 cells
500 cells
1000 cells
Erf+/+
Erf-/-
Erf+/+
Erf-/-
Erf+/+
Erf-/-
Erf+/+
Erf-/-
Erf+/+
Erf-/-
Erf+/+
Erf-/-

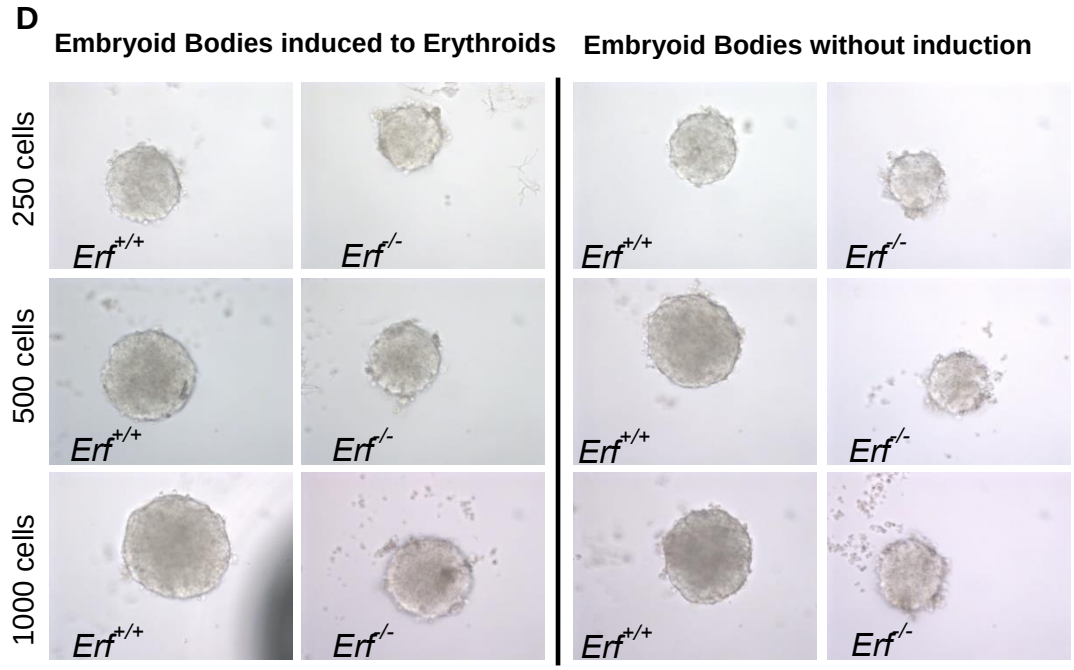

Figure 21. Morphology of *Erf*$^{-/-}$ Embryoid bodies induced to hematopoietic lineage. (A) 500 and 1000 cells, **(B)** 100, 500 and 1000 cells, **(C), (D)** 250, 500 and 1000 cells were used for the formation of EBs with (left) or without induction to hematopoietic lineage (right). *Erf*$^{-/-}$ are compared to *Erf*$^{+/+}$ embryoid bodies. Magnification is 10x.

At day 2, EBs are collected and plated in suspension in the same differentiation media. At day 4, EBs have developed the first erythroid precursors which come from the primitive wave, representing the embryonic day E6.5 of the embryo (Keller et al., 1993). From day 6 onwards, 85% of EBs contain early hematopoietic (CD34, Sca-1) and erythroid (Ter119) cells of the both primitive and definitive wave. Markers, like Flk-1 for mesoderm, endothelial and the early hematopoietic cell can be used for detection of populations in each day as shown in Table 6, but we did not have this capability (Carotta et al., 2004). We performed expansion of EBs from day 6 to day 10 form an initial number of 500 ESCs, we trypsinised them, counted total cells (Figure 22A) and then performed flow cytometry with the marker of erythroid lineage CD71 and Ter119, in order to test the more immature to more mature erythroid progenitors (Figure 22B -F). We distinguished the populations in R1-R2 ($CD71^+$ $Ter119^-$) and R1-R4 ($CD71^+$ $Ter119^+$). Enucleated cells ($CD71^-$ $Ter119^+$) were very few.

Table 7. Marker expression of cells at different time points of expansion from EBs (Carotta et al., 2004)**.**

	EB		ES-EP				FL-EP	
Marker	Day 6, %	Day 7, %	Day 14, %	Day 21, %	Day 40, %	Day 82, %	Day 7, %	Day 14, %
Multipotent								
Sca-1	8.6 ± 1.9	2.0 ± 0.7	1.1 ± 0.6	< 1	< 1	< 0.1	4.8 ± 2.9	2.3 ± 2.4
CD34	5.5 ± 2.3	25.3 ± 7.7	15.9 ± 1.3	13.9 ± 0.1	8.8 ± 1.6	< 1	11.6 ± 6.1	6.5 ± 2.1
CD117	61.2 ± 5	50.1 ± 10.0	45.6 ± 11	38.4 ± 2.3	64.0 ± 9.1	62.0 ± 7.7	59.5 ± 6.4	57.5 ± 3.5
Erythroid								
Ter119	2.9 ± 1.4	40.0 ± 4.4	75.6 ± 7.9	94.3 ± 2.4	88.5 ± 5.7	69.6 ± 14.8	42.2 ± 3.0	31.5 ± 5.5
[MFI of Ter119]	[13.9 ± 8.3]	[185.4 ± 81.5]	[191.7 ± 64.8]	[425.5 ± 120.9]	[175.0 ± 42.44]	[42.0 ± 1.4]	[28.6 ± 1.5]	[91.5 ± 33.4]
Ter119/CD117	0.9 ± 0.3	35.0 ± 15.2	47.0 ± 5.7	37.9 ± 3.2	65.0 ± 23.5	13.9 ± 2.0	11.0 ± 2.8	13.0 ± 0.7
Myeloid								
Mac1	< 0.1	3.7 ± 2.1	< 1	< 1	< 0.1	< 0.1	7.3 ± 4.0	< 1
Lymphoid								
B220	1.0 ± 0.4	< 1	< 1	< 0.1	< 0.1	< 0.1	1.2 ± 0.1	< 1
CD19	< 0.1	< 1	< 0.1	< 0.1	< 0.1	< 0.1	2.2 ± 0.8	< 1
CD4	< 0.1	< 1	< 0.1	< 0.1	< 0.1	< 0.1	2.4 ± 1.5	< 1
Endothelial								
Flk-1	41.6 ± 8.7	< 0.1	< 0.1	< 0.1	< 0.1	ND	1.6 ± 0.6	1.1 ± 1.6
Proliferating cell marker								
CD71	91.0	98 ± 1.2	99.0 ± 0.8	99.8 ± 0.2	99.7 ± 0.3	ND	99.0 ± 1.4	99.2 ± 0.4

Unfortunately, this system had much variation and could not provide strong evidence for the role of *Erf* in erythropoiesis. At day 5 and 6, cells had produced R3-4 populations, whereas in day 7 to 10 they had only R1-R2 populations (Figure 22). This is strange as the proportion of R3-4 population should increase by the time. However, when we look at day 7, 9 and 10 where the cells have not differentiated to R3-4 populations, we can conclude that *Erf*$^{-/-}$ have reduced proportion of this population. This is consistent with the reduced cells in peripheral blood of embryos. However, we could not make any conclusions because of these variations.

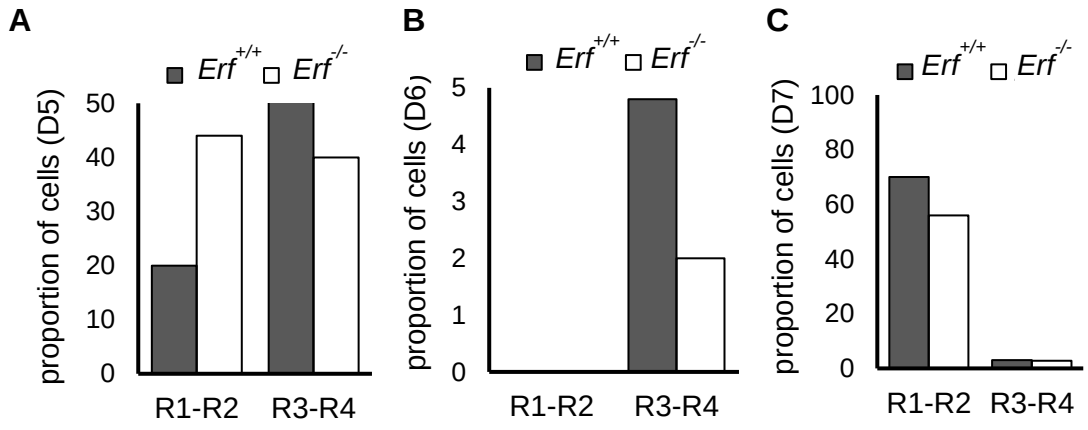

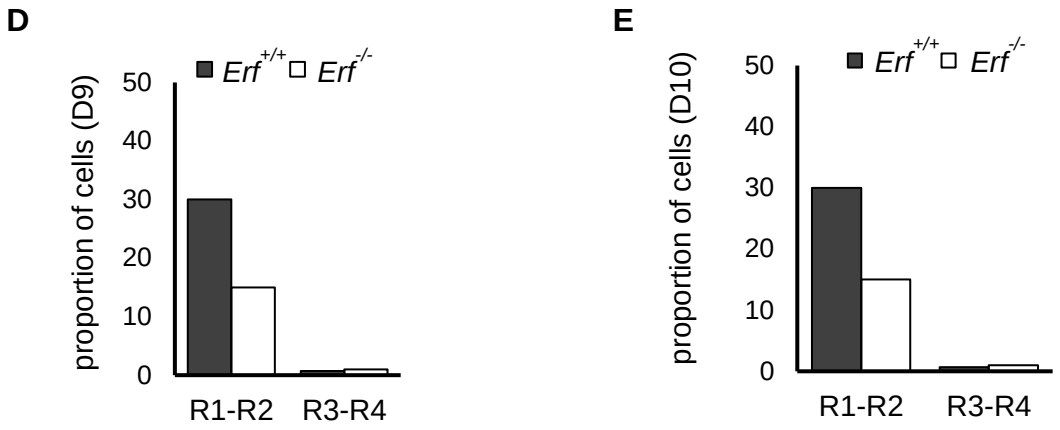

Figure 22. Proportion of erythroblast in *Erf*$^{-/-}$ Embryoid bodies. (A) Proportion of R1,2 and R3,4 population at day 5 of EBs (D5), **(B)** day 6 (D6), **(C)** day 7 (D7), **(D)** day 9 (D9) and **(E)** day 10 (D10). EBs formed from murine 500 ESCs with the method of hanging drop in media for induction to hematopoietic cells. At day 2, the cultured in suspension in same media and the collected at day 5, 6, 7, 9 and 10 for flow cytometry with the markers for erythroblast CD71 and Ter119. *Erf*$^{-/-}$ are compared to *Erf*$^{+/+}$ embryoid bodies. Each experiment performed once. R1-R2: CD71^{+}Ter119^{-}, R3-R4: CD71^{+}Ter119^{+}.

14. Ex vivo expansion and differentiation of *Erf*$^{ed/ed}$ fetal liver ertythroblasts

Our current data indicate a decreased number of embryonic erythrocytes and a decreased differentiation of the R2 to the R3 population in the fetal liver as the underlying defect. To that extend, we used ex vivo expansion and differentiation of embryonic liver–derived erythroblasts in order to determine the possible phenotypic and molecular changes leading to the decreased numbers of embryonic erythrocytes in *Erf*$^{ed/ed}$ embryos.

Given the absence of laboratories with the relevant expertise in the country at this period, we acquired and utilized the techniques of expansion and differentiation of erythroblasts, during an one month secondment in the Dr. Marieke von Lindern's lab, an expert in the field of mouse erythroid development. Initially, primary fetal liver-derived erythroblasts from *Erf*$^{ed/ed}$ embryos at embryonic day E12.5 to E13.5 were expanded in medium supplemented with specific growth factors of erythropoiesis. In order to study self-renewal and differentiation of erythroid progenitors, established approaches were used. We examined proliferation defects by counting cell

every day, but our data indicate that *Erf*$^{ed/ed}$ mice erythroblasts had no difference both in total numbers and the proliferation rate at E12.5 as E13.5 fetal livers (Figure 23). Results have been estimated by three *Erf*$^{ed/ed}$ out of 12 littermates at E13.5 and from only 1 *Erf*$^{ed/ed}$ out of 17 at E12.5. In figure 23, because we had only one *Erf*$^{ed/ed}$ in E12.5, we show results for each sample separately in order to examine all variations. Our travel did not permit us to know the genotype before we left, as liver samples should be arrived to Netherlands no more than 6 hours.

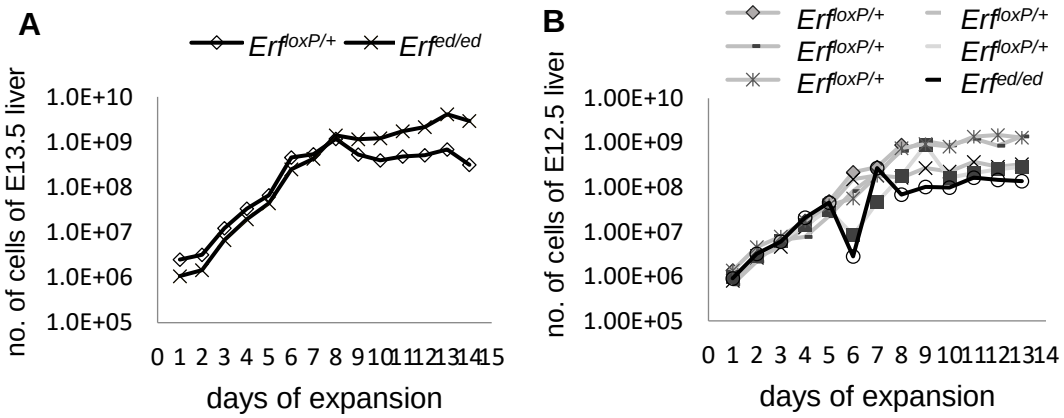

Figure 23. (A) *Erf*$^{ed/ed}$ cell cultures initiated from fetal livers yield of extensively proliferating cells. (A) Cells from E13.5 livers were grown in expansion media for 41 days and cells were remained in a density < 2 x10^6 cells/ml and (B) from E12.5 livers. Cells were counted every day and diluted properly. Number of cells in each day was estimated according to the counting and the dilution that was made. *Erf*$^{ed/ed}$ are compared to *Erf*$^{loxP/+}$ littermates. All values are means of 4 *Erf*$^{loxP/+}$ biological samples and 3 *Erf*$^{ed/ed}$ from 3 litters at E13.5 and 5 *Erf*$^{loxP/+}$ biological samples and 1 *Erf*$^{ed/ed}$ from 1 litters at E12.5. Each experiment performed once. Statistical analysis was performed using the unpaired t-test with two-tailed distribution.

To study the differentiation process, erythroid cells grew in specific erythroid maturation media and cells were isolated at time points of 0, 12, 24, 36 and 48 hours. In order to distinguish the maturation stages of the erythroblasts according to both cell and nuclear size, we used casy machine at the referred time points. As shown Figure 24 A, B, total volume of cells was counted in E13.5 and E12.5 erythroblast, respectively, after differentiation at 12, 24, 36 and 48 hours. In order to distinguish the premature to more mature erythroblasts, cells

that had diameter < and > 7.5 μM were measured separately in casy machine (Figure 24 C, D respectively). E12.5 livers had also been distinguished based onsize (data are not shown). Our data indicate no difference in diameter of cells both in E13.5 and E12.5 livers. E13.5 liver also stained with benzidine in order to distinguish hemoglobin content but no differences were found (Figure 24 E). Moreover, in order to examine the stage of differentiation of erythroblasts, we performed flow cytometry with the markers CD71 and Ter119, whose dynamic expression distinguishes R1 – R5 erythroblast populations, as well as with CD44 that exhibits a progressive and dramatic decrease from proerythroblasts to reticulocytes. Our results did not show any difference in flow cytometry between littermates (Figure 24 F).

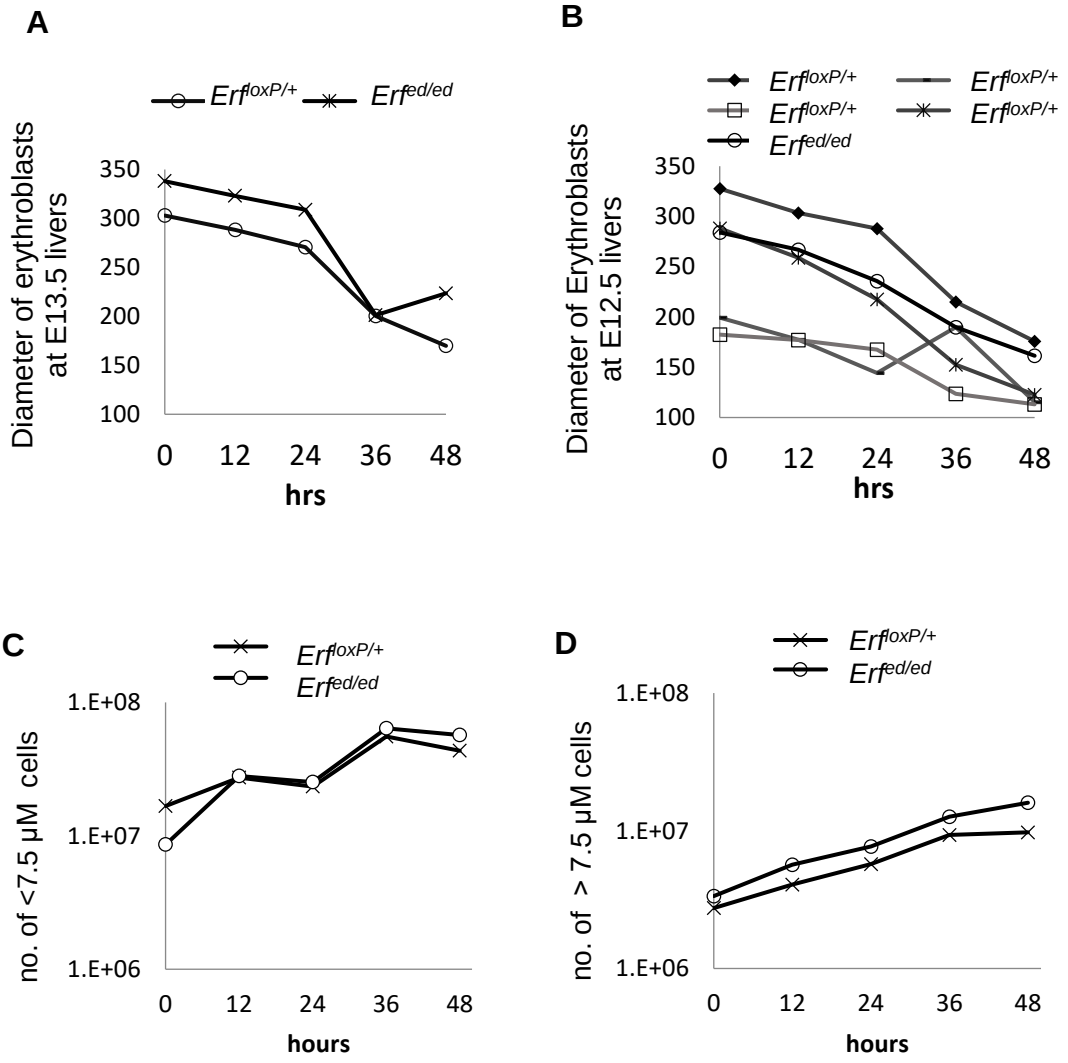

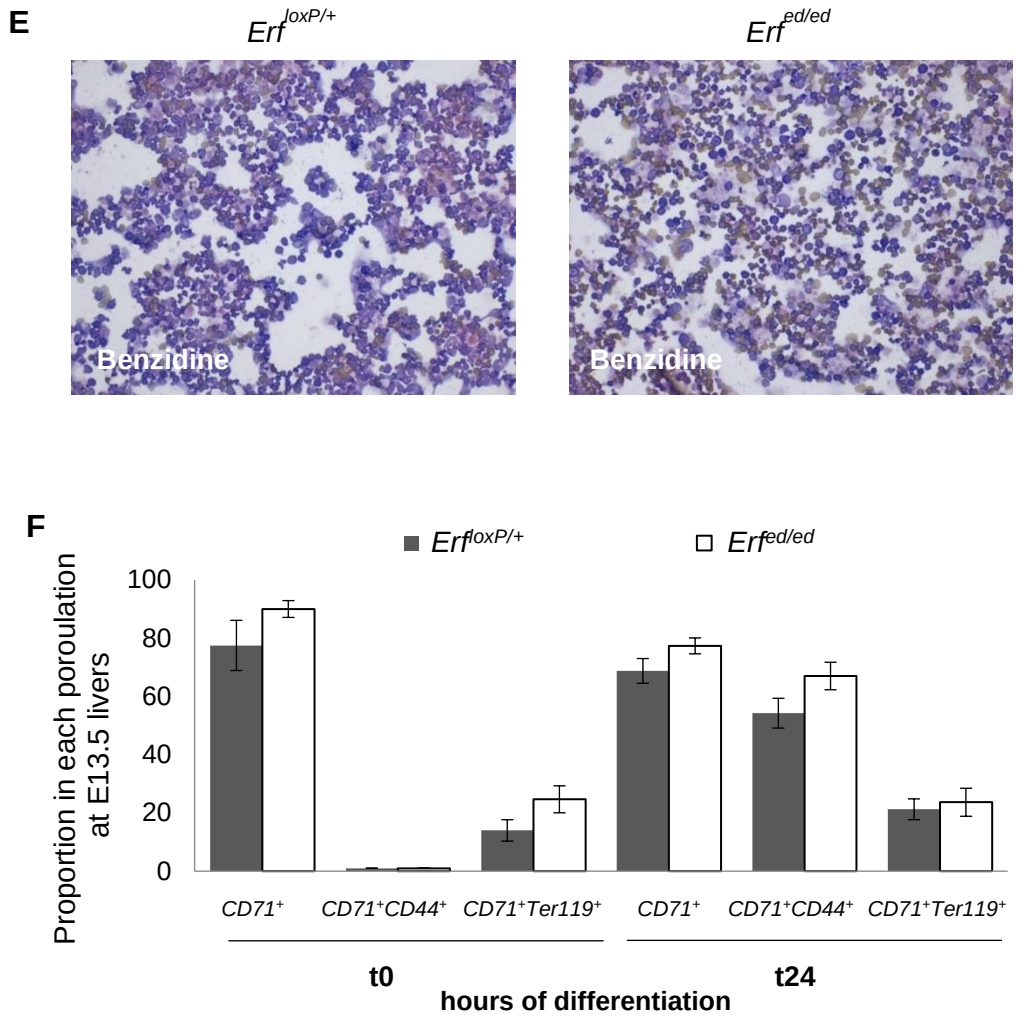

Figure 24. *Erf*$^{ed/ed}$ maintain their ability to mature ex vivo. (A) Cells from E13.5 and **(B)** E12.5 livers were grown in differentiation media for 12, 24, 36 and 48 hrs and mean volume of the cells was measured on casy machine. **(C)** Number of cells from E13.5 were distinguished as <7.5 μM and **(D)** >7.5 μM on casy machine at 12, 24, 36 and 48 hrs differentiation. **(E)** Benzidine staining at E13.5 blood smears after 24 hrs of differentiation. **(F)** Proportion of cells positive for CD44, CD71 and Ter119 after 0 and 24 hrs differentiation of E13.5 livers based on flow cytometry. *Erf*$^{ed/ed}$ are compared to *Erf*$^{loxP/+}$ littermates. All values are means of 4 *Erf*$^{loxP/+}$ biological samples and 3 *Erf*$^{ed/ed}$ from 3 litters at E13.5 and 5 *Erf*$^{loxP/+}$ biological samples and 1 *Erf*$^{ed/ed}$ from 1 litters at E12.5. Each experiment performed once. Statistical analysis was performed using the unpaired t-test with two-tailed distribution.

To examine if the addition of growth factors press the system to a physiological growth even though *Erf*$^{ed/ed}$ mice may have an intrinsic defect, we performed expansion and differentiation of erythroblasts with gradient concentrations of stem cell factor (SCF) and erythropoietin (epo), respectively.

SCF is essential for proliferation and erythropoietin is crucial for survival in low concentrations, but in big quantities it is crucial for differentiation of erythroblasts.

To that extend, we tested expansion of *Erf*$^{ed/ed}$ erythroblasts with gradient concentrations of SCF 30, 3, 1, 0.3, 0.1, 0.03, 0.01 ng/ml for 24 and 28 hrs in the presence of 0.1 u/ml epo for survival. To study differentiation, erythroblasts cultivated with gradient concentrations of 3, 1, 0.3, 0.1, 0.03 and 0.01 ng/ml erythropoietin for 12 hrs. Cells plated in gradient concentrations after 5 days of expansion and all erythroblasts derived from E13.5 fetal livers.. At time points, number of *Erf*$^{floxP/+}$ cells and *Erf*$^{ed/ed}$ was counted and cells distinguished base on a mean volume <7.5 μM as in indicator of more mature erythroblasts. The mean volume of the cells was measured on casy machine. All values are means of 4 *Erf*$^{floxP/+}$ biological samples and 2 *Erf*$^{ed/ed}$ from 2 litters. Moreover, samples analyzed for flow cytometry against CD71, Ter11 and CD44 (data not shown). Statistical analysis was performed using the unpaired t-test with two-tailed distribution.

We were initially surprised by the lack of any differences in ex vivo culture. We know from previous experiments that R1/R2 portion in knockout fetal livers is increased in vivo and a small differentiation delay occurs. However, these data are consistent with the transcriptome of *Erf*$^{floxP/+}$ and *Erf*$^{ed/ed}$ E13.5 liver cells, analyzed by RNA-seq that found no molecular target. Given that we do not observe any differentiation blockage but severe quantitative differences, the lack of differences is not surprising. For example, if a progenitor cell had failed to proliferate/differentiate effectively, considering its small proportion in the total liver population and the lack of any unique cell type specific gene markers, it would not have produced any detectable difference. Analysis of subpopulation may be required to identify the affected cell type. This analysis however is hampered by the lack of efficient specific markers and the minimal numbers of the potentially interesting cell types.

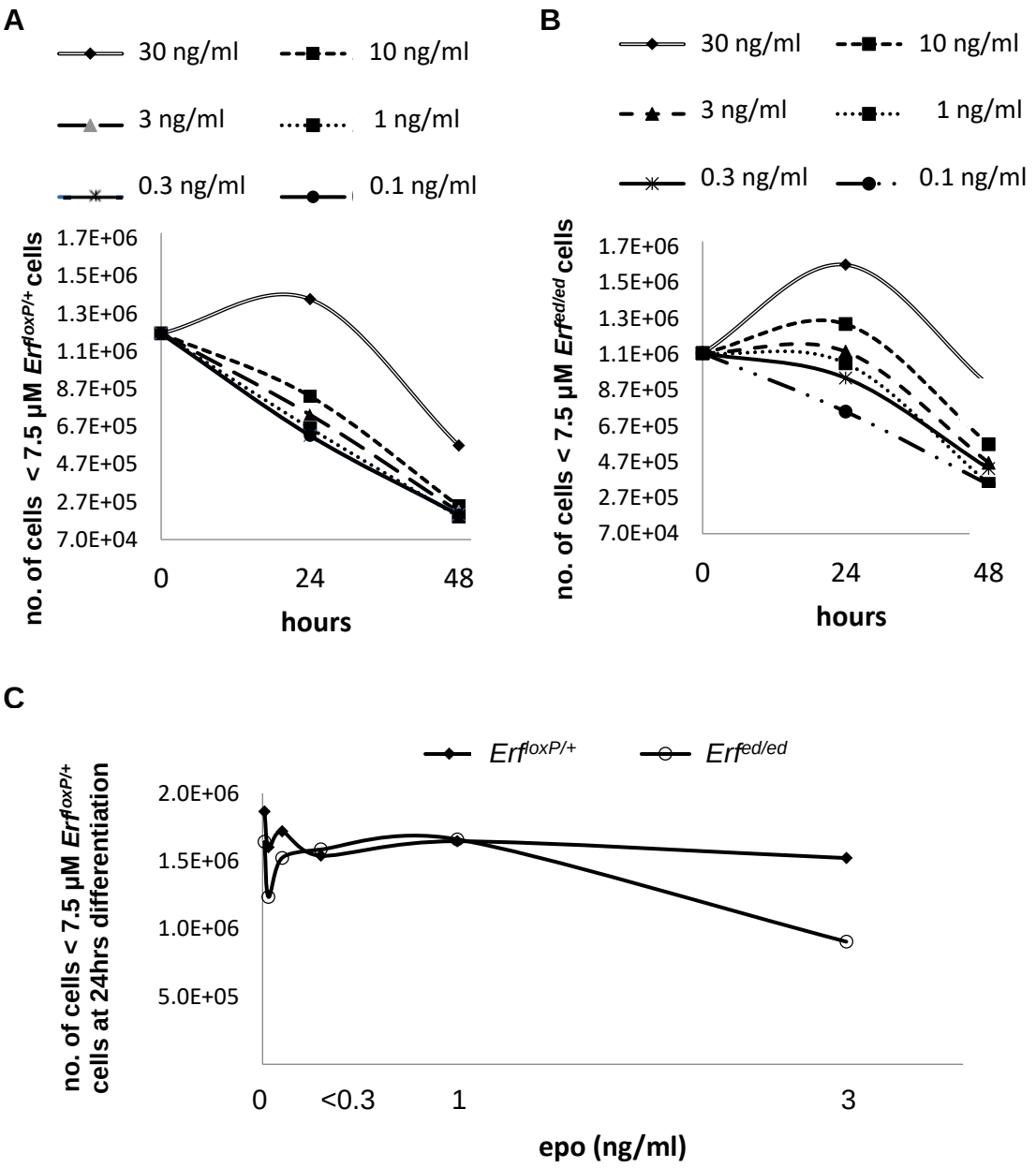

Figure 25. Grandient concentrations of SCF and erythropoietin does not affect *Erf*$^{ed/ed}$ differentiation ex vivo. (A) Number of *Erf*$^{loxP/+}$ cells and **(B)** *Erf*$^{ed/ed}$ distinguished on a mean volume <7.5 µM after expansion with gradient concentrations of SCF for 24 and 48 hrs. SCF: 30, 3, 1, 0.3, 0.1 ng/ml. **(C)** Number of *Erf*$^{loxP/+}$ cells and *Erf*$^{ed/ed}$ distinguished on a mean volume volume <7.5 µM after expansion with gradient concentrations of epo for 24 hrs. Epo: 1, 0.3, 0.1, 0.03, 0.01 ng/ml All erythroblasts derived from E13.5 fetal livers. The mean volume of the cells was measured on casy machine. All values are means of 4 *Erf*$^{loxP/+}$ biological samples and 2 *Erf*$^{ed/ed}$ from 2 litters Statistical analysis was performed using the unpaired t-test with two-tailed distribution.

15. Molecular targets of Erf in hematopoietic cells

To discover the molecular targets of Erf, we performed RNA-seq analysis at E13.5 livers. Provided that the total blood cell counts in periphery drops at 3 % at E14.5 compared to 50% at E13.5, we assumed that the critical day is E13.5. For the RNA-seq analysis, RMA from *Erfl*$^{loxP/+}$ and 2 *Erf*$^{ed/ed}$ livers from the same litter was isolated. Analysis revealed no differences in the transcriptome of *Erf*$^{ed/ed}$ compared *to Erfl*$^{loxP/+}$ livers. We were surprised by the lack of any differences in the transcriptome and the 20% expression of Erf, analyzed by RNA-seq. However, given that we do not observe any differentiation blockage but severe quantitative differences, the lack of differences is not surprising. For example, if a progenitor cell had failed to proliferate/differentiate effectively, considering its small proportion in the total liver population and the lack of any unique cell type specific gene markers, it would not have produced any detectable difference.

To discover a possible target of Erf, we studied RunX1 as it has a lot of feature that could make him a conceivable target. First of all *Runx1* is expressed in HSCs and downstream myeloid cells, but its expression is decreased in maturing erythroid cells (North et al., 2004). Consistent with the reduced HSCs after the transplantation assay, Erf may block the Runx1 activation and cells finally to differentiate. Cooperation of Runx1 with PU.1 is critical for the commitment to myeloid lineages (de Bruijn et al., 2000), making it a target of Erf. Moreover, Runx1 is crucial for the emergence of hematopoietic stem cells from the hemogenic endothelium from the AGM.

For this reason, we performed Real time PCR in cDNAs from peripheral blood at E10.5. Runx1 transcript variants that encode different protein isoforms result from 2 alternate promoters (P1 and P2) as well as from alternate splicing (Martinez et al., 2016). The Runx1 isoforms derived from P2 are expressed in a variety of tissues, such as brain, kidney, pancreas, heart and liver but expression of P1-derived isoform is predominantly expressed in hematopoietic stem cell, megakaryocytes and T lymphocytes present in thymus and spleen (Martinez et al., 2016). Each promoter leads to 2 alternative splicing resulting to 4 different products (Martinez et al., 2016). Three different primer sets were used in RT-PCR for the 2 variants derived from promoter P1 (Runx1P1) and 2

variants derived from promoter P2 (Runx1P2) and one for all the 4 variants (RunX1). RT-PCR was performed in E10.5 peripheral blood of 7 *Erf*$^{floxP/+}$ and 5 *Erf*$^{ed/ed}$ samples from three litters. Samples are represented as ratio to *Erf*$^{floxp/+}$ littermates. Values for *Erf*$^{ed/ed}$ and *Erf*$^{floxP/+}$ cells were compared to the average value of the *Erf*$^{floxP/+}$ littermates.

Our results show no significant differences in the mRNA levels of Runx1 in all the three primer sets (Figure 26). However, primers for all 4 variants (RunX1) had a better efficiency in Real-Time, in contrast to primers for promoter P1 and P2 in which we had also no product in a lot of samples. So, our data indicate that either Erf does not influence mRNA levels of RunX1 or the effect has begun very early in hemopoiesis, for example from the moment of the emergence of hematopoietic cells and cannot be detected.

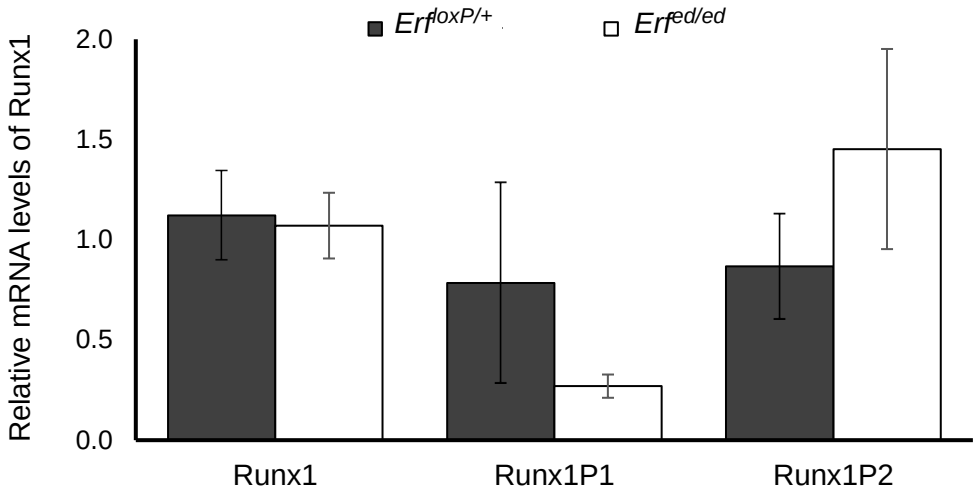

Figure 26. *Erf*$^{ed/ed}$ have normal mRNA levels of RunX1. mRNA level of Runx1 were quantified by RT-PCR. Primers for the 4 variants of RunX1 (RunX1), primers fro the 2 vaviants that come from promoter P1 and prmoter P2 were employed. Each experiment performed once. Values for *Erf*$^{ed/ed}$ and *Erf*$^{floxP/+}$ cells are compared to the average value of the *Erf*$^{floxP/+}$ littermates. Samples are represented as ratio to *Erf*$^{floxp/+}$ littermates. All values are means ± SE of at at least 5 samples from 3 litters. Statistical analysis was performed using the unpaired t-test with two-tailed distribution.

Part II. Craniosynostosis

Craniosynostosis is a disease that leads to the premature fusion of cranial sutures and affects 1 of 2,000 children. Here, we indicate for first time that Erf reduced dosage causes craniosynostosis in both mice and humans.

1. Craniosynostosis in mice with reduced dosage of Erf

Initially, we observed that *Erf*$^{floxP/-}$ mice appeared smaller and their head was intricate, a phenotype similar to craniosynostosis (Figure 1 A). To study more precisely the skulls of *Erf*$^{floxP/-}$ mice, we performed staining with alizarin and alcian blue, which stain osteoblasts and chondrocytes, respectively (Figure 1 B), as well we performed μicro-CT scans to study the phenotype in more details (Figure 1 C). The μicro-CT scans were performed in cooperation with Dr. Stephen Twigg and Dr. Andrew Wilkie of the Clinical Genetics Group, at the Weatherall Institute of Molecular Medicine, at University of Oxford. Our results indicate that sagittal (S), coronal (C) and lambdoid (L) sutures were normal in the *Erf*$^{+/-}$ mutant (Figure 1 C, i), but the *Erf*$^{floxP/-}$ littermates have craniosynostosis of the sagittal and coronal sutures (Figure 1 C, ii) or sagittal, coronal and lambdoid sutures (Figure 1 C, iii). The reason of craniosynostosis in *Erf*$^{floxP/-}$ and not in *Erf*$^{+/-}$ was studied by Real-time PCR by E. Vorgia, a previous member in the lab, finding that *Erf*$^{floxP/-}$ mice had transcription levels of Erf at 30% compared to *Erf*$^{+/+}$. This demonstrates that the *Erf*^{floxP} allele is hypomorphic, conceivably due to the intronic *PGKneo* cassette, which may reduce the efficiency of the transcript production. So, our results indicate that haploinsufficiency of Erf leads to the premature fusion of cranial sutures in mice.

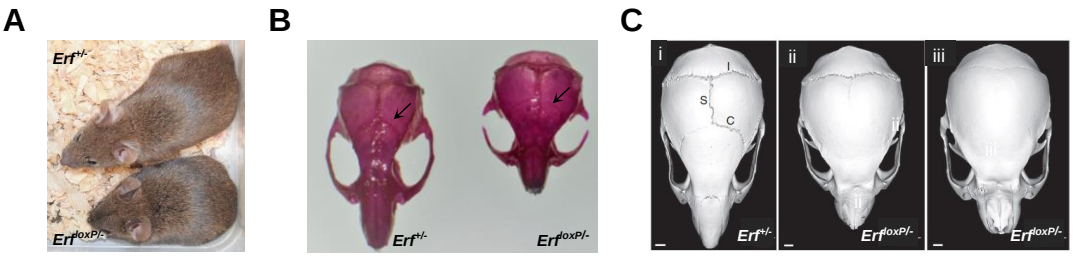

Figure 1. *Erf*$^{floxP/-}$ mice have craniosynostosis. (A) *Erf*$^{floxP/-}$ mice appear smaller and with strange head compared to *Erf*$^{+/-}$. Age: 2 months **(B)** Skulls of

Erf$^{loxP/-}$ mice are smaller and the sagittal sutures are not obvious compared to *Erf*$^{+/-}$ (arrow). Alcian and alizarin staining was performed to distinguish chondrocytes and osteoblasts, respectively. Red: osteoblasts, Blue: Chondrocytes, which are visible a little in the nose indicating a normal situation. **(C)** μicro-CT scanning of the heads of mice aged 9 weeks. Note normal morphology and patent sagittal (S), coronal (C) and lambdoid (L) sutures in the *Erf*$^{+/-}$ mutant (**i**), whereas the *Erf*$^{loxP/-}$ littermates have craniosynostosis of the sagittal and coronal sutures (**ii**) or sagittal, coronal and lambdoid sutures (**iii**).

2. Craniosynostosis in hymans with mutations of ERF

Next, we investigated the role of Erf in craniosynostosis in humans. Analysis of the genome of patients with craniosynostosis (by Dr. Stephen Twigg and Dr. Andrew Wilkie) revealed specific mutations in the *Erf* gene. The number of patients that were examined and the type of craniosynostosis they had as well some of their phenotypes are shown in Table 6 and Figure 2.

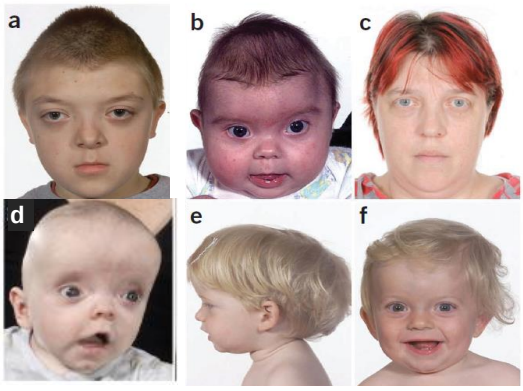

Figure 2. Patients with craniosynostosis have ERF mutations. (a-f) Phenotypes of humans with craniosynostosis.

Specifically, *ERF* is consisted of 4 exons (Figure 3 A) and encodes a ubiquitously expressed member of the ETS family of transcription factors (numbering 28 in humans), which functions as a negative transcriptional regulator, by competing with other ETS family members for DNA binding or due to interaction with other targets. ERF functional characterized motifs are located in the N-terminal DNA-binding (ETS), central ERK interaction and C-terminal repressor domains (Figure 3A,B). DNA binding targets a core motif (5′-GGA(A/T)-3′), with little sequence discrimination from other ETS family

members. The identified *ERF* mutations were diverse: the three missense changes (one recurrent) were located in critical residues in the DNA-binding ETS domain or disrupted the initiation codon, whereas the remaining eight mutations comprised a splice-site mutation, two nonsense changes and three frameshift mutations (one recurrent, present in three families) (Figure 3).

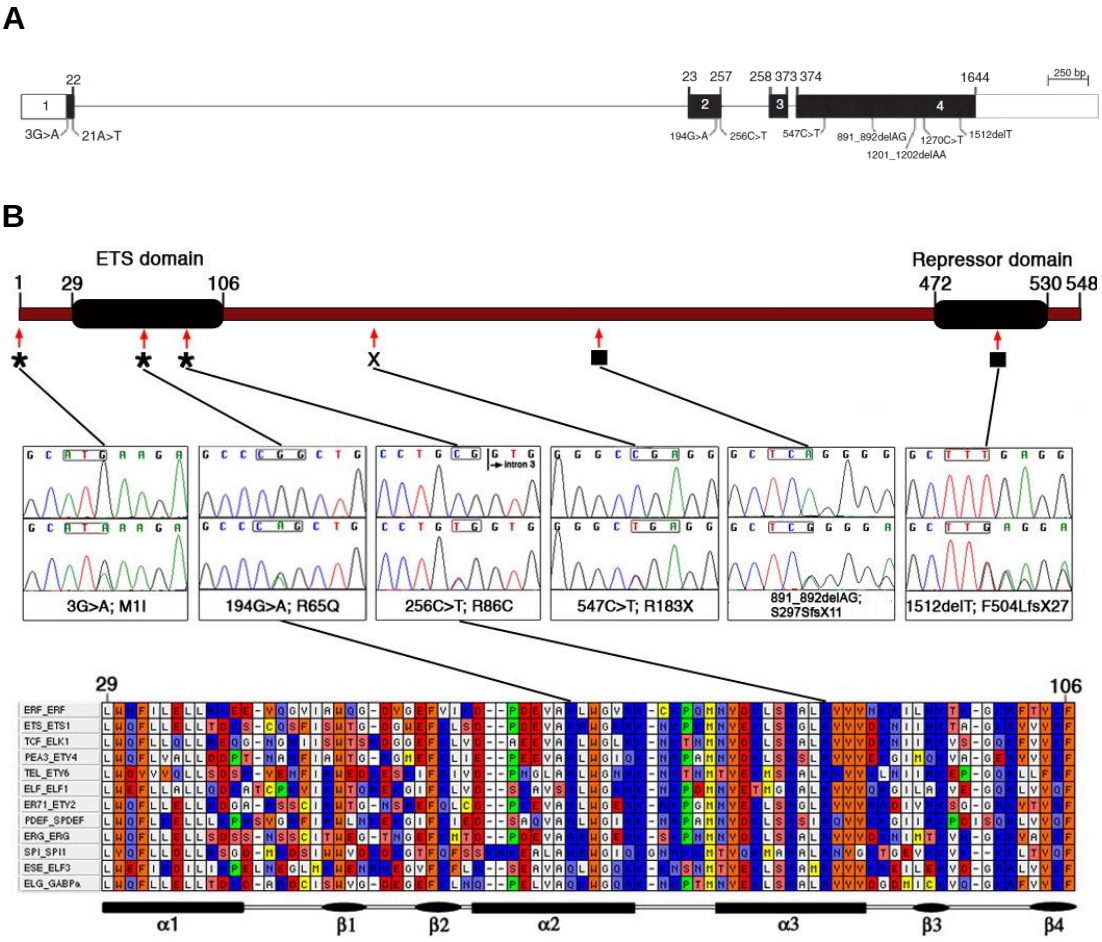

Figure 3. Exon and domain structure of ERF and mutations identified in craniosynostosis. (A) *ERF* comprises 4 exons extending over 7.6 kb and (**B**) encodes a 548-amino-acid protein. The positions of serine (S) and threonine (T) sites phosphorylated by ERK4 are indicated. Two missense substitutions, pArg65Gln and p.Arg86Cys, localize to the ETS DNA-binding domain and one frameshift occurs in the repressor domain. Shown below is the ETS domain sequence from a representative member of each ETS subfamily in humans. Fully and partially conserved residues are indicated.

Table 2 Mutations of *ERF* present in 12 families

Family	Proband	Proband craniosynostosis phenotype[a]	Individuals with mutations[b]	cDNA change	Predicted amino-acid change	*De novo* mutation
1	OX2158	M	II-2, III-3, IV-1, IV-2	c.547C>T	p.Arg183*	–
2	OX2729	NA	II-1	c.1512delT	p.Phe504Leufs*27	–
3	OX2789	P	II-1	c.891_892delAG	p.Gly299Argfs*9	–
4	OX3247	UL	II-2, III-1	c.256C>T	p.Arg86Cys	+
5	OX3248	S	II-1, III-1	c.194G>A	p.Arg65Gln	–
6	OX3801	M	II-1, III-1, III-2, IV-2	c.3G>A	p.0	+
7	OX3970	M	II-2, III-1, III-2	c.891_892delAG	p.Gly299Argfs*9	–
8	OX4097	M	II-1	c.891_892delAG	p.Gly299Argfs*9	+
9	OX4626	P	II-2, III-1, III-2	c.1270C>T	p.Gln424*	–
10	OX4708	M	II-1	c.256C>T	p.Arg86Cys	+
11	OX4902	S	II-2, II-3, III-1	c.21A>T	p.Gly8_Phe9ins147	–
12	OX5072	P	II-1	c.1201_1202delAA	p.Lys401Glufs*10	–

[a]M, multiple-suture synostosis; P, pansynostosis; S, sagittal synostosis; UL, unilateral lambdoid synostosis; NA, not available.
[b]Details are given in **Supplementary Figure 1**.

3. Crucial mutations for ERF activity

To study the significance of each mutation in the activity for Erf, we created constructs that have the substitution of arginine to glutamine (194G>A;R65Q) and the arginine to cysteine (256C>T;R86C) at the DNA binding domain of the protein but also the frameshift mutation in the repressor domain (1512delT; F504LfsX27). In one way, the mutations have been inserted in the pSG5 plasmid containing both ERF DNA binding and repressor domain. Then, this plasmid co-transfected in HeLa cells with the plasmid pGL3 basic or the pGL3 enhancer that both contain the GATA1 DNA binding sequence on which the Erf binds. When Erf is active then the luciferase gene cannot be transcribed. In a second way, psG424 plasmid was employed for ERF mutations to be inserted, after the DNA binding domain of Gal4. Then each plasmid was co-transfected with the pGl3 control Gal4 DNA binding sequence plasmid or the pGL3 enhancer Gal4 DNA binding sequence plasmid and the levels of luciferase were quantified after transfection in HeLa cells. Our results indicate that both mutations for arginine to glutamine (194G>A;R65Q) and the arginine to cysteine (256C>T;R86C) at the DNA binding domain are crucial for the activity of Erf (Figure 4A), but also the mutation in repressor domain (1512delT; F504LfsX27) (Figure 4B). However, we observed a repression of luciferase expression when we transfected the 1512delT mutation of Erf with its (non-gal4) binding domain (Figure 4A), but this occurs because binding of Erf in the

promoter compete the binding efficiency of other ets factors that can activate the expression.

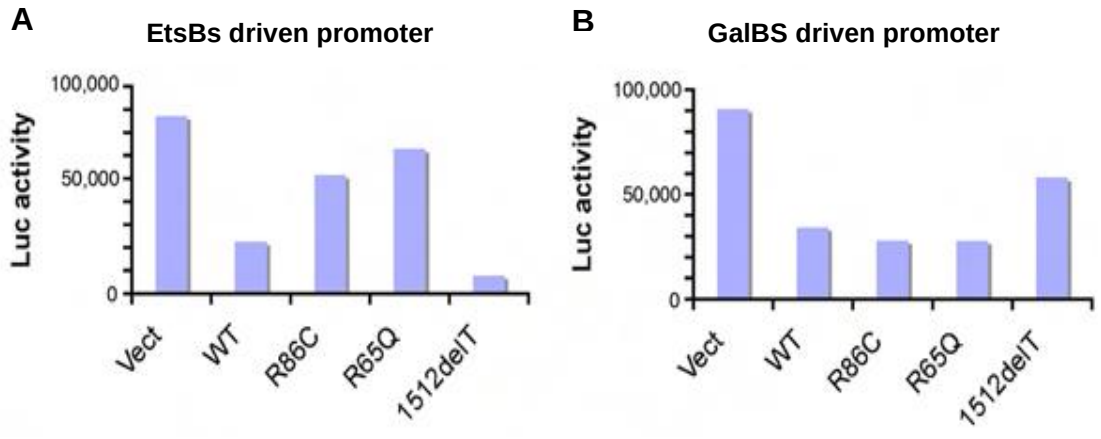

Figure 4. ERF DNA binding mutants R86C, R65Q and repressor domain mutant (1512delT) fail to repress luciferase expression. (A) Ets-binding mutants (R86C, R65Q) fail to repress Ets-binding containing promoters**.** The deletion 1512T can retain suppressor activity because its DNA binding domain can compete endogenous activation factors. **(B)** The deletion/frameshift (1512T) failed on Gal4 DNA binding sequence. Ets binding mutations show suppression as Gal4 binding domain is functional.

4. RUNX2 and Erf DNA binding motifs are common

To explore the nuclear targets of Erf, chromatin immunoprecipitation (ChIP) of Erf in mouse embryonic fibroblasts (MEFs) was performed by A. Zaragoulias, a previous member of our lab. By comparing the enriched sequences from fibroblasts maintained without fetal calf serum (FCS) for 4 h (–FCS: inactive Erk1/2, nuclear Erf) to those from cells supplemented with FCS (+FCS: Erk1/2 phosphorylation and nuclear entry, consequent phosphorylation and nuclear export of Erf), we could identify the component of the ChIP-seq signal attributable to dynamic Erf binding (defined by a −FCS/+FCS ratio of >3). Signals of dynamic binding were divided according to if they were found within 1 kb of a transcriptional start sites (TSS; putative promoter) or at greater distances (non-TSS; putative enhancer). MEME analysis identified two major sequences enriched near TSSs, one corresponding to the ETS-binding consensus and the other to the sequence bound by Ronin-Hcfc1. In non-TSSs, which are believed to identify tissue-specific interactions of ETS factors, the

three most highly specific sequence motifs were 5′-TGANTCA-3′, 5′-TGTGG-3′ and 5′-TTCCT-3′, where N represents any nucleotide, corresponding to consensus motifs for AP-1, RUNX and ETS factors, respectively. This suggests that Erf-binding sites frequently lie close to the binding sites for other transcription factors. However, RunX2 is a known factor, which is involved in osteogenesis, so we focused on if ERF is really associated with RunX2. The ChIP-seq data identified sites of dynamic binding within introns of *Runx2*, which might reflect direct regulation of transcription. Alternatively, Erf may regulate osteogenesis by altering the balance of positive and negative regulatory complexes formed on DNA targets by Runx2 and other Ets proteins. Moreover, Little *et al.*(Little et al., 2012) identified enrichment of a hybrid ETS-RUNX binding motif very similar to the sequence (5′-GGATGTGG-3′) in our data set.

For this reason, we examined the effects of ERF and RUNX2 on transactivation using a DNA-binding target containing this core sequence in 3 different sequences (d1: 5'-CTAGAGA**GGATGTGG**TTT-3' and d5: 5'-CTAGAGA**GGATG**ATCCTGTGGTTT-3', d10: 5'-CTAGAGAGGATGATGGAT**GGATGTGG**TTT-3'). These core sequences were cloned in the pGL3 promoter plasmid, which has a luciferace gene under its promoter, while Erf and RunX2 were cloned in the pSG5 plasmid, separately each one (see methods section for the specific enzymes and method that was used). pSG5-Erf, pSG5-Runx2 and pGL3-d1, d5, d10 motifs co-transfected in HeLa cells and repressor activity of Erf on Runx2 was estimated through expression of luciferase gene. Our results indicate that whereas RUNX2 alone elicited 1.6-fold upregulation of expression, this induction was suppressed by ERF, which lowered expression to below the basal level, similar to the effect of ERF added alone (Figure 5A), indicating antagonism by ERF of RUNX2-mediated transactivation in this model situation. Note here that this result has been observed in all three sequence cores (d1, d5, d10) that were employed.

Given that the ChIP-seq data showed potential interactions of Erf and Runx2 at numerous targets (Figure 5B), further work will be required to identify critical factors in osteogenic dysregulation in the *ERF* or *RUNX2* haploinsufficiency states. However, the position of ERF downstream of the RAS-MEK-ERK cascade and the delayed onset of suture ossification associated with *ERF* haploinsufficiency make ERF an attractive target for therapeutic modulation.

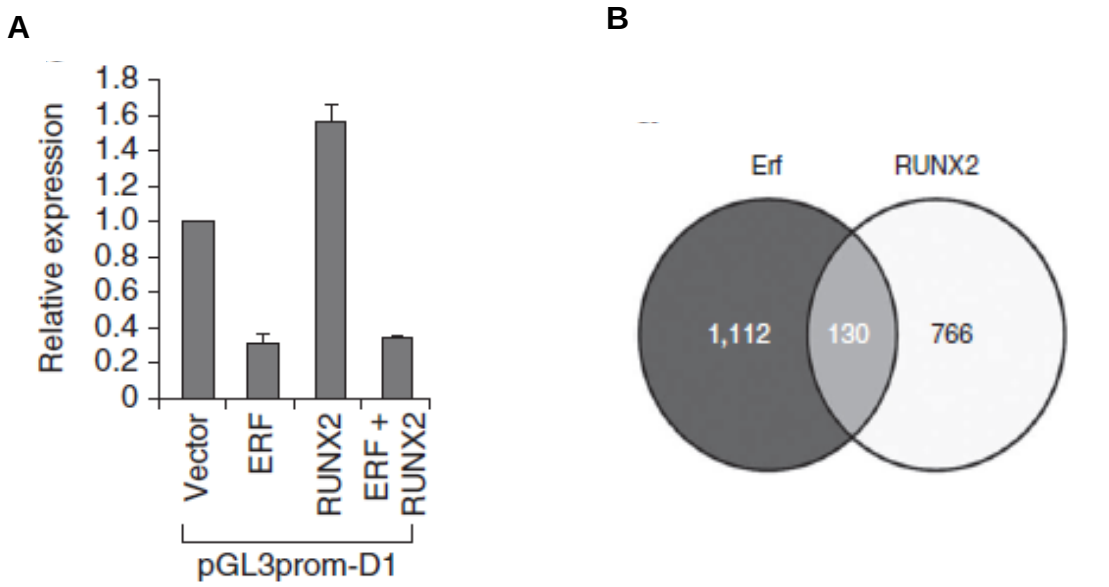

Figure 5. RunX2 inhibition by Erf. (A) Transactivation analysis using the hybrid Erf-Runx2 binding target identified by ChIP-seq (5′-agaGGATGTGGttt-3′, core target capitalized). HeLa cells were transfected with 1 µg of empty vector or with vectors encoding *ERF* or *RUNX2* cDNA, alone or in combination. Results were normalized relative to reporter expression detected with empty vector and are expressed as the mean ± s.e. of four independent experiments. **(B)** Overlapping transcriptional targets of Erf and RUNX2 identified by ChIP-seq. Comparison of non-TSS mouse Erf targets with −FCS/+FCS > 3 identified in this work (*n* = 2,033) with orthologous human RUNX2 targets identified by Little *et al.* (*n* = 1,603). To improve the specificity of linkage to regulated genes, ChIP-seq peaks more than 40 kb away from the closest RefSeq gene were excluded.

4. Discussion

In this study, we demonstrate for first time that *Erf* is detrimental to embryonic erythropoiesis. Mice lacking *Erf* in embryo proper at E5 (MeoxCre), to bypass lethality due to placenta defects (Papadaki et al., 2007), exhibited severe anemia and died around embryonic day (E) 14.5. Our data indicate that *Erf* elimination decreases, but does not block, the primitive and definitive yolk sac-derived erythropoiesis waves and impairs fetal liver definitive hematopoiesis with decreased numbers of precursor and mature cells and inefficient differentiation of immature erythroid precursors. Moreover, Erf appears to be necessary for hematopoietic stem cells that support adult hematopoiesis, for maintenance or differentiation, as evident by their impaired repopulation ability (Proposed model figure).

1. Erf is required for the primitive yolk sac derived erythroblasts

The ontogeny of the hematopoietic system is a complex process with multiple waves of hemopoietic potential, emerging from different anatomical sites (Palis et al., 1999; Palis, 2014). The first hematopoietic progenitors that emerge in the yolk sac at embryonic day E7.5 are called primitive wave. Primitive progenitors generate the first circulating blood cells of erythroid, megakaryocyte and macrophage lineages (Kingsley et al., 2004; Fraser et al., 2007) and provide the majority of circulating blood cells until E12.5 (Palis, 2014).

The reduced numbers of blood cells at E9.5 and onwards in the $Erf^{ed/ed}$ embryos, counted from peripheral blood at E9.5 and onwards, indicate that the cells of primitive wave are reduced. Because of the onset of anemia as early as E9.5, we initially examined erythropoiesis at E9.5 when erythroblasts mature semi-synchronously. At E9.5, the yolk sacs revealed normal mesothelium and visceral endoderm junctions, but the blood islands contained fewer and larger primitive erythroblasts in $Erf^{ed/ed}$ mice. On the contrary, the yolk sac vasculature of $Erf^{ed/ed}$ embryos appeared normal and as a result we excluded vasculogenesis as the reason of lethality. Provided that more than 95 % of the circulating erythroid cells from E9.5 to E12.5 derive from the primitive wave of hematopoietic progenitors in the yolk sac (Fraser et al., 2007), the reduced numbers of circulating blood cells would suggest a defect in primitive

erythropoiesis. In addition, both morphology of cells and the mRNA reduced levels of εy globin, which is expressed in the mature cells of primitive wave, show that *Erf*$^{ed/ed}$ have more immature primitive cells. All these data suggest that *Erf* may affect the onset or differentiation rate of these cells. Future studies must be done in order to prove if *Erf* is required for the formation of hemogenic endothelium, the emergence of cells from it or the maintenance of primitive cells in bloodstream. Techniques like immunofluorescence in the AGM region or culture of EBs toward differentiation to hematopoietic cells and isolation of hemangioblast, hemogenic endothelium and their descendants in the proper days would be appropriate.

2. Erf is required for the definitive yolk sac derived erythroblasts

Shortly after the production of primitive wave, a second wave also begins in the yolk sac at embryonic day E8.25, called the definitive wave and comprises erythroid and myeloid progenitors (EMPs) (Palis et al., 1999; Bertrand et al., 2005; Tober et al., 2007) that begin to colonize the fetal liver at embryonic day E9.5, until a third wave takes place of them in the bone marrow. At E10.5, numbers of EMPs were examined at peripheral blood before they migrate to the fetal liver.

To explore the effect of *Erf* elimination on the progenitors of the definitive hematopoietic wave that emerges in the yolk sac, peripheral blood was isolated at E10.5 and the c-Kit ^{high}, CD41^{+}, CD16/32^{+} erythroid-myeloid progenitor cells (EMP) cells were quantitated by flow cytometry. Both the number and proportion of EMPs was decreased at 50%. The number of definitive erythroid progenitors (BFU-E and CFU-E), defined by their ability to form colonies in semisolid media, was also significantly reduced at E10.5. Taken together, these data confirm that the yolk sac-derived EMP wave of hematopoietic potential is also impaired in early stages of their development by the loss of *Erf*.

3. Erf is required for the differentiation of definitive erythroblasts in fetal liver

The increased anemia at E13.5 – E14.5 indicated a profound lack of definitive erythroid cells which are produced at this time in the fetal liver and

make up the majority of the circulating cells at these time points (Houssaint, 1981; Palis et al., 1999). *Erf*$^{ed/ed}$ embryos show additional differentiation defects in definitive erythropoiesis after EMPs have homed to the fetal liver. Analysis of E11.5 – E13.5 *Erf*$^{ed/ed}$ embryos revealed significantly reduced liver size and liver cell numbers compared to their *Erf*$^{loxP/+}$ littermates. This is consistent with the decrease in EMPs in the bloodstream at E10.5. To examine if this reduction is due to the colonization and/or the expansion of the erythroid progenitors to the liver, we analyzed BFU-E and CFU-E numbers at E11.5 – E13.5. BFU-E/CFU-E colony assays reveal increased proportion of BFU-E and CFU-E at E12.5 - E13.5 livers, indicating an additional defect in differentiation process. Proportion of CFU-E colonies in E11.5 fetal livers were also increased but proportion of BFU-E, the more immature colonies, was similar and as a result we excluded the reason of the increased proportion of CFU-E due to the delay of the emergence of the cells. However, the total number of cells are reduced as a result of the reduced production of cells in bloodstream. Additionally, flow cytometry of liver cells indicates increased proportion of R1 (CD71^{low}, Ter119^{-}), R2 (CD71^{high}, Ter119^{-}) proerythroblasts and reduced proportion of the mature R3 (CD71^{high}, Ter119^{+}), R4 (CD71^{high}, Ter119^{+}) populations at E12.5 livers. The total number of cells are reduced again as a result of the reduced production of cells in bloodstream. This is consistent with the colony assay as we know that R1 cells comprise ≥ 40% CFU-Es, R2 contain only a few CFU-Es and R3 – R5 contain no erythroid progenitors (Sieff et al., 2010). These data suggest an additional role for Erf in R1-R2 towards R3 differentiation.

4. Erf is required for HSC development

Erf appears to have a crucial role in the differentiation of HSCs emerging from the AGM at E10.5, migrating to the liver and ultimately constituting the adult HSCs in the bone marrow (Medvinsky and Dzierzak, 1996).

Transplantation of *Erf*$^{ed/ed}$ liver cells into irradiated mice shows that recipients could not live beyond 4 weeks, suggesting a defect in short-term HSCs. Addition of spleen helper cells from wt mice to assess long-term HSCs, indicate a marginal contribution from the *Erf*$^{ed/ed}$ cells 5 months after transplantation.

These data allude to a defect in HSC maintenance or differentiation ability that may have implications in adult pathologies and needs further examination.

However, it still remains unknown in which stage and cell type of maintenance, expansion or maturation *Erf* is crucial. Future studies must be done by deletion of Erf with retrovirus in adult bone marrow HSCs, cultivation in specific media for maintance of only the HSC proportion and examination of each stage of differentiation with specific markers.

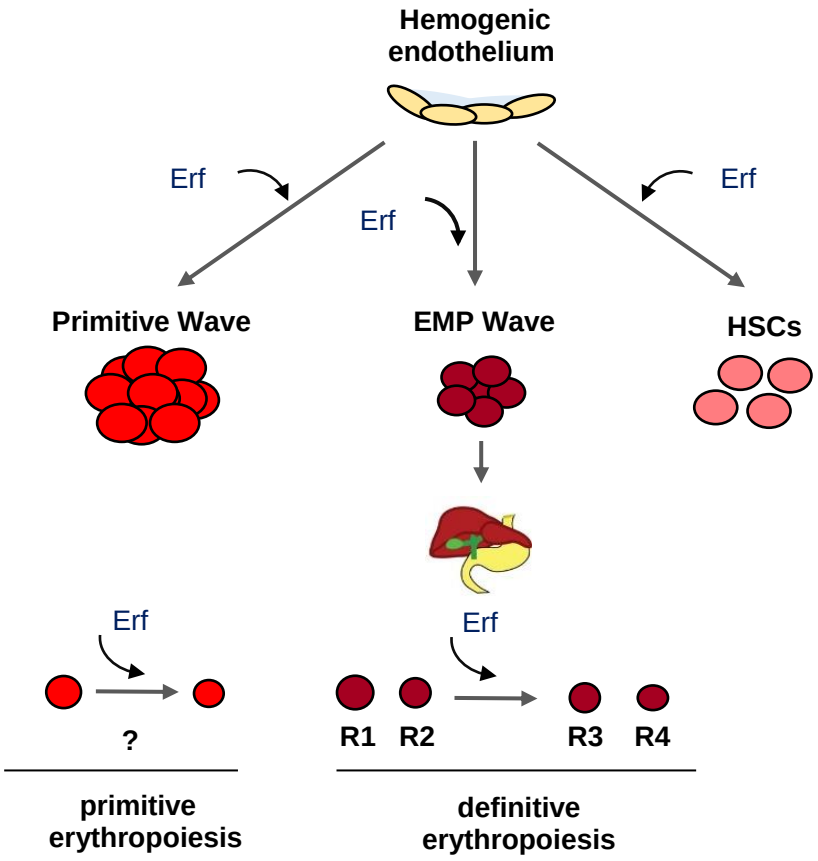

Proposed model. **Erf is involved in different waves and aspects of hematopoiesis.** It is required for both primitive and definitive yolk sac derived hematopoiesis, as well as for the production or the maintenance of HSCs. It is also required for the rate of differentiation of R2 to R3 maturing cells in the fetal liver.

5. Erf is required for normal osteogenesis

We have demonstrated for first time that reduced dosage of Erf causes complex craniosynostosis, a disease of premature fusion of the cranial sutures, in both mice and humans.

Erf$^{loxP/-}$ mice have reduced protein levels of *Erf* ~ 30% of normal exhibit postnatal multiple-suture synostosis. Haploinsufficiency of Erf was the reason of craniosynstosis. Using chromatin immunoprecipitation in mouse embryonic fibroblasts and high-throughput sequencing, we found that Erf binds preferentially to elements away from promoters that contain Runx or AP-1 motifs. Runx2 is known that has two different promoters P1 and P2 that produce 4 variants (Stock and Otto, 2005). P1 is expressed in highly differentiating cells, while P2 in mesenchymal or pre-osteoblasts and chondrocytes (Stock and Otto, 2005). Erf may compete with activating ETS factors that act together with Runx2 in multifactor transcriptional complexes or compete the binding of the same Runx2. One suggestion is that low levels of Erf may lead to Runx2 constant activation in mesenchymal cells or in the osteoblasts, resulting in differentiation to osteoblasts or mature, respectively in a faster way. Our results are consistent with the fact that activation of Erk leads to maturation of mesenchymal to osteogenesis (Salasznyk et al., 2004).

Future studies must be done to find the specific progenitor that Erf is related to and next to discover Erf targets. Moreover, therapeutic assays could be done by increasing the quantity of Erf through regulation of Erk kinase by specific inhibitors. To rescue the craniosynostosis phenotype in mice would be a big step for treatment in humans.

6. Quantity of Erf is crucial for survival

The extent of defects in both hemopoiesis and osteogenesis appear to be Erf quantity dependent. Haploinsufficiency of Erf (*Erf*$^{loxP/-}$) leads to craniosynostosis, while heterozygous mice appear no defects. Moreover, total absence of Erf in the embryo leads to death due to anemia, while reduced levels of *Erf* lead to survival with non-mendelian frequences.

The quantity effect is observed in both hemogenic endothelium *Lyve1*$^{Cre/+}$ *Erf*$^{loxP/loxP}$ mice and *Erf*$^{loxP/-}$ embryos. Similar to the epiblast-deleted *Erf*$^{ed/ed}$

embryos, the *Lyve1*$^{Cre/Cre}$ *Erf*$^{floxP/loxP}$ embryos appear anemic, have reduced BFU-E/CFU-E colonies in the bloodstream at E10.5, and reduced numbers of total cells and erythroid precursors in the liver at E14.5. On the other hand, *Lyve1*$^{Cre/+}$ *Erf*$^{floxP/loxP}$ mice had reduced numbers of CFU-Es compared to *Erf*$^{+/+}$, bit increased numbers compared to *Lyve1*$^{Cre/Cre}$ *Erf*$^{floxP/loxP}$*.* The same results have been observed and been statistical significant in all *Erf*$^{floxP/-}$ mice for both primitive and definitive assays. Moreover, in contrast to the *Lyve1*$^{Cre/Cre}$ *Erf*$^{floxP/loxP}$ embryos, *Lyve1*$^{Cre/+}$ *Erf*$^{floxP/loxP}$ as wells as *Erf*$^{floxP/-}$ mice were viable albeit with sub-mendelian frequencies, indicating a quantity dependent defect.

Analysis of the *Erf* expression in fetal livers showed that heterozygous *Lyve1*-cre embryos have significantly higher expression than the homozygous *Lyve1*-cre as well as the *Meox2*-cre embryos. This would suggest that the frequency of *Erf* elimination and/or the level of expression of *Erf* in EMPs may be critical for the severity of the defect and thus survival.

However, Lyve1 is expressed in the definitive wave at E8.5 and comprises a marker for discrimination of definitive from primitive yolk sac derived cells (L. K. Lee et al., 2016). On the contrary, we noticed that *Lyve1*$^{Cre/Cre}$ *Erf*$^{floxP/loxP}$ embryos had also reduced total cells at E10.5 - E12.5 peripheral blood, when the majority of the erythroblasts is the primitive wave. This could not be explained neither based on the microenvironment of yolk sac as Lyve1 is not known to be expressed there based on primitive erythropoieisis.

7. Hematopoietic cell autonomous defect

The apparent defect in the production and differentiation of the primitive and definitive erythroid lineage in the absence of *Erf*, appears to be a cell autonomous event.

The cell types and contacts of yolk sacs as well as the vascular system of yolk sac and embryo looked normal, indicating the cell autonomous character of primitive cells. Moreover, the embryo weight and the anatomy of the hearts the three layers of placenta did not reveal abnormalities.

As evidenced, the elimination of *Erf* in the Lyve1-expressing hemogenic endothelium cells of the yolk sac leads to lethality, indicating a cell autonomous

defect. Moreover, the reduced number of the liver derived HSCs at the transplantation assay confirms the cell autonomous activity of definitive cells.

Elimination of Erf in fetal livers (*Alfp - cre;Erf*$^{loxP/loxP}$) did not lead to lethality, verifying that hepatocytes are not responsible for lethality. Moreover, the stromal cells of the liver looked normal after immunostaining with specific markers (data not shown). Our data demonstrate the cell autonomous defect of hematopoietic cells.

8. The RTK/Ras/Erk pathway in hemopoiesis and osteogenesis

Erf is a member of the *ets*-family of transcription factors and an effector in the RTK/Ras/Erk pathway, which both have been involved in diverse facets of hematopoiesis (Le Gallic et al., 1999).

Erk has been reported to lead to tight junctions between endothelial cells in the AGM region of zebrafish, thus repressing the emergence of hematopoietic stem cells from hemogenic endothelium but promoting the arterial endothelial identity (C. Zhang et al., 2014). After the artery – vein specification, Erk is inactivated by Smad1/5 through recruitment of histone deacetylases and finally leads to the EHT (C. Zhang et al., 2014). This is consistent with the fewer number of HSCs that are found in the transplants with *Erf*$^{ed/ed}$ livers, but also with the reduced numbers of EMPs and primitive cells, as it is known that there is also hemogenic endothelium in the yolk sac of mice (Padron-Barthe et al., 2014). BMP4 which is upstream of Smad, is known to be important not only for hemogenic endothelium and initiation of HSCs production, but also for differentiation to mature osteoblasts (Lan et al., 2014). We could make a hypothesis that BMP4 could regulate Erk signaling both in hemopoiesis and osteogenesis. Erf is transported to cytoplasm and as result EHT is blocked and osteoblasts mature.

According to osteogenesis, gain of function mutations in Fgf2 (Byun et al., 2014) leads to overactivation of Erk pathway and increased osteogenesis. This is consistent with our results that lead to increased osteogenesis in the absence of Erf. Moreover, Fgf2 is required for the differentiation of mesoderm to hemangioblast in the heart, so next its inactivation is important for

hemangioblast to differentiate to the next cell type. This indicates a dual role of Fgf2 both in osteogenesis and hemopoiesis.

In addition, oncogenic H-Ras protein leads to block of terminal differentiation of CFU-E progenitors in vivo, which can explain the differentiation defect of CFU-E and R2 population in *Erf*$^{ed/ed}$ livers (J. Zhang et al., 2003).

9. Possible targets of Erf in hemopoiesis and osteogenesis

Ets transcription factors recognize a common DNA-binding motif and may antagonize each other on a variety of targets (Hollenhorst et al., 2011). Erf, a transcriptional repressor, may ensure the absence of spurious activation by other ets-family proteins or repress the transcription of non-ets genes, leading to the proper differentiation programs and homeostasis (Hollenhorst et al., 2011).

Overexpression of PU-1 ets family protein, is reported to block the differentiation of BFU-E / CFU-E to mature erythrocytes (Schuetze et al., 1993). Moreover, expression of PU.1 is important for differentiation of multipotent hematopoietic cells to osteoclasts. Osteoclasts are cells that act as macrophage against osteoblast. To that extend, Erf could compete the binding of PU.1 in order CFU-E to differentiate to mature erythrocytes or hematopoietic cells to differentiate to osteoclasts resulting normal osteogenesis. The archetypal fusion gag-Myb-Ets oncoprotein, encoded by E26 retrovirus, induces acute leukemia and can block both myeloid and erythroid differentiation at the stage of BFU-E / CFU-E (Rascle et al., 1996), which is consistent with the absence of Erf. Erf has been again reported to promote erythroid differentiation in K52 cells (Athanasiou et al., 2003). Moreover, overactivation of E26 Ets1 protein leads to increased mineralization (Rabault and Ghysdael, 1994), and Erf may antagonize Ets1 that also has a role in erythroid differentiation process (Clausen et al., 1997).

Another plausible hypothesis on the diverse effects of Erf in hematopoiesis is its interplay with the Runx factors. *Runx1* is expressed in HSCs and downstream myeloid cells, but its expression is decreased in maturing erythroid cells (North et al., 2004). Consistent with the reduced HSCs after the transplantation assay, Erf may block the Runx1 activation and cells finally to

differentiate. Cooperation of Runx1 with PU.1 is critical for the commitment to myeloid lineages (de Bruijn et al., 2000). Moreover, Runx1 transcription appears to be regulated via ets factor binding to one of its enhancers (Nottingham et al., 2007). It is conceivable Erf to antagonize PU.1 and suppress Runx1 indirectly.

Runx2 is highly expressed in HSCs and is decreased as they mature (Kuo et al., 2009). In osteogenesis, Runx2 leads to maturation of osteoblasts. Another, possibility is Erf to antagonize or repressTwist1 only in HSCs. Overexpression of Twist1 leads to activation of Runx1 in HSCs (C. Y. Dong et al., 2014), while it leads to the inactivation of Runx2 in osteoblasts (Qin et al., 2012). Finally, we have shown that the Runx-Erf interplay on osteogenic targets may be important for bone development and craniosynostosis (Twigg et al., 2013). It is conceivable that a similar interplay may also be relevant in hematopoietic development with Erf and Runx1 or Runx2 in very early stages of hematopoiesis in bloodstream or at the region of AGM, where HSCs are produced as we did not observe any difference in mRNA levels of Runx1 at E10.5 bloodstream.

10. Difficulties in finding Erf molecular targets

In spite of the wide effect of *Erf* on hematopoiesis, it remains unclear if there is a common underlying mechanism or if there are distinct downstream effectors involved in the different cell types affected.

The fact that in the absence of Erf we have quantitative differences rather than a block in any specific differentiation step or the cell cycle, makes determination of possible mechanisms even more challenging. Indeed, transcriptional analysis of E13.5 livers, before the collapse of peripheral blood levels, failed to reveal statistically significant differences in genes or pathways between wt and *Erf*-null cells (unpublished data). This would be consistent with a quantitative rather than an instructive effect. This conclusion is also supported by the apparent difference in viability of the Lyve1-cre heterozygous and homozygous animals in which the observed difference may be the result of the extent of the deletion. In addition, our unpublished data indicate a minimal but

statistically significant sub-mendelian frequency of the viable *Erf*$^{loxP/-}$ animals, suggesting an effect because of the timing and/or the extent of *Erf* expression.

Given that we do not observe any differentiation blockage but severe quantitative differences, the lack of differences is not surprising. For example, if a progenitor cell had failed to proliferate/differentiate effectively, considering its small proportion in the total liver population and the lack of any unique cell type specific gene markers, it would not have produced any detectable difference.

11. Biological significance

Our data strongly suggest an important role of Erf in all 3 waves primitive, EMP and HSC, of hematopoiesis during ontogeny. Erf activity is regulated by phosphorylation and nucleo-cytoplasmic shuttling and thus could be an appealing target for intervention. However, further experiments are needed to elucidate its precise mechanism and the stage of action during hematopoietic differentiation or self-renewal or maintenance, particularly in the HSC.

Understanding the molecular mechanisms controlling the potential of erythroid cells to expand and differentiate and identifying how this potential may be modified or lost would be useful for both basic research and clinical applications. The molecular role of *Erf* in mouse development and specifically in erythropoiesis is not appreciated, yet. Elucidation of the role of *Erf* in hematopoietic development not only further our understanding on these processes but is also be relevant in understanding adult hematopoietic disorders as the myelodysplastic syndrome (MDS).

Because of the Erf regulation via nuclear export after RTK activation, *Erf* KO is simulating aberrant MAPK signaling that can be relevant in these processes. Thus, validating the role of Erf in hematopoiesis will also offer a new target for possible intervention in cases where the gene is intact but the protein is inactivated due to inappropriate signaling.

5. References

Adolfsson, L.E., Lundgren, M., Tilling, B., et al. (2005). Short-term safety and tolerability of double-dose salmeterol/fluticasone propionate in adult asthmatic patients. Clin. Drug Investig. *25*, 231-241.

Aiuti, A., Cicchini, C., Bernardini, S., et al. (1998). Hematopoietic support and cytokine expression of murine-stable hepatocyte cell lines (MMH). Hepatology *28*, 1645-1654.

Akashi, K., Traver, D., Miyamoto, T., et al. (2000). A clonogenic common myeloid progenitor that gives rise to all myeloid lineages. Nature *404*, 193-197.

Allegra, M., Zaragkoulias, A., Vorgia, E., et al. (2012). Semaphorin-7a reverses the ERF-induced inhibition of EMT in Ras-dependent mouse mammary epithelial cells. Mol. Biol. Cell *23*, 3873-3881.

Allen, A., Fisher, C., Premawardhena, A., et al. (2010). Adaptation to anemia in hemoglobin E-ss thalassemia. Blood *116*, 5368-5370.

Alter, B.P. (1979). Fetal erythropoiesis in stress hematopoiesis. Exp. Hematol. *7 Suppl 5*, 200-209.

Athanasiou, M., Blair, D.G., and Mavrothalassitis, G. (2003). ERF, an ETS-related transcriptional repressor, can induce erythroid differentiation. Anticancer Res. *23*, 2143-2153.

Athanasiou, M., LeGallic, L., Watson, D.K., et al. (2000a). Suppression of the Ewing's sarcoma phenotype by FLI1/ERF repressor hybrids. Cancer Gene Ther. *7*, 1188-1195.

Athanasiou, M., Mavrothalassitis, G., Sun-Hoffman, L., et al. (2000b). FLI-1 is a suppressor of erythroid differentiation in human hematopoietic cells. Leukemia *14*, 439-445.

Ayres-Silva Jde, P., Manso, P.P., Madeira, M.R., et al. (2011). Sequential morphological characteristics of murine fetal liver hematopoietic microenvironment in Swiss Webster mice. Cell Tissue Res. *344*, 455-469.

Bankston, P.W., and Pino, R.M. (1980). The development of the sinusoids of fetal rat liver: morphology of endothelial cells, Kupffer cells, and the transmural migration of blood cells into the sinusoids. Am. J. Anat. *159*, 1-15.

Barker, J.E. (1968). Development of the mouse hematopoietic system. I. Types of hemoglobin produced in embryonic yolk sac and liver. Developmental biology *18*, 14-29.

Belaoussoff, M., Farrington, S.M., and Baron, M.H. (1998). Hematopoietic induction and respecification of A-P identity by visceral endoderm signaling in the mouse embryo. Development *125*, 5009-5018.

Bertrand, J.Y., Jalil, A., Klaine, M., et al. (2005). Three pathways to mature macrophages in the early mouse yolk sac. Blood *106*, 3004-3011.

Bethlenfalvay, N.C., and Block, M. (1970). Fetal erythropoiesis. Maturation in megaloblastic (yolk sac) erythropoiesis in the C 57 B1-6J mouse. Acta Haematol. *44*, 240-245.

Bialek, P., Kern, B., Yang, X., et al. (2004). A twist code determines the onset of osteoblast differentiation. Dev. Cell *6*, 423-435.

Bose, R., Karthaus, W.R., Armenia, J., et al. (2017). ERF mutations reveal a balance of ETS factors controlling prostate oncogenesis. Nature.

Brotherton, T.W., Chui, D.H., Gauldie, J., et al. (1979). Hemoglobin ontogeny during normal mouse fetal development. Proceedings of the National Academy of Sciences of the United States of America *76*, 2853-2857.

Bulger, M., Schubeler, D., Bender, M.A., et al. (2003). A complex chromatin landscape revealed by patterns of nuclease sensitivity and histone modification within the mouse beta-globin locus. Molecular and cellular biology *23*, 5234-5244.

Byun, M.R., Kim, A.R., Hwang, J.H., et al. (2014). FGF2 stimulates osteogenic differentiation through ERK induced TAZ expression. Bone *58*, 72-80.

Cantor, A.B., and Orkin, S.H. (2002). Transcriptional regulation of erythropoiesis: an affair involving multiple partners. Oncogene *21*, 3368-3376.

Carotta, S., Pilat, S., Mairhofer, A., et al. (2004). Directed differentiation and mass cultivation of pure erythroid progenitors from mouse embryonic stem cells. Blood *104*, 1873-1880.

Chang, L., and Karin, M. (2001). Mammalian MAP kinase signalling cascades. Nature *410*, 37-40.

Chen, M.J., Yokomizo, T., Zeigler, B.M., et al. (2009). Runx1 is required for the endothelial to haematopoietic cell transition but not thereafter. Nature *457*, 887-891.

Chen, W.S., Manova, K., Weinstein, D.C., et al. (1994). Disruption of the HNF-4 gene, expressed in visceral endoderm, leads to cell death in embryonic ectoderm and impaired gastrulation of mouse embryos. Genes & development *8*, 2466-2477.

Cheng, J.T., Cobb, M.H., and Baer, R. (1993). Phosphorylation of the TAL1 oncoprotein by the extracellular-signal-regulated protein kinase ERK1. Molecular and cellular biology *13*, 801-808.

Choi, K., Kennedy, M., Kazarov, A., et al. (1998). A common precursor for hematopoietic and endothelial cells. Development *125*, 725-732.

Chun, K., Teebi, A.S., Azimi, C., et al. (2003). Screening of patients with craniosynostosis: molecular strategy. Am. J. Med. Genet. A *120A*, 470-473.

Ciau-Uitz, A., Monteiro, R., Kirmizitas, A., et al. (2014). Developmental hematopoiesis: ontogeny, genetic programming and conservation. Exp. Hematol. *42*, 669-683.

Ciurea, A.V., and Toader, C. (2009). Genetics of craniosynostosis: review of the literature. J. Med. Life *2*, 5-17.

Clausen, P.A., Athanasiou, M., Chen, Z., et al. (1997). ETS-1 induces increased expression of erythroid markers in the pluripotent erythroleukemic cell lines K562 and HEL. Leukemia *11*, 1224-1233.

Coffin, J.D., Florkiewicz, R.Z., Neumann, J., et al. (1995). Abnormal bone growth and selective translational regulation in basic fibroblast growth factor (FGF-2) transgenic mice. Mol. Biol. Cell *6*, 1861-1873.

Connerney, J., Andreeva, V., Leshem, Y., et al. (2006). Twist1 dimer selection regulates cranial suture patterning and fusion. Developmental dynamics : an official publication of the American Association of Anatomists *235*, 1345-1357.

Corlu, A., Lamy, I., Ilyin, G.P., et al. (1998). Hematopoiesis-promoting activity of rat liver biliary epithelial cells: involvement of a cell surface molecule, liver-regulating protein. Exp. Hematol. *26*, 382-394.

Dang, S.M., Kyba, M., Perlingeiro, R., et al. (2002). Efficiency of embryoid body formation and hematopoietic development from embryonic stem cells in different culture systems. Biotechnol. Bioeng. *78*, 442-453.

Davis, R.J. (2000). Signal transduction by the JNK group of MAP kinases. Cell *103*, 239-252.

de Bruijn, M.F., Speck, N.A., Peeters, M.C., et al. (2000). Definitive hematopoietic stem cells first develop within the major arterial regions of the mouse embryo. EMBO J. *19*, 2465-2474.

Deckelbaum, R.A., Holmes, G., Zhao, Z., et al. (2012). Regulation of cranial morphogenesis and cell fate at the neural crest-mesoderm boundary by engrailed 1. Development *139*, 1346-1358.

Delaney, C., Heimfeld, S., Brashem-Stein, C., et al. (2010). Notch-mediated expansion of human cord blood progenitor cells capable of rapid myeloid reconstitution. Nat. Med. *16*, 232-236.

Dennis, J.E., and Charbord, P. (2002). Origin and differentiation of human and murine stroma. Stem cells *20*, 205-214.

Detrich, H.W., 3rd, Kieran, M.W., Chan, F.Y., et al. (1995). Intraembryonic hematopoietic cell migration during vertebrate development. Proceedings of the National Academy of Sciences of the United States of America *92*, 10713-10717.

Dong, C., Davis, R.J., and Flavell, R.A. (2002). MAP kinases in the immune response. Annu. Rev. Immunol. *20*, 55-72.

Dong, C., Yang, D.D., Wysk, M., et al. (1998). Defective T cell differentiation in the absence of Jnk1. Science *282*, 2092-2095.

Dong, C.Y., Liu, X.Y., Wang, N., et al. (2014). Twist-1, a novel regulator of hematopoietic stem cell self-renewal and myeloid lineage development. Stem cells *32*, 3173-3182.

Dooley, K.A., Davidson, A.J., and Zon, L.I. (2005). Zebrafish scl functions independently in hematopoietic and endothelial development. Developmental biology *277*, 522-536.

Dzierzak, E., and Philipsen, S. (2013). Erythropoiesis: development and differentiation. Cold Spring Harb. Perspect. Med. *3*, a011601.

Elorza, A., Hyde, B., Mikkola, H.K., et al. (2008). UCP2 modulates cell proliferation through the MAPK/ERK pathway during erythropoiesis and has no effect on heme biosynthesis. J. Biol. Chem. *283*, 30461-30470.

Fantoni, A., De la Chapelle, A., Rifkind, R.A., et al. (1968). Erythroid cell-development in fetal mice: synthetic capacity for different proteins. J. Mol. Biol. *33*, 79-91.

Farace, M.G., Brown, B.A., Raschella, G., et al. (1984). The mouse beta h1 gene codes for the z chain of embryonic hemoglobin. J. Biol. Chem. *259*, 7123-7128.

Fehling, H.J., Lacaud, G., Kubo, A., et al. (2003). Tracking mesoderm induction and its specification to the hemangioblast during embryonic stem cell differentiation. Development *130*, 4217-4227.

Forrest, C.R., and Hopper, R.A. (2013). Craniofacial syndromes and surgery. Plast. Reconstr. Surg. *131*, 86e-109e.

Fraser, S.T., Isern, J., and Baron, M.H. (2007). Maturation and enucleation of primitive erythroblasts during mouse embryogenesis is accompanied by changes in cell-surface antigen expression. Blood *109*, 343-352.

Friedrich, C., Zausch, E., Sugrue, S.P., et al. (1996). Hematopoietic supportive functions of mouse bone marrow and fetal liver microenvironment: dissection of granulocyte, B-lymphocyte, and hematopoietic progenitor support at the stroma cell clone level. Blood *87*, 4596-4606.

Gao, X., Johnson, K.D., Chang, Y.I., et al. (2013). Gata2 cis-element is required for hematopoietic stem cell generation in the mammalian embryo. J. Exp. Med. *210*, 2833-2842.

Garcia-Porrero, J.A., Godin, I.E., and Dieterlen-Lievre, F. (1995). Potential intraembryonic hemogenic sites at pre-liver stages in the mouse. Anat. Embryol. (Berl.) *192*, 425-435.

Gekas, C., Dieterlen-Lievre, F., Orkin, S.H., et al. (2005). The placenta is a niche for hematopoietic stem cells. Dev. Cell *8*, 365-375.

Gering, M., and Patient, R. (2005). Hedgehog signaling is required for adult blood stem cell formation in zebrafish embryos. Dev. Cell *8*, 389-400.

Godin, I., Dieterlen-Lievre, F., and Cumano, A. (1995). Emergence of multipotent hemopoietic cells in the yolk sac and paraaortic splanchnopleura in mouse embryos, beginning at 8.5 days postcoitus. Proceedings of the National Academy of Sciences of the United States of America *92*, 773-777.

Godin, I., Garcia-Porrero, J.A., Dieterlen-Lievre, F., et al. (1999). Stem cell emergence and hemopoietic activity are incompatible in mouse intraembryonic sites. J. Exp. Med. *190*, 43-52.

Goetze, S., Kim, S., Xi, X.P., et al. (2000). Troglitazone inhibits mitogenic signaling by insulin in vascular smooth muscle cells. J. Cardiovasc. Pharmacol. *35*, 749-757.

Goldie, L.C., Lucitti, J.L., Dickinson, M.E., et al. (2008). Cell signaling directing the formation and function of hemogenic endothelium during murine embryogenesis. Blood *112*, 3194-3204.

Gritsman, K., Yuzugullu, H., Von, T., et al. (2014). Hematopoiesis and RAS-driven myeloid leukemia differentially require PI3K isoform p110alpha. J. Clin. Invest. *124*, 1794-1809.
Guruharsha, K.G., Kankel, M.W., and Artavanis-Tsakonas, S. (2012). The Notch signalling system: recent insights into the complexity of a conserved pathway. Nat. Rev. Genet. *13*, 654-666.
Haar, J.L., and Ackerman, G.A. (1971). Ultrastructural changes in mouse yolk sac associated with the initiation of vitelline circulation. Anat. Rec. *170*, 437-455.
Hernandez-Hernandez, A., Ray, P., Litos, G., et al. (2006). Acetylation and MAPK phosphorylation cooperate to regulate the degradation of active GATA-1. EMBO J. *25*, 3264-3274.
Herrera, R., Hubbell, S., Decker, S., et al. (1998). A role for the MEK/MAPK pathway in PMA-induced cell cycle arrest: modulation of megakaryocytic differentiation of K562 cells. Exp. Cell Res. *238*, 407-414.
Hirschi, K.K. (2012). Hemogenic endothelium during development and beyond. Blood *119*, 4823-4827.
Hollenhorst, P.C., McIntosh, L.P., and Graves, B.J. (2011). Genomic and biochemical insights into the specificity of ETS transcription factors. Annu. Rev. Biochem. *80*, 437-471.
Houssaint, E. (1981). Differentiation of the mouse hepatic primordium. II. Extrinsic origin of the haemopoietic cell line. Cell Differ. *10*, 243-252.
Hsu, C.L., Kikuchi, K., and Kondo, M. (2007). Activation of mitogen-activated protein kinase kinase (MEK)/extracellular signal regulated kinase (ERK) signaling pathway is involved in myeloid lineage commitment. Blood *110*, 1420-1428.
Huang, G., Zhang, P., Hirai, H., et al. (2008). PU.1 is a major downstream target of AML1 (RUNX1) in adult mouse hematopoiesis. Nat. Genet. *40*, 51-60.
Huber, T.L., Kouskoff, V., Fehling, H.J., et al. (2004). Haemangioblast commitment is initiated in the primitive streak of the mouse embryo. Nature *432*, 625-630.
Iseki, S., Wilkie, A.O., and Morriss-Kay, G.M. (1999). Fgfr1 and Fgfr2 have distinct differentiation- and proliferation-related roles in the developing mouse skull vault. Development *126*, 5611-5620.
Jacob, S., Wu, C., Freeman, T.A., et al. (2007). Expression of Indian Hedgehog, BMP-4 and Noggin in craniosynostosis induced by fetal constraint. Ann. Plast. Surg. *58*, 215-221.
Jacobs-Helber, S.M., Ryan, J.J., and Sawyer, S.T. (2000). JNK and p38 are activated by erythropoietin (EPO) but are not induced in apoptosis following EPO withdrawal in EPO-dependent HCD57 cells. Blood *96*, 933-940.
Jang, Y.Y., and Sharkis, S.J. (2007). A low level of reactive oxygen species selects for primitive hematopoietic stem cells that may reside in the low-oxygenic niche. Blood *110*, 3056-3063.
Ji, R.P., Phoon, C.K., Aristizabal, O., et al. (2003). Onset of cardiac function during early mouse embryogenesis coincides with entry of primitive erythroblasts into the embryo proper. Circ. Res. *92*, 133-135.
Jiang, X., Iseki, S., Maxson, R.E., et al. (2002). Tissue origins and interactions in the mammalian skull vault. Developmental biology *241*, 106-116.
Johnson, D., and Wilkie, A.O. (2011). Craniosynostosis. Eur. J. Hum. Genet. *19*, 369-376.
Kamata, T., Kang, J., Lee, T.H., et al. (2005). A critical function for B-Raf at multiple stages of myelopoiesis. Blood *106*, 833-840.
Kassebaum, N.J., Jasrasaria, R., Naghavi, M., et al. (2014). A systematic analysis of global anemia burden from 1990 to 2010. Blood *123*, 615-624.
Kataoka, H., Hayashi, M., Nakagawa, R., et al. (2011). Etv2/ER71 induces vascular mesoderm from Flk1+PDGFRalpha+ primitive mesoderm. Blood *118*, 6975-6986.
Kellendonk, C., Opherk, C., Anlag, K., et al. (2000). Hepatocyte-specific expression of Cre recombinase. Genesis *26*, 151-153.

Keller, G., Kennedy, M., Papayannopoulou, T., et al. (1993). Hematopoietic commitment during embryonic stem cell differentiation in culture. Molecular and cellular biology *13*, 473-486.

Kim, J.W., and Ahn, Y.H. (1998). CCAAT/enhancer binding protein regulates the promoter activity of the rat GLUT2 glucose transporter gene in liver cells. Biochem. J. *336 (Pt 1)*, 83-90.

Kina, T., Ikuta, K., Takayama, E., et al. (2000). The monoclonal antibody TER-119 recognizes a molecule associated with glycophorin A and specifically marks the late stages of murine erythroid lineage. British journal of haematology *109*, 280-287.

Kinder, S.J., Tsang, T.E., Quinlan, G.A., et al. (1999). The orderly allocation of mesodermal cells to the extraembryonic structures and the anteroposterior axis during gastrulation of the mouse embryo. Development *126*, 4691-4701.

Kingsley, P.D., Malik, J., Emerson, R.L., et al. (2006). "Maturational" globin switching in primary primitive erythroid cells. Blood *107*, 1665-1672.

Kingsley, P.D., Malik, J., Fantauzzo, K.A., et al. (2004). Yolk sac-derived primitive erythroblasts enucleate during mammalian embryogenesis. Blood *104*, 19-25.

Kissa, K., and Herbomel, P. (2010). Blood stem cells emerge from aortic endothelium by a novel type of cell transition. Nature *464*, 112-115.

Klemsz, M., Hromas, R., Raskind, W., et al. (1994). PE-1, a novel ETS oncogene family member, localizes to chromosome 1q21-q23. Genomics *20*, 291-294.

Kodandapani, R., Pio, F., Ni, C.Z., et al. (1996). A new pattern for helix-turn-helix recognition revealed by the PU.1 ETS-domain-DNA complex. Nature *380*, 456-460.

Kozhevnikova, M.N., Mikaelian, A.S., and Starostin, V.I. (2009). [Molecular genetic and immunophenotypic analysis of antigen profiling, osteogenic and adipogenic potentials of mesenchymal stromal cells from fetal liver and adult bone marrow in rats]. Tsitologiia *51*, 526-538.

Kubo, H., and Alitalo, K. (2003). The bloody fate of endothelial stem cells. Genes & development *17*, 322-329.

Kuo, Y.H., Zaidi, S.K., Gornostaeva, S., et al. (2009). Runx2 induces acute myeloid leukemia in cooperation with Cbfbeta-SMMHC in mice. Blood *113*, 3323-3332.

Lai, C.F., Chaudhary, L., Fausto, A., et al. (2001). Erk is essential for growth, differentiation, integrin expression, and cell function in human osteoblastic cells. J. Biol. Chem. *276*, 14443-14450.

Lan, Y., He, W., Li, Z., et al. (2014). Endothelial Smad4 restrains the transition to hematopoietic progenitors via suppression of ERK activation. Blood *123*, 2161-2171.

Lancrin, C., Sroczynska, P., Stephenson, C., et al. (2009). The haemangioblast generates haematopoietic cells through a haemogenic endothelium stage. Nature *457*, 892-895.

Le Gallic, L., Sgouras, D., Beal, G., Jr., et al. (1999). Transcriptional repressor ERF is a Ras/mitogen-activated protein kinase target that regulates cellular proliferation. Molecular and cellular biology *19*, 4121-4133.

Le Gallic, L., Virgilio, L., Cohen, P., et al. (2004). ERF nuclear shuttling, a continuous monitor of Erk activity that links it to cell cycle progression. Molecular and cellular biology *24*, 1206-1218.

Lee, D., Park, C., Lee, H., et al. (2008). ER71 acts downstream of BMP, Notch, and Wnt signaling in blood and vessel progenitor specification. Cell Stem Cell *2*, 497-507.

Lee, L.K., Ghorbanian, Y., Wang, W., et al. (2016). LYVE1 Marks the Divergence of Yolk Sac Definitive Hemogenic Endothelium from the Primitive Erythroid Lineage. Cell reports *17*, 2286-2298.

Lemaigre, F.P. (2003). Development of the biliary tract. Mech. Dev. *120*, 81-87.

Lenox, L.E., Perry, J.M., and Paulson, R.F. (2005). BMP4 and Madh5 regulate the erythroid response to acute anemia. Blood *105*, 2741-2748.

Levi, B., Wan, D.C., Wong, V.W., et al. (2012). Cranial suture biology: from pathways to patient care. J. Craniofac. Surg. *23*, 13-19.

Lewis, T.S., Shapiro, P.S., and Ahn, N.G. (1998). Signal transduction through MAP kinase cascades. Adv. Cancer Res. *74*, 49-139.

Li, P., Pashmforoush, M., and Sucov, H.M. (2012). Mesodermal retinoic acid signaling regulates endothelial cell coalescence in caudal pharyngeal arch artery vasculogenesis. Developmental biology *361*, 116-124.

Little, G.H., Noushmehr, H., Baniwal, S.K., et al. (2012). Genome-wide Runx2 occupancy in prostate cancer cells suggests a role in regulating secretion. Nucleic Acids Res. *40*, 3538-3547.

Liu, B., Chen, S., Johnson, C., et al. (2014). A ciliopathy with hydrocephalus, isolated craniosynostosis, hypertelorism, and clefting caused by deletion of Kif3a. Reprod. Toxicol. *48*, 88-97.

Liu, D., Pavlopoulos, E., Modi, W., et al. (1997). ERF: genomic organization, chromosomal localization and promoter analysis of the human and mouse genes. Oncogene *14*, 1445-1451.

Liu, F., and Patient, R. (2008). Genome-wide analysis of the zebrafish ETS family identifies three genes required for hemangioblast differentiation or angiogenesis. Circ. Res. *103*, 1147-1154.

Lizama, C.O., Hawkins, J.S., Schmitt, C.E., et al. (2015). Repression of arterial genes in hemogenic endothelium is sufficient for haematopoietic fate acquisition. Nat Commun *6*, 7739.

Lucitti, J.L., Jones, E.A., Huang, C., et al. (2007). Vascular remodeling of the mouse yolk sac requires hemodynamic force. Development *134*, 3317-3326.

Luis, T.C., Ichii, M., Brugman, M.H., et al. (2012). Wnt signaling strength regulates normal hematopoiesis and its deregulation is involved in leukemia development. Leukemia *26*, 414-421.

Luis, T.C., Naber, B.A., Roozen, P.P., et al. (2011). Canonical wnt signaling regulates hematopoiesis in a dosage-dependent fashion. Cell Stem Cell *9*, 345-356.

Marais, R., Wynne, J., and Treisman, R. (1993). The SRF accessory protein Elk-1 contains a growth factor-regulated transcriptional activation domain. Cell *73*, 381-393.

Martinez, M., Hinojosa, M., Trombly, D., et al. (2016). Transcriptional Auto-Regulation of RUNX1 P1 Promoter. PLoS One *11*, e0149119.

Mavrothalassitis, G.J., and Papas, T.S. (1991). Positive and negative factors regulate the transcription of the ETS2 gene via an oncogene-responsive-like unit within the ETS2 promoter region. Cell Growth Differ. *2*, 215-224.

McGrath, K.E., Frame, J.M., Fegan, K.H., et al. (2015). Distinct Sources of Hematopoietic Progenitors Emerge before HSCs and Provide Functional Blood Cells in the Mammalian Embryo. Cell reports *11*, 1892-1904.

McGrath, K.E., Koniski, A.D., Malik, J., et al. (2003). Circulation is established in a stepwise pattern in the mammalian embryo. Blood *101*, 1669-1676.

Medlock, E.S., and Haar, J.L. (1983). The liver hemopoietic environment: I. Developing hepatocytes and their role in fetal hemopoiesis. Anat. Rec. *207*, 31-41.

Medvinsky, A., and Dzierzak, E. (1996). Definitive hematopoiesis is autonomously initiated by the AGM region. Cell *86*, 897-906.

Medvinsky, A., Rybtsov, S., and Taoudi, S. (2011). Embryonic origin of the adult hematopoietic system: advances and questions. Development *138*, 1017-1031.

Mefford, H.C., Shafer, N., Antonacci, F., et al. (2010). Copy number variation analysis in single-suture craniosynostosis: multiple rare variants including RUNX2 duplication in two cousins with metopic craniosynostosis. Am. J. Med. Genet. A *152A*, 2203-2210.

Minegishi, N., Ohta, J., Yamagiwa, H., et al. (1999). The mouse GATA-2 gene is expressed in the para-aortic splanchnopleura and aorta-gonads and mesonephros region. Blood *93*, 4196-4207.

Mishina, Y., and Snider, T.N. (2014). Neural crest cell signaling pathways critical to cranial bone development and pathology. Exp. Cell Res. *325*, 138-147.

Mo, Y., Vaessen, B., Johnston, K., et al. (2000). Structure of the elk-1-DNA complex reveals how DNA-distal residues affect ETS domain recognition of DNA. Nat. Struct. Biol. *7*, 292-297.

Moore, M.A., and Metcalf, D. (1970). Ontogeny of the haemopoietic system: yolk sac origin of in vivo and in vitro colony forming cells in the developing mouse embryo. British journal of haematology *18*, 279-296.

Morioka, K., Tone, S., Mukaida, M., et al. (1998). The apoptotic and nonapoptotic nature of the terminal differentiation of erythroid cells. Exp. Cell Res. *240*, 206-217.

Morriss-Kay, G.M., and Wilkie, A.O. (2005). Growth of the normal skull vault and its alteration in craniosynostosis: insights from human genetics and experimental studies. J. Anat. *207*, 637-653.

Mucenski, M.L., McLain, K., Kier, A.B., et al. (1991). A functional c-myb gene is required for normal murine fetal hepatic hematopoiesis. Cell *65*, 677-689.

Muller, A.M., Medvinsky, A., Strouboulis, J., et al. (1994). Development of hematopoietic stem cell activity in the mouse embryo. Immunity *1*, 291-301.

Mundlos, S., Otto, F., Mundlos, C., et al. (1997). Mutations involving the transcription factor CBFA1 cause cleidocranial dysplasia. Cell *89*, 773-779.

Murray, H.L. (1932). Tubal Gestation as seen by the Gynaecologist: An Analytical Study of Certain Aspects, Clinical and Pathological, of a Consecutive Series of 146 cases. Proc. R. Soc. Med. *25*, 1375-1385.

Nagata, Y., Moriguchi, T., Nishida, E., et al. (1997). Activation of p38 MAP kinase pathway by erythropoietin and interleukin-3. Blood *90*, 929-934.

Nieminen, P., Morgan, N.V., Fenwick, A.L., et al. (2011). Inactivation of IL11 signaling causes craniosynostosis, delayed tooth eruption, and supernumerary teeth. Am. J. Hum. Genet. *89*, 67-81.

North, T.E., Stacy, T., Matheny, C.J., et al. (2004). Runx1 is expressed in adult mouse hematopoietic stem cells and differentiating myeloid and lymphoid cells, but not in maturing erythroid cells. Stem cells *22*, 158-168.

Nottingham, W.T., Jarratt, A., Burgess, M., et al. (2007). Runx1-mediated hematopoietic stem-cell emergence is controlled by a Gata/Ets/SCL-regulated enhancer. Blood *110*, 4188-4197.

Okano, K., Hibi, A., Miyaoka, T., et al. (2012). Inhibitory effects of the transcription factor Ets-1 on the expression of type I collagen in TGF-beta1-stimulated renal epithelial cells. Mol. Cell. Biochem. *369*, 247-254.

Okuda, K.S., Astin, J.W., Misa, J.P., et al. (2012). lyve1 expression reveals novel lymphatic vessels and new mechanisms for lymphatic vessel development in zebrafish. Development *139*, 2381-2391.

Padron-Barthe, L., Temino, S., Villa del Campo, C., et al. (2014). Clonal analysis identifies hemogenic endothelium as the source of the blood-endothelial common lineage in the mouse embryo. Blood *124*, 2523-2532.

Pages, G., Guerin, S., Grall, D., et al. (1999). Defective thymocyte maturation in p44 MAP kinase (Erk 1) knockout mice. Science *286*, 1374-1377.

Palis, J. (2014). Primitive and definitive erythropoiesis in mammals. Front. Physiol. *5*, 3.

Palis, J., Malik, J., McGrath, K.E., et al. (2010). Primitive erythropoiesis in the mammalian embryo. Int. J. Dev. Biol. *54*, 1011-1018.

Palis, J., Robertson, S., Kennedy, M., et al. (1999). Development of erythroid and myeloid progenitors in the yolk sac and embryo proper of the mouse. Development *126*, 5073-5084.

Paniushina, O.V., Bueverova e, I., Satdykova, G.P., et al. (2004). [Comparative investigation of mesenchymal stem cells isolated from the bone marrow and embryonic liver of mouse and rat]. Izv. Akad. Nauk. Ser. Biol., 659-664.

Papadaki, C., Alexiou, M., Cecena, G., et al. (2007). Transcriptional repressor erf determines extraembryonic ectoderm differentiation. Molecular and cellular biology *27*, 5201-5213.

Perrimon, N., Pitsouli, C., and Shilo, B.Z. (2012). Signaling mechanisms controlling cell fate and embryonic patterning. Cold Spring Harb. Perspect. Biol. *4*, a005975.

Peschle, C., Mavilio, F., Care, A., et al. (1985). Haemoglobin switching in human embryos: asynchrony of zeta----alpha and epsilon----gamma-globin switches in primitive and definite erythropoietic lineage. Nature *313*, 235-238.

Qi, H., Aguiar, D.J., Williams, S.M., et al. (2003). Identification of genes responsible for osteoblast differentiation from human mesodermal progenitor cells. Proceedings of the National Academy of Sciences of the United States of America *100*, 3305-3310.

Qin, Q., Xu, Y., He, T., et al. (2012). Normal and disease-related biological functions of Twist1 and underlying molecular mechanisms. Cell Res. *22*, 90-106.

Rabault, B., and Ghysdael, J. (1994). Calcium-induced phosphorylation of ETS1 inhibits its specific DNA binding activity. J. Biol. Chem. *269*, 28143-28151.

Racke, F.K., Lewandowska, K., Goueli, S., et al. (1997). Sustained activation of the extracellular signal-regulated kinase/mitogen-activated protein kinase pathway is required for megakaryocytic differentiation of K562 cells. J. Biol. Chem. *272*, 23366-23370.

Raman, M., Chen, W., and Cobb, M.H. (2007). Differential regulation and properties of MAPKs. Oncogene *26*, 3100-3112.

Raouf, A., and Seth, A. (2000). Ets transcription factors and targets in osteogenesis. Oncogene *19*, 6455-6463.

Rascle, A., Ferrand, N., Gandrillon, O., et al. (1996). Myb-Ets fusion oncoprotein inhibits thyroid hormone receptor/c-ErbA and retinoic acid receptor functions: a novel mechanism of action for leukemogenic transformation by E26 avian retrovirus. Molecular and cellular biology *16*, 6338-6351.

Rhodes, J., Hagen, A., Hsu, K., et al. (2005). Interplay of pu.1 and gata1 determines myelo-erythroid progenitor cell fate in zebrafish. Dev. Cell *8*, 97-108.

Rich, I.N. (1992). The developmental biology of hemopoiesis: effect of growth factors on the colony formation by embryonic cells. Exp. Hematol. *20*, 368-370.

Rich, I.N., and Kubanek, B. (1979). The ontogeny of erythropoiesis in the mouse detected by the erythroid colony-forming technique. I. Hepatic and maternal erythropoiesis. J. Embryol. Exp. Morphol. *50*, 57-74.

Richmond, T.D., Chohan, M., and Barber, D.L. (2005). Turning cells red: signal transduction mediated by erythropoietin. Trends Cell Biol. *15*, 146-155.

Robb, L., Lyons, I., Li, R., et al. (1995). Absence of yolk sac hematopoiesis from mice with a targeted disruption of the scl gene. Proceedings of the National Academy of Sciences of the United States of America *92*, 7075-7079.

Robert-Moreno, A., Guiu, J., Ruiz-Herguido, C., et al. (2008). Impaired embryonic haematopoiesis yet normal arterial development in the absence of the Notch ligand Jagged1. EMBO J. *27*, 1886-1895.

Rugh, J.D., Lemke, R.R., and Dal Santo, F.B. (1990). Hysteresis in jaw positioning following lateral stretches. J. Dent. Res. *69*, 470-472.

Saba-El-Leil, M.K., Vella, F.D., Vernay, B., et al. (2003). An essential function of the mitogen-activated protein kinase Erk2 in mouse trophoblast development. EMBO reports *4*, 964-968.

Sabapathy, K., Kallunki, T., David, J.P., et al. (2001). c-Jun NH2-terminal kinase (JNK)1 and JNK2 have similar and stage-dependent roles in regulating T cell apoptosis and proliferation. J. Exp. Med. *193*, 317-328.

Salanga, M.C., Meadows, S.M., Myers, C.T., et al. (2010). ETS family protein ETV2 is required for initiation of the endothelial lineage but not the hematopoietic lineage in the Xenopus embryo. Developmental dynamics : an official publication of the American Association of Anatomists *239*, 1178-1187.

Salasznyk, R.M., Klees, R.F., Hughlock, M.K., et al. (2004). ERK signaling pathways regulate the osteogenic differentiation of human mesenchymal stem cells on collagen I and vitronectin. Cell communication & adhesion *11*, 137-153.

Samokhvalov, I.M. (2012). Return to the hematopoietic stem cell origin. Cell regeneration *1*, 9.

Samokhvalov, I.M., Samokhvalova, N.I., and Nishikawa, S. (2007). Cell tracing shows the contribution of the yolk sac to adult haematopoiesis. Nature *446*, 1056-1061.

Sanchez-Lara, P.A., Carmichael, S.L., Graham, J.M., Jr., et al. (2010). Fetal constraint as a potential risk factor for craniosynostosis. Am. J. Med. Genet. A *152A*, 394-400.

Sasaki, K., and Iwatsuki, H. (1997). Origin and fate of the central macrophages of erythroblastic islands in the fetal and neonatal mouse liver. Microsc. Res. Tech. *39*, 398-405.

Sasaki, K., and Matsumura, G. (1986). A karyometrical study of circulating erythroblasts of yolk sac origin in the mouse embryo. Arch. Histol. Jpn. *49*, 535-541.

Sasaki, K., and Sonoda, Y. (2000). Histometrical and three-dimensional analyses of liver hematopoiesis in the mouse embryo. Arch. Histol. Cytol. *63*, 137-146.

Sato, M., Suzuki, S., and Senoo, H. (2003). Hepatic stellate cells: unique characteristics in cell biology and phenotype. Cell Struct. Funct. *28*, 105-112.

Schaeffer, H.J., and Weber, M.J. (1999). Mitogen-activated protein kinases: specific messages from ubiquitous messengers. Molecular and cellular biology *19*, 2435-2444.

Schlereth, S.L., Neuser, B., Caramoy, A., et al. (2014). Enrichment of lymphatic vessel endothelial hyaluronan receptor 1 (LYVE1)-positive macrophages around blood vessels in the normal human sclera. Invest. Ophthalmol. Vis. Sci. *55*, 865-872.

Schuetze, S., Stenberg, P.E., and Kabat, D. (1993). The Ets-related transcription factor PU.1 immortalizes erythroblasts. Molecular and cellular biology *13*, 5670-5678.

Scott, E.W., Simon, M.C., Anastasi, J., et al. (1994). Requirement of transcription factor PU.1 in the development of multiple hematopoietic lineages. Science *265*, 1573-1577.

Sgouras, D.N., Athanasiou, M.A., Beal, G.J., Jr., et al. (1995). ERF: an ETS domain protein with strong transcriptional repressor activity, can suppress ets-associated tumorigenesis and is regulated by phosphorylation during cell cycle and mitogenic stimulation. EMBO J. *14*, 4781-4793.

Shalaby, F., Ho, J., Stanford, W.L., et al. (1997). A requirement for Flk1 in primitive and definitive hematopoiesis and vasculogenesis. Cell *89*, 981-990.

Shalaby, F., Rossant, J., Yamaguchi, T.P., et al. (1995). Failure of blood-island formation and vasculogenesis in Flk-1-deficient mice. Nature *376*, 62-66.

Shelly, C., Petruzzelli, L., and Herrera, R. (1998). PMA-induced phenotypic changes in K562 cells: MAPK-dependent and -independent events. Leukemia *12*, 1951-1961.

Si-Tayeb, K., Lemaigre, F.P., and Duncan, S.A. (2010). Organogenesis and development of the liver. Dev. Cell *18*, 175-189.

Sieff, C.A., Yang, J., Merida-Long, L.B., et al. (2010). Pathogenesis of the erythroid failure in Diamond Blackfan anaemia. British journal of haematology *148*, 611-622.

Silver, L., and Palis, J. (1997). Initiation of murine embryonic erythropoiesis: a spatial analysis. Blood *89*, 1154-1164.

Spyropoulos, D.D., Pharr, P.N., Lavenburg, K.R., et al. (2000). Hemorrhage, impaired hematopoiesis, and lethality in mouse embryos carrying a targeted disruption of the Fli1 transcription factor. Molecular and cellular biology *20*, 5643-5652.

Srinivas, S., Watanabe, T., Lin, C.S., et al. (2001). Cre reporter strains produced by targeted insertion of EYFP and ECFP into the ROSA26 locus. BMC Dev. Biol. *1*, 4.

Steiner, R. (1973). On the kinetics of erythroid cell differentiation in fetal mice. II. DNA and hemoglobin measurements of individual erythroblasts during gestation. J. Cell. Physiol. *82*, 219-230.

Steiner, R., and Vogel, H. (1973). On the kinetics of erythroid cell differentiation in fetal mice. I. Microspectrophotometric determination of the hemoglobin content in erythroid cells during gestation. J Cell Physiol *81*, 323-338.

Stock, M., and Otto, F. (2005). Control of RUNX2 isoform expression: the role of promoters and enhancers. J. Cell. Biochem. *95*, 506-517.

Sumanas, S., Gomez, G., Zhao, Y., et al. (2008). Interplay among Etsrp/ER71, Scl, and Alk8 signaling controls endothelial and myeloid cell formation. Blood *111*, 4500-4510.

Sumanas, S., and Lin, S. (2006). Ets1-related protein is a key regulator of vasculogenesis in zebrafish. PLoS Biol. *4*, e10.

Tallquist, M.D., and Soriano, P. (2000). Epiblast-restricted Cre expression in MORE mice: a tool to distinguish embryonic vs. extra-embryonic gene function. Genesis *26*, 113-115.

Taoudi, S., Bee, T., Hilton, A., et al. (2011). ERG dependence distinguishes developmental control of hematopoietic stem cell maintenance from hematopoietic specification. Genes & development *25*, 251-262.

Tavian, M., Cortes, F., Charbord, P., et al. (1999). Emergence of the haematopoietic system in the human embryo and foetus. Haematologica *84 Suppl EHA-4*, 1-3.

Terrace, J.D., Currie, I.S., Hay, D.C., et al. (2007). Progenitor cell characterization and location in the developing human liver. Stem cells and development *16*, 771-778.

Thompson, C.B., Wang, C.Y., Ho, I.C., et al. (1992). cis-acting sequences required for inducible interleukin-2 enhancer function bind a novel Ets-related protein, Elf-1. Molecular and cellular biology *12*, 1043-1053.

Ting, M.C., Wu, N.L., Roybal, P.G., et al. (2009). EphA4 as an effector of Twist1 in the guidance of osteogenic precursor cells during calvarial bone growth and in craniosynostosis. Development *136*, 855-864.

Tober, J., Koniski, A., McGrath, K.E., et al. (2007). The megakaryocyte lineage originates from hemangioblast precursors and is an integral component both of primitive and of definitive hematopoiesis. Blood *109*, 1433-1441.

Tremblay, K.D., and Zaret, K.S. (2005). Distinct populations of endoderm cells converge to generate the embryonic liver bud and ventral foregut tissues. Developmental biology *280*, 87-99.

Trimborn, T., Gribnau, J., Grosveld, F., et al. (1999). Mechanisms of developmental control of transcription in the murine alpha- and beta-globin loci. Genes & development *13*, 112-124.

Trivedi, A.K., Bararia, D., Christopeit, M., et al. (2007). Proteomic identification of C/EBP-DBD multiprotein complex: JNK1 activates stem cell regulator C/EBPalpha by inhibiting its ubiquitination. Oncogene *26*, 1789-1801.

Turjanski, A.G., Vaque, J.P., and Gutkind, J.S. (2007). MAP kinases and the control of nuclear events. Oncogene *26*, 3240-3253.

Twigg, S.R., Forecki, J., Goos, J.A., et al. (2015). Gain-of-Function Mutations in ZIC1 Are Associated with Coronal Craniosynostosis and Learning Disability. Am. J. Hum. Genet. *97*, 378-388.

Twigg, S.R., and Wilkie, A.O. (2015). A Genetic-Pathophysiological Framework for Craniosynostosis. Am. J. Hum. Genet. *97*, 359-377.

Verykokakis, M., Papadaki, C., Vorgia, E., et al. (2007). The RAS-dependent ERF control of cell proliferation and differentiation is mediated by c-Myc repression. J. Biol. Chem. *282*, 30285-30294.

Vorgia, E., Zaragkoulias, A., Peraki, I., et al. (2017). Suppression of Fgf2 by ETS2 repressor factor (ERF) is required for chorionic trophoblast differentiation. Mol. Reprod. Dev.

Wang, L., Liu, T., Xu, L., et al. (2013). Fev regulates hematopoietic stem cell development via ERK signaling. Blood *122*, 367-375.

Wang, Q., Stacy, T., Binder, M., et al. (1996). Disruption of the Cbfa2 gene causes necrosis and hemorrhaging in the central nervous system and blocks definitive hematopoiesis. Proceedings of the National Academy of Sciences of the United States of America *93*, 3444-3449.

Wang, W.C., Morales, K.H., Scher, C.D., et al. (2005). Effect of long-term transfusion on growth in children with sickle cell anemia: results of the STOP trial. J. Pediatr. *147*, 244-247.

Wang, X.Y., Lan, Y., He, W.Y., et al. (2008). Identification of mesenchymal stem cells in aorta-gonad-mesonephros and yolk sac of human embryos. Blood *111*, 2436-2443.

Wareing, S., Eliades, A., Lacaud, G., et al. (2012a). ETV2 expression marks blood and endothelium precursors, including hemogenic endothelium, at the onset of blood development. Developmental dynamics : an official publication of the American Association of Anatomists *241*, 1454-1464.

Wareing, S., Mazan, A., Pearson, S., et al. (2012b). The Flk1-Cre-mediated deletion of ETV2 defines its narrow temporal requirement during embryonic hematopoietic development. Stem cells *30*, 1521-1531.

Wasylyk, B., Hagman, J., and Gutierrez-Hartmann, A. (1998). Ets transcription factors: nuclear effectors of the Ras-MAP-kinase signaling pathway. Trends Biochem. Sci. *23*, 213-216.

Watson, D.K., Smyth, F.E., Thompson, D.M., et al. (1992). The ERGB/Fli-1 gene: isolation and characterization of a new member of the family of human ETS transcription factors. Cell Growth Differ. *3*, 705-713.

Watson, E.D., and Cross, J.C. (2005). Development of structures and transport functions in the mouse placenta. Physiology (Bethesda) *20*, 180-193.

Waugh, R.E., Huang, Y.S., Arif, B.J., et al. (2013). Development of membrane mechanical function during terminal stages of primitive erythropoiesis in mice. Exp. Hematol. *41*, 398-408 e392.

Wechsler, M.E., Hermann, B.P., and Bizios, R. (2015). Adult Human Mesenchymal Stem Cell Differentiation at the Cell Population and Single-Cell Levels Under Alternating Electric Current. Tissue engineering. Part C, Methods.

Weissman, I.L. (2006). Medicine: politic stem cells. Nature *439*, 145-147.

Whitelaw, D.A. (1990). Acute rheumatic fever in adults. S. Afr. Med. J. *78*, 305-308.

Whitelaw, E., Tsai, S.F., Hogben, P., et al. (1990). Regulated expression of globin chains and the erythroid transcription factor GATA-1 during erythropoiesis in the developing mouse. Molecular and cellular biology *10*, 6596-6606.

Wilkie, A.O., Byren, J.C., Hurst, J.A., et al. (2010). Prevalence and complications of single-gene and chromosomal disorders in craniosynostosis. Pediatrics *126*, e391-400.

Wong, P.M., Chung, S.W., Chui, D.H., et al. (1986). Properties of the earliest clonogenic hemopoietic precursors to appear in the developing murine yolk sac. Proceedings of the National Academy of Sciences of the United States of America *83*, 3851-3854.

Xiao, G., Gopalakrishnan, R., Jiang, D., et al. (2002). Bone morphogenetic proteins, extracellular matrix, and mitogen-activated protein kinase signaling pathways are required for osteoblast-specific gene expression and differentiation in MC3T3-E1 cells. J. Bone Miner. Res. *17*, 101-110.

Xiao, G., Jiang, D., Thomas, P., et al. (2000). MAPK pathways activate and phosphorylate the osteoblast-specific transcription factor, Cbfa1. J. Biol. Chem. *275*, 4453-4459.

Yordy, J.S., and Muise-Helmericks, R.C. (2000). Signal transduction and the Ets family of transcription factors. Oncogene *19*, 6503-6513.

Zhang, C., Lv, J., He, Q., et al. (2014). Inhibition of endothelial ERK signalling by Smad1/5 is essential for haematopoietic stem cell emergence. Nat Commun *5*, 3431.

Zhang, J., Socolovsky, M., Gross, A.W., et al. (2003). Role of Ras signaling in erythroid differentiation of mouse fetal liver cells: functional analysis by a flow cytometry-based novel culture system. Blood *102*, 3938-3946.

Zhao, H., Feng, J., Ho, T.V., et al. (2015). The suture provides a niche for mesenchymal stem cells of craniofacial bones. Nat. Cell Biol. *17*, 386-396.

Zhen, F., Lan, Y., Yan, B., et al. (2013). Hemogenic endothelium specification and hematopoietic stem cell maintenance employ distinct Scl isoforms. Development *140*, 3977-3985.

6. Publications

This work was published as first author in Molecular and Cellular Biology.

It has been accepted and it is going to be published on-line in few days.

The Ets2 repressor factor (*Erf*) is required for effective for primitive and definitive hematopoiesis.

Ioanna Peraki,[1, 2] James Palis[3] and George Mavrothalassitis[1, 2, #]

[1] Medical School, University of Crete and [2] IMBB, FORTH, Heraklion, Crete 71003, Greece [3] Department of Pediatrics, Center for Pediatric Biomedical Research, University of Rochester Medical Center, Rochester, NY 14642, USA

Running title: *Erf* is required for erythropoiesis

Address correspondence to George Mavrothalassitis, mavro@imbb.forth.gr

Word count for Introduction, Results and Discussion is 3105

Word count for Materials and Methods is 972

Keywords: *Erf*, mouse, embryo, anemia, primitive wave, definitive wave, HSCs, hemogenic endothelium, differentiation, fetal liver

Abstract

Erf is a ubiquitously expressed ets-DNA-binding containing transcriptional repressor. *Erf* haploinsufficiency causes craniosynostosis in human and mice, while its absence in mice leads to failed chorioallantoic fusion and death at E10.5. In this study, we show that *Erf* is required in all three waves of embryonic hematopoiesis. Mice lacking *Erf* in embryo proper exhibited severe anemia and died around embryonic day (E) 14.5. *Erf* epiblast specific knockout embryos had reduced numbers of circulating blood cells from E9.5 onwards with the development of severe anemia by E14.5. Elimination of *Erf* resulted in both reduced and more immature primitive erythroblasts at E9.5-10.5. Reduced definitive erythroid colony forming activity was found in the bloodstream of E10.5 embryos and in the fetal liver at E11.5-13.5. Finally, elimination of *Erf* resulted in impaired repopulation ability, indicating that Erf is necessary for hematopoietic stem cell maintenance or differentiation. We conclude that Erf is required for both primitive and erythro-myeloid progenitor waves of HSC-independent hematopoiesis, as well as the normal function of HSCs.

Introduction

The ontogeny of the hematopoietic system is a complex process with multiple waves of hemopoietic potential emerging from different anatomical sites (1). The first hematopoietic progenitors that emerge in the yolk sac at embryonic day E7.5 generate the first circulating blood cells of erythroid, megakaryocyte and macrophage lineages. (2-4). Shortly after, at embryonic day E8.25, a second wave of hematopoietic progenitors, termed erythro-myeloid progenitors (EMPs) emerge in the yolk sac and colonize the fetal liver at embryonic day E10.5 (5-8). A third wave of hematopoietic potential, consisted of adult repopulating hematopoietic stem cells (HSCs) emerges from large arterial vessels beginning at E10.5, which colonizes the fetal liver but ultimately engrafts the bone marrow to provide life-long postnatal blood cell production (9-12).

Several *ets* genes have been shown to play a crucial role in distinct steps of hematopoiesis. PU.1 regulates the HSCs to myeloid commitment (13, 14). Other transcription factors of the ets family have also been shown to regulate hematopoiesis. *Etv2* regulates the emergence of blood and endothelial cells activating *Flk1* gene that is critical for initiation of hemangioblast formation (15-20) and is also required for the formation of hemogenic endothelium at the onset of yolk sac hematopoiesis (21). *Erg* is a critical regulator for HSC maintenance during embryonic development (22). *Fev* regulates the number of *Runx1* expressing cells by transcriptionally activating *Erk2*, to enhance ERK signaling (23), while PU.1 synergizes with Runx1 and determines its hematopoietic specific expression (24).

Erf is a ubiquitously expressed ets-family gene that has been suggested to enhance erythroid differentiation. Erf is regulated by Erk1/2 phosphorylation and nucleocytoplasmic shuttling. In its non-phosphorylated nuclear form, Erf blocks cell proliferation arresting cells at G0/G1 phase in a cell type-specific manner, it can suppress ets- and ras-induced tumorigenicity in fibroblasts, cell lines derived from Ewing's Sarcomas harboring the EWS-FLI1 rearrangement, and the epithelial to mesenchymal transition via semaphorin7a inhibition (25-30). *Erf*-null embryos fail to undergo chorioallantoic fusion and labyrinth development because of a block in chorion trophoblast stem cell (Ch-TSC) differentiation, resulting in the fetal demise at E10.5 (31). Finally, Erf haploinsufficiency causes craniosynostosis in humans and in mice, identifying *Erf* as a novel regulator of osteogenesis within the RAS-ERK signaling pathway (32).

Here, we demonstrate that elimination of *Erf* in the murine embryo proper at E5, leads to severe anemia and fetal death at E14.5. Employing histological, cellular, molecular and in vivo repopulation assays, we show that *Erf* is required for the timely or quantitative production of both primitive and definitive yolk sac derived hematopoiesis, as well as the production or maintenance of HSCs. In addition, *Erf* is required for the efficient maturation of erythroid precursors into mature erythrocytes. Thus, our data indicate that *Erf* is required throughout hematopoietic development for the homeostasis of this complex system.

Materials and Methods

Generation of conditional *Erf*$^{-/-}$ mice. Elimination of *Erf* in epiblast-derived tissues (*Erf*$^{ed/ed}$) was achieved by the intercross of *Meox2*$^{tm1(cre)Sor/J}$ (Jackson Laboratory, stock no 003755) with the *Erf*$^{loxP/loxP}$ mice (32) to generate *Meox2*$^{tm1(cre)Sor/J}$;*Erf*$^{+/-}$ and cross those with *Erf*$^{loxP/loxP}$ to totally eliminate *Erf* in the embryo proper. *Lyve1*$^{tm1.1(EGFP/cre)Cys/J}$ mice (Jackson Laboratory, stock no 012601) were crossed with the *Erf*$^{loxP/loxP}$ to eliminate *Erf* in the hemogenic endothelium (33) and finally in the definitive yolk sac derived wave (34). The liver specific *Alfp-Cre*;*Erf*$^{loxP/loxP}$ mice were used to eliminate *Erf* in hepatic cells (35).

Tissue collection and histological analysis. Timed-pregnant female mice were sacrificed at specified days of gestation by cervical dislocation according to institutional guidelines. The uteri were isolated from the peritoneum and placentas were removed using #5 watchmaker's forceps. The remaining whole yolk sacs were rinsed in PBS to remove vestiges of maternal blood and placed in IMDM media (ThermoFisher, cat. no. 12440053) with 2% FBS (Biochrom cat. no.50115). Blood was collected from separated embryos. Fetal livers were isolated from embryos not subjected to bleeding and dissociated by gentle pipetting in IMDM with 2% FBS. Cells were counted on a hematocytometer. Blood, collected on slides, was left to dry, fixed with methanol for 10 min, stained with Giemsa (Merck) for 2 minutes, washed with excess water, dried and mounted for observation.

For hematoxylin/eosin staining, yolk sacs were fixed with 4% paraformaldehyde for 1 hr at room temperature, dehydrated gradually with ethanol 70%, 90%, 100% for 30 min at room temperature, cleared in xylol for 30 min and impregnated with paraffin at 58^{o} C twice, for 30 min each. Five µM paraffin sections were stained with hematoxylin/eosin. For immunostaining, yolk sacs were fixed with 4% PFA for 1 hr at room temperature, washed extensively with PBS, stained with rat anti – PECAM1 (Pharmingen, cat. no. 553370) overnight at 4^{o} C and then incubated with anti-rat FITC conjugated antibody (Sigma, cat. no. F0382) in 1:50 dilution for 1 hour at room temperature.

Hematopoietic colony assays. Erythroid colony-forming units (CFU-E) and burst-forming units (BFU-E) were analyzed from bloodstream and fetal livers at E10.5 and E11.5 - E13.5, respectively. Fifty thousand cells were plated in 1 ml of 1.2 % Serum-free methylcellulose (Stem Cell Technologies, cat. no. H4100) supplemented with 37% FBS, 1.25 % w/v BSA, 0.25 µM β–mercaptoethanol, 0.01 % Sodium Bicarbonate, 10 ng/ml IL-3 (Peprotech, cat. no.213-13), 10 ng/ml IL-6 (Peprotech, cat. no.216-16), 1 ng/ml GM-CSF (Peprotech, cat. no.315-03), and 2 u/ ml erythropoietin (gift from Dr. Marieke von Lindern). Additionally, SCF 100 ng/ml (supernatant of CHO producer cells) was added in colonies from E10.5 blood. The cells were cultured in 35 mm dishes at 37^{o}C with 5% CO_2 and 100% humidity. The numbers of colonies were scored after 3 days for CFU-E and 7 days for BFU-E.

Flow cytometric analysis. Single cell suspensions were prepared from E11.5 - E13.5 livers, stained with biotinylated rat anti-Ter119 antibody (Biolegend, cat.

no.116203), a marker for all stages of differentiation from early proerythroblasts to mature erythrocytes, streptavidin-PerCP (Biolegend, cat. no.405213) and FITC-coupled rat anti-CD71, a marker for all erythroblasts except mature erythrocytes (Biolegend, cat. no.113805) in PBS/1% fetal bovine for 15 minutes at 4°C. Blood cells were stained with FITC-coupled anti - CD16/32 (Biolegend, cat. no. 101305), PE-coupled anti - c-Kit (Biolegend, cat. no. 105807) and APC-coupled anti - CD41 (Biolegend, cat. no. 133913), markers of EMPs. Stained cells were analyzed in a MoFloT High-Performance Cell Sorter and FlowJo V10 software.

Real-time quantitative PCR. Total RNA was extracted from peripheral blood and fetal livers at E10.5 – E11.5, using Trizol reagent (Invitrogen, cat. no. 15596018) according to manufacturer's instructions. mRNA was subjected to reverse transcription using SuperScript First strand Synthesis kit (Invitrogen, cat. no. 11904-018). Expression levels of *β*major globin, detected mainly in definitive blood cells (Fw: 5´ - CACAAACCCCAGAAACAGACA- 3; Rv: 5´ - CTGACAGATGCTCTCTTGGG - 3´), *βH1* globin (Fw: 5 ´- CTCAAGGAGAC CTTTGCTCA - 3´; Rv: AGTCCCCATGGAGTCAAAGA) and *εy* globin, detected in primitive erythroid cells (Fw: 5´-GGAGAGTCCATTAAGAACCTAGACAA-3´; Rv: 5´-CTG TGAATTCATTGCCGAAGTAC- 3), were examined with Real-time polymerase chain reactions. Reactions were performed with 5 ng of total cDNA using the 2 x BrilliantIII SYBRGREEN QPCR mastermix (Stratagene, cat. no. 600882-51) in an Applied Biosystems StepOne plus Real-Time PCR machine. All expression levels were normalized to *Gapdh* levels (Fw: 5´ - CCAGTATGACTCCACTCACG.- 3´, Rv: 5´ - GACTCCACGACATACTCAGC -

3´) in the same cDNA. To distinguish *Alfp-cre* homozygous from heterozygous mice, quantitative Real-time PCR was performed with a general *Cre* primer (Fw: 5´ - GCG GTC TGG CAG TAA AAA CTA TC -3 ; Rv: 5´ GTG AAA CAG CAT TGC TGT CAC TT) in 10 ng DNA.

Reconstitution analysis. Mice at 6 weeks of age were lethally irradiated with 950 rad. Five hundred thousand fetal liver cells at E13.5 were injected intravenously into the lethally irradiated recipient $Erf^{+/+}$ mice. For the competitive repopulation studies 4 x 10^5 fetal liver cells from E12.5 embryos were co-injected intravenously with 2 x 10^5 spleen cells into lethally irradiated recipient $Erf^{+/+}$ mice. The animals were monitored twice a week for viability and general health. All mice were of mixed C57B6/SV129 background. The engraftment of donor cells was analyzed after 5 months. DNA from blood was extracted with the FlexiGene DNA kit (cat.no. 51204) and PCR for the detection of the loxP allele or the deletion of *Erf* was performed with the primers m11671F: 5'-ACGCCACAGCCCACCTCTCC -3', 11771R**:** 5'–CAGCAAAAGCTCAGGGAGTG-3' and 4021F: 5'–GCACTGCTAGCTCTGAATGG-3', 11771R: 5'–CAGCAAAAGCTCAGGGAGTG- 3' respectively.

Statistical Analysis. Statistical analysis was carried out using the 2 tailed unpaired *t*-test equipped with Excel 2016. For all graphs, data are presented as means ± standard error. The Pearson's chi-square test was used to evaluate the actual over the expected frequency of the genotypes. A * *P* value < 0.05, ** *P* value < 0.005 and *** *P* value < 0.0005 denoted statistical significance.

184

185

Results

***Erf*$^{ed/ed}$ embryos die in utero due to severe anemia.** We have previously shown that elimination of *Erf* in mice leads to lethality at E10.5 because of failed chorioallantoic fusion and labyrinth development (31), while *Erf* haploinsufficiency leads to defective suture development and craniosynostosis (32). To investigate other developmental processes that *Erf* may regulate bypassing the placental defect, we eliminated *Erf* in the epiblast at E5, crossing *Erf*$^{loxP/loxP}$ mice with mice expressing the cre recombinase under the control of the *Meox2* gene (36) in order to delete *Erf* in the embryos but not in the placenta (*Erf*$^{ed/ed}$). Elimination of *Erf* in the epiblast, resulted in embryonic death around E14.5 (Figure 1A). The embryos were pale indicative of anemia (Figure 1B). *Erf*$^{ed/ed}$ embryos contained approximately 50% of normal circulating primitive erythroblasts between E9.5 through E12.5. The blood levels of *Erf*$^{ed/ed}$ fetuses subsequently dropped precipitously by E14.5 to less than 5% of the normal (Figure 1C). A few *Erf* knockout fetuses exhibited somewhat higher levels of circulating blood at E14.5, consistent with the occasional survival until E15.5 or E16.5. The mutant embryos did not appear to have defects in other tissues (data not shown) and overall embryo size was comparable (Supplemental figure 1). The anemia and fetal demise did not appear to be of placental origin, as its development appeared unaffected in the *Erf*$^{ed/ed}$ embryos (Supplemental figure 2) but rather a defect in the embryo proper where *Erf* elimination exceeded 90% (Supplemental figure 3A-C)

***Erf* elimination impairs primitive erythropoiesis.** Because of the onset of anemia as early as E9.5, we initially examined erythropoiesis at E9.5 and

E10.5, when erythroblasts mature semi-synchronously. At E9.5, the *Erf*$^{ed/ed}$ yolk sac revealed normal mesothelium and visceral endoderm junctions, but the blood islands contained fewer and larger primitive erythroblasts (Figure 2A). On the contrary, the yolk sac vasculature of *Erf*$^{ed/ed}$ embryos appeared normal (Figure 2B). More than 95 % of the circulating erythroid cells from E9.5 to E12.5 derive from the primitive wave of hematopoietic progenitors in the yolk sac (4). Thus, the reduced numbers of circulating blood cells would suggest a defect in primitive erythropoiesis. In the absence of *Erf*, primitive erythroblasts at E10.5 are larger and contain enlarged nuclei with less condensed chromatin, features consistent with a delay in their maturation (Figure 2C). Globin mRNA levels analyzed by real-time PCR, indicate that *εy*-globin expression primitive erythroblasts of *Erf*$^{ed/ed}$ embryo was significantly lower than their *Erf*-expressing littermates at both E10.5 and E11.5 (Figure 2D), consistent with delayed maturation (37). These data indicate that elimination of *Erf* results in both decreased numbers and delayed maturation of primitive erythroid precursors.

***Erf* elimination impairs yolk sac-derived definitive erythroblasts.** The first circulating definitive erythroid cells that emerge at E11.5 - E12.5 are derived from EMP / BFU-E that have seeded the fetal liver (38). The profound anemia at E13.5 – 14.5 suggested a defect in EMP. To explore the effect of *Erf* elimination on the progenitors of the definitive hematopoietic wave that emerges in the yolk sac, peripheral blood was isolated at E10.5 and the c-Kit^{high}, CD41^{+}, CD16/32^{+} erythroid-myeloid progenitor cells (EMP) cells were quantitated by flow cytometry (38) (Figure 3A). As shown in figure 3B, *Erf*$^{ed/ed}$ embryos have half as many phenotypic EMPs compared to their *Erf*-expressing

236 littermates. Consistent with the loss of phenotypic EMP, the number of definitive
237 erythroid progenitors (BFU-E and CFU-E), defined by their ability to form
238 colonies in semisolid media, was also significantly reduced at E10.5 (Figure
239 3C). Taken together, these data confirm that the yolk sac-derived EMP wave of
240 hematopoietic potential is also impaired by the loss of *Erf*.
241
242 **Elimination of *Erf* in hemogenic endothelium recapitulates the *Erf*$^{ed/ed}$**
243 **hematopoietic phenotype in definitive hematopoiesis.** To determine if Erf
244 exerts a cell autonomous effect on hematopoietic development, we deleted *Erf*
245 in the hemogenic endothelium, utilizing the *Lyve1*$^{tm1.1(EGFP/cre)Cys}$ mice, which
246 express the cre recombinase under the control of the *Lyve1* gene. Recently, it
247 has been shown that *Lyve1* is expressed in hemogenic endothelium and
248 specifically marks EMP but not the primitive hematopoietic wave that emerges
249 from the yolk sac (34). Later, *Lyve1* is also expressed in blood and lymphatic
250 vessels, lymph nodes, liver, spleen sinuses and lung and endocardial
251 endothelial cells (33, 39, 40). *Lyve1*$^{tm1.1(EGFP/cre)Cys/tm1.1(EGFP/cre)Cys}$ *Erf*$^{loxP/loxP}$
252 (*Lyve1*$^{Cre/Cre}$ *Erf*$^{loxP/loxP}$) mice died in utero and appeared anemic, a phenotype
253 analogous to the epiblast-specific *Erf*$^{ed/ed}$ embryos. They were pale (Figure 4A),
254 and showed reduced BFU-Es / CFU-E at E10.5 (Figure 4B), indicating a defect
255 in EMPs before their migration to the liver. At E13.5 they exhibited decreased
256 liver cell numbers and severely reduced blood cells in the bloodstream at E14.5
257 (Figure 4C and D, respectively). Both the small liver size and the reduced
258 number of circulating blood cells suggest impaired EMP-derived
259 hematopoiesis, similar to that observed in epiblast *Erf*-null embryos (see

below). This would be indicative of a cell-autonomous defect of *Erf* elimination, specifically in the definitive hematopoietic wave of the yolk sac.

Surprisingly, in contrast to the *Lyve1*$^{Cre/Cre}$ *Erf*$^{loxP/loxP}$ embryos, *Lyve1*$^{Cre/+}$ *Erf*$^{loxP/loxP}$ mice were viable albeit with sub-mendelian frequencies (Supplemental figure 3D). Analysis, of the *Erf* expression in fetal livers showed that heterozygous *Lyve1*-cre embryos have significantly higher expression than the homozygous *Lyve1*-cre as well as the *Meox2*-cre embryos (Supplemental figure 3C). This would suggest that the frequency of *Erf* elimination and/or the level of expression of *Erf* in EMPs may be critical for the severity of the defect and thus survival.

***Erf* elimination compromises fetal liver erythropoiesis.** The increased anemia at E13.5 – E14.5 indicated a profound lack of definitive erythroid cells which are produced at this time in the fetal liver and make up the majority of the circulating cells at these time points (5, 41). Analysis of E11.5 – E13.5 *Erf*$^{ed/ed}$ embryos revealed significantly reduced liver size and liver cell numbers compared to their *Erf*$^{loxP/+}$ littermates (Figure 5A, Supplemental figure 4A). To examine if this reduction is due to the colonization of the liver and/or the expansion of the erythroid progenitors in the liver, we analyzed BFU-E and CFU-E numbers at E11.5 – E13.5. Consistent with the reduced EMP in the yolk sac and in the bloodstream, *Erf*$^{ed/ed}$ embryos contained fewer BFU-E and CFU-E in the liver compared to their *Erf*$^{loxP/+}$ littermates (Figure 5B and Figure 5C). Interestingly, BFU-E abundance in *Erf*$^{ed/ed}$ embryo livers at E11.5 was comparable to their *Erf*$^{loxP/+}$ littermates, whereas it was increased at E12.5 - E13.5 (Supplemental figure 4B). The abundance of CFU-Es in the *Erf*$^{ed/ed}$

285 embryo livers was increased compared to *Erf*$^{loxP/+}$ littermates throughout E11.5
286 – E13.5 (Supplemental figure 4C). In addition, non-erythroid liver cells
287 appeared unaffected as *Erf*$^{ed/ed}$ embryos had comparable numbers of
288 hepatocytes and stromal cells and comparable rates of liver cell proliferation
289 and apoptosis (Supplemental figure 5 and unpublished data). We further tested
290 the possible contribution of hepatic cells, eliminating *Erf* specifically in the
291 hepatocytes after crossing the *Erf*$^{loxP/loxP}$ mice with the *Alfp-Cre* mice (35). *Alfp*
292 *-cre;Erf*$^{loxP/loxP}$ mice were normal with no hematopoietic defects (not shown). All
293 these data indicate that Erf elimination may also affect erythroid maturation in
294 the fetal liver.
295 We thus examined erythroid maturation analyzing the abundance of the R1-R4
296 populations in E12.5 fetal liver by CD71 and Ter119 staining and flow cytometry
297 (Figure 5D). This analysis suggested that indeed the early precursor cells and
298 the proerythroblasts (R1), as well as the proerythroblasts and the early
299 basophilic proerythroblasts (R2) are more abundant in *Erf*$^{ed/ed}$ embryo livers,
300 while the early and late basophilic erythroblasts (R3) and the
301 polychromatophilic and orthochromatic erythroblast (R4) populations (42) are
302 less abundant (Figure 5E). Consistent with the colony assays, these data
303 indicate that in addition to the initial colonization, there is also a defect in the
304 maturation of the erythroid precursors in the fetal liver. This apparent reduced
305 rate of maturation was not due to a defect in cell cycle at E13.5 (Supplemental
306 figure 6), or the lack of erythroblast contacts with macrophages, as they were
307 evident in E12.5 livers (Supplemental figure 7). It was also not evident at E11.5,
308 the earlier stages of liver population by EMPs (Supplemental figure 8). It would

thus appear that the maturational defect of the *Erf*$^{ed/ed}$ liver erythroblasts is cell autonomous.

***Erf* is required for HSC development.** The dramatic decrease in peripheral blood at E14.5 raised the possibility that not only the EMPs but also the HSCs may be affected by the *Erf* loss. Therefore, we examined the role of *Erf* in hematopoietic stem cell maintenance and differentiation via both non-competitive and competitive repopulation experiments to evaluate short-term and long-term HSCs. Fifteen to 23 days after the transplantation of E13.5 liver cells in irradiated mice of the same haplotype, 3 of 4 mice repopulated with *Erf*$^{ed/ed}$ cells, died in contrast to the mice transplanted with *Erf*-competent cells, indicating a defect in short term HSCs (Figure 6A). For the competitive repopulation assays, E12.5 fetal liver cells were co-injected with spleen cells from *wt* animals in irradiated *wt* host mice of the same genetic background (Figure 6A). Donor HSC engraftment was estimated with semiquantitive PCR 5 months after the injection. Our data suggest that in contrast to the *Erf*$^{loxP/+}$ cells that contributed to almost all the hematopoietic cells of the irradiated animals, the *Erf*$^{ed/ed}$ cells had marginally detectable contribution (Figure 6B), suggesting that the long-term HSCs may also be affected by the elimination of *Erf*.

Discussion

In this study, we demonstrate for first time that elimination of *Erf* in the murine embryo proper at E5 is detrimental to embryonic erythropoiesis and leads to embryonic death around E14.5 due to severe anemia. Our data indicate that *Erf* elimination decreases, but does not block, the primitive and definitive yolk sac-derived erythropoiesis waves, and the efficiency of fetal HSCs that support adult hematopoiesis.

A wave of primitive erythroid progenitors emerges from the yolk sac at E7.5 – E9.0 (5), providing the majority of circulating blood cells until E12.5 (4). The reduced numbers of blood cells at E9.5 and onwards in the $Erf^{ed/ed}$ embryos, indicate a defect in the production and/or differentiation of these cells. The immature cell morphology and the decreased expression of *ey*-globin suggest that $Erf^{ed/ed}$ *may* affect the onset or differentiation rate of these cells.

The second, EMP, wave emerging from the yolk sac at E8.25 and colonizing the fetal liver (5), is also reduced in the absence of *Erf.* Both the number of EMP assessed by flow cytometry and the number of BFU-E and CFU-E colony-forming cells, circulating in the bloodstream of E10.5 embryos, are reduced in $Erf^{ed/ed}$ embryos. $Erf^{ed/ed}$ embryos show additional differentiation defects in definitive erythropoiesis after EMPs have homed to the fetal liver. Consistent with the decrease in EMPs, total cells in the liver, as well as erythroid precursor cells, are decreased in the absence of *Erf*. However, both BFU-E/CFU-E colony assays and flow cytometry of liver cells indicate increased proportion of R1, R2 proerythroblasts and reduced proportion of the mature R3, R4 populations. These data suggest an additional role for Erf in R2-R3 differentiation. The apparent defect in the production and differentiation of the definitive erythroid

lineage in the absence of *Erf*, appears to be a cell autonomous event, as evidenced by the elimination of *Erf* in the Lyve1-expressing hemogenic endothelium cells of the yolk sac. Similar to the epiblast-deleted $Erf^{ed/ed}$ embryos, the $Lyve1^{Cre/Cre}$ $Erf^{loxP/loxP}$ embryos appear anemic, have reduced BFU-E/CFU-E colonies in the bloodstream at E10.5, and reduced numbers of total cells and erythroid precursors in the liver at E14.5.

Finally, *Erf* appears to also have a crucial role in the differentiation of HSCs emerging from the AGM at E10.5, migrating to the liver and ultimately constituting the adult HSCs in the bone marrow. Transplantation of $Erf^{ed/ed}$ liver cells into irradiated mice shows that recipients could not live beyond 4 weeks, suggesting a defect in short-term HSCs. Addition of spleen helper cells from wt mice to assess long-term HSCs, indicate a marginal contribution from the $Erf^{ed/ed}$ cells 5 months after transplantation. These data allude to a defect in HSC maintenance or differentiation ability that may have implications in adult pathologies and needs further examination.

In spite of the wide effect of *Erf* on hematopoiesis, it remains unclear if there is a common underlying mechanism or if there are distinct downstream effectors involved in the different cell types affected. The fact that in the absence of Erf we have quantitative differences rather than a block in any specific differentiation step or the cell cycle, makes determination of possible mechanisms even more challenging. Indeed, transcriptional analysis of E13.5 livers, before the collapse of peripheral blood levels, failed to reveal statistically significant differences in genes or pathways between wt and *Erf*-null cells (unpublished data). This would be consistent with a quantitative rather than an instructive effect. This conclusion is also supported by the apparent difference

in viability of the Lyve1-cre heterozygous and homozygous animals in which the observed difference may be the result of the extent of the deletion. In addition, our unpublished data indicate a minimal but statistically significant sub-mendelian frequency of the viable *Erf*$^{loxP/-}$ animals, suggesting an effect because of the timing and/or the extent of *Erf* expression.

Erf is a member of the *ets*-family of transcription factors and an effector in the RTK/ras/erk pathway, which both have been involved in diverse facets of hematopoiesis. Erk has been reported to negatively affect fetal hemopoiesis, leading to tight junctions between endothelial cells in the AGM region of zebrafish, repressing the emergence of HSCs and promoting the arterial endothelial identity (43). Such an effect would be consistent with the apparent decrease of the HSCs observed in the absence of *Erf*, and the reduced numbers of EMPs and primitive cells, that emerge from the hemogenic endothelium in the yolk sac (44). In addition, oncogenic *H-Ras* blocks the terminal differentiation of CFU-E progenitors in vivo (45), consistent with the differentiation defect of the R2 population observed in *Erf*$^{ed/ed}$ livers.

Ets transcription factors recognize a common DNA-binding motif (46) and may antagonize each other on a variety of targets. Erf, a transcriptional repressor, may ensure the absence of spurious activation by other ets-family proteins leading to the proper differentiation programs and homeostasis. Overexpression of PU-1 is reported to block the differentiation of BFU-E / CFU-E to mature erythrocytes (47). The archetypal fusion gag-Myb-Ets oncoprotein, encoded by E26 retrovirus, induces acute leukemia and can block both myeloid and erythroid differentiation at the stage of BFU-E / CFU-E (48). Overactivation of *Etv2* leads to the upregulation of *Fli1* (49), which promotes the formation of

the vascular system (50) and the upregulation of *PU.1*. *Fli1* was identified as a proto-oncogene in erythroleukemias induced by retroviral integration (51). Finally, Erf itself has been reported to promote erythroid differentiation (26) and may antagonize Ets1 that may also have a role in this process (52). Thus, elimination of *Erf* may affect the entire regulatory network of ets factors in hematopoiesis.

Another plausible hypothesis on the diverse effects of Erf in hematopoiesis is its interplay with the RUNX factors. *Runx1* is expressed in HSCs and downstream myeloid cells, but its expression is decreased in maturing erythroid cells (53). Cooperation of Runx1 with PU.1 is critical for the commitment to myeloid lineages (13). *Runx2* is highly expressed in HSCs and is decreased as they mature (54). Runx1 transcription appears to be regulated via ets factor binding to one of its enhancers (24), while Runx2 may also be regulated by Erf or other ets proteins (32). Finally, we have recently shown that the Runx-Erf interplay on osteogenic targets may be important for bone development and craniosynostosis (32). It is conceivable that a similar interplay may also be relevant in hematopoietic development.

Taken together, our data strongly suggest an important role of Erf in all 3 waves primitive, EMP and HSC, of hematopoiesis during ontogeny. Erf activity is regulated by phosphorylation and nucleo-cytoplasmic shuttling and thus could be an appealing target for intervention. However, further experiments are needed to elucidate its precise mechanism and the stage of action during hematopoietic differentiation, particularly in the HSC differentiation.

Acknowledgments

We thank C. Kourouniotis, DVM, and the IMBB animal facility staff for expert animal support and Mrs Z. Vlata for Flow Cytometry analysis. Dr Marieke von Lindern (Sanquin, Amsterdam, Netherlands) for help with cell cultures and materials. We thank Dr. Kathleen McGrath for advice regarding the flow cytometric analysis of EMP and Anne Koniski for advice regarding erythroid colony assays.

Funding information

Greek Ministry of Education grant SYNERGASIA 09SYN-11-902 to GM and National Institutes of Health (USA) grant R01 HL130670 to JP.

Author contribution

I.P. designed and performed experiments and wrote the manuscript, J.P. designed experiments and wrote the manuscript, G.M. conceived the project, designed experiments and wrote the manuscript.

Conflicts of interest

The authors declare no conflict.

References

1. **Dzierzak E, Speck NA.** 2008. Of lineage and legacy: the development of mammalian hematopoietic stem cells. Nat Immunol **9:**129-136.

2. **Palis J, Malik J, McGrath KE, Kingsley PD.** 2010. Primitive erythropoiesis in the mammalian embryo. Int J Dev Biol **54:**1011-1018.

3. **Kingsley PD, Malik J, Fantauzzo KA, Palis J.** 2004. Yolk sac-derived primitive erythroblasts enucleate during mammalian embryogenesis. Blood **104:**19-25.

4. **Fraser ST, Isern J, Baron MH.** 2007. Maturation and enucleation of primitive erythroblasts during mouse embryogenesis is accompanied by changes in cell-surface antigen expression. Blood **109:**343-352.

5. **Palis J, Robertson S, Kennedy M, Wall C, Keller G.** 1999. Development of erythroid and myeloid progenitors in the yolk sac and embryo proper of the mouse. Development **126:**5073-5084.

6. **Bertrand JY, Jalil A, Klaine M, Jung S, Cumano A, Godin I.** 2005. Three pathways to mature macrophages in the early mouse yolk sac. Blood **106:**3004-3011.

7. **Tober J, Koniski A, McGrath KE, Vemishetti R, Emerson R, de Mesy-Bentley KK, Waugh R, Palis J.** 2007. The megakaryocyte lineage originates from hemangioblast precursors and is an integral component both of primitive and of definitive hematopoiesis. Blood **109:**1433-1441.

8. **Rich IN, Kubanek B.** 1979. The ontogeny of erythropoiesis in the mouse detected by the erythroid colony-forming technique. I. Hepatic and maternal erythropoiesis. J Embryol Exp Morphol **50:**57-74.

9. **Muller AM, Medvinsky A, Strouboulis J, Grosveld F, Dzierzak E.** 1994. Development of hematopoietic stem cell activity in the mouse embryo. Immunity **1:**291-301.

10. **Godin I, Dieterlen-Lievre F, Cumano A.** 1995. Emergence of multipotent hemopoietic cells in the yolk sac and paraaortic splanchnopleura in mouse embryos, beginning at 8.5 days postcoitus. Proc Natl Acad Sci U S A **92:**773-777.

11. **Medvinsky A, Dzierzak E.** 1996. Definitive hematopoiesis is autonomously initiated by the AGM region. Cell **86:**897-906.

12. **de Bruijn MF, Speck NA, Peeters MC, Dzierzak E.** 2000. Definitive hematopoietic stem cells first develop within the major arterial regions of the mouse embryo. EMBO J **19:**2465-2474.

13. **Imperato MR, Cauchy P, Obier N, Bonifer C.** 2015. The RUNX1-PU.1 axis in the control of hematopoiesis. Int J Hematol **101:**319-329.

14. **Scott EW, Simon MC, Anastasi J, Singh H.** 1994. Requirement of transcription factor PU.1 in the development of multiple hematopoietic lineages. Science **265:**1573-1577.

15. **Liu F, Patient R.** 2008. Genome-wide analysis of the zebrafish ETS family identifies three genes required for hemangioblast differentiation or angiogenesis. Circ Res **103:**1147-1154.

16. **Lee D, Park C, Lee H, Lugus JJ, Kim SH, Arentson E, Chung YS, Gomez G, Kyba M, Lin S, Janknecht R, Lim DS, Choi K.** 2008. ER71 acts downstream of BMP, Notch, and Wnt signaling in blood and vessel progenitor specification. Cell Stem Cell **2:**497-507.

17. **Sumanas S, Gomez G, Zhao Y, Park C, Choi K, Lin S.** 2008. Interplay among Etsrp/ER71, Scl, and Alk8 signaling controls endothelial and myeloid cell formation. Blood **111:**4500-4510.

18. **Kataoka H, Hayashi M, Nakagawa R, Tanaka Y, Izumi N, Nishikawa S, Jakt ML, Tarui H, Nishikawa S.** 2011. Etv2/ER71 induces vascular mesoderm from Flk1+PDGFRalpha+ primitive mesoderm. Blood **118:**6975-6986.

19. **Wareing S, Mazan A, Pearson S, Gottgens B, Lacaud G, Kouskoff V.** 2012. The Flk1-Cre-mediated deletion of ETV2 defines its narrow temporal requirement during embryonic hematopoietic development. Stem Cells **30:**1521-1531.

20. **Okano K, Hibi A, Miyaoka T, Inoue T, Sugimoto H, Tsuchiya K, Akiba T, Nitta K.** 2012. Inhibitory effects of the transcription factor Ets-1 on the expression of type I collagen in TGF-beta1-stimulated renal epithelial cells. Mol Cell Biochem **369:**247-254.

21. **Wareing S, Eliades A, Lacaud G, Kouskoff V.** 2012. ETV2 expression marks blood and endothelium precursors, including hemogenic endothelium, at the onset of blood development. Dev Dyn **241:**1454-1464.

22. **Taoudi S, Bee T, Hilton A, Knezevic K, Scott J, Willson TA, Collin C, Thomas T, Voss AK, Kile BT, Alexander WS, Pimanda JE, Hilton DJ.** 2011. ERG dependence distinguishes developmental control of hematopoietic stem cell maintenance from hematopoietic specification. Genes Dev **25:**251-262.

23. **Wang L, Liu T, Xu L, Gao Y, Wei Y, Duan C, Chen GQ, Lin S, Patient R, Zhang B, Hong D, Liu F.** 2013. Fev regulates hematopoietic stem cell development via ERK signaling. Blood **122:**367-375.

24. **Nottingham WT, Jarratt A, Burgess M, Speck CL, Cheng JF, Prabhakar S, Rubin EM, Li PS, Sloane-Stanley J, Kong ASJ, de Bruijn MF.** 2007. Runx1-mediated hematopoietic stem-cell emergence is controlled by a Gata/Ets/SCL-regulated enhancer. Blood **110:**4188-4197.

25. **Allegra M, Zaragkoulias A, Vorgia E, Ioannou M, Litos G, Beug H, Mavrothalassitis G.** 2012. Semaphorin-7a reverses the ERF-induced inhibition of EMT in Ras-dependent mouse mammary epithelial cells. Mol Biol Cell **23:**3873-3881.

26. **Athanasiou M, Blair DG, Mavrothalassitis G.** 2003. ERF, an ETS-related transcriptional repressor, can induce erythroid differentiation. Anticancer Res **23:**2143-2153.

27. **Athanasiou M, LeGallic L, Watson DK, Blair DG, Mavrothalassitis G.** 2000. Suppression of the Ewing's sarcoma phenotype by FLI1/ERF repressor hybrids. Cancer Gene Ther **7:**1188-1195.

28. **Le Gallic L, Sgouras D, Beal G, Jr., Mavrothalassitis G.** 1999. Transcriptional repressor ERF is a Ras/mitogen-activated protein kinase target that regulates cellular proliferation. Mol Cell Biol **19:**4121-4133.

29. **Sgouras DN, Athanasiou MA, Beal GJ, Jr., Fisher RJ, Blair DG, Mavrothalassitis GJ.** 1995. ERF: an ETS domain protein with strong transcriptional repressor activity, can suppress ets-associated tumorigenesis and is regulated by phosphorylation during cell cycle and mitogenic stimulation. EMBO J **14:**4781-4793.

30. **Verykokakis M, Papadaki C, Vorgia E, Le Gallic L, Mavrothalassitis G.** 2007. The RAS-dependent ERF control of cell proliferation and differentiation is mediated by c-Myc repression. J Biol Chem **282:**30285-30294.

31. **Papadaki C, Alexiou M, Cecena G, Verykokakis M, Bilitou A, Cross JC, Oshima RG, Mavrothalassitis G.** 2007. Transcriptional repressor erf determines extraembryonic ectoderm differentiation. Mol Cell Biol **27:**5201-5213.

32. **Twigg SR, Vorgia E, McGowan SJ, Peraki I, Fenwick AL, Sharma VP, Allegra M, Zaragkoulias A, Sadighi Akha E, Knight SJ, Lord H, Lester T, Izatt L, Lampe AK, Mohammed SN, Stewart FJ, Verloes A, Wilson LC, Healy C, Sharpe PT, Hammond P, Hughes J, Taylor S, Johnson D, Wall SA, Mavrothalassitis G, Wilkie AO.** 2013. Reduced dosage of ERF causes complex craniosynostosis in humans and mice and links ERK1/2 signaling to regulation of osteogenesis. Nat Genet **45:**308-313.

33. **Goode DK, Obier N, Vijayabaskar MS, Lie ALM, Lilly AJ, Hannah R, Lichtinger M, Batta K, Florkowska M, Patel R, Challinor M, Wallace K, Gilmour J, Assi SA, Cauchy P, Hoogenkamp M, Westhead DR, Lacaud G, Kouskoff V, Gottgens B, Bonifer C.** 2016.

549 Dynamic Gene Regulatory Networks Drive Hematopoietic Specification and
550 Differentiation. Dev Cell **36:**572-587.
551 34. **Lee LK, Ghorbanian Y, Wang W, Wang Y, Kim YJ, Weissman IL, Inlay MA, Mikkola HK.**
552 2016. LYVE1 Marks the Divergence of Yolk Sac Definitive Hemogenic Endothelium
553 from the Primitive Erythroid Lineage. Cell Rep **17:**2286-2298.
554 35. **Kellendonk C, Opherk C, Anlag K, Schutz G, Tronche F.** 2000. Hepatocyte-specific
555 expression of Cre recombinase. Genesis **26:**151-153.
556 36. **Tallquist MD, Soriano P.** 2000. Epiblast-restricted Cre expression in MORE mice: a tool
557 to distinguish embryonic vs. extra-embryonic gene function. Genesis **26:**113-115.
558 37. **Kingsley PD, Malik J, Emerson RL, Bushnell TP, McGrath KE, Bloedorn LA, Bulger M,**
559 **Palis J.** 2006. "Maturational" globin switching in primary primitive erythroid cells.
560 Blood **107:**1665-1672.
561 38. **McGrath KE, Frame JM, Fegan KH, Bowen JR, Conway SJ, Catherman SC, Kingsley PD,**
562 **Koniski AD, Palis J.** 2015. Distinct Sources of Hematopoietic Progenitors Emerge
563 before HSCs and Provide Functional Blood Cells in the Mammalian Embryo. Cell Rep
564 **11:**1892-1904.
565 39. **Dellinger MT, Meadows SM, Wynne K, Cleaver O, Brekken RA.** 2013. Vascular
566 endothelial growth factor receptor-2 promotes the development of the lymphatic
567 vasculature. PLoS One **8:**e74686.
568 40. **Gordon EJ, Gale NW, Harvey NL.** 2008. Expression of the hyaluronan receptor LYVE-1
569 is not restricted to the lymphatic vasculature; LYVE-1 is also expressed on embryonic
570 blood vessels. Dev Dyn **237:**1901-1909.
571 41. **Houssaint E.** 1981. Differentiation of the mouse hepatic primordium. II. Extrinsic
572 origin of the haemopoietic cell line. Cell Differ **10:**243-252.
573 42. **Sieff CA, Yang J, Merida-Long LB, Lodish HF.** 2010. Pathogenesis of the erythroid
574 failure in Diamond Blackfan anaemia. Br J Haematol **148:**611-622.

43. **Zhang C, Lv J, He Q, Wang S, Gao Y, Meng A, Yang X, Liu F.** 2014. Inhibition of endothelial ERK signalling by Smad1/5 is essential for haematopoietic stem cell emergence. Nat Commun **5:**3431.

44. **Padron-Barthe L, Temino S, Villa del Campo C, Carramolino L, Isern J, Torres M.** 2014. Clonal analysis identifies hemogenic endothelium as the source of the blood-endothelial common lineage in the mouse embryo. Blood **124:**2523-2532.

45. **Zhang J, Socolovsky M, Gross AW, Lodish HF.** 2003. Role of Ras signaling in erythroid differentiation of mouse fetal liver cells: functional analysis by a flow cytometry-based novel culture system. Blood **102:**3938-3946.

46. **Hollenhorst PC, McIntosh LP, Graves BJ.** 2011. Genomic and biochemical insights into the specificity of ETS transcription factors. Annu Rev Biochem **80:**437-471.

47. **Schuetze S, Stenberg PE, Kabat D.** 1993. The Ets-related transcription factor PU.1 immortalizes erythroblasts. Mol Cell Biol **13:**5670-5678.

48. **Rascle A, Ferrand N, Gandrillon O, Samarut J.** 1996. Myb-Ets fusion oncoprotein inhibits thyroid hormone receptor/c-ErbA and retinoic acid receptor functions: a novel mechanism of action for leukemogenic transformation by E26 avian retrovirus. Mol Cell Biol **16:**6338-6351.

49. **Wong KS, Proulx K, Rost MS, Sumanas S.** 2009. Identification of vasculature-specific genes by microarray analysis of Etsrp/Etv2 overexpressing zebrafish embryos. Dev Dyn **238:**1836-1850.

50. **Brown LA, Rodaway AR, Schilling TF, Jowett T, Ingham PW, Patient RK, Sharrocks AD.** 2000. Insights into early vasculogenesis revealed by expression of the ETS-domain transcription factor Fli-1 in wild-type and mutant zebrafish embryos. Mech Dev **90:**237-252.

51. **Ben-David Y, Giddens EB, Letwin K, Bernstein A.** 1991. Erythroleukemia induction by Friend murine leukemia virus: insertional activation of a new member of the ets gene family, Fli-1, closely linked to c-ets-1. Genes Dev **5:**908-918.

52. **Clausen PA, Athanasiou M, Chen Z, Dunn KJ, Zhang Q, Lautenberger JA, Mavrothalassitis G, Blair DG.** 1997. ETS-1 induces increased expression of erythroid markers in the pluripotent erythroleukemic cell lines K562 and HEL. Leukemia **11:**1224-1233.

53. **North TE, Stacy T, Matheny CJ, Speck NA, de Bruijn MF.** 2004. Runx1 is expressed in adult mouse hematopoietic stem cells and differentiating myeloid and lymphoid cells, but not in maturing erythroid cells. Stem Cells **22:**158-168.

54. **Kuo YH, Zaidi SK, Gornostaeva S, Komori T, Stein GS, Castilla LH.** 2009. Runx2 induces acute myeloid leukemia in cooperation with Cbfbeta-SMMHC in mice. Blood **113:**3323-3332.

Figure legends

Figure 1. *Erf*$^{ed/ed}$ mice are embryonic lethal and appear anemic. (**A**) Pregnant mice were sacrificed at the indicated day of gestation and the genotype of the embryos was analyzed. The graph indicates the percentages of alive *Erf*$^{ed/ed}$ embryos. The data are from 160 litters with at least 5 litters for each gestation stage (Supplemental Table 1). Chi square test showed statistical important decrease with the expected mendelian distribution, after E13.5. (**B**) Representative microphotographs of embryos at E13.5 showing an apparent anemia and lack of other gross morphology differences of *Erf*$^{ed/ed}$ embryos compared to their *Erf*$^{floxP/+}$ littermates. (**C**) Number of blood cells from the yolk sac and embryo proper at the indicated day of gestation. *Erf*$^{ed/ed}$ embryos exhibit statistically significant decrease throughout E9.5 – E13.5 exacerbated at E14.5. Samples are represented in a logarithmic scale. All values are means ± SE from 35 litters with at least 7 litters for each gestation stage (Supplemental Table 2). Statistical analysis performed using the unpaired t-test with two-tailed distribution. *, P < 0.05, **, P < 0.005, ***, P < 0.0005 for *Erf*$^{floP/+}$ vs *Erf*$^{ed/ed}$.

Figure 2. *Erf*$^{ed/ed}$ yolk sacs exhibit immature primitive erythroid progenitors. (A) Sagittal sections of paraffin-embedded yolk sacs from E9.5 *Erf*$^{ed/ed}$ and *Erf*$^{floxP/+}$ embryos stained with H&E. ve: visceral endoderm, m: mesothelium, bi: blood islands. **(B)** Fluorescent microphotographs of yolk sac from *Erf*$^{floxP/+}$ and *Meox2cre;Erf*$^{ed/ed}$ (*Erf*$^{ed/ed}$) at E10.5 stained with the angiogenesis marker PECAM-1. The white boxes on the images on the left indicate the magnified area of the image on the right. **(C)** Representative microphotographs of giemsa stained peripheral blood cells from E10.5

embryos. *Erf*$^{ed/ed}$ cells exhibit larger primitive precursor cells with less condensed chromatin and larger nuclei than their *Erf*-expressing littermates. Arrow indicates the most immature, larger, progenitors while filled arrow indicates the most mature, smaller, progenitors in each genotype. **(D)** *εy* globin mRNA levels, normalized to *Gapdh* mRNA levels, were determined by qPCR in blood cells from E10.5 and E11.5 *Erf*$^{ed/ed}$ and *Erf*$^{floxp/+}$ embryos. All values are means ± SE of at least 6 biological samples of each genotype from 6 litters at E10.5 and of at least 11 biological samples of each genotype from 7 litters at E11.5.

Figure 3. *Erf*$^{ed/ed}$ have decreased definitive progenitors in bloodstream. **(A)** Representative flow cytometry analysis of blood from E10.5 embryos stained with anti-c-Kit, anti-CD41 and anti CD16/32 antibodies. Cells expressing high levels of c-Kit (left panel) that were positive for CD41 and CD16/32 (right panel) were considered the EMP fraction. **(B)** EMP (c-Kit ^{high}, CD41^{+}, CD16/32^{+}) cells from E10.5 *Erf*$^{ed/ed}$ and *Erf*$^{floxP/+}$ embryonic blood werecompared to the average number of the *Erf*$^{floxP/+}$ EMP cells of the litter. All values are means ± SE of 4 biological samples of each genotype from 3 litters. Statistical analysis was performed using the unpaired t-test with two-tailed distribution. ***, P < 0.0005. **(C)** Number of BFU-E and CFU-E colonies derived from E10.5 *Erf*$^{ed/ed}$ and *Erf*$^{floxP/+}$ embryo blood were compared to the average number of the *Erf*$^{floxP/+}$ BFU-E / CFU-E colonies of the litter. All values are means ± SE of 6 biological samples of each genotype from 3 litters. Statistical analysis was performed using the unpaired t-test with two-tailed distribution. *, P < 0.05, **, P < 0.005, ***, P < 0.0005.

Figure 4. Elimination of *Erf* in definitive yolk sac wave leads to anemia. (**A**) Representative microphotographs of embryos at E13.5 showing an apparent anemia of *Lyve1*$^{tm1.1(EGFP/cre)Cys/tm1.1(EGFP/cre)Cys}$;*Erf*$^{loxP/loxP}$ (Lyve1$^{Cre/Cre}$ Erf$^{loxP/loxP}$) embryos compared to their *Erf*$^{+/+}$ littermates. (**B**) Number of BFU-E and CFU-E colonies derived from E10.5 *Lyve1*$^{Cre/Cre}$ *Erf*$^{loxP/loxP}$ and *Erf*$^{+/+}$ embryo blood were compared to the average number of the *Erf*$^{+/+}$ BFU-E / CFU-E colonies of the litter. All values are means ± SE of 4 biological samples from 2 litters. Statistical analysis was performed using the unpaired t-test with two-tailed distribution. *, P < 0.05. (**C**) Total liver cell counts of *Lyve1* $^{Cre/Cre}$ *Erf*$^{loxP/loxP}$ embryos compared to the *Erf*$^{+/+}$ littermates at E13.5. All values are means ± SE of 2 biological samples of each genotype from 2 litters. Statistical analysis was performed using the unpaired t-test with two-tailed distribution. *, P < 0.05, **, P < 0.005. (**D**) Total cell counts of *Lyve*$^{Cre/Cre}$ *Erf*$^{loxP/loxP}$ embryos compared to the *Erf*$^{+/+}$ littermates at E14.5 bloodstream. All values are means ± SE of 2 biological samples of each genotype from 2 litters. Statistical analysis was performed using the unpaired t-test with two-tailed distribution. *, P < 0.05.

Figure 5. *Erf*$^{ed/ed}$ have decreased differentiation rate in the fetal liver. (A) Total number of liver cells, **(B)** number of BFU-Es per liver at E11.5 – E13.5. and (**C**) number of CFU-Es at E11.5 – E13.5. Graphs of the values for *Erf*$^{ed/ed}$ and *Erf*$^{loxP/+}$ embryos compared to the average value of the *Erf*$^{loxP/+}$ littermates. All values are means ± SE of samples of at least 6 litters per gestation day (Supplemental Table 3) for total cells in liver and at least 6 litters per gestation day (Supplemental Table 4) for BFU-E / CFU-E colonies. Statistical analysis was performed using the unpaired t-test with two-tailed distribution. *, P < 0.05,

, P < 0.005, ***, P < 0.0005. (D**) Representative flow cytometry of *Erf*$^{ed/ed}$ E12.5 liver cells stained for Ter119, a marker for early proerythroblasts to mature erythrocytes (R3 – R5), and CD71, a marker for all proerythroblasts, except mature erythrocytes (R1-R4). (**E**) Comparison of R1-4 populations of E12.5 embryonic liver cells, analyzed by flow cytometry as in (D). Values for *Erf*$^{ed/ed}$ and *Erf*$^{floxP/+}$ cells are compared to the average value of the *Erf*$^{floxP/+}$ littermates. Samples are represented as ratio to *Erf*$^{floxp/+}$ littermates. All values are means ± SE of at least 6 biological samples of each genotype from at least 4 litters. Statistical analysis was performed using the unpaired t-test with two-tailed distribution. *, P < 0.05, **, P < 0.005, ***, P < 0.0005.

Figure 6. *Erf*$^{ed/ed}$ have reduced HSCs in liver transplant recipients. (A) Outline of repopulation experiments of sublethally irradiated mice with E13.5 liver cells (liver cells) or competitive repopulation experiments with E12.5 liver donor cells (+ helper) from *Erf*$^{ed/ed}$ and *Erf*$^{floxP/+}$ embryos assayed 1 (1m) or 5 (5m) months after irradiation. **(B)** Detection of the repopulating cells in the competitive repopulation experiment 5 months after irradiation by semiquantitative PCR. Transplanted *Erf*-expressing cells are detected by the presence of the 170 bp band (loxP, left panel) while *Erf*-null cells by the expression of the 178 bp band (del, right panel) generated after the excision of the *Erf* gene. The 101 bp wt *Erf* band (wt) and the 206 bp band from the GRCm38.p4 locus (GRC) were used as PCR controls. Lanes 100, 50, 10, 1 are quantitation controls containing 100 %, 50 %, 10 %, 1 % *Erf*$^{floxP/+}$ or *Erf*$^{ed/ed}$ DNA mixed with *Erf*$^{+/+}$ DNA. The numbers below indicate the percentage of the test band compared to the 100% sample.

714

Figure 1

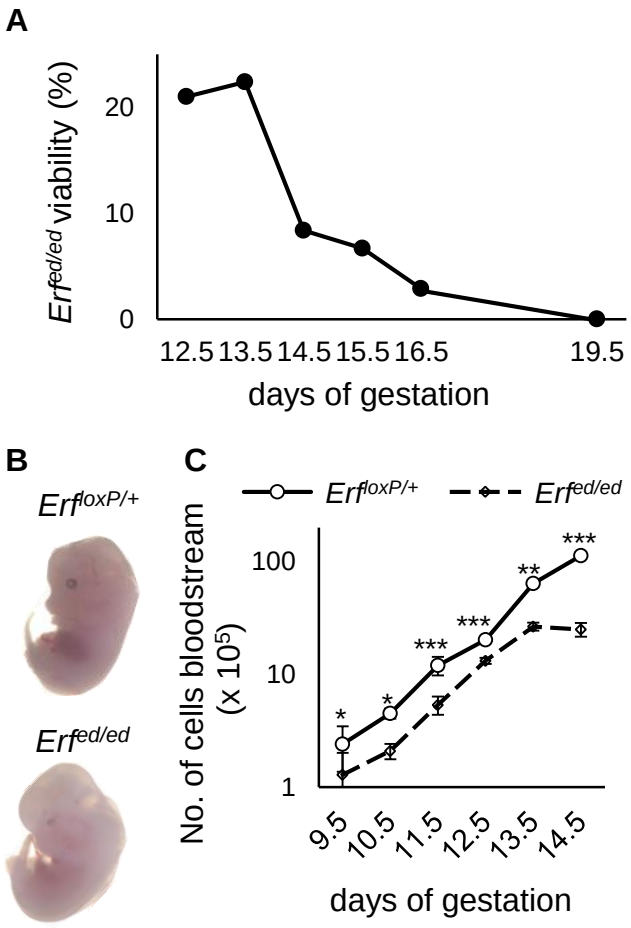
A
Erfed/ed viability (%)
20
10
0
12.5 13.5 14.5 15.5 16.5
19.5
days of gestation
B
ErfloxP/+
Erfed/ed
C
ErfloxP/+
Erfed/ed
No. of cells bloodstream (x 10^5)
100
10
1
*
*
***
***
**
***
9.5
10.5
11.5
12.5
13.5
14.5
days of gestation

Figure 2

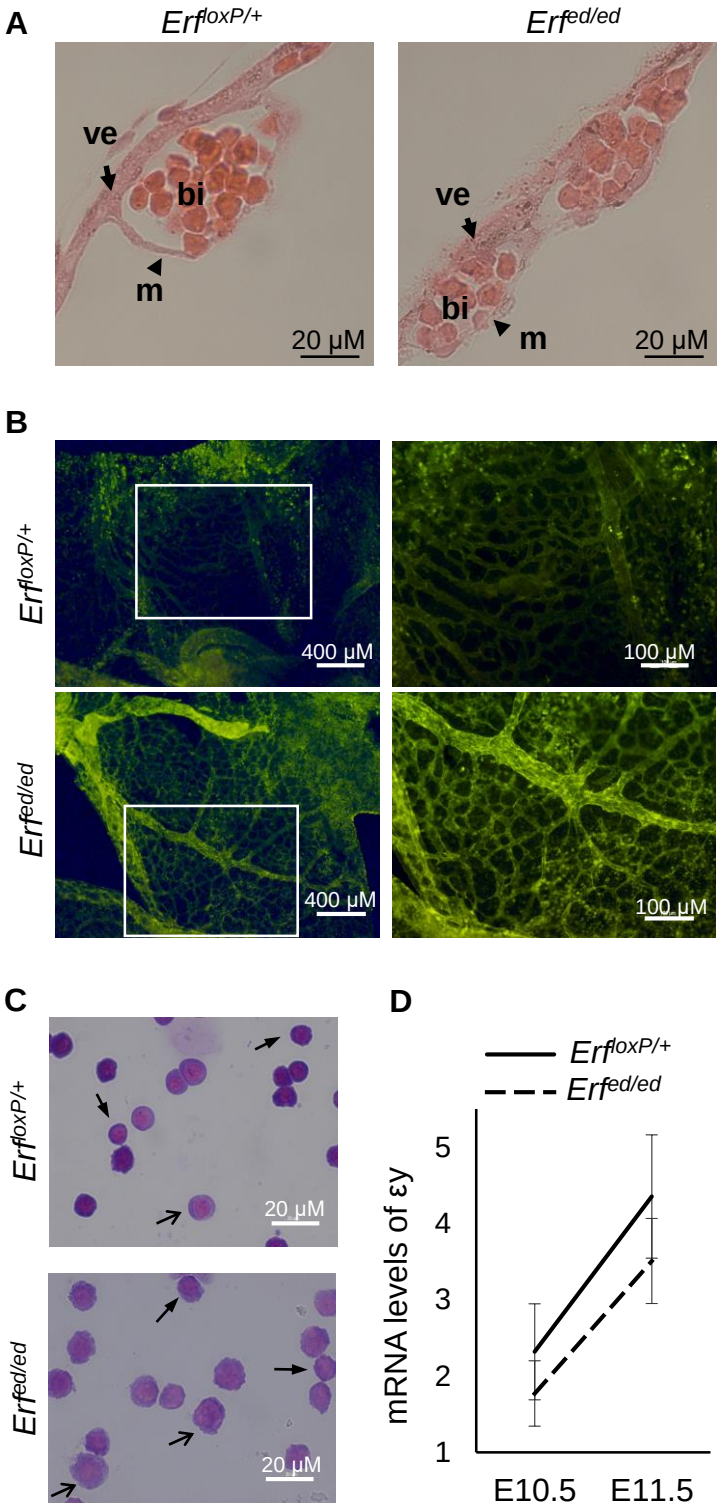
A
Erf^floxP/+
Erf^ed/ed
ve
bi
m
20 μM
ve
bi
m
20 μM
B
Erf^floxP/+
400 μM
100 μM
Erf^ed/ed
400 μM
100 μM
C
Erf^floxP/+
20 μM
Erf^ed/ed
20 μM
D
Erf^floxP/+
Erf^ed/ed
mRNA levels of εy
5
4
3
2
1
E10.5
E11.5

Figure 3

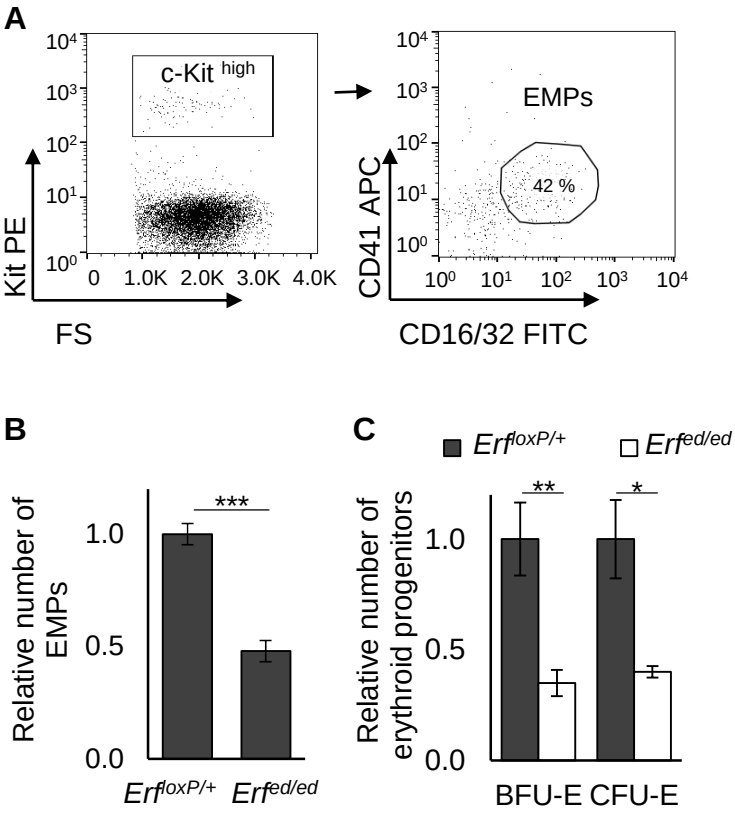
A
c-Kit high
Kit PE
FS
EMPs
42 %
CD41 APC
CD16/32 FITC
B
Relative number of EMPs
***
Erf floxP/+
Erf ed/ed
C
Erf floxP/+
Erf ed/ed
Relative number of erythroid progenitors
**
*
BFU-E
CFU-E

Figure 4

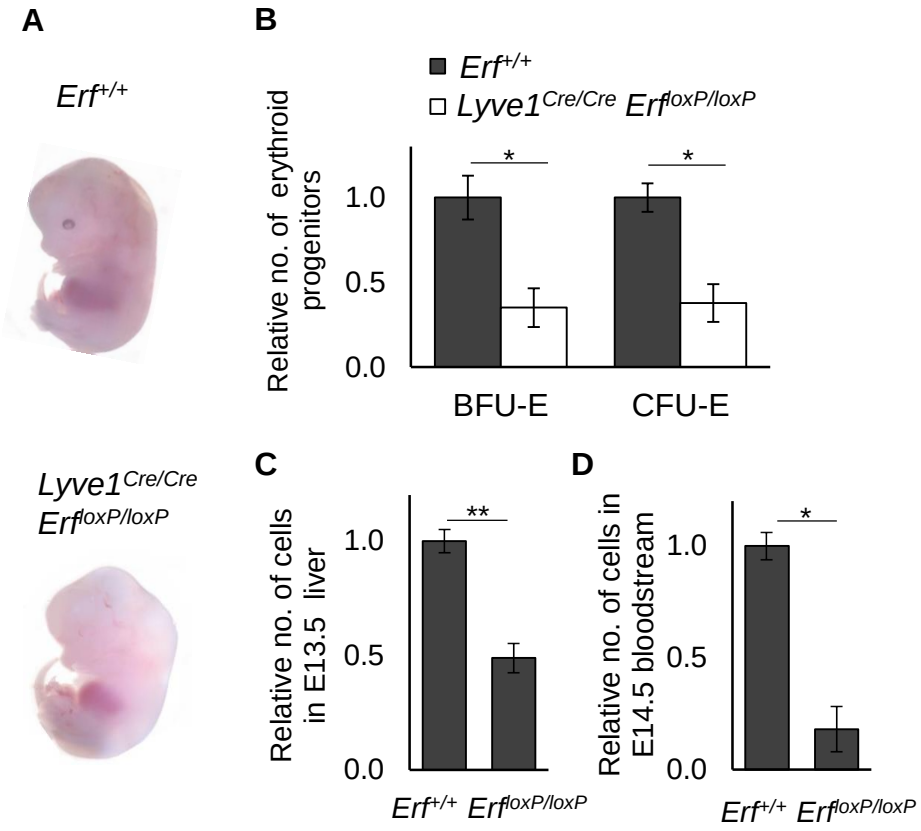
A
Erf+/+
Lyve1Cre/Cre
ErfloxP/loxP
B
Erf+/+
Lyve1Cre/Cre ErfloxP/loxP
Relative no. of erythroid progenitors
1.0
0.5
0.0
*
*
BFU-E
CFU-E
C
Relative no. of cells in E13.5 liver
**
Erf+/+ ErfloxP/loxP
D
Relative no. of cells in E14.5 bloodstream
*
Erf+/+ ErfloxP/loxP

Figure 5

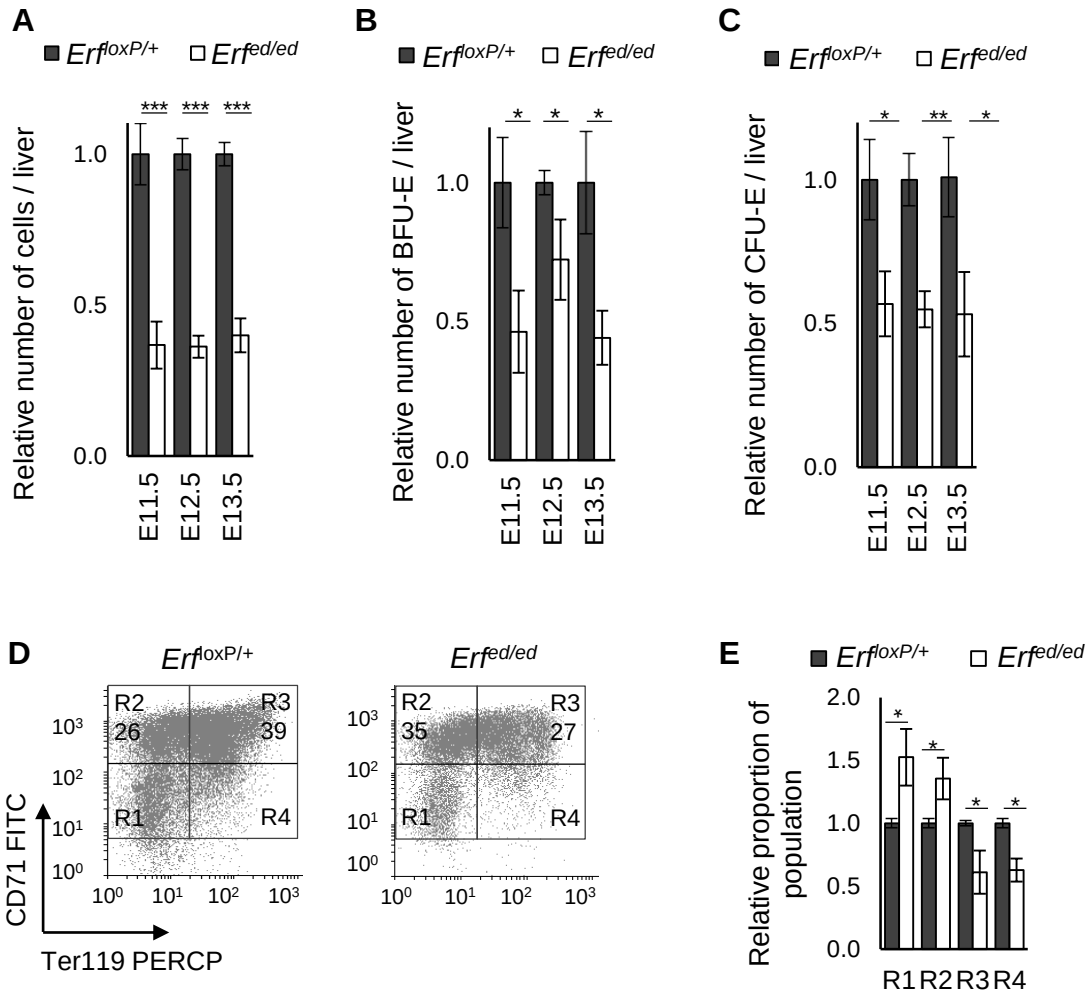
A
Erf floxP/+
Erf ed/ed
Relative number of cells / liver
1.0
0.5
0.0
***
***
***
E11.5
E12.5
E13.5
B
Erf floxP/+
Erf ed/ed
Relative number of BFU-E / liver
1.0
0.5
0.0
*
*
*
E11.5
E12.5
E13.5
C
Erf floxP/+
Erf ed/ed
Relative number of CFU-E / liver
1.0
0.5
0.0
*
**
*
E11.5
E12.5
E13.5
D
Erf floxP/+
Erf ed/ed
R2
R3
26
39
R1
R4
35
27
CD71 FITC
Ter119 PERCP
E
Erf floxP/+
Erf ed/ed
Relative proportion of population
2.0
1.5
1.0
0.5
0.0
R1 R2 R3 R4

Figure 6

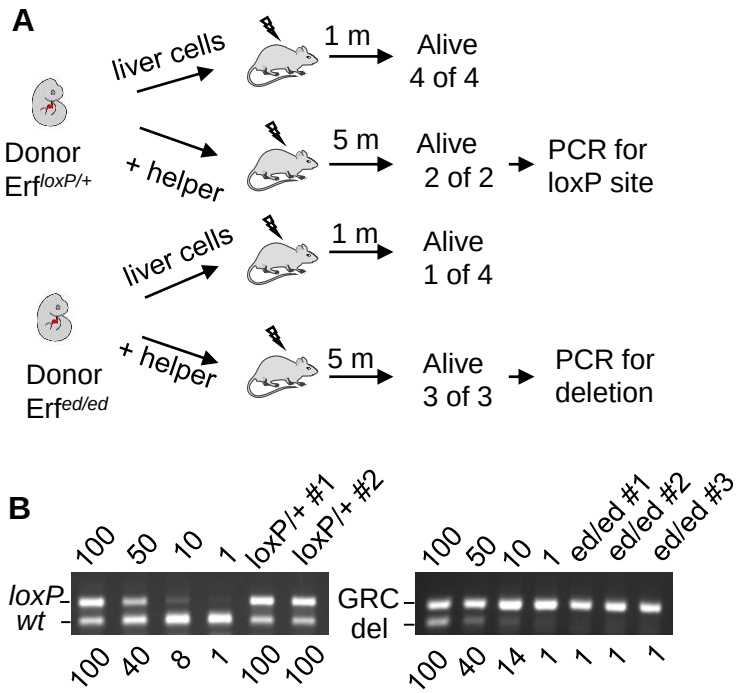
A
liver cells
1 m
Alive
4 of 4
Donor
Erf loxP/+
+ helper
5 m
Alive
2 of 2
PCR for
loxP site
liver cells
1 m
Alive
1 of 4
Donor
Erf ed/ed
+ helper
5 m
Alive
3 of 3
PCR for
deletion
B
100
50
10
1
loxP/+ #1
loxP/+ #2
ed/ed #1
ed/ed #2
ed/ed #3
loxP
wt
GRC
del
100
40
8
1
100
100
100
40
14
1
1
1
1

Supplemental Methods

Histologic analysis. Embryos and placentas were fixed in 4% paraformaldehyde at 4°C overnight, the tissues were washed in PBS, cryoprotected in 30% sucrose/PBS with gentle agitation at 4°C overnight, embedded in 7.5% w/v gelatin (Fluka, cat. No. 48723) containing 1.5% w/v sucrose and were frozen in 2-methylbutane at - 30°C. Specimens were cut into 7 μm sections in cryostat, collected on poly-L-lysine-coated slides and stained with hematoxylin/eosin (Sigma, cat. no HHS16) or subjected to in situ hybridization.

In situ-hybridization. The in situ hybridization with 4311, Tef5 and Pl1 probes for spongiotrophoblasts, syncytiotrophoblasts and giant cells respectively, was performed as previously described (31). Briefly, samples were fixed with 4 % PFA, incubated with proteinase K 20 μg/ml for 5 min at RT, washed with 0,2 % glycine in 1x PBS, fixed in 4 % PFA and washed in 1 x PBS for 5 min at RT. Then they were incubated with an acetylation mix containing triethenolamine 0.1 M (Merck, cat. no. 8379), NaOH 10N, and acetic anydrate 0.25% (Merck, cat. no. A6404) for 10 min, RT, washed with 1x PBS and hybridised with RNA probe in a concentration 1 ng/μl in hybridization buffer (50 % formamide 5 x Denhardts, 5x SSC, yeast tRNA 200 μg/ml, herring sperm DNA 0,5 mg/ml) at 55^{o}C for 16-18 hrs. After hybridization, samples were washed in 2× SSC for 30 min at 55°C, incubated in 20 μg/ml RNase for 30 min at 37°C, washed in 2× SSC / 50% formamide for 20 min and then 2× SSC (twice) at 55°C. Samples were blocked for non - specific

binding with 10% FCS for 1 hr at RT and then they were incubated with alkaline phosphatase (AP)-conjugated anti-digoxigenin (Roche cat.no. 11093274910) at 37°C, overnight. The hybridization was examined with NBT/BCIP solution (Roche, cat. no. 11681451001). Samples were photographed with 63x lens on a Zeis Axio Scope microscope fitted with ProgRess Jenoptik camera.

Real-time quantitative PCR for Erf. Total RNA was extracted from whole embryos, fetal livers and yolk sacs at E12.5, using Trizol reagent (Invitrogen, cat. no. 15596018) according to manufacturer's instructions. Reverse transcription of mRNA was employed by the SuperScript first strand synthesis kit (Invitrogen, cat. no. 11904-018). The reactions were performed with 100 ng of total cDNA utilizing the 2 x BrilliantIII SYBRGREEN QPCR mastermix (Stratagene, cat. no. 600882-51) in an Applied Biosystems StepOne plus Real-Time PCR machine. Expression levels of Erf were detected with the Erf primers (Fw: 5′ - TGTGGCACTTTATCCTGGAG - 3; Rv: 5′ - CTTGTAGGTGAACCGTTTCC – 3′). All expression levels were normalized to Gapdh levels (Fw: 5′ - CCAGTATGACTCCACTCACG.- 3′, Rv: 5′ - GACTCCACGACATACTCAGC - 3′) in the same cDNA. Annealing was performed at 56^{o}C for 20 sec for both Erf and Gapdh.

Fluorescence staining and confocal microscopy. Cryosections from E11.5 or E12.5 embryos were blocked in 5 % fetal bovine serum , 2% BSA, 0.5 % Triton solution in PBS for 1 hr and stained with the following antibodies: rat anti-Ter119 (Biolegend, cat. no.116203) or rat anti-CD71 antibody (Biolegend, cat. no.113805) for detection of all proerythroblasts to maturing enucleated

erythroblasts, rabbit anti-HNF4a for hepatocytes, rabbit anti - pH3 (Merck Millipore, cat. no, 07-424) for proliferating cells and rat anti - F4/80 (Biolegend, cat. no,123109) for the macrophages. The antibodies were diluted in 1 % fetal bovine serum, 0.4 % BSA in PBS and incubated overnight at 4°C, washed 3 times in PBS and stained with anti-rat CF555 (Sigma, cat. no. SAB4600060), anti-rabbit FITC (Sigma, cat. no. F0382) and anti-rabbit CF555 (Sigma, cat. no. SAB4600068), in 1:1000, 1:50 and 1:1000 dilution, respectively. Nuclei were stained with TO-PRO-3 iodide (Invitrogen cat. no. T3605) for 5 min at RT and the slides were mounted with mowiol (Sigma, cat. no. 81381). Analysis of apoptotic cells was performed with the In Situ cell dead kit TMR Red (Roche, cat. no. 12156792910) according to manual instructions.

Additionally, BrdU staining was employed in fetal livers with the following the method. Pregnant mice were injected with 50 μg Brdu (Sigma, cat. no B5002) per gr of the animal for 2 hrs. Then, embryos were dissected, fixated and frozen for cryosections. Sections were fixed in 4% paraformaldehyde in 1x PBS for 10 min, RT and then washed with 1xPBS for 3 times. Samples were incubated in a solution containing HCl 2N and 0.5% Triton in 1xPBS for 30 min, at 37^{o}C in glass bottle. Then, washes with a neutralization buffer containing sodium tetraborate 0.1M, pH 8.5 were performed for 5 min in 3 times. Blocking as mentioned before followed and then samples were incubated with rat anti-Brdu (Bio-rad, cat. no. OBT0030G) in dilution 1:800, overnight, at 4^{o}C. Next day, washes followed and samples were incubated with anti-rat CF555 (Sigma, cat. no. SAB4600060) for 1 hr, RT. The staining of nuclei was performed as before. All samples were analyzed by confocal microscope and processed with Leica 2.6.0 confocal imaging software.

Cell cycle analysis. Fetal livers were isolated from E13.5 embryos and dissociated by gentle pipetting in IMDM with 2% FBS. Cells were counted in hematocytometer and cells were incubated in 0.25% Triton, 1% BSA in 1x PBS for 15 min at 4°C. Then, 5 x 10^5 cells were centrifuged at 300 g and stained with 300 µl of a PBS solution containing propidium iodide 20 µg/ml and RNAse A (Qiagen, cat. no. 19101) 250 µg/ml for 20 minutes, at 4°C. Samples were analyzed by BD FACSCalibur Flow cytometer.

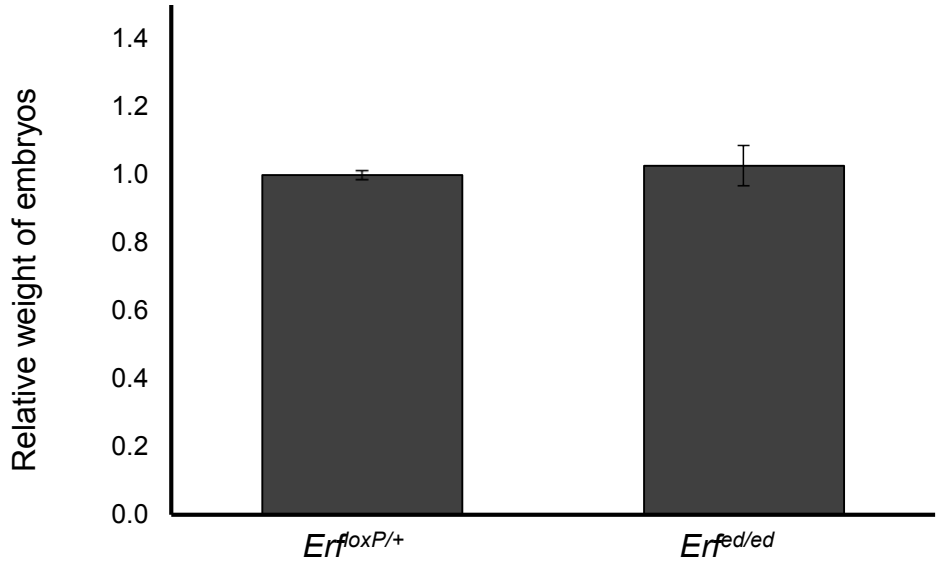

Supplemental Figure 1. Weight of *Erf*$^{ed/ed}$ embryos is comparable to their *Erf*$^{floxP/+}$ littermates. Dissected embryos were weighed and their weight was compared to the average weight of the *Erf*$^{floxp/+}$ embryos of each litter. The graph indicates the relative embryo weight of the respective genotype at embryonic day 13.5. All values are means ± SE of 10 biological samples from 8 litters. No statistical significance was observed using unpaired t-test with two-tailed distribution.

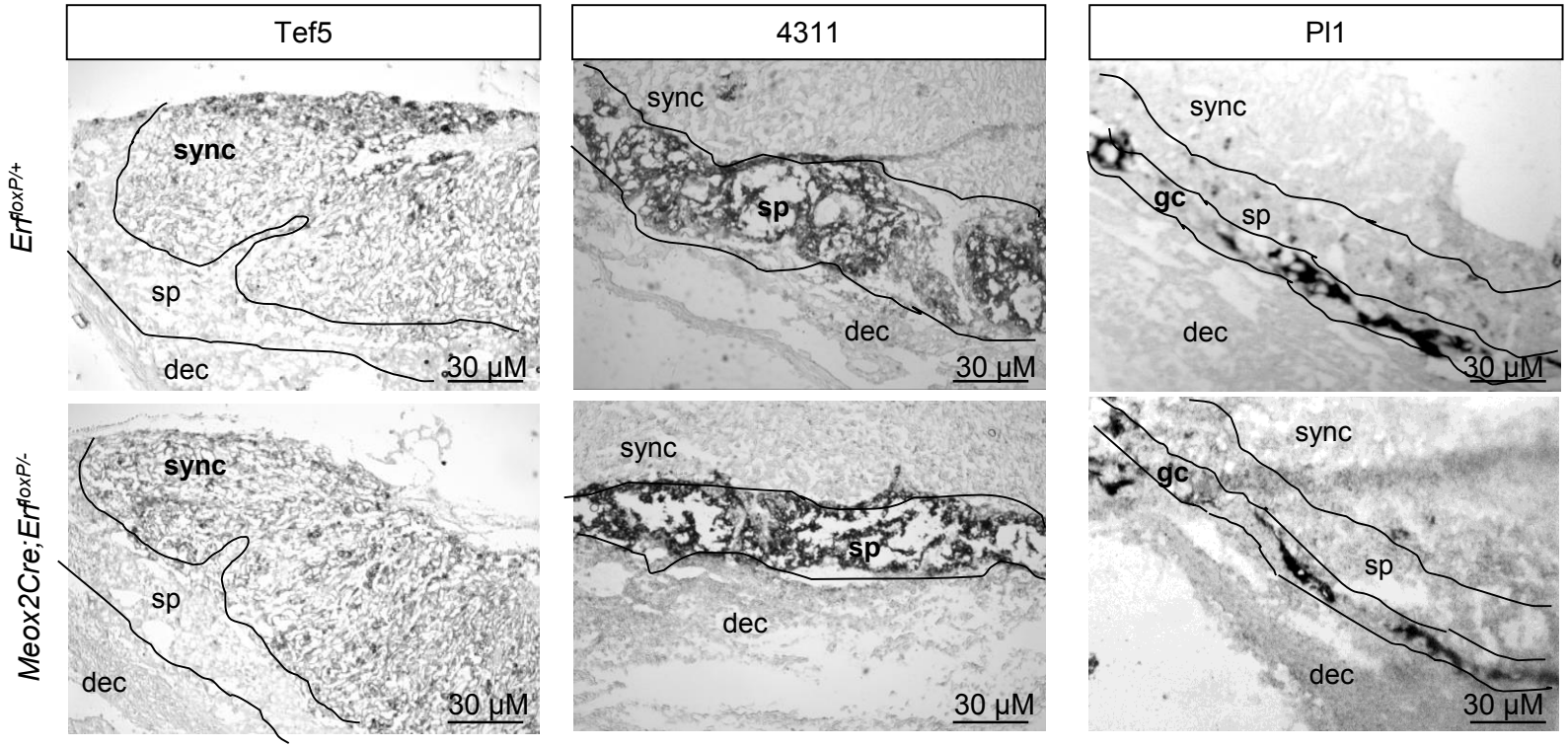

Supplemental Figure 2. *Erf*$^{ed/ed}$ embryos have no placenta defects. RNA in Situ hybridization on cryosections from E13.5 placentas with the cell type specific markers Tef5, 4311 that label the syncytiotrophoblast and the spongiotrophoblast respectively and from E12.5 placenta with the marker Pl1 that labels giant cells layer. Placentas of *Meox2cre;Erf*$^{floxP/-}$ concepti that nurture *Erf*$^{ed/ed}$ embryos appear comparable to their *Erf*$^{floxP/+}$ counterparts. sync: synciotrophoblast, sp: spongiotrophoblast, dec: decidua, gc: giant cells.

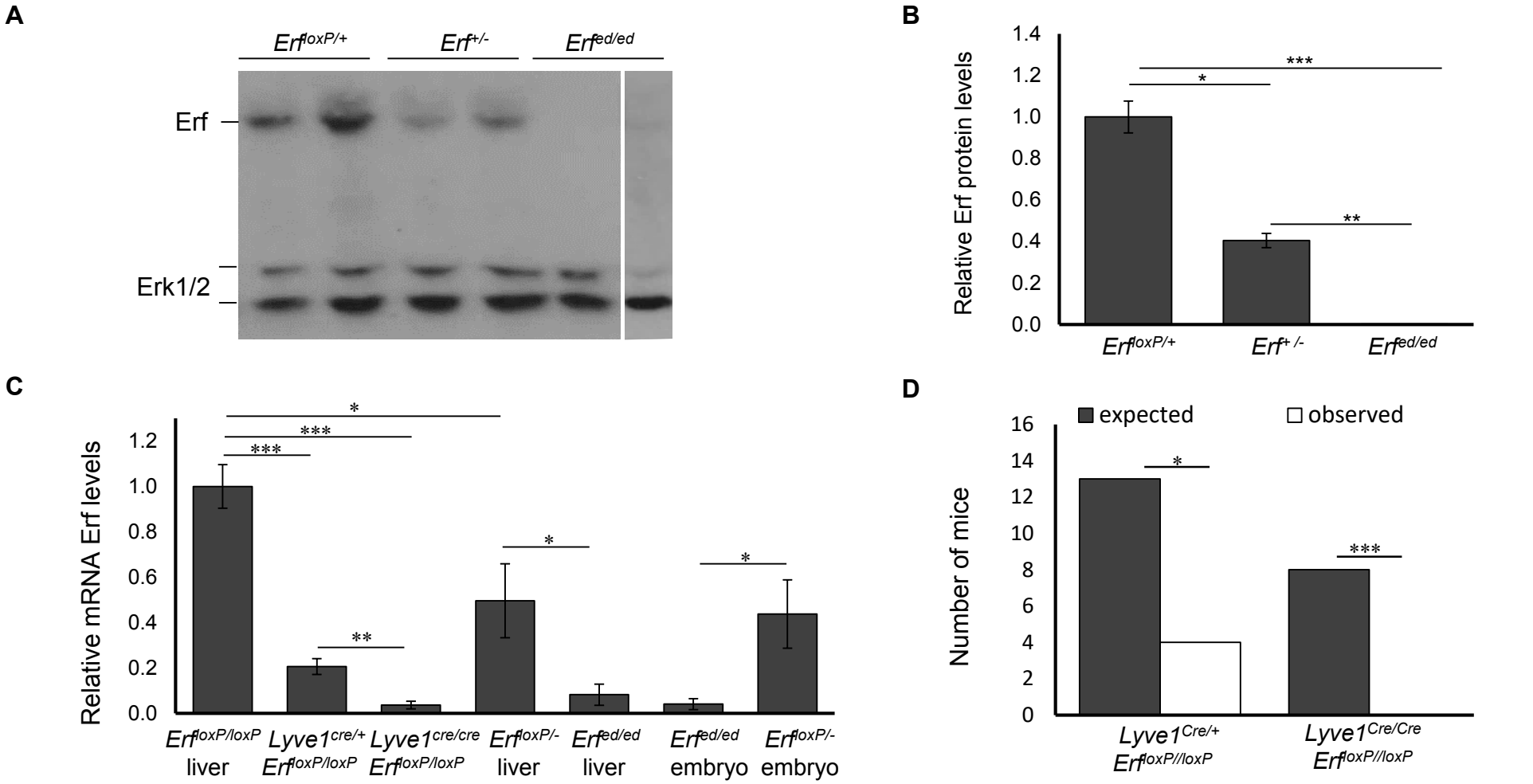

Supplemental Figure 3. Quantity differences in Erf expression. (A) Protein levels of Erf were determined by western blot from *Erf*$^{floxP/+}$, *Erf*$^{+/-}$ and *Erf*$^{ed/ed}$ E12.5 embryos. Erk1/2 antibody was used for normalization. All samples except for the last one were loaded in the same blot. **(B)** Quantification of Erf protein levels from *Erf*$^{floxP/+}$, *Erf*$^{+/-}$ and *Erf*$^{ed/ed}$ E12.5 embryos. Samples are represented as ratio to *Erf*$^{floxp/+}$ littermates after normalization with Erk1/2 quantities. **(C)** mRNA levels of Erf were determined in fetal livers of *Erf*$^{floxP/loxP}$, *Lyve1*$^{Cre/+}$ *Erf*$^{floxP/loxP}$ and *Lyve1*$^{Cre/Cre}$ *Erf*$^{floxP/loxP}$ E12.5 embryos as well in both livers and whole embryos of *Erf*$^{floxP/-}$ and *Erf*$^{ed/ed}$ at E12.5, employing the qPCR method. Samples were normalized to Gapdh mRNA levels and were quantified corresponding to the 2 loxP alleles. **(D)** Number of animals born with the *Lyve1*$^{Cre/+}$ *Erf*$^{floxP/loxP}$ or the *Lyve1*$^{Cre/+}$ *Erf*$^{floxP/loxP}$ genotype. Chi square test showed statistical important differences of the actual over expected numbers of total 100 mice from 16 different litters. All values are means ± SE of at least 5 samples from 5 litters**.** Statistical analysis was performed using the unpaired t-test with two-tailed distribution. *, P < 0.05, P < 0.05, ***, P < 0.0005.

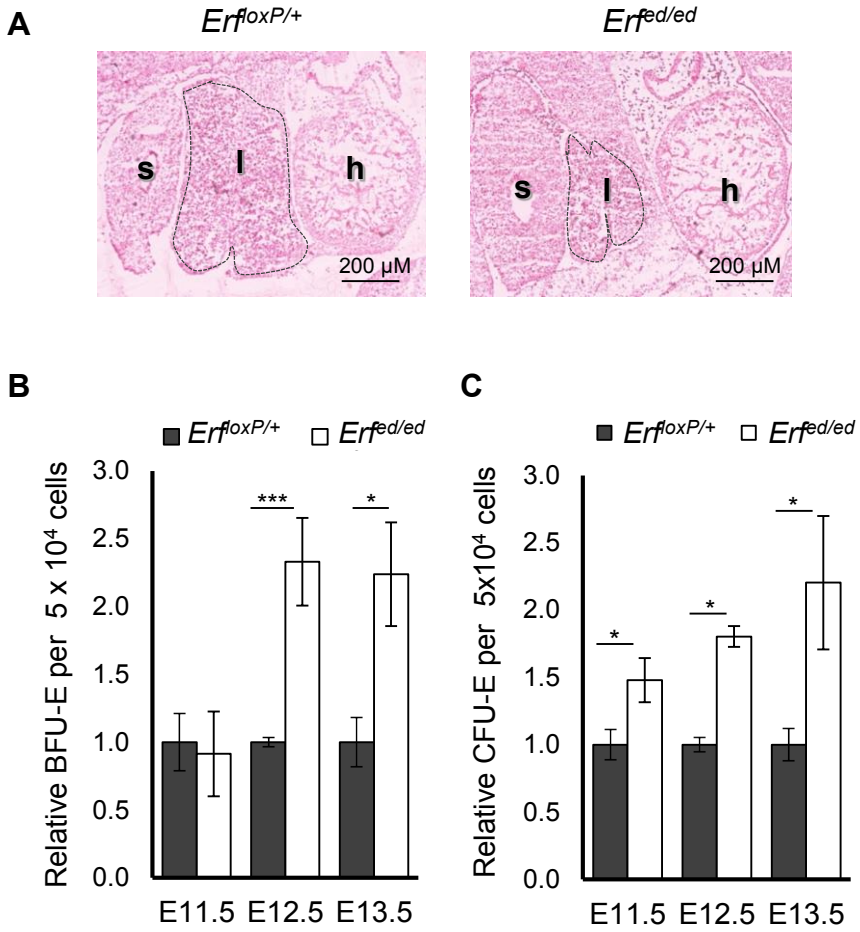

Supplemental Figure 4. *Erf*$^{ed/ed}$ livers have decreased numbers but increased proportion of BFU-Es and CFU-Es. **(A)** Sagittal sections from E11.5 *Erf*$^{ed/ed}$ and *Erf*$^{loxP/+}$ embryos stained with Hematoxylin and Eosin. s: stomach, l: liver, h: heart. **(B)** Proportion of BFU-E and **(C)** CFU-E at 11.5 – 13.5 d.p.c. Samples are represented as ratio to *Erf*$^{loxp/+}$ littermates. All values are means ± SE of samples from at least from 6 litters per gestation day (Supplemental Table 4). Statistical analysis was performed using the unpaired t-test with two-tailed distribution. *, $P < 0.05$, ***, $P < 0.0005$.

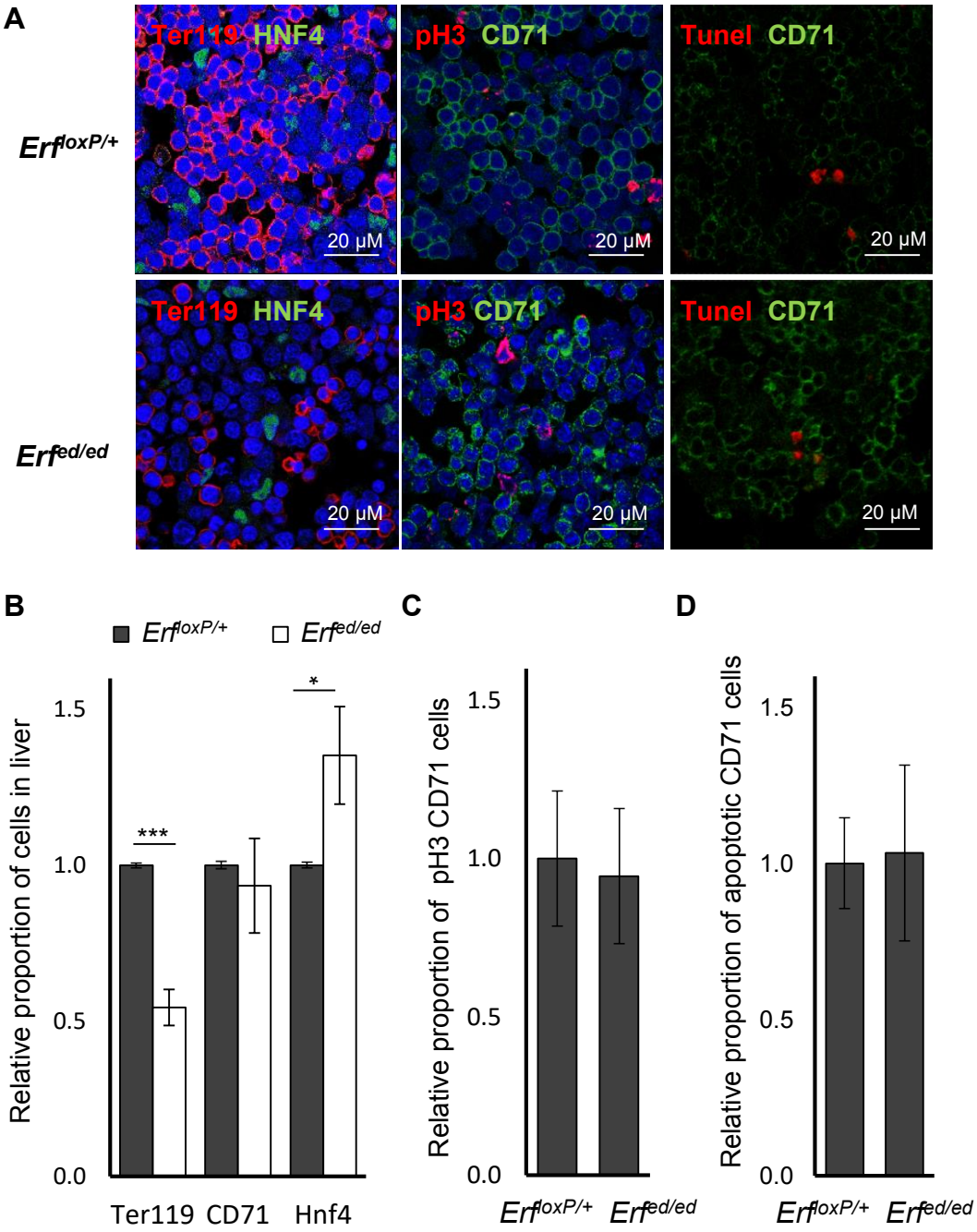

Supplemental Figure 5. *Erf* does not affect hepatic cells, growth rate or apoptosis. (A) Confocal microscopy images of sagittal sections of livers from E12.5 $Erf^{ed/ed}$ and $Erf^{floxP/+}$ embryos stained with the anti-Ter119 antibody for detection of the mature erythroblasts R3 – R5, anti-HNF4 antibody for hepatocytes (left panels), anti-CD71 antibody for the erythroblasts R1 – R4 and anti-pH3 antibody for proliferating cells (middle panels) or with In Situ cell dead kit TMR (Tunel) for detection of apoptotic CD71 cells (right panels). Nuclei were stained with TOPRO-3 (blue). **(B)** Proportion of Ter119, HNF4 and CD71 cells in E12.5 livers. The graph shows the values for $Erf^{ed/ed}$ and $Erf^{floxP/+}$ embryos, compared to the average value of the $Erf^{floxP/+}$ littermates. All values are means ± SE of at least 10 biological samples of each genotype from 8 litters. Statistical analysis was performed using the unpaired t-test with two-tailed distribution. ***, $P < 0.0005$. **(C)** Proportions of CD71 cells are positive for pH3 at E12.5 livers. The values for $Erf^{ed/ed}$ and $Erf^{floxP/+}$ embryos were compared to the average value of the $Erf^{floxP/+}$ littermates. All values are means ± SE of 4 biological samples of each genotype from 3 litters. *, $P < 0.05$. **(D)** Proportion of apoptotic cells (Tunel positive) at E12.5 livers. The values for $Erf^{ed/ed}$ and $Erf^{floxP/+}$ embryos were compared to the average value of the $Erf^{floxP/+}$ littermates. All values are means ± SE of at least 2 biological samples of each genotype from 2 litters. Statistical analysis was performed using the unpaired t-test with two-tailed distribution. *, $P < 0.05$.

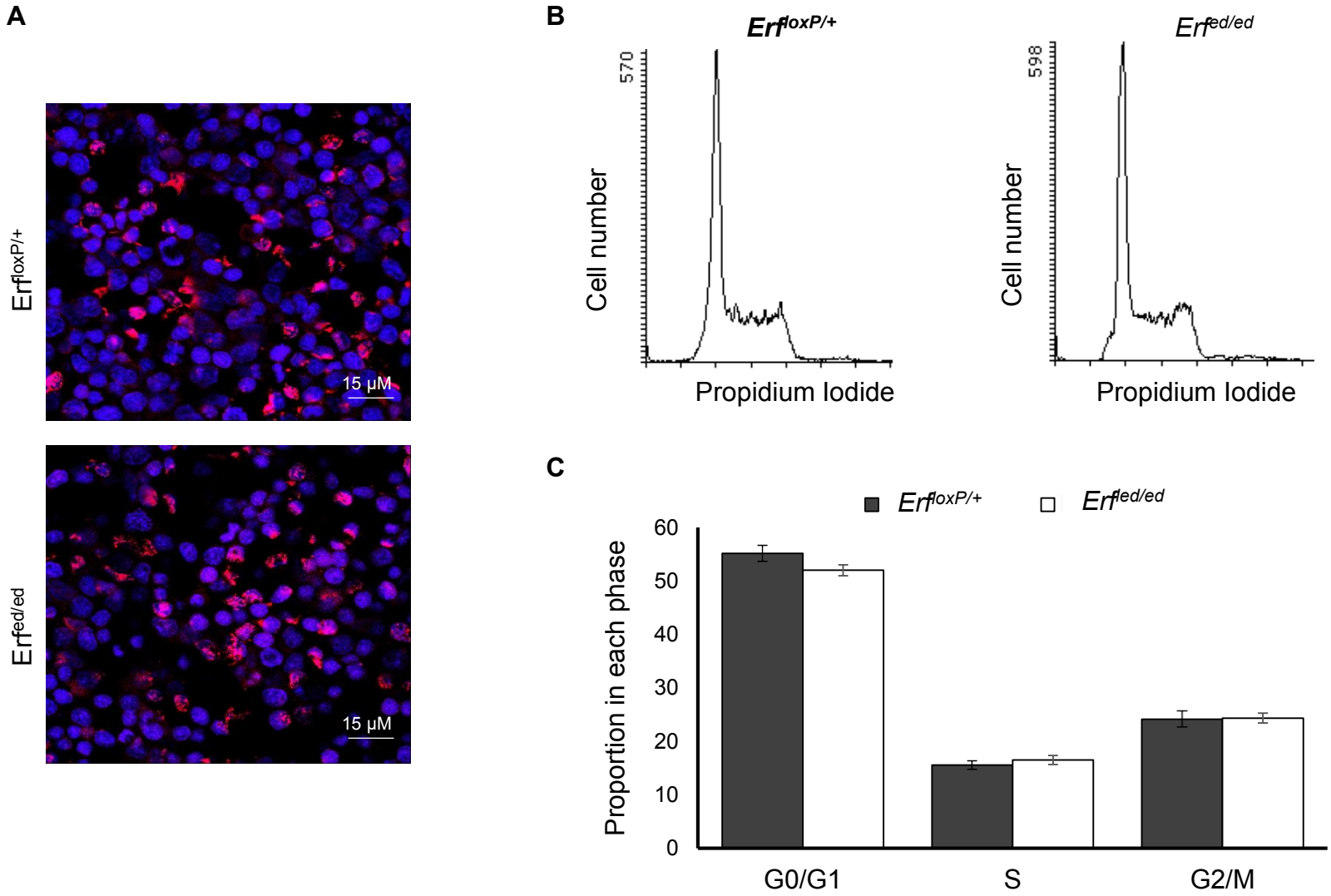

Supplemental Figure 6. *Erf*$^{ed/ed}$ erythroblasts have normal cell cycle progression. (A) Confocal microscopy images of sagittal sections of livers from E12.5 *Erf*$^{ed/ed}$ and *Erf*$^{floxP/+}$ embryos stained with BrdU, a marker of proliferating cells (red). Nuclei were stained with TOPRO-3 (blue). **(B)** Representative flow cytometry profiles of cell cycle of E13.5 *Erf*$^{ed/ed}$ and *Erf*$^{floxP/+}$ fetal livers stained with propidium iodide. **(C)** Proportions of phases G0/G1, S and G2/M of cell cycle at E13.5 livers. All values are means ± SE of 6 biological samples of each genotype from 2 litters.

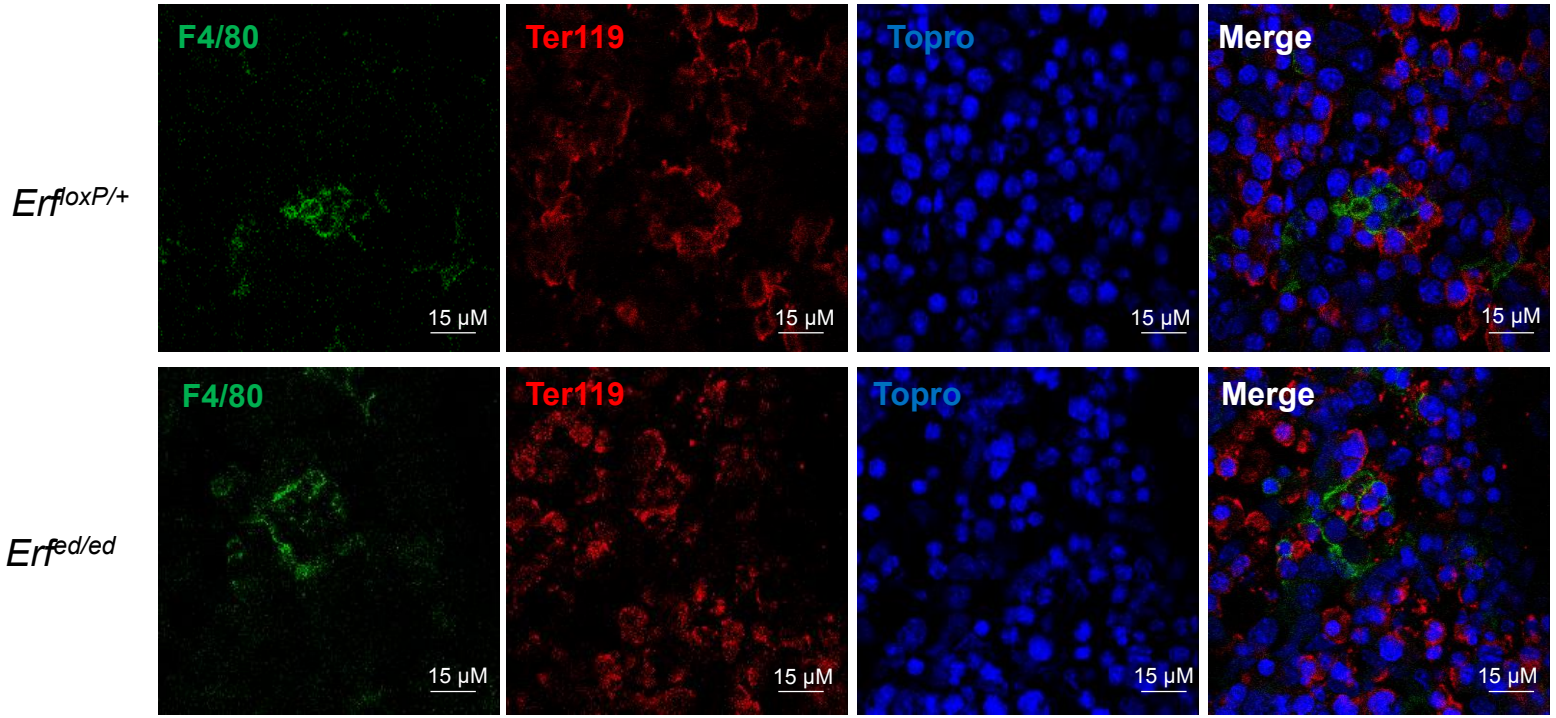

Supplemental Figure 7. *$Erf^{ed/ed}$* have normal macrophages – erythroblasts contacts. Confocal microscopy images of sagittal sections of livers from E12.5 *$Erf^{ed/ed}$* and *$Erf^{floxP/+}$* embryos stained with anti-F4/80 antibody, a marker for macrophages (green) and Ter119, a marker for maturing erythroblasts (red). Nuclei were stained with TOPRO-3 (blue).

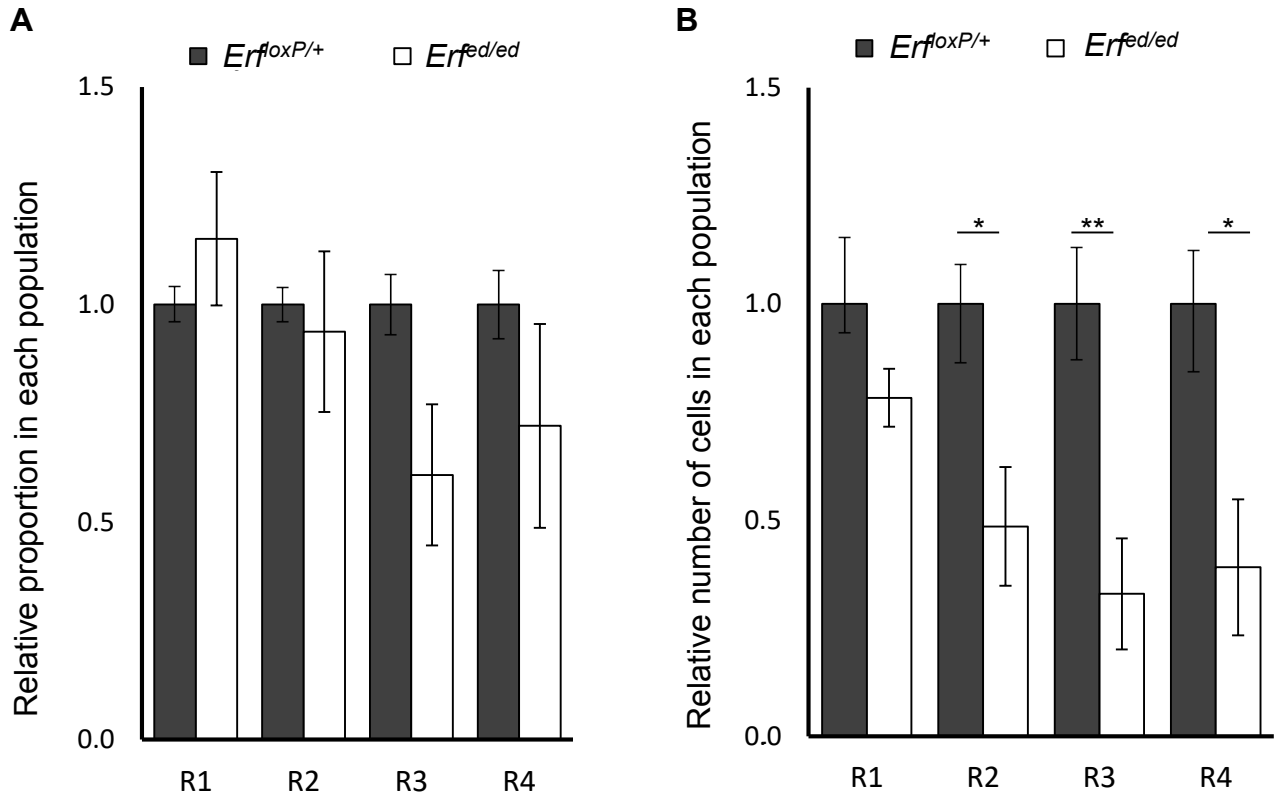

Supplemental Figure 8. *Erf*$^{ed/ed}$ have reduced progenitor erythroid cells at E11.5. (A) Proportions and **(B)** total cells of R1-4 populations from E11.5 embryonic liver cells. Liver cells were stained with anti-CD71 and anti-Ter119 antibodies and were analyzed by flow cytometry based on the dynamic expression of CD71 and Ter119 markers. The graphs show the values for *Erf*$^{ed/ed}$ and *Erf*$^{floxP/+}$ embryos compared to the average value of the *Erf*$^{floxP/+}$ littermates. All values are means ± SE of at least 6 biological samples of each genotype of at least 4 litters. Statistical analysis was performed using the unpaired t-test with two-tailed distribution. *, $P < 0.05$, **, $P < 0.005$. .

Supplemental Tables

Supplemental Table 1. Number of *Erf*$^{ed/ed}$ embryos in each gestation day, whose lethality was measured as shown in Figure 1a.

Embryonic day	No. of litters	No. of *Erf*$^{ed/ed}$ *embryos*	No. of total embryos
9.5	5	6	48
10.5	12	12	86
11.5	12	17	91
12.5	39	45	219
13.5	27	32	152
14.5	15	9	102
15.5	5	2	26
16.5	5	1	23
adult	38	0	248

Supplemental Table 2. Number of embryos, whose number of cells in bloodstream was counted in each gestation day (epiblast derived conditional mice) as shown in Figure 1c.

		No. of embryos for peripheral blood counts	
Embryonic day	litters	*Erf*$^{floxP/+}$	*Erf*$^{ed/ed}$
9.5	3	9	4
10.5	9	24	15
11.5	9	15	11
12.5	5	13	7
13.5	3	3	4
14.5	6	13	7

Supplemental Table 3. Number of liver samples in each gestation day and genotype, which was used for counting total cells in liver as shown in Figure 5a. .

		No. of liver samples	
Embryonic day	litters	*Erf*$^{floxP/+}$	*Erf*$^{ed/ed}$
11.5	6	17	8
12.5	9	22	15
13.5	13	28	24

Supplemental Table 4. Number of samples used in each gestation day and genotype for counting proportion and numbers of BFU-E / CFU-E per liver as shown in Figure 5b, c and Supplemental figure 4b,c.

		No. of samples for BFU-E / CFU-E analysis	
Embryonic day	litters	*Erf*$^{floxP/+}$	*Erf*$^{ed/ed}$
11.5	3	6	5
12.5	5	10	9
13.5	4	9	8

nature genetics

Reduced dosage of *ERF* causes complex craniosynostosis in humans and mice and links ERK1/2 signaling to regulation of osteogenesis

Stephen R F Twigg[1], Elena Vorgia[2,3,16], Simon J McGowan[4,16], Ioanna Peraki[2,3,16], Aimée L Fenwick[1,16], Vikram P Sharma[1,5], Maryline Allegra[2], Andreas Zaragkoulias[3], Elham Sadighi Akha[6], Samantha J L Knight[6], Helen Lord[7], Tracy Lester[7], Louise Izatt[8], Anne K Lampe[9], Shehla N Mohammed[8], Fiona J Stewart[10], Alain Verloes[11], Louise C Wilson[12], Chris Healy[13], Paul T Sharpe[13], Peter Hammond[14], Jim Hughes[15], Stephen Taylor[4], David Johnson[5], Steven A Wall[5], George Mavrothalassitis[2,3] & Andrew O M Wilkie[1,5]

The extracellular signal–related kinases 1 and 2 (ERK1/2) are key proteins mediating mitogen-activated protein kinase signaling downstream of RAS: phosphorylation of ERK1/2 leads to nuclear uptake and modulation of multiple targets[1]. Here, we show that reduced dosage of ERF, which encodes an inhibitory ETS transcription factor directly bound by ERK1/2 (refs. 2–7), causes complex craniosynostosis (premature fusion of the cranial sutures) in humans and mice. Features of this newly recognized clinical disorder include multiple-suture synostosis, craniofacial dysmorphism, Chiari malformation and language delay. Mice with functional Erf levels reduced to ~30% of normal exhibit postnatal multiple-suture synostosis; by contrast, embryonic calvarial development appears mildly delayed. Using chromatin immunoprecipitation in mouse embryonic fibroblasts and high-throughput sequencing, we find that ERF binds preferentially to elements away from promoters that contain RUNX or AP-1 motifs. This work identifies ERF as a novel regulator of osteogenic stimulation by RAS-ERK signaling, potentially by competing with activating ETS factors in multifactor transcriptional complexes.

We used exome sequencing[8] to analyze the DNA from a 15-year-old boy with craniosynostosis affecting all sutures of the cranial vault. His 7-year-old brother had metopic, sagittal and left coronal synostosis, and their mother exhibited exorbitism and midface hypoplasia but did not have documented craniosynostosis (**Fig. 1**). After excluding previously described variants and genomic regions for which the brothers did not share the maternal allele, 135 non-synonymous sequence changes remained, including 5 nonsense mutations (**Supplementary Table 1**). One of the nonsense mutations (c.547C>T; p.Arg183*) was present in *ERF*, encoding an inhibitory ETS family transcription factor located on chromosome 19q13.2. ERF was previously shown to be a prominent binding target of the paralogous ERK1/2 kinases[7], key effectors of the RAS-MEK-ERK signal transduction cascade; the transcriptional activity of ERF is primarily regulated by ERK1/2-mediated phosphorylation, which leads to its export from the nucleus[5,6]. We considered *ERF* as a candidate because activation of ERK1/2 signaling was previously shown in craniosynostosis[9,10]. We confirmed segregation of the mutation from the maternal grandmother to the two affected children (family 1; **Supplementary Fig. 1**).

To analyze the possible contribution of *ERF* mutation to the pathological phenotype, we sequenced the gene in 411 samples from unrelated subjects with craniosynostosis (**Table 1**) and 288 northern European controls. Heterozygous loss-of-function mutations were present in an additional 11 samples from affected individuals but were not identified in normal controls ($P = 0.004$, Fisher's exact test) (**Fig. 2** and **Table 2**). No deletions were identified in 276 mutation-negative samples. We analyzed earlier generations, finding 26 mutation-positive individuals in total (**Supplementary Fig. 1**). In 4 families, the mutation had arisen *de novo* from a parent ($n = 2$), grandparent ($n = 1$) or great-grandparent ($n = 1$) (**Supplementary Fig. 2**). The occurrence

[1]Clinical Genetics Group, Weatherall Institute of Molecular Medicine, University of Oxford, Oxford, UK. [2]Institute of Molecular Biology and Biotechnology, Foundation for Research and Technology–Hellas, Heraklion, Greece. [3]School of Medicine, University of Crete, Heraklion, Greece. [4]Computational Biology Research Group, Weatherall Institute of Molecular Medicine, University of Oxford, Oxford, UK. [5]Craniofacial Unit, Oxford University Hospitals National Health Service (NHS) Trust, Oxford, UK. [6]National Institute for Health Research (NIHR) Biomedical Research Centre, Oxford and Wellcome Trust Centre for Human Genetics, University of Oxford, Oxford, UK. [7]Molecular Genetics Laboratory, Oxford University Hospitals NHS Trust, Oxford, UK. [8]Clinical Genetics, Guy's and St. Thomas' NHS Foundation Trust, London, UK. [9]South East of Scotland Clinical Genetics Service, NHS Lothian, Edinburgh, UK. [10]Northern Ireland Regional Genetics Service, Belfast City Hospital, Belfast, UK. [11]Département de Génétique, Assistance Publique–Hôpitaux de Paris (AP-HP)–Hôpital Robert Debré, Paris, France. [12]North East Thames Regional Genetics Service, Great Ormond Street Hospital for Children NHS Trust, London, UK. [13]Department of Craniofacial Development and Stem Cell Biology, Dental Institute, King's College London, London, UK. [14]Molecular Medicine Unit, University College London (UCL) Institute of Child Health, London, UK. [15]Medical Research Council (MRC) Molecular Haematology Unit, Weatherall Institute of Molecular Medicine, University of Oxford, Oxford, UK. [16]These authors contributed equally to this work. Correspondence should be addressed to G.M. (mavro@imbb.forth.gr) or A.O.M.W. (awilkie@hammer.imm.ox.ac.uk).

Received 10 July 2012; accepted 3 January 2013; published online 27 January 2013; doi:10.1038/ng.2539

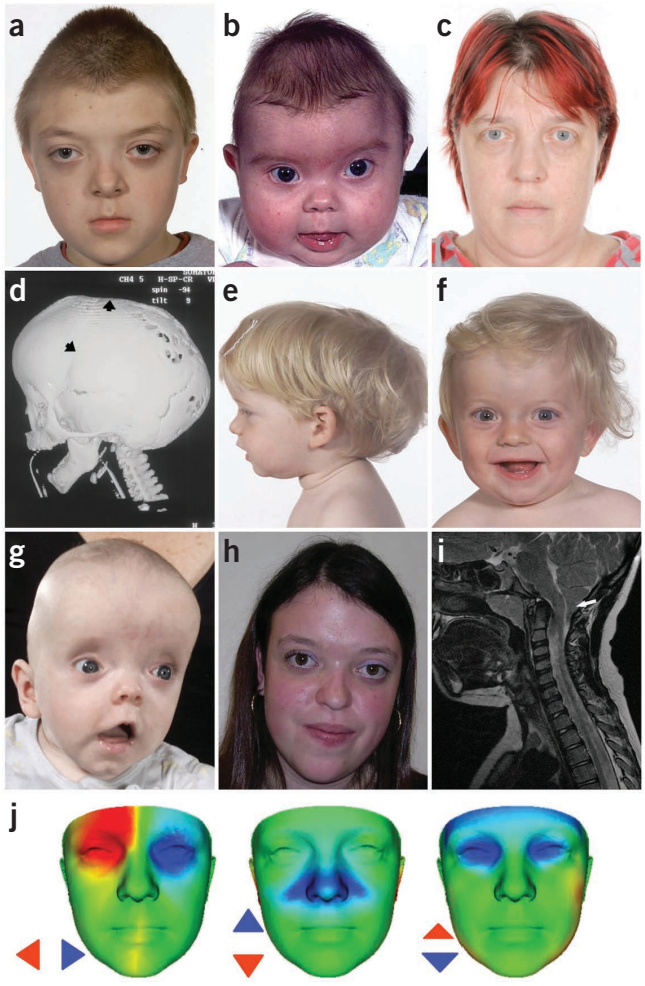

Figure 1 Clinical features of subjects heterozygous for *ERF* mutations. (**a**–**d**) Family 1 showing subject IV-1, aged 10 years, on whom exome sequencing was performed (**a**), his brother IV-2, aged 4 months (**b**), and their mother III-3, aged 37 years (**c**). The CT head scan of IV-2, aged 5 months (**d**), shows synostosis of the left coronal and sagittal sutures (arrows) associated with multiple craniolacunae; the lambdoid and squamosal sutures remain patent. (**e**–**h**) Subjects identified in follow-up sequencing had clinical diagnoses ranging from non-syndromic sagittal synostosis (**e**, III-1 in family 5, aged 1.6 years) or unilateral lambdoid synostosis (**f**, III-1 in family 4, aged 1.2 years) to *FGFR2* mutation–negative Crouzon syndrome (**g**, II-1 in family 10, aged 4 months; **h**, III-1 in family 7, aged 18 years). (**i**) Magnetic resonance brain imaging (sagittal, T1 view) of III-1 in family 4, aged 7.1 years, showing Chiari malformation (12-mm herniation of cerebellar tonsils through the foramen magnum, arrow). (**j**) Comparison of average faces between *ERF*-mutant ($n = 14$) and control ($n = 381$) subjects. Red and blue coloring denote normalized displacement at over 1.5 s.d., highlighting shared features of hypertelorism (left), vertical nasal displacement (middle) and prominent forehead with exorbitism (right). Written consent was provided for the publication of all photographs.

of mutations only in samples from affected individuals and the identification of multiple *de novo* cases establish that *ERF* mutations are the cause of craniosynostosis in these families.

ERF comprises 4 exons (**Fig. 2a**) and encodes a ubiquitously expressed member of the ETS family of transcription factors (numbering 28 in humans)[11], which acts as a negative transcriptional regulator, either by competing with other ETS family members for DNA binding or through interaction with unique targets[2,3]. Functionally characterized motifs in ERF include the N-terminal DNA-binding (ETS), central ERK interaction and C-terminal repressor domains (**Fig. 2b**); DNA binding targets a core motif (5′-GGA(A/T)-3′), with little sequence discrimination from other ETS family members[12]. The identified *ERF* mutations were diverse: the three missense changes (one recurrent) were located in critical residues in the DNA-binding ETS domain or disrupted the initiation codon, whereas the remaining eight mutations comprised a splice-site mutation, two nonsense changes and three frameshift mutations (one recurrent, present in three families) (**Fig. 2**, **Table 2** and **Supplementary Fig. 3a**). Immunoblotting of fibroblasts or lymphoblastoid cells from affected individuals showed lower expression of full-length ERF associated with the initiation codon and nonsense mutations but not the missense substitutions affecting the ETS domain (**Supplementary Fig. 3b**). DNA-binding domain alterations did not repress transcription from ETS binding site–containing promoters (**Supplementary Fig. 3c).**These data suggest that the predominant pathophysiological mechanism is heterozygous loss of function (haploinsufficiency).

We analyzed the phenotype associated with this new syndrome in the 26 mutation-positive individuals (**Supplementary Table 2**). Of 14 pediatric cases, 13 had craniosynostosis; in the 8 with accurate assessment by three-dimensional computed tomography (CT) of the skull, fusion affected the sagittal ($n = 7$), lambdoid ($n = 5$), coronal ($n = 3$) and metopic ($n = 1$) sutures (**Fig. 1d** and **Supplementary Table 3**), a pattern distinct from those observed in other monogenic types of craniosynostosis, in which the coronal suture is most commonly affected[13]. Seven of 12 probands had syndromic multiple-suture synostosis (**Table 1**), representing a 13-fold enrichment compared to other diagnostic groups ($P = 3 \times 10^{-5}$, Fisher's exact test), but 3 subjects presented with single-suture synostosis of the sagittal ($n = 2$) or lambdoid ($n = 1$) sutures (**Fig. 1e**,**f**). In half of the families, a diagnosis of Crouzon syndrome had been suggested because of exorbitism and midface hypoplasia (**Fig. 1a**,**c**,**g**,**h** and **Supplementary Fig. 4**); however, *FGFR2* genetic testing[14,15] was normal. Chiari type I malformations were diagnosed in four cases (**Fig. 1i**); pathologically raised intracranial pressure was documented in nine cases by invasive monitoring or skull radiology. Twelve pediatric cases (86%) had behavioral or learning problems, particularly affecting concentration and language acquisition (**Supplementary Table 2**). Notably, despite the multiple-suture involvement, many affected individuals presented after infancy, and primary surgery was frequently delayed (**Supplementary Fig. 5**). Extracranial growth was normal, except for occasional mild shortening of the digits; no health problems of later onset were consistently found in carrier adults, in many of whom mild craniofacial signs or macrocephaly was the only clinical feature.

Table 1 Subjects with craniosynostosis analyzed for *ERF* mutations by DNA sequencing

	Non-syndromic		Syndromic		Combined	
	Total	*ERF* mutation positive	Total	*ERF* mutation positive	Total	*ERF* mutation positive
Metopic	46	0	13	0	59	0
Sagittal	70	1	16	1	86	2
Unicoronal	99	0	16	0	115	0
Bicoronal	25	0	24	0	49	0
Uni- or bilambdoid	13	1	0	0	13	1
Multisuture	26	1	40	7	66	8
Sutures not specified	6	0	18	1	24	1
Combined	285	3	127	9	412	12

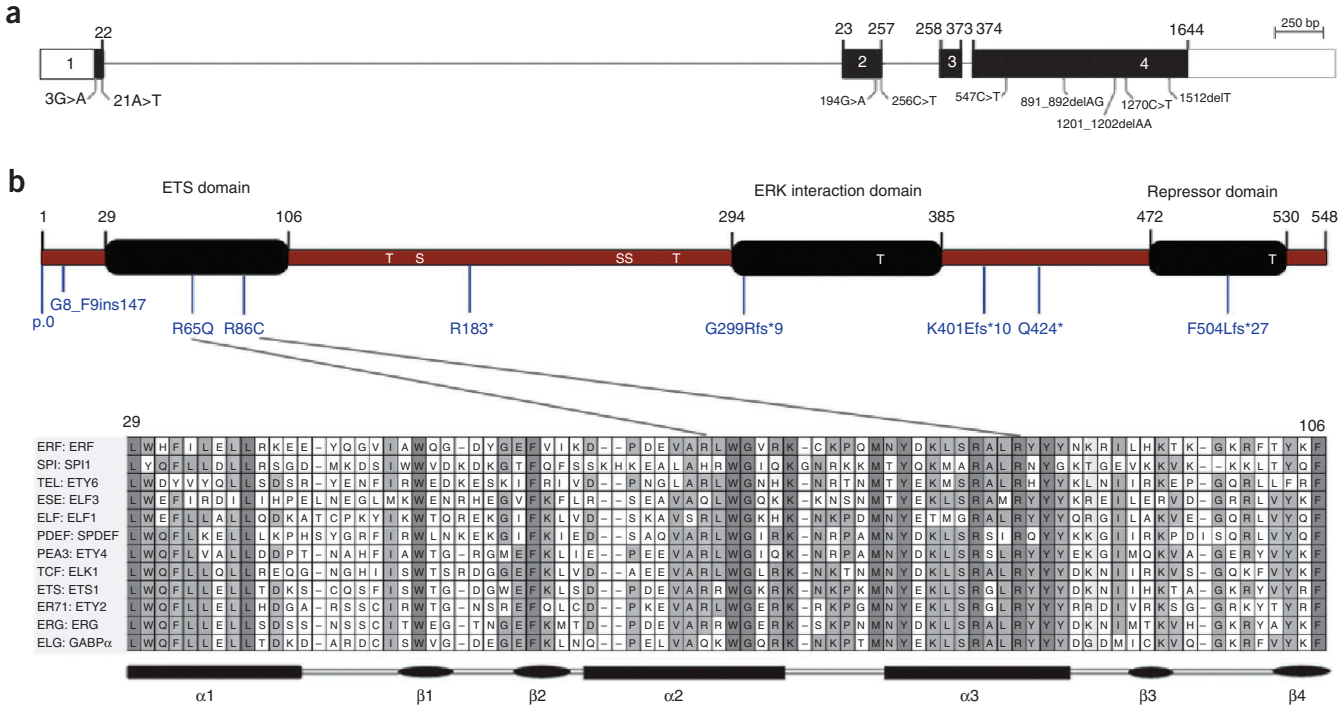

Figure 2 Exon and domain structure of ERF and mutations identified in craniosynostosis. (**a**,**b**) *ERF* comprises 4 exons (**a**) extending over 7.6 kb and encodes a 548-amino-acid protein (**b**). The positions of serine (S) and threonine (T) sites phosphorylated by ERK[4] are indicated. Two missense substitutions, p.Arg65Gln and p.Arg86Cys, localize to the ETS DNA-binding domain. Shown below is the ETS domain sequence from a representative member of each ETS subfamily in humans. Fully and partially conserved residues are shaded dark and light gray, respectively.

No genotype-phenotype correlation was found. In 6 families, including 14 carriers of *ERF* mutation, we used three-dimensional scanning[16] to document the facial phenotype; this analysis showed that hypertelorism, shortening and/or vertical displacement of the nose and prominent orbits and forehead were consistently present but varied in severity (**Fig. 1j**, **Supplementary Fig. 6** and **Supplementary Movies 1–6**). This newly recognized disorder, which we term ERF-related craniosynostosis, was identified in 5 of 402 (1.2%) of individuals requiring surgery for craniosynostosis in our extended Oxford cohort[13] (including children born between 1998 and 2006).

A specific role for ERF was not previously suspected, either in the cranial sutures or in osteogenesis more generally. In the mouse, heterozygous loss of function of the orthologous gene ($Erf^{+/-}$) is not associated with any abnormality, whereas homozygous loss ($Erf^{-/-}$) causes severe placental defects resulting in death by embryonic day (E) 10.5 (ref. 17). To explore the function of Erf during development, we engineered mice harboring a conditional allele (Erf^{loxP}) containing a selectable marker, *PGKneo*, located within intron 1, together with tandem *loxP* sites to enable Cre-mediated excision (**Supplementary Fig. 7a**). RT-PCR analysis of *Erf* cDNA in dissected E16.5 mouse calvaria showed that, in $Erf^{loxP/-}$ compound heterozygotes, *Erf* transcription was reduced to 29% of the wild-type level (**Fig. 3a**). This indicates that the Erf^{loxP} allele is hypomorphic, probably because the intronic *PGKneo* cassette reduces the efficiency of transcript production. Both heterozygous ($Erf^{loxP/+}$) and homozygous ($Erf^{loxP/loxP}$) conditional mice were grossly normal, but compound conditional and null heterozygotes ($Erf^{loxP/-}$) had domed heads that became apparent during the first 3–6 weeks of life. μCT scanning showed craniosynostosis affecting multiple calvarial sutures (**Fig. 3b–f** and **Supplementary Fig. 7b**,**c**). No other specific skeletal abnormalities were evident with Alizarin red and Alcian blue staining (**Supplementary Fig. 7d**). As in humans, the cranial sutures seem to be particularly sensitive to reduced *Erf* dosage, but the threshold level required for manifestation of the disease phenotype is lower in mice.

To explore the developmental origins of craniosynostosis in mice, we examined *Erf* expression and calvarial osteogenesis in E16.5 calvariae by whole-mount RNA *in situ* hybridization and RT-PCR.

Table 2 Mutations of *ERF* present in 12 families

Family	Proband	Proband craniosynostosis phenotype[a]	Individuals with mutations[b]	cDNA change	Predicted amino-acid change	*De novo* mutation
1	OX2158	M	II-2, III-3, IV-1, IV-2	c.547C>T	p.Arg183*	–
2	OX2729	NA	II-1	c.1512delT	p.Phe504Leufs*27	–
3	OX2789	P	II-1	c.891_892delAG	p.Gly299Argfs*9	–
4	OX3247	UL	II-2, III-1	c.256C>T	p.Arg86Cys	+
5	OX3248	S	II-1, III-1	c.194G>A	p.Arg65Gln	–
6	OX3801	M	II-1, III-1, III-2, IV-2	c.3G>A	p.0	+
7	OX3970	M	II-2, III-1, III-2	c.891_892delAG	p.Gly299Argfs*9	–
8	OX4097	M	II-1	c.891_892delAG	p.Gly299Argfs*9	+
9	OX4626	P	II-2, III-1, III-2	c.1270C>T	p.Gln424*	–
10	OX4708	M	II-1	c.256C>T	p.Arg86Cys	+
11	OX4902	S	II-2, II-3, III-1	c.21A>T	p.Gly8_Phe9ins147	–
12	OX5072	P	II-1	c.1201_1202delAA	p.Lys401Glufs*10	–

[a]M, multiple-suture synostosis; P, pansynostosis; S, sagittal synostosis; UL, unilateral lambdoid synostosis; NA, not available. [b]Details are given in **Supplementary Figure 1**.

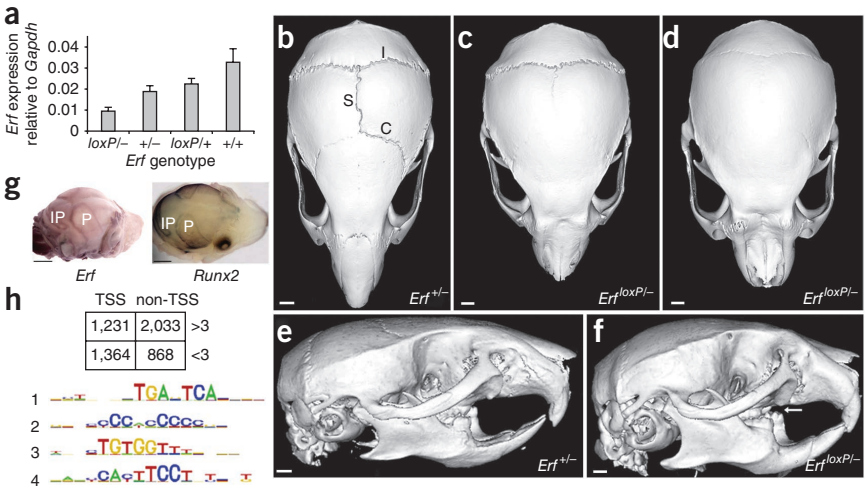

Figure 3 Analysis of *Erf* in mouse mutants and embryonic fibroblasts. (**a**) Quantitative RT-PCR of *Erf* in E16.5 calvariae of different genotypes, showing reduced expression from Erf^{loxP} relative to the wild-type *Erf* allele. Error bars, s.e.m. (**b**–**f**) μCT scanning of the heads of mice aged 9 weeks. Note normal morphology and patent sagittal (S), coronal (C) and lambdoid (L) sutures in the $Erf^{+/-}$ mutant, top view (**b**), side view (**e**), whereas the $Erf^{loxP/-}$ littermates have craniosynostosis of the sagittal and coronal sutures (**c**) or sagittal, coronal and lambdoid sutures (**d**). Note dental malocclusion (arrow) on the side view (**f**) of the skull in **d**. Scale bars, 1.12 mm in **b**,**e**, 1.01 mm in **c**,**d**,**f**. (**g**) Whole-mount RNA *in situ* hybridization of *Erf* and *Runx2* in wild-type E16.5 mouse calvariae. Note similar expression patterns coinciding with osteogenic fronts of parietal (P) and interparietal (IP) bones. Scale bars, 1 mm. (**h**) Summary of ChIP-seq analysis using antibody to Erf in MEFs. Top, shown are the number of peaks identified according to whether they were located within 1 kb of a TSS and whether they showed loss of binding in the presence of FCS (–FCS/+FCS > 3). Bottom, MEME analysis of the 2,033 non-TSS dynamically bound peaks (–FCS/+FCS > 3) identifies enrichment for motifs corresponding to binding sites for AP-1 (motif 1, 5′-TGANTCA-3′), RUNX (motif 3, 5′-TGTGG-3′) and ETS (motif 4, 5′-TTCCT-3′). Motif 2 was also observed in TSS peaks (**Supplementary Fig. 9a**).

In wild-type animals, *Erf* was expressed along the osteogenic margins of the developing calvarial bones, in a similar distribution to that observed for the master osteogenic regulator *Runx2* (**Fig. 3g**); in humans, haploinsufficiency for orthologous *RUNX2* causes cleidocranial dysplasia associated with defective calvarial ossification, whereas complete duplications occur in craniosynostosis[18–22]. Comparison of wild-type and $Erf^{loxP/-}$ mutants for transcripts of *Spp1* (encoding osteopontin) or *Bglap2* (encoding osteocalcin; data not shown), markers of late osteogenic differentiation[23], showed similar sutural gaps (**Supplementary Fig. 8a**). However, quantitation of transcripts in E16.5 calvariae showed modest (up to twofold) downregulation of multiple osteogenic markers in $Erf^{loxP/-}$ mutants compared to wild-type littermates, which was significant ($P < 0.05$, *t* test) in the *Prkg2* and *Serinc5* transcripts (**Supplementary Fig. 8b**)[24]. At this stage of development, therefore, ossification seems to be mildly delayed in $Erf^{loxP/-}$ embryos. However, by postnatal day (P) 14, the coronal sutures of the $Erf^{loxP/-}$ but not of the $Erf^{+/+}$ pups were variably fused (**Supplementary Fig. 8c**). Further detailed analysis of intermediate time points will be necessary to document the timing of craniosynostosis in the $Erf^{loxP/-}$ mutants and to determine the relative contributions to this pathology of altered proliferation, differentiation and apoptosis[25].

To gain insight into the nuclear targets of Erf, we employed chromatin immunoprecipitation (ChIP) in mouse embryonic fibroblasts (MEFs), using a previously characterized antibody specific to the C-terminal domain[3,26], combined with high-throughput sequencing (ChIP-seq). By comparing the enriched sequences from fibroblasts maintained without fetal calf serum (FCS) for 4 h (–FCS: inactive Erk1/2, nuclear Erf) to those from cells supplemented with FCS (+FCS: Erk1/2 phosphorylation and nuclear entry, consequent phosphorylation and nuclear export of Erf)[4,5,26], we could identify the component of the ChIP-seq signal attributable to dynamic Erf binding (defined by a –FCS/+FCS ratio of >3). We divided signals of dynamic binding according to whether they occurred within 1 kb of a transcriptional start sites (TSS; putative promoter) or at greater distances (non-TSS; putative enhancer) (**Fig. 3h** and **Supplementary Tables 4** and **5**). MEME analysis[27] identified two major sequences enriched near TSSs (**Supplementary Fig. 9a**), one corresponding to the ETS-binding consensus[12] and the other to the sequence bound by Ronin-Hcfc1 (ref. 28); these motifs are virtually identical to those in promoters bound by ETS1 (ref. 29). In non-TSSs, which are believed to identify tissue-specific interactions of ETS factors[29], the three most highly specific sequence motifs were 5′-TGANTCA-3′, 5′-TGTGG-3′ and 5′-TTCCT-3′, where N represents any nucleotide, corresponding to consensus motifs for AP-1, RUNX and ETS factors, respectively (**Fig. 3h** and **Supplementary Fig. 9a**). This suggests that Erf-binding sites frequently lie close to the binding sites for other transcription factors; corroborating this idea, enrichment of both AP-1 and RUNX sites was observed in ChIP-seq studies of other ETS proteins[29,30]. The non-randomness of these associations was confirmed by showing that closely adjacent AP-1–ETS and RUNX-ETS sites exhibited polarity, consistent with interactions between pairs of transcription factors when binding DNA with specific orientation and separation (**Supplementary Fig. 9b**,**c** and **Supplementary Tables 6** and **7**)[29–33]. MetaCore analysis of non-TSS ChIP-seq targets

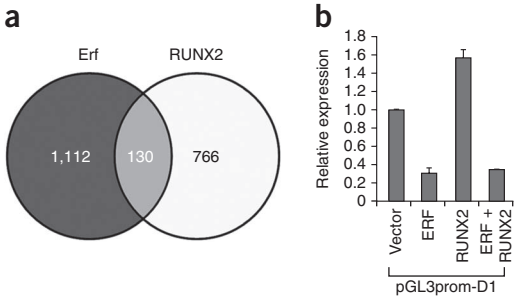

Figure 4 Overlapping transcriptional targets of Erf and RUNX2 identified by ChIP-seq. (**a**) Comparison of non-TSS mouse Erf targets with –FCS/+FCS > 3 identified in this work ($n = 2,033$) with orthologous human RUNX2 targets identified by Little *et al.* ($n = 1,603$)[38]. To improve the specificity of linkage to regulated genes, ChIP-seq peaks more than 40 kb away from the closest RefSeq gene were excluded. Peaks were assigned to the gene with the closest exon. (**b**) Transactivation analysis using the hybrid Erf-Runx2 binding target identified by ChIP-seq (5′-agaGGATGTGGttt-3′, core target capitalized). HeLa cells were transfected with 1 μg of empty vector or with vectors encoding *ERF* or *RUNX2* cDNA, alone or in combination. Results were normalized relative to reporter expression detected with empty vector and are expressed as the mean ± s.e.m. of four independent experiments.

with a −FCS/+FCS ratio of >3 (n = 2,033) identified epithelial-to-mesenchymal transition (EMT) as the process showing the greatest enrichment (**Supplementary Fig. 10**); the RAS-MEK-ERK cascade and downstream AP-1 factors are located within the center of this network. Validating this analysis, ERF was recently identified experimentally as a negative regulator of EMT[34].

The identification of frequent RUNX-binding motifs within distal (non-TSS) Erf targets is of interest because Runx2 is a key dosage-sensitive regulator of calvarial osteogenesis[18,35]. The ChIP-seq data identified two sites of dynamic binding within introns of *Runx2*, which might reflect direct regulation of transcription (**Supplementary Table 6**). Alternatively, Erf may regulate osteogenesis by altering the balance of positive and negative regulatory complexes formed on DNA targets by Runx2 and other Ets proteins (such as Ets2)[36,37]. We explored this hypothesis in two ways. First, we compared our Erf ChIP-seq data with a data set of 1,603 RUNX2-occupied regions in human prostate cancer cells[38]. There were 130 orthologous genes that were nearest to and had signals within 40 kb of a ChIP-seq peak in each of the data sets (**Fig. 4a** and **Supplementary Table 8**), a highly significant overlap ($P = 4 \times 10^{-11}$, hypergeometric test); moreover, Little *et al.*[38] identified enrichment of a hybrid ETS-RUNX binding motif very similar to the sequence (5′-GGATGTGG-3′) in our data set (**Supplementary Fig. 9c**). Second, we examined the effects of ERF and RUNX2 on transactivation using a DNA-binding target containing this core sequence. Whereas RUNX2 alone elicited 1.6-fold upregulation of expression, this induction was suppressed by ERF, which lowered expression to below the basal level, similar to the effect of ERF added alone (**Fig. 4b**), indicating antagonism by ERF of RUNX2-mediated transactivation in this model situation. Given that the ChIP-seq data showed potential interactions of Erf and Runx2 at numerous targets (**Fig. 4a** and **Supplementary Table 8**), further work will be required to identify critical factors in osteogenic dysregulation in the *ERF* or *RUNX2* haploinsufficiency states.

Our genetic observations in humans and mice will focus renewed attention on the role of Ets factors in regulating osteogenesis, which although documented, is not well defined[36,37,39]. Direct Erk1/2-mediated phosphorylation was previously linked to stabilization and/or activation of Runx2 (refs. 40,41); we speculate that additional indirect control of Runx2 action by Erk1/2 (ref. 42) may be mediated by its control of Erf localization. Our data provide a pathway-based phenotypic link with *FGFR2* mutations, as several individuals with *ERF*-related craniosynostosis were previously diagnosed with Crouzon syndrome (**Supplementary Table 2**)[14,15]. The position of ERF downstream of the RAS-MEK-ERK cascade and the delayed onset of suture ossification associated with *ERF* haploinsufficiency (**Supplementary Fig. 5**) make ERF an attractive target for therapeutic modulation.

URLs. MLPA, http://www.mrc-holland.com/; MEME-ChIP, http://meme.nbcr.net/meme/; UCSC Genome Browser, http://genome.ucsc.edu/; PolyPhen-2, http://genetics.bwh.harvard.edu/pph2/; SeqMonk, http://www.bioinformatics.babraham.ac.uk/projects/seqmonk/; GeneGo MetaCore, http://www.genego.com/metacore.php; JASPAR transcription factor binding profile database, http://jaspar.genereg.net/; Bowtie sequence alignment, http://bowtie-bio.sourceforge.net/index.shtm; Multi-Image Genome viewer (MIG), https://mig.molbiol.ox.ac.uk/mig/; HomoloGene, http://www.ncbi.nlm.nih.gov/homologene.

METHODS

Methods and any associated references are available in the online version of the paper.

Accession codes. Human *ERF* mRNA and genomic sequences are available as NCBI reference sequences NM_006494.2 and NC_000019.9, respectively. Mouse *Erf* mRNA sequence is available as NCBI reference sequence NM_010155.3. Human ETS DNA-binding protein sequences are available at UniProt under accession P50548 (ERF), P17947 (SPI1), P41212 (ETV6), P78545 (ELF3), P32519 (ELF1), O95238 (SPDEF), P43268 (ETV4), P19419 (ELK1), P14921 (ETS1), O00321 (ETV2), P11308 (ERG) and Q06546 (GABPα). *Erf* ChIP-seq data have been deposited at the Gene Expression Omnibus (GEO) under accession GSE42936.

Note: Supplementary information is available in the online version of the paper.

ACKNOWLEDGMENTS

We thank R. Boehm, H. Care, C. Langman, J. Phipps and E. Sweeney for clinical assistance, L. Gregory, P. Piazza and staff at the High-Throughput Genomics facility at the Wellcome Trust Centre for Human Genetics for exome sequencing, C. Babbs, S. Butler, J. Frankland, C. Rode and T. Rostron for technical help, K. Kourouniotis for blastocyst injections and expert animal support, E. Giannoulatou for bioinformatics assistance, and B. Graves and P. Hollenhorst for discussions. We thank J. Heath (University of Birmingham), G. Schwabe (Charité University Hospital) and D. Rice (University of Helsinki) for the gifts of the *Spp1*, *Runx2* and *Bglap2* probes, respectively. This work was funded by the Greek Ministry of Education grants PYTHAGORAS II KA2092, PENED 03ED626, HERAKLEITOS II KA 3396 and SYNERGASIA 09SYN-11-902 to G.M., the NIHR Biomedical Research Centre, with funding from the Department of Health's NIHR Biomedical Research Centres funding scheme (S.J.L.K. and A.O.M.W.), the Oxford Craniofacial Unit Charitable Fund (V.P.S.), the Department of Health, UK, Quality, Improvement, Development and Initiative Scheme (QIDIS) (V.P.S.) and the Wellcome Trust (090532, S.J.L.K.; 093329, S.R.F.T. and A.O.M.W.). The views expressed in this publication are those of the authors and not necessarily those of the Department of Health, UK.

AUTHOR CONTRIBUTIONS

S.R.F.T. designed and performed experiments and wrote the manuscript. M.A., I.P., A.L.F., E.V., A.Z., E.S.A., S.J.L.K., H.L. and T.L. performed experiments. S.J.M., J.H. and S.T. performed bioinformatic analyses. V.P.S. performed experiments and assessed patients. L.I., A.K.L., S.N.M., F.J.S., A.V., L.C.W., D.J. and S.A.W. identified and assessed patients. C.H. and P.T.S. performed and analyzed μCT scans. P.H. performed and analyzed three-dimensional facial imaging. G.M. conceived the project, designed experiments and wrote the manuscript. A.O.M.W. conceived the project, assessed patients, designed experiments and wrote the manuscript.

COMPETING FINANCIAL INTERESTS

The authors declare competing financial interests: details are available in the online version of the paper.

Published online at http://www.nature.com/doifinder/10.1038/ng.2539.
Reprints and permissions information is available online at http://www.nature.com/reprints/index.html.

1. Plotnikov, A., Zehorai, E., Procaccia, S. & Seger, R. The MAPK cascades: signaling components, nuclear roles and mechanisms of nuclear translocation. *Biochim. Biophys. Acta* **1813**, 1619–1633 (2011).
2. Mavrothalassitis, G.J. & Papas, T.S. Positive and negative factors regulate the transcription of the *ETS2* gene via an oncogene-responsive–like unit within the *ETS2* promoter region. *Cell Growth Differ.* **2**, 215–224 (1991).
3. Sgouras, D.N. *et al.* ERF: an ETS domain protein with strong transcriptional repressor activity, can suppress ets-associated tumorigenesis and is regulated by phosphorylation during cell cycle and mitogenic stimulation. *EMBO J.* **14**, 4781–4793 (1995).
4. Le Gallic, L., Sgouras, D., Beal, G. & Mavrothalassitis, G. Transcriptional repressor ERF is a Ras/mitogen-activated protein kinase target that regulates cellular proliferation. *Mol. Cell Biol.* **19**, 4121–4133 (1999).
5. Le Gallic, L., Virgilio, L., Cohen, P., Biteau, B. & Mavrothalassitis, G. ERF nuclear shuttling, a continuous monitor of Erk activity that links it to cell cycle progression. *Mol. Cell Biol.* **24**, 1206–1218 (2004).
6. Polychronopoulos, S. *et al.* The transcriptional ETS2 repressor factor associates with active and inactive Erks through distinct FXF motifs. *J. Biol. Chem.* **281**, 25601–25611 (2006).
7. von Kriegsheim, A. *et al.* Cell fate decisions are specified by the dynamic ERK interactome. *Nat. Cell Biol.* **11**, 1458–1464 (2009).
8. Ng, S.B. *et al.* Exome sequencing identifies the cause of a mendelian disorder. *Nat. Genet.* **42**, 30–35 (2010).
9. Kim, H.-J. Erk pathway and activator protein 1 play crucial roles in FGF2-stimulated premature cranial suture closure. *Dev. Dyn.* **227**, 335–346 (2003).

10. Shukla, V., Coumoul, X., Wang, R.-H., Kim, H.-S. & Deng, C.-X. RNA interference and inhibition of MEK-ERK signaling prevent abnormal skeletal phenotypes in a mouse model of craniosynostosis. *Nat. Genet.* **39**, 1145–1150 (2007).
11. Hollenhorst, P.C., McIntosh, L.P. & Graves, B.J. Genomic and biochemical insights into the specificity of ETS transcription factors. *Annu. Rev. Biochem.* **80**, 437–471 (2011).
12. Wei, G.-H. Genome-wide analysis of ETS-family DNA-binding *in vitro* and *in vivo*. *EMBO J.* **29**, 2147–2160 (2010).
13. Wilkie, A.O.M. *et al.* Prevalence and complications of single-gene and chromosomal disorders in craniosynostosis. *Pediatrics* **126**, e391–e400 (2010).
14. Kan, S.-H. *et al.* Genomic screening of fibroblast growth-factor receptor 2 reveals a wide spectrum of mutations in patients with syndromic craniosynostosis. *Am. J. Hum. Genet.* **70**, 472–486 (2002).
15. Lajeunie, E. *et al.* Mutation screening in patients with syndromic craniosynostoses indicates that a limited number of recurrent *FGFR2* mutations accounts for severe forms of Pfeiffer syndrome. *Eur. J. Hum. Genet.* **14**, 289–298 (2006).
16. Hammond, P. & Suttie, M.J. Large-scale phenotyping of 3D facial morphology. *Hum. Mutat.* **33**, 817–825 (2012).
17. Papadaki, C. *et al.* Transcriptional repressor Erf determines extraembryonic ectoderm differentiation. *Mol. Cell Biol.* **27**, 5201–5213 (2007).
18. Mundlos, S. *et al.* Mutations involving the transcription factor CBFA1 cause cleidocranial dysplasia. *Cell* **89**, 773–779 (1997).
19. Park, M.-H. *et al.* Differential expression patterns of Runx2 isoforms in cranial suture morphogenesis. *J. Bone Miner. Res.* **16**, 885–892 (2001).
20. Komori, T. Signaling networks in RUNX2-dependent bone development. *J. Cell Biochem.* **112**, 750–755 (2011).
21. Mefford, H.C. *et al.* Copy number variation analysis in single-suture craniosynostosis: multiple rare variants including *RUNX2* duplication in two cousins with metopic craniosynostosis. *Am. J. Med. Genet.* **152A**, 2203–2210 (2010).
22. Varvagiannis, K. *et al.* Pure *de novo* partial trisomy 6p in a girl with craniosynostosis. *Am. J. Med. Genet. A.* published online; doi:10.1002/ajmg.a.35727 (10 January 2013).
23. Iseki, S., Wilkie, A.O.M. & Morriss-Kay, G.M. Fgfr1 and Fgfr2 have distinct differentation- and proliferation-related roles in the developing mouse skull vault. *Development* **126**, 5611–5620 (1999).
24. Hecht, J. *et al.* Detection of novel skeletogenesis target genes by comprehensive analysis of a *Runx2*$^{-/-}$ mouse model. *Gene Expr. Patterns* **7**, 102–112 (2007).
25. Morriss-Kay, G.M. & Wilkie, A.O.M. Growth of the normal skull vault and its alteration in craniosynostosis: insights from human genetics and experimental studies. *J. Anat.* **207**, 637–653 (2005).
26. Verykokakis, M., Papadaki, C., Vorgia, E., Le Gallic, L. & Mavrothalassitis, G. The RAS-dependent ERF control of cell proliferation and differentiation is mediated by c-Myc repression. *J. Biol. Chem.* **282**, 30285–30294 (2007).
27. Bailey, T.L. *et al.* MEME SUITE: tools for motif discovery and searching. *Nucleic Acids Res.* **37**, W202–W208 (2009).
28. Dejosez, M. *et al.* Ronin/Hcf-1 binds to a hyperconserved enhancer element and regulates genes involved in the growth of embryonic stem cells. *Genes Dev.* **24**, 1479–1484 (2010).
29. Hollenhorst, P.C. *et al.* DNA specificity determinants associate with distinct transcription factor functions. *PLoS Genet.* **5**, e1000778 (2009).
30. Hollenhorst, P.C. *et al.* Oncogenic ETS proteins mimic activated RAS/MAPK signaling in prostate cells. *Genes Dev.* **25**, 2147–2157 (2011).
31. Goetz, T.L., Gu, T.L., Speck, N.A. & Graves, B.J. Auto-inhibition of Ets-1 is counteracted by DNA binding cooperativity with core-binding factor α2. *Mol. Cell Biol.* **20**, 81–90 (2000).
32. Hess, J., Porte, D., Munz, C. & Angel, P. AP-1 and Cbfa/runt physically interact and regulate parathyroid hormone–dependent MMP13 expression in osteoblasts through a new osteoblast-specific element 2/AP-1 composite element. *J. Biol. Chem.* **276**, 20029–20038 (2001).
33. D'Alonzo, R.C., Selvamurugan, N., Karsenty, G. & Partridge, N.C. Physical interaction of the activator protein-1 factors c-Fos and c-Jun with Cbfa1 for collagenase-3 promoter activation. *J. Biol. Chem.* **277**, 816–822 (2002).
34. Allegra, M. *et al.* Semaphorin-7a reverses the ERF-induced inhibition of EMT in Ras-dependent mouse mammary epithelial cells. *Mol. Biol. Cell* **23**, 3873–3881 (2012).
35. Lou, Y. *et al.* A Runx2 threshold for the cleidocranial dysplasia phenotype. *Hum. Mol. Genet.* **18**, 556–568 (2009).
36. Sumarsono, S.H. *et al.* Down's syndrome–like skeletal abnormalities in *Ets2* transgenic mice. *Nature* **379**, 534–537 (1996).
37. Vary, C.P.H. *et al.* Involvement of Ets transcription factors and targets in osteoblast differentiation and matrix mineralization. *Exp. Cell Res.* **257**, 213–222 (2000).
38. Little, G.H. *et al.* Genome-wide Runx2 occupancy in prostate cancer cells suggests a role in regulating secretion. *Nucleic Acids Res.* **40**, 3538–3547 (2012).
39. Wai, P.Y. *et al.* Ets-1 and runx2 regulate transcription of a metastatic gene, osteopontin, in murine colorectal cancer cells. *J. Biol. Chem.* **281**, 18973–18982 (2006).
40. Ge, C. *et al.* Identification and functional characterization of ERK/MAPK phosphorylation sites in the Runx2 transcription factor. *J. Biol. Chem.* **284**, 32533–32543 (2009).
41. Park, O.-J., Kim, H.-J., Woo, K.-M., Baek, J.-H. & Ryoo, H.-M. FGF2-activated ERK mitogen-activated protein kinase enhances Runx2 acetylation and stabilization. *J. Biol. Chem.* **285**, 3568–3574 (2010).
42. Matsushita, T. *et al.* Extracellular signal–regulated kinase 1 (ERK1) and ERK2 play essential roles in osteoblast differentiation and in supporting osteoclastogenesis. *Mol. Cell Biol.* **29**, 5843–5857 (2009).

ONLINE METHODS

Subjects. The clinical study was approved by Oxfordshire Research Ethics Committee B (reference C02.143) and Riverside Research Ethics Committee (reference 09/H0706/20). Written informed consent to obtain samples for genetics research was obtained from each child's parent or guardian. In most probands, the clinical diagnosis of craniosynostosis was confirmed by CT scanning, although some individuals had only skull radiography. Venous blood was obtained for DNA extraction and the preparation of lymphoblastoid cell lines. Fibroblast cultures were established from skin biopsies obtained from scalp incision during surgical intervention.

Exome sequencing and segregation analysis. We used an Agilent SureSelect Human All Exon kit (v.1; 38 Mb) to capture exonic DNA from a library prepared from 3 μg of DNA extracted from whole blood (subject IV-1 in family 1). Enriched DNA was sequenced on an Illumina Genome Analyzer IIx platform (51-bp paired-end reads), and the 3.1 Gb of sequence generated was mapped with Bowtie software[43] (hg19 genome), which gave an average coverage of 43-fold. Variants were called using SAMtools[44] (**Supplementary Table 9**). The proband and his brother and parents were genotyped using an Illumina HumanCytoSNP-12 BeadChip (300k). Chromosomal regions where the two affected boys shared the same maternal allele were identified and used to filter the exome data.

Mutation screening. Mutation analysis was performed by sequencing genomic PCR amplification products (BigDye Terminator v3.1, Applied Biosystems). Copy-number variation was analyzed by multiplex ligation–dependent probe amplification (MLPA). RNA was extracted from whole blood (PAXgene tubes, Qiagen) and lymphoblastoid cell lines (TRIzol, Invitrogen), and cDNA was synthesized with the RevertAid First-Strand cDNA kit (Thermo). The sequences of the primers for genomic and cDNA amplification and for MLPA and the details of all experimental conditions are provided in **Supplementary Table 10**. cDNA numbering for *ERF* starts at the A of the ATG initiation codon (+1).

Three-dimensional facial imaging. Images were captured with a commercial photogrammetric device and manually landmarked, as were an additional 381 images of healthy controls for comparison. Dense surface model and signature analyses were undertaken as described[16,45]. Face signatures were visualized as color-coded heat maps, derived from lateral, vertical and depth differences at 24,000 surface points compared to corresponding positions on the mean face of the matched controls.

Protein blots. Protein immunoblots were performed as described[4]. Cells or homogenized embryos were lysed in RIPA buffer (150 mM NaCl, 1% NP-40, 0.5% deoxycholic acid, 0.1% SDS, 50 mM Tris-(hydroxymethyl)-aminomethane, pH 8.0, 1 μg/ml aprotinin and 1 μg/ml leupeptin, 1 mM phenylmethylsulfonyl fluoride, 1 mM orthovanadate, 10 mM β-glycerophosphate) containing protease and phosphatase inhibitors. Equal amounts of protein were separated by discontinuous SDS electrophoresis and transferred onto nitrocellulose. ERF was detected with S17S rabbit polyclonal antibody to ERF (1:1,000 dilution), and ERK1/2 was detected with rabbit polyclonal antibody to ERK1/2 (Cell Signaling Technology, 9102; 1:1,000 dilution) in TBS with 0.1% Tween. Proteins were detected with horseradish peroxidase–conjugated secondary antibody to rabbit (Jackson ImmunoResearch; 1:5,000 dilution) and visualized by chemiluminescence. Autoradiographs were quantified using US National Institutes of Health (NIH) ImageJ software.

Promoter assays. Mutations identified in affected individuals were introduced into wild-type *ERF* cDNA by site-directed mutagenesis (QuikChange, Stratagene), cloned into pSG5-*ERF* and pSG424-*ERF* expression vectors[3] and sequence verified. The ability of wild-type and mutated ERF to repress transcriptional activity was determined in HeLa cells. The pGL333 reporter (with three copies of the GATA1 ets-binding site (ebs) and a minimal TK1 promoter), generated by transferring the corresponding promoter fragment from pBLCAT333 (ref. 46) into the pGL3-Basic vector (Promega), was used to determine repression on ebs-containing promoters. The pGLGal4 reporter (gal4 DNA-binding site and the SV40 promoter), generated by transferring the corresponding promoter fragment from SV40/GAL4 (ref. 3) into the pGL3-Basic vector, was used to assess ebs-independent repression.

For studies of RUNX2 and ERF interaction, the SfiI restriction fragment from pENTR223.1-*RUNX2* plasmid (Open Biosystems), containing *RUNX2* cDNA, was cloned into the EcoRI site of the pSG5 expression vector (Agilent Technologies) to generate pSG5-*RUNX2*. Double-stranded oligonucleotides encompassing the core Ets-Runx binding site (**Supplementary Table 10**) were cloned directionally between the NheI and BglII sites of the pGL3-Promoter luciferase reporter vector (Promega) to generate pGL3prom-D1. HeLa cells were transfected with the calcium phosphate method using 0.5 μg of pGL3prom-D1 reporter, 0.5 μg of pRSV-Gal for transfection efficiency control, 1 μg of pSG5-*ERF* and/or 1 μg of pSG5-*RUNX2*, and/or 0–2 μg of pSG5 to a total of 3 μg of DNA. All pairwise comparisons were significant ($P < 0.01$, *t* test), with the exception of ERF versus ERF and RUNX2.

Generation of conditional Erf^{loxP} mice. Mice were maintained in specific pathogen–free facilities at the Institute of Molecular Biology and Biotechnology, Heraklion, Greece, or the Biomedical Services Unit, Oxford. Protocols were approved through the General Directorate of Veterinary Services, Heraklion, Region of Crete, or the University of Oxford Local Ethical Review process. Experimental procedures were performed in accordance with the European Union DIRECTIVE 2010/63/EU and/or the UK Animals (Scientific Procedures) Act, 1986 (Project License 30/2660).

The *Erf*-targeting vector (**Supplementary Fig. 7a**) was prepared by inserting a *loxP* sequence (ApaI site 16 bp 3′ of the *Erf* stop codon) and a *PGKneo-loxP* cassette (BstZ17I site 350 bp 5′ of *Erf* exon 2) within the 7.3-kb *Erf* genomic fragment 59A. *loxP* orientation was verified by sequencing, and the targeting fragment was inserted into pBSTK9 (ref. 47). R1 ES cells were electroporated and selected as described[17], and clones were screened by Southern blotting using a 2.2-kb BamHI-XbaI fragment (int-probe) for homologous recombination and absence of additional insertions. Positive clones were tested for the presence of the 3′ *loxP* site by PCR amplification using StopF2 and 5578R. Recombination after transfection with Cre recombinase–expressing plasmid was tested by PCR using Intr1-2 and 5578R (**Supplementary Fig. 7a** and **Supplementary Table 10**).

Chimeric mice were generated by microinjection of embryonic stem cell (ES) clones as described[17]. Cells from clone 89 were injected into 3.5-d post-conception C57BL/6 blastocysts and implanted into pseudopregnant CD1 females[48]. Male offspring with high levels of chimerism were mated to CBA×C57BL/6 females to produce $Erf^{loxP/+}$ heterozygous mice. $Erf^{loxP/-}$ compound heterozygotes were obtained from an $Erf^{+/-} \times Erf^{loxP/+}$ cross ($Erf^{+/-}$ animals were sourced either from a previously described knockout line[17] or by crossing $Erf^{loxP/loxP}$ mice with $Meox2^{tm1(cre)Sor}$/J mice[49]). At birth, $Erf^{loxP/-}$ mice were on average ~18% lighter than their littermates, but they exhibited catch-up growth by 6 weeks of age.

Skeletal preparations and immunohistochemistry. Skeletons were fixed in 95% ethanol and stained overnight with Alcian blue (0.03% in 95% ethanol:20% acetic acid). After several washes with 95% ethanol, skeletons were rehydrated, treated with 2% KOH (12 h) and stained in 1% KOH containing 75 μg/ml Alizarin red S (24 h). Excess stain was removed in 1% KOH:20% glycerol, and, after washing in 0.2% KOH:20% glycerol, skeletons were stored in 50% glycerol.

The skulls of P14 mice were fixed overnight in 4% paraformaldehyde, decalcified using Calci-Clear (Raymond A Lamb) and embedded in paraffin. Immunohistochemistry was performed using a polyclonal antibody to RUNX2 (M-70, Santa Cruz Biotechnology) on 8-μm sections that were counterstained with hematoxylin.

μCT analyses. Specimens for μCT were scanned using a General Electric Locus SP μCT scanner (GE Healthcare). Specimens were immobilized using cotton gauze, scanned to produce voxel size volumes of 14–28 μm and characterized further by making three-dimensional isosurfaces, generated and measured using Microview (GE).

Whole-mount RNA *in situ* hybridization. Embryos were dissected and fixed in 4% paraformaldehyde and then dehydrated. *In situ* hybridization

was performed as described[50] using digoxigenin-incorporated riboprobes. The *Erf* probe (554 bp) was amplified from mouse cDNA with the primers mErfF2 and mErfR1 (**Supplementary Table 10**) and was cloned into pGEM-T Easy (Promega). The *Spp1*, *Runx2* and *Bglap2* probes were kind gifts from J. Heath, G. Schwabe and D. Rice, respectively. For detection with antibody, specimens were incubated with antibody to digoxigenin conjugated with alkaline phosphatase (1:1,000 dilution in 2% FCS; Roche, 11093274910). Expression patterns were visualized with the BM Purple kit (Roche). Whole mounts were analyzed using a Leica MZFLIII microscope and LASAF software (Leica Microsystems).

ChIP-seq assays. For chromatin immunoprecipitation (ChIP), 20–25 × 10^6 MEFs from E13.5 wild-type embryos were grown in DMEM, either supplemented with 10% FCS (+FCS) or in its absence (–FCS), for 4 h to induce Erf nuclear localization. ChIP was performed as described[26] with S17S rabbit polyclonal antibody to Erf, which was previously shown to be specific for Erf[3]. Cells were fixed with 1% formaldehyde in PBS for 10 min at room temperature, and nuclei were isolated and sonicated in 50 mM HEPES, pH 7.9, 140 mM NaCl, 1 mM EDTA, 1% Triton X-100, 0.1% sodium deoxycholate and 1% SDS. Samples were incubated with antibody overnight at 4 °C and were then incubated for 2 h with agarose-coupled protein G. Immunoprecipitated material was washed, cross-linking was reversed overnight at 65 °C, and DNA was purified by phenol extraction and ethanol precipitation. ChIP-seq libraries were prepared and sequenced using the standard Illumina protocol.

ChIP-seq analysis. Paired-end reads from ChIP-seq and input samples were aligned to the mouse genome build using Bowtie (version 0.12.3)[43]. Peaks were called with SeqMonk (version 0.19), using the contig generator function (peak merge distance of 50 bp, minimum peak size of 50 bp, minimum fold enrichment relative to input of fivefold). The number of reads in a union set of peaks from the –FCS and +FCS samples was quantified and normalized for total aligned read count in each ChIP-seq and input sample using the SeqMonk quantification function. The in-house Perl script Smonker.pl was used to normalize the peaks against input, to calculate the difference in enrichment for each peak in the –FCS and +FCS samples, and to store these values in a GFF3 file. Peaks were annotated for overlap (within 1 kb) with TSSs (UCSC Known Gene mm9 build) and problematic copy-number regions of the mm9 genome (ploidy peaks)[51] using the in-house Perl script intersectandappend.pl. The resulting annotated and quantified peaks were stored in a Multi-Image Genome viewer (MIG) SQL database. Peaks were filtered in MIG on the basis of the calculated relative enrichments between the two samples and their overlap with TSSs to produce two data sets (TSS and non-TSS). Peaks associated with ploidy regions were excluded.

Motif analysis. The *de novo* identification of over-represented motifs around the center of each peak (300 bp) was performed using MEME-ChIP tools[27]. The frequency of identified motifs in enriched and control peaks was calculated using the in-house program MotifQuant.pl. DNase I hypersensitive regions from adult fibroblast cells (from the Encyclopedia of DNA Elements (ENCODE) Project via the UCSC table browser, file wgEncodeUwDnaseFibroblastC57bl6MAdult8wksPkRep1) that overlap with TSSs or not, as appropriate, were used as control regions. MotifQuant.pl randomly sampled from these control sets the same number of peaks as in the test set and repeated this sampling 1,000 times to produce a mean frequency and a normal distribution for motif occurrence.

For the motif analyses presented in **Supplementary Figure 9b**,**c** and **Supplementary Tables 6** and **7**, ETS-binding motifs were defined by the sequences 5′-GGAA-3′ or 5′-GGAT-3′; AP-1 by 5′-TCANTGA-3′ and RUNX by 5′-TGTGG-3′ (of which 35% matched the extended 5′-TGTGGT-3′ consensus) (JASPAR database). Pathway analysis of gene lists from ChIP-seq peaks was performed using GeneGo MetaCore (**Supplementary Fig. 10**).

Comparison with RUNX2 ChIP-seq data. We extracted the list of 1,603 ChIP-seq peaks obtained for RUNX2 binding in a human prostate cancer cell line (**Table S3** from ref. 38). From this list, we obtained the subset of 896 peaks located within 40 kb upstream or downstream of RefSeq genes, choosing the gene closest to the coordinates of the ChIP-seq peak. We converted the RefSeq ID for each annotated gene to the HomoloGene ID and compared the resulting list to Erf ChIP-seq data (**Supplementary Table 4**, non-TSS), also restricted to a 40-kb window on either side of each gene. Significance of the overlap was tested using a hypergeometric distribution. The list of 130 shared genes (**Fig. 4a**) is provided in **Supplementary Table 8**.

43. Langmead, B., Trapnell, C., Pop, M. & Salzberg, S.L. Ultrafast and memory-efficient alignment of short DNA sequences to the human genome. *Genome Biol.* **10**, R25 (2009).
44. Li, H. *et al.* The Sequence Alignment/Map format and SAMtools. *Bioinformatics* **25**, 2078–2079 (2009).
45. Hammond, P. The use of 3D face shape modelling in dysmorphology. *Arch. Dis. Child.* **92**, 1120–1126 (2007).
46. Watson, D.K. *et al.* The *ERGB/Fli-1* gene: isolation and characterization of a new member of the family of human *ETS* transcription factors. *Cell Growth Differ.* **3**, 705–713 (1992).
47. Spyropoulos, D.D. *et al.* Hemorrhage, impaired hematopoiesis, and lethality in mouse embryos carrying a targeted disruption of the *Fli1* transcription factor. *Mol. Cell Biol.* **20**, 5643–5652 (2000).
48. Hogan, B. *Manipulating the Mouse Embryo: a Laboratory Manual* (Cold Spring Harbor Laboratory Press, Plainview, New York, 1994).
49. Tallquist, M.D. & Soriano, P. Epiblast-restricted Cre expression in MORE mice: a tool to distinguish embryonic vs. extra-embryonic gene function. *Genesis* **26**, 113–115 (2000).
50. Wilkinson, D.G. *In-situ Hybridization: a Practical Approach* (Oxford University Press, Oxford, 1992).
51. Kowalczyk, M.S. *et al.* Intragenic enhancers act as alternative promoters. *Mol. Cell* **45**, 447–458 (2012).

doi:10.1038/ng.2539

Received: 15 June 2016 | Revised: 23 January 2017 | Accepted: 23 January 2017

DOI 10.1002/mrd.22780

RESEARCH ARTICLE

WILEY WILEY Molecular Reproduction & Development

Suppression of *Fgf2* by ETS2 repressor factor (ERF) is required for chorionic trophoblast differentiation

Elena Vorgia[1,2] | Andreas Zaragkoulias[1] | Ioanna Peraki[1,2] | George Mavrothalassitis[1,2]

[1] Medical School, University of Crete, Heraklion, Crete, Greece

[2] IMBB, FORTH, Heraklion, Crete, Greece

Correspondence
Prof. George Mavrothalassitis, Medical School, University of Crete, A. Kalokairinou, Voutes, Heraklion, Crete 71003, Greece.
Email: mavro@imbb.forth.gr

Funding information
Greek Ministry of Education, Grant number: PYTHAGORAS II KA2092; PENED, Grant number: 03ED626; HERAKLEITOS II KA, Grant number: 3396; SYNERGASIA, Grant number: 09SYN-11-902

ETS2 repressor factor (ERF) is a ubiquitous transcriptional repressor regulated by Extracellular signal-regulated kinase 1/2 (ERK1/2) phosphorylation. Homozygous deletion of *Erf* in mice blocks chorionic trophoblast differentiation, resulting in the failure of chorioallantoic fusion and subsequent embryo death. Fibroblast growth factor (FGF) signaling is important for proper trophoblast stem cell (TSC) differentiation and development of the hemochorial placenta. Lack of *Fgf2* promotes TSC differentiation, while FGF4 or FGF2 is required for murine TSC maintenance. Here, we show that low in vivo *Fgf2* mRNA abundance occurs in patches of placental chorion cells and ex vivo in TSCs. This expression is repressed via direct interaction of ERF with the *Fgf2* transcription unit is increased in the absence of ERF, and is decreased in the presence of an ERF mutant resistant to ERK phosphorylation. Thus, FGF2 inhibition by ERF appears to be necessary for proper chorionic TSC differentiation, and may account for the block of chorionic trophoblast differentiation in *Erf*-knockout animals. The differentiation of ERF-overexpressing TSC lines also suggests that ERF may have an FGF2-independent effect during the commitment towards syncytiotrophoblasts.

KEYWORDS
placenta, syncytiotrophoblast, transcriptional repression

1 | INTRODUCTION

The placenta is an ephemeral, but vital, composite organ. It is the first organ to develop, and placental defects invariably result in early embryonic death (Cross et al., 2003; Georgiadis, Ferguson-Smith, & Burton, 2008). Although anatomically different, human and rodent placentas possess analogous cell types whose development is governed by similar mechanisms (Cross, 2005; Douglas, Vande Voort, Kumar, Chang, & Golos, 2009). Thus, given the ethical and practical limitations, the mouse placenta serves as an appropriate experimental model of human placenta development (Soncin, Natale, & Parast, 2015).

The first differentiation event of mammalian embryonic development segregates the trophectoderm and the inner cell mass (Senner & Hemberger, 2010). Trophectoderm cells are maintained and proliferate under strong fibroblast growth factor (FGF) signaling originating from the inner cell mass, and give rise to all placental trophoblast subtypes. Trophoblast stem cells (TSCs) inhabit the region of the placenta called the chorion and either remain as stem cells or differentiate into trophoblast giant cells, spongiotrophoblasts, syncytiotrophoblasts of the labyrinth, or glycogen trophoblasts. Syncytiotrophoblasts form the labyrinth of the placenta that functions as the main transport surface for gas and nutrient exchange between fetal and maternal circulation (Hu & Cross, 2010; Hughes et al., 2004; Watson & Cross, 2005).

Ex vivo maintenance of the TSC phenotype in mouse cells is dependent on stimulation by FGF4 (Erlebacher, Price, & Glimcher, 2004; Kubaczka et al., 2014; Tanaka, Kunath, Hadjantonakis, Nagy, & Rossant, 1998). FGF/MAPK (Mitogen-activated protein kinase) signaling is unambiguously crucial for early trophoblast proliferation. FGF4 binds to FGF receptor 2, thus activating RAS/MAPK signaling (Kunath, Strumpf, & Rossant, 2004). Extracellular signal-regulated

Abbreviations: ChIP, chromatin immunoprecipitation; dpc, day post coitum; *Erf*-KO, ETS2 repressive factor [knockout]; ERK, extracelular signal-regulated kinase; FGF, fibroblast growth factor; TSC, trophoblast stem cell.

Elena Vorgia and Andreas Zaragkoulias contributed equally to this work.

kinase (ERK) activation by FGF appears to be required for the emergence or survival of TSCs in humans and mice (Daoud et al., 2005; Yang et al., 2006). Recent studies indicate that FGF2 may have a role in placenta development, and can support the TSC phenotype and derivation more efficiently than FGF4 (Ohinata & Tsukiyama, 2014). Surprisingly, very little is currently known about the regulation of FGFs in placenta development.

The maintenance or differentiation of TSC-derived cell types is regulated by key transcription factors, such as MASH2 for spongiotrophoblasts, HAND1 for trophoblast giant cells, and the GCM1 for syncytiotrophoblasts (Hughes et al., 2004; Rossant & Cross, 2001). Terminal differentiation within the chorionic plate depends on the expression of the ETS-domain transcriptional repressor ERF (ETS repressor factor) (Papadaki et al., 2007). ERK1/2 phosphorylates ERF, resulting in its nuclear export and inactivation of ERF-targeted gene transcription; elimination of *Erf* may, therefore, recapitulate some aspects of ERK1/2 activation during placenta development. Expression of *Erf* precedes the expression of *Gcm1* during the differentiation of chorionic plate TSCs and chorioallantoic fusion. Thus, *Erf* may be required for the proper commitment of cell progenitors towards the syncytiotrophoblast lineage. Indeed, ex vivo differentiation of *Erf*-knockout (*Erf*-KO) TSCs is delayed, based on the sustained expression of the TSC marker genes *Cdx2* (Strumpf et al., 2005), *Eomes* (Russ et al., 2000), and *Esrrb* (Luo et al., 1997), and on decreased levels of the spongiotrophoblast lineage marker *Tpbpa* (Simmons, Forteir, & Cross, 2007).

The mechanism by which *Erf* may affect chorionic trophoblast cell differentiation remains elusive. Here, we employed molecular and cellular approaches to elucidate steps in the differentiation process. Our findings suggest that ERF binds to *Fgf2* regulatory elements and suppresses its transcription in chorionic trophoblast cells, thereby allowing TSC differentiation to syncytiotrophoblasts and chorioallantoic fusion.

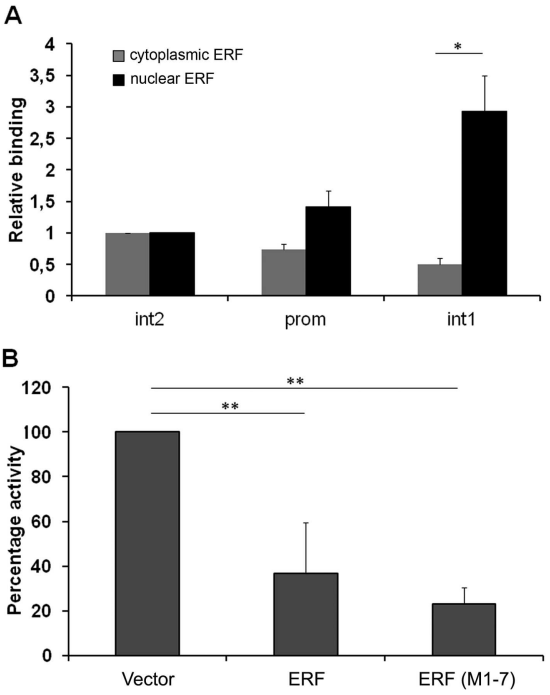

FIGURE 1 ERF binds *Fgf2* and can repress promoter activity. (A) Chromatin immunoprecipitation assays were performed in exponentially growing (grey bars) or 4-hr serum-deprived TSCs (black bars). The binding shown is relative to the distal site in intron 2. Prom, FGF2-promoter primer set; int1, FGF2-intron 1 primer set; int2, FGF2-intron2 primer set (see section 4). Values shown are the average of three independent experiments. (B) HeLa cells co-transfected with 0.2 μg of the −1078/−168 pGL3-basic-Luc *Fgf2* promoter construct, 1.7 μg of empty vector (pSG5), wild-type *Erf* (pSG5-ERF), or the nuclear *Erf* mutant (pSG5-M1-7), as indicated, plus 1 μg of the RSV-LacZ (transfection efficiency control). Luciferase activity of the samples were normalized to and presented as percentage of activity in the empty vector (pSG5; 100%). The data shown are mean ± standard deviation from at least three independent experiments. *, $p < 0.01$

2 | RESULTS

2.1 | ERF binds the *Fgf2* gene and suppresses its transcription

Many genes are involved in the lineage specification of TSCs during the formation of the placenta. We previously showed that ERF is required for proper labyrinth formation, as well as ex vivo differentiation of TSCs (Papadaki et al., 2007), but the underlying mechanism was unclear. Analysis of genome-wide ERF DNA-binding sites by chromatin immunoprecipitation (ChIP) and sequencing in mouse embryonic fibroblasts (Figure S1) (Twigg et al., 2013) identified putative ERF binding on the promoter and first intron regions of *Fgf2*.

We first performed ChIP experiments on actively proliferating or differentiating TSCs to determine if ERF binds *Fgf2*. Increased ERF binding of the promoter and first intron regions, but not distal intron 2 region, of *Fgf2* was observed under differentiation conditions (Figure 1A), which is consistent with the ChIP-sequencing results obtained from mouse embryo fibroblasts (Twigg et al., 2013). Additional support for this direct relationship was obtained from transcription assays using an *Fgf2* promoter-luciferase hybrid reporter in the presence of either wild-type ERF or an ERF mutant (M1-7), which has seven putative serine/threonine MAPK phosphorylation sites mutated to alanine and localizes exclusively in the nucleus (Le Gallic et al., 1999), thus, simulating growth factor-deprivation conditions. Over 60% repression was observed using the wild-type *Erf*-expressing plasmid; this was increased to 80% using the nuclear *Erf* mutant, ERF-M1-7 (Figure 1B). The ChIP and reporter data together suggest that ERF may directly bind *Fgf2* and suppress its transcription.

2.2 | ERF suppresses *Fgf2* expression in TSCs

Fgf2 expression during differentiation in either wild-type or *Erf*-KO TSCs was examined to evaluate the biological relevance of its transcriptional inhibition by ERF. The cells were subjected to a standard ex vivo differentiation protocol, involving withdrawal of embryonic fibroblast-condition medium, FGF4, and heparin. *Fgf2* expression, as measured by quantitative PCR was marginal but detectable in both wild-type and *Erf*-KO TSCs; its expression in *Erf*-KO TSCs was significantly higher. Interestingly, *Fgf2* abundance increased

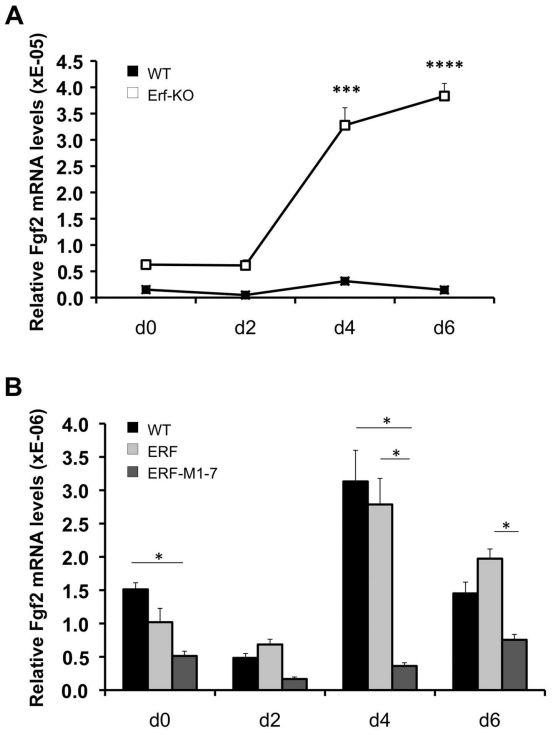

FIGURE 2 *Fgf2* expression in TSCs is suppressed by ERF. (A) TSCs were subjected to the standard differentiation protocol, and the abundance of *Fgf2* mRNA was estimated by quantitative PCR in relation to *Gapdh* mRNA levels over time. (A) Wild-type (black squares) versus *Erf*-KO (white squares) TSCs. (B) Wild-type TSCs (black), TSCs overexpressing wild-type ERF (light grey), versus TSCs overexpressing ERF-M1-7 (dark grey). The graphs present the average of at least five independent experiments. *, $p < 0.05$; ***, $p < 0.001$; ****, $p < 0.0001$

by almost an order of magnitude during the differentiation of *Erf*-KO but not wild-type TSCs (Figure 2A), suggesting that ERF may suppress spurious *Fgf2* transcription during differentiation.

We next established ERF-overexpressing TSC lines to examine if ERF levels and nuclear localization affect *Fgf2* expression, and possibly TSC differentiation and lineage specification. Both wild-type and ERF-M1-7 were introduced into TSCs via plasmids containing cytomegalovirus (CMV)-driven coding sequences. A limited number of stable clones was obtained after G418 selection and expansion. These surviving clones were then tested for ERF protein expression and gross morphology (Figure S2). Quantification of ERF abundance revealed a moderate overexpression of about fourfold in four wild-type ERF and twofold in three ERF-M1-7 clones, suggesting that high ERF levels may be detrimental to TSCs (Figure S2A). Cells with ERF-M1-7 always possessed significantly lower *Fgf2* transcript than the already low levels in the wild-type ERF lines, either in maintenance or differentiation media (Figure 2B), implying that ERF can suppress even marginal *Fgf2* expression in TSCs, and that this suppression is even more prominent during differentiation.

2.3 | Low *Fgf2* levels affect TSC differentiation

TSC self-renewal in culture depends on FGF4 (Himeno, Tanaka, & Kunath, 2008; Tanaka et al., 1998). Given the structural and functional similarities between FGF2 and FGF4, and the apparent activation of *Fgf2* in the absence of *Erf*, we examined the ability of FGF2 to support murine TSC self-renewal. Cells were grown in maintenance medium in the presence of a 25, 2.5, 0.8, or 0 ng/ml FGF2 for 6 D, with regular sampling to evaluate the expression of the TSC markers *Eomes* and *Cdx2* by quantitative PCR; the 25 ng/ml concentration was comparable to the amount of FGF4 normally used. *Cdx2* abundance remained high with 25 or 2.5 ng/ml FGF2 (Figure 3A), whereas *Eomes* abundance remained high only at 25 ng/ml FGF2 (Figure 3B). The rapid decrease in *Eomes* levels with 25 ng/ml FGF2 does not appear to be a result of differentiation, as its abundance was constant for the duration of the experiment and no morphological evidence of differentiation was observed after 6 D in culture, whereas differentiated cells were readily observed at ≤2.5 ng/ml FGF2. These data suggest that FGF2 can support TSC maintenance, which is consistent with a recent report by Ohinata and Tsukiyama (2014) indicating that FGF2 can be used to derive TSCs from mouse blastocysts.

We further compared the efficiency of FGF2 versus FGF4 in the maintenance of the TSC characteristics at the suboptimal concentrations of 2.5 and 0.8 ng/ml, using the expression of the TSC-specific genes *Cdx2*, *Esrrb*, and *Eomes* as a measure of their undifferentiated state. The abundance of each TSC marker transcript decreased in all conditions

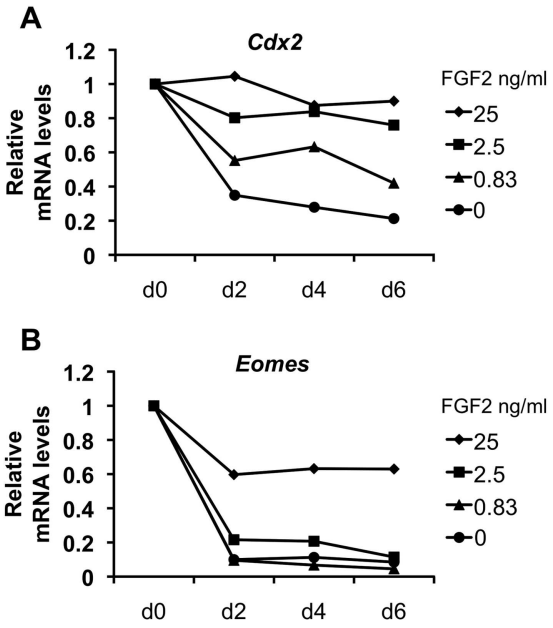

FIGURE 3 FGF2 can support maintenance of stem cell characteristics in TSCs. TSCs were cultured for 6 days in the presence of 25 ng/ml (diamonds), 2.5 ng/ml (squares), 0.83 ng/ml (triangles), or the absence of FGF2 (circles). The abundance of *Cdx2* (A) and *Eomes* (B) was evaluated by quantitative PCR, and expressed relative to the levels of cells growing under normal maintenance conditions with 25 ng/ml FGF4 (d0). Graphs show the average of at least three independent experiments. Most of the pair-wise comparisons among the four different FGF2 concentrations for a given day were statistically significant (not indicated; assessed by two-way ANOVA)—*insignificant* differences for *Cdx2* (A) were between 25 ng/ml and 2.5 ng/ml as well as 0.8 ng/ml and 0 ng/ml at days 2 and 6 and between 25 ng/ml and 2.5 ng/ml, 25 ng/ml or 2.5 ng/ml, and 0.8 ng/ml at Day 4; for *Eomes* (B) were between 0.8 ng/ml and 0 ng/ml at Day 2 and 2.5 ng/ml and 0 ng/ml at Day 6

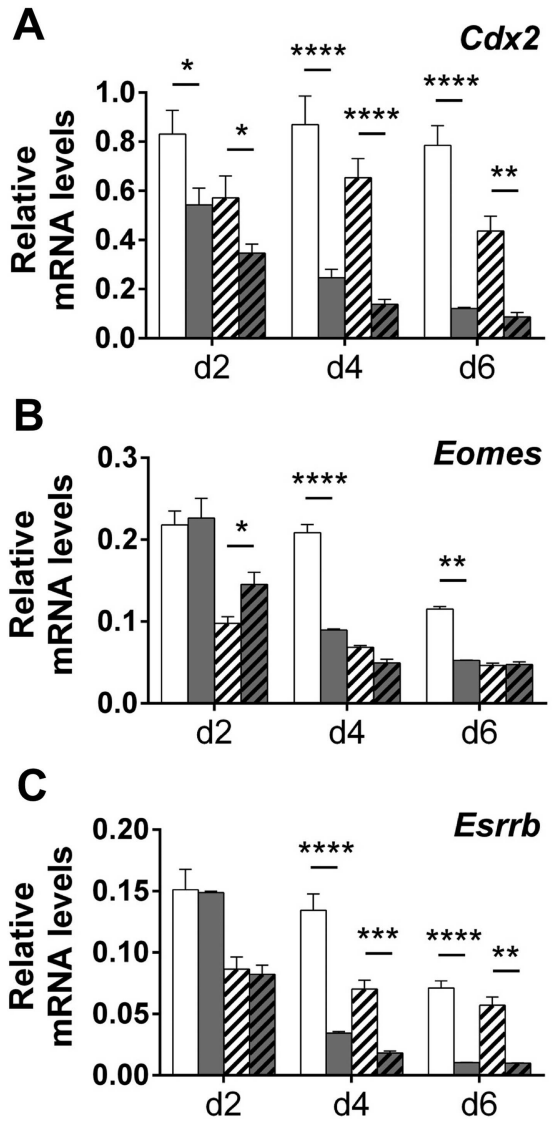

FIGURE 4 Low levels of FGF2 can affect TSC differentiation. TSCs were culture in differentiation media supplemented with FGF2 (white bars) or FGF4 (grey bars) at 2.5 ng/ml (solid bars) or 0.8 ng/ml (striped bars). Transcript abundance of *Cdx2* (A), *Eomes* (B), and *Esrrb* (C) was analyzed by quantitative PCR after 2, 4, and 6 days, as indicated. The values shown are relative to *Gapdh* level. Graphs present the average of three independent experiments. *, $p < 0.05$; **, $p < 0.01$; ***, $p < 0.001$, or ****, $p < 0.0001$

compared to cells growing in maintenance media. In the presence of 2.5 or 0.8 ng/ml FGF2, however, both *Cdx2* and *Esrrb* transcription was higher than in the equivalent FGF4 cultures after 4 and 6 days (Figure 4A and C); *Eomes* expression was higher after 4 and 6 days of culture, but only at 2.5 ng/ml of FGF2 versus FGF4 (Figure 4B). These data suggest that even sub-nanogram-per-ml concentrations of FGF2 may partially maintain TSC characteristics and/or block or delay their differentiation.

2.4 | Low *Fgf2* levels may account for the *Erf*-KO phenotype

We previously showed that elimination of *Erf* from the placenta leads to failure of chorioallantoic fusion, while ex vivo differentiation of *Erf*-KO TSCs delayed attenuation of stem cell marker expression (Papadaki et al., 2007). Similar to *Erf*-KO conditions, low levels of FGF2 in media delayed the loss of stem cell marker expression during TSC differentiation (Figures 3 and 4). Considering that ERF can suppress *Fgf2* transcription in TSCs, we examined *Fgf2* transcript abundance in the developing mouse placenta. At day post-coitum (dpc) 8.5, *Erf* is expressed across the chorion basal layer; by dpc 9.5, its expression occurs in clusters along the chorion basal layer, allowing chorioallantoic fusion (Papadaki et al., 2007).

Analysis of wild-type and $Erf^{-/-}$ mouse placentas at dpc 9.5 for *Fgf2* mRNA by in situ hybridization revealed marginal transcript abundance, consistent with the quantitative PCR data on TSCs, but *Fgf2* mRNA was detectable along the basal chorion layer in distinct cell clusters (Figure 5, upper panels). In contrast, all the cells in the chorion layer appear to possess *Fgf2* mRNA in $Erf^{-/-}$ placentas (Figure 5, lower panels). This clustered pattern of *Fgf2* transcription is reminiscent of the *Erf* expression pattern at the same developmental stage (Papadaki et al., 2007), and is consistent with the hypothesis that *Fgf2* may account for the failure of chorioallantoic fusion in *Erf*-KO animals.

2.5 | ERF may contribute to syncytiotrophoblast lineage development

Spurious *Fgf2* expression in the absence of *Erf* may be responsible for the maintenance of the chorionic trophoblasts in the undifferentiated state observed in $Erf^{dl1/dl1}$ animals, thus contributing to the failed chorioallantoic fusion. Timing of this *Erf* effect during placenta development coincides with the elimination of ERK activity in the labyrinth (Rossant & Cross, 2001), suggesting that nuclear ERF may be required for proper TSC differentiation. Therefore, we utilized our ERF-overexpressing TSC lines to decipher the effect of ERF on TSC differentiation and lineage specification.

TSCs overexpressing either wild-type or ERF-M1-7 were subjected to the standard ex vivo differentiation protocol, and expression of markers characteristic of the different TSC-derived lineages were determined by quantitative PCR. Similar to the parental and *Erf*-KO TSCs, wild-type and ERF-M1-7-overexpressing cells lose their stem cell characteristics, as evidenced by decreased *Cdx2* expression (Figure 6A). Expression of *Gcm1*, which marks chorioallantoic fusion points and is required for differentiation towards syncytiotrophoblasts (Anson-Cartwright et al., 2000; Cross, 2005; Hughes et al., 2004; Papadaki et al., 2007), increased in the presence of ERF-M1-7 late in the differentiation process (Figure 6B). Although TSCs do not differentiate in vitro towards syncytiotrophoblasts without extensive genetic manipulation (Cross, 2005), cells expressing ERF-M1-7 exhibited increased expression of the syncytiotrophoblast markers *Cx26* (Figure 6C), and *Tfeb* (Figure 6D). The abundance of *Tpbpa* (*4311*), a spongiotrophoblast-specific marker, and *Pl1*, a giant cells marker (Tanaka et al., 1998), did not significantly change (Figure S3). These observations suggest that in addition to its role in *Fgf2* regulation, nuclear localization of ERF in the absence of ERK activity may contribute to syncytiotrophoblast differentiation, or proliferation during normal placenta development.

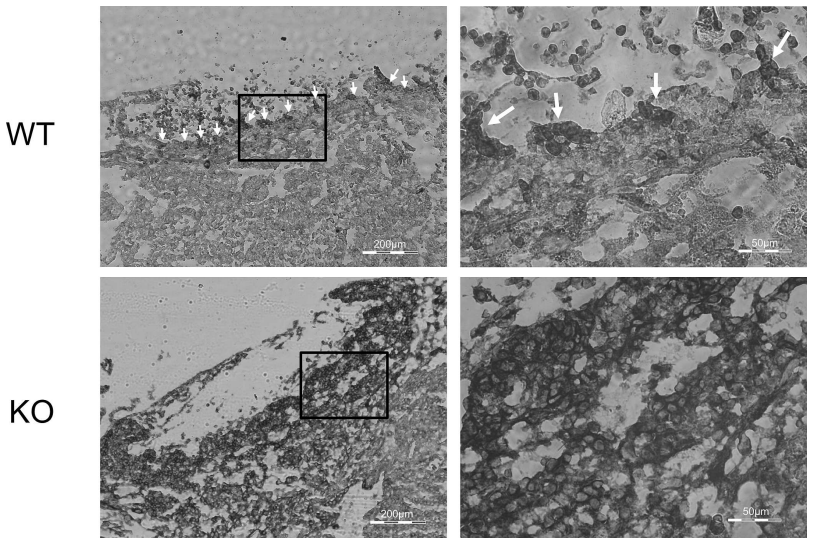

FIGURE 5 *Fgf2* expression in the basal chorion layer of the placenta at 9.5 dpc. In situ hybridization of cryosections from dpc 9.5 wild-type (upper panels) and $Erf^{-/-}$ (lower panels) placentas with *Fgf2* antisense RNA probe. Microphotographs obtained with a 5x (left panels) or 20x (right panels) objective from the labyrinth/basal chorion layer are shown. The black rectangle in the pictures on the left indicates the corresponding area of the picture on the right. The arrows in the wild-type placentas indicate *Fgf2* expression along the basal chorion layer. Scale bars, 200 μm (left); 50 μm (right)

3 | DISCUSSION

ERF is a ubiquitously expressed transcriptional repressor regulated exclusively by ERK1/2 via phosphorylation and nuclear export (Polychronopoulos et al., 2006). ERF appears to affect diverse cell type-specific processes involving case-specific targets and co-factors—that is, proliferation and tumorigenesis via c-*Myc* regulation mediated by E2Fs (Verykokasis, Papadaki, Vorgia, Le Gallic, & MavroThalassitis, 2007); epithelial-to-mesenchymal transition via SEMA7A regulation (Allegra et al., 2012); cell motility via EGR1

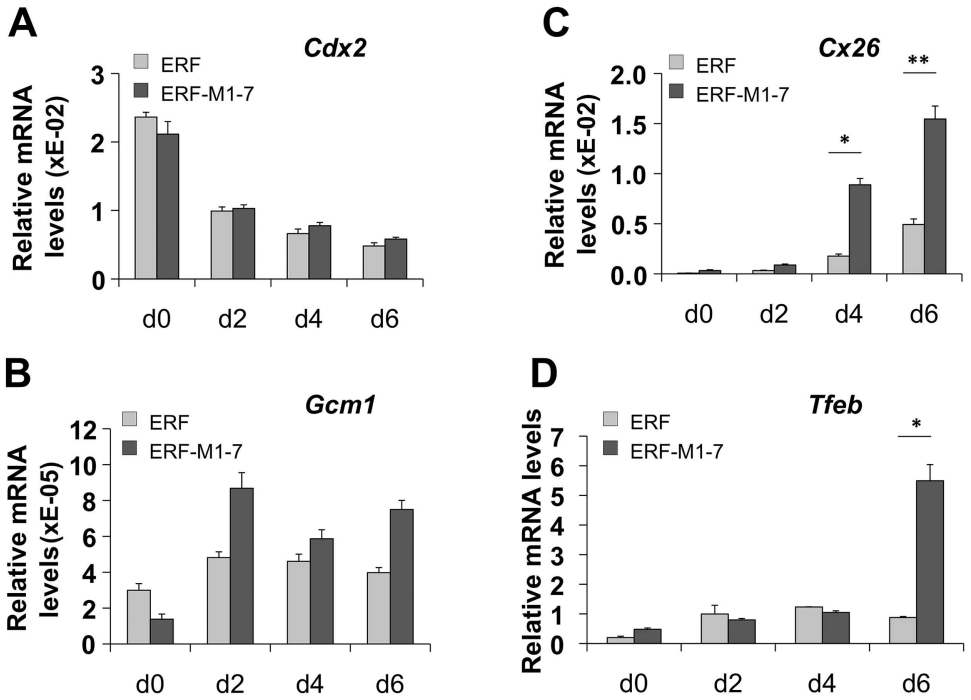

FIGURE 6 Nuclear ERF induces TSC differentiation. TSCs overexpressing wild-type ERF (light grey) or ERF-M1-7 (dark grey) were subjected to the standard differentiation protocol, and the mRNA abundance of *Cdx2* (A), *Gcm1* (B), *Cx26* (C), and *Tfeb* (D) were analyzed by quantitative PCR in relation to *Gapdh* mRNA levels. Graphs present the average of at least four independent experiments. *, $p < 0.05$; **, $p < 0.01$

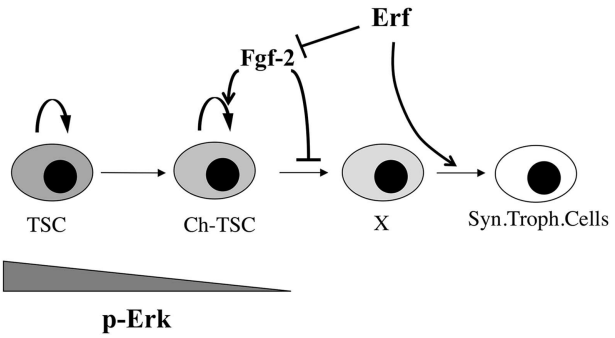

FIGURE 7 Model of ERF function in placenta development. Schematic of the role of FGF2 and ERF in trophoblast differentiation. Minimization of ERK activity allows ERF to inhibit *Fgf2* transcription, allowing chorionic trophoblasts to differentiate towards syncytiotrophoblasts

cooperation (Tarcic et al., 2012); and cranial suture development and craniosynostosis via RUNX2 interplay (Twigg et al., 2013). *Erf* ablation in mice results in embryo death at embryonic Day 10.5 due to failed placenta chorionic trophoblast differentiation and the absence of chorioallantoic fusion (Papadaki et al., 2007), although how *Erf* may contribute to chorion cell differentiation was unclear.

Genome-wide analysis of ERF DNA-binding sites in embryo fibroblasts (Twigg et al., 2013) identified a strong interaction of ERF with *Fgf2*. FGF signaling plays a pivotal role in TSC differentiation: FGF4 expressed by the inner cell mass is required for trophectoderm maintenance (Arman, Haffner-Krausz, Chen, Heath, & Lonai, 1998), while maintenance of murine TSCs requires FGF4 (Tanaka et al., 1998) or FGF2 (Ohinata & Tsukiyama, 2014). Attenuation of FGF2 signaling is also required for the differentiation of TSCs in humans (Sudheer, Bhusan, Fauler, Lehrach, & Adjaye, 2012). Thus, regulation of *Fgf2* is a plausible mechanism of action for ERF. The interaction originally detected in murine embryonic fibroblasts was also evident in TSCs, and was enhanced when cells were induced to differentiate. Consistent with ERF function as a repressor, reporter assays indicated that ERF suppressed transcription from the *Fgf2* promoter while endogenous *Fgf2* mRNA in TSCs increased in the absence of ERF but decreased in the presence of nuclear ERF. Direct regulation of *Fgf2* by ERF is also consistent with the known role of *Ets* genes in the regulation of FGF signaling (Tsang & Dawid, 2004). Thus, we propose a model where ERF suppresses *Fgf2* expression in order for chorionic trophoblasts to differentiate toward syncytiotrophoblasts (Figure 7). This model is consistent with our previous model (Papadaki et al., 2007), and now includes the stage, when *Fgf2* inactivation may be important for proper differentiation. We additionally suggest that decreased ERK activity in the placenta during development may increase nuclear ERF localization, which in turn suppresses *Fgf2* transcription and further decreases ERK activity, together allowing for proper TSC differentiation.

Many *Fgf* family members are expressed in the placenta, although the degree and subtype varies among species (Pfarrer et al., 2006; Zhong et al., 2006). *Fgf2* expression is marginal in most cases, and its complex post-transcriptional regulation, multiple isoforms (Prats, Vagner, Prats, & Amalric, 1992; Touriol, Roussigne, Gensac, Prats, & Prats, 2000), and possible autocrine or paracrine activity (Chlebova et al., 2009; Presta et al., 2000) complicates determining which cells expressing FGF2 are regulated by FGF2 signaling. *Fgf2* and *Erf* expression in the developing placenta would be consistent with the hypothesis that ERF suppresses a paracrine FGF2 function, as activation of ERK1/2 by FGF inhibits the ability of ERF to act as a transcriptional repressor. Unfortunately, we could not determine if *Erf* and *Fgf2* are expressed in distinct chorion cells, by double in situ hybridization or immunodetection, due to the very low abundance of *Fgf2* transcript.

Our data suggest that even low levels of FGF2 are sufficient to delay or even block ex vivo differentiation of TSCs, and may explain the delayed differentiation we observed in *Erf*-KO TSCs (Papadaki et al., 2007). Yet, even low levels of FGF2 cannot account for all the ERF-dependent changes in syncytiotrophoblast differentiation of TSCs (Figure 6C, D and S4). TSCs are reported to spontaneously differentiate to giant cells and spongiotrophoblasts ex vivo, but differentiation towards syncytiotrophoblasts requires the concerted action of several genes (Hughes et al., 2004; Simmons et al., 2008). Activin may promote differentiation of chorionic trophoblasts towards syncytiotrophoblasts in the absence of FGF4 (Natale, Hemberger, Hughes, & Cross, 2009), and *Erf* can affect Phosphoinositol-3-kinase-mediated transforming growth factor-β signaling via Semaphorin 7a (Allegra et al., 2012) during the epithelial-to-mesenchymal transition. Nuclear ERF may also affect semaphorins in the placenta, facilitating syncytiotrophoblast differentiation. Indeed, *SEMA*7A is expressed throughout the human placenta (Saben et al., 2014); *SEMA*3A is reported to provide a chemorepulsive signal from the umbilical cord (Marzioni et al., 2004); and *SEMA*3B may be involved in some cases of preeclampsia (Kaitu'u-Lino et al., 2014; Zhou et al., 2013). Yet, little is known about their function in human placental cells much less about their role in the mouse placenta. Further experiments are needed to elucidate the induction of the ERF syncytiotrophoblast phenotype in relation to activin and semaphorins.

4 | MATERIALS AND METHODS

4.1 | Cell cultures

The *Erf*-wild-type and −KO TSC lines derived from 3.5 dpc blastocysts of 129/Sv x C57BL/6 mice (Papadaki et al., 2007) were maintained in an undifferentiated state using 70% mouse embryonic fibroblast-condition medium, 30% RPMI medium supplemented with 20% fetal bovine serum (FBS) (Gibco), 25 ng/ml FGF4 (Peprotech), and 1 μg/ml heparin (Sigma–Aldrich). Wild-type TSCs were derived from male blastocyst while *Erf*-KO lines were derived from both male and female blastocysts. Differentiation was induced by plating 2×10^5 cells in 60 mm culture dishes, and replacing the medium 24 hr later (Day 0) with 80% RPMI, 20% FBS.

HeLa cells were maintained in DMEM medium supplemented with 10% FBS.

4.2 | Stable transfection

TSC clones overexpressing ERF were produced by the stable integration of pCMV-HA-ERF and pCMV-HA-ERF-M1-7 plasmids into wild-type TSCs. The plasmids were generated by cloning the corresponding fragments from pSG5-ERF and pSG5-M17 (Le Gallic et al., 1999), respectively, into the BamHI site of the vector pCMV-HA (Vandenheuvel & Harlow, 1993). TSCs were transfected with Lipofectamin 2000 (Invitrogen, Carlsbad, CA), according to the manufacturer's instructions, and selected with 300 μg/ml G418 for 10–13 d. Individual clones were expanded and characterized. Four clones overexpressing wild-type ERF and three clones expressing ERF-M1-7 maintained their TSC characteristics, as determined by the expression of stem cell markers and the absence of differentiation markers. Clones were monitored regularly for these stem cell characteristics, and were discarded if evidence of spontaneous differentiation was noted.

4.3 | Western blot analysis

Whole-cell protein extracts were analyzed by electrophoresis and immunoblotting with the S17S anti-ERF rabbit polyclonal antibody (1:1000 dilution) from Le Gallic et al. (1999). The abundance of total ERK1/2, determined by the p44/42 MAPK antibody (1:1000 dilution) (Cell Signaling), was used as loading control. Autoradiograms were scanned and quantified with ImageJ (Schindelin et al., 2012).

4.4 | RNA analysis and quantitative PCR

Total RNA was isolated using Trizol (Invitrogen), following the manufacturer's instructions. RNA was then treated with DNase (Ambion, Austin, TX), reverse transcribed with an AffinityScript Multi-Temperature cDNA Synthesis Kit (Stratagene, La Jolla, CA), and amplified with Brilliant SYBR Green QPCR Master Mix reagent (Stratagene) on an MxPro3005 instrument (Stratagene). All RNA analysis experiments had a minimum of three independent biological replicates, with two technical replicates.

All primer sets (Table 1) had comparable amplification efficiencies of 96.5–98.0%, as indicated by the 3-log standard curves established for each one. Abundance of the housekeeping marker, *Gapdh*, remained fairly constant during the differentiation process across all lines and conditions, with a Ct mean value of 13.13 ± 0.67 (standard deviation) (see Table S1); this is consistent with previous assessments (Veazey & Golding, 2011) and transcriptome analysis (Table S2) (Ralston et al., 2010), supporting the validity of *Gapdh* as a reference transcript for TSC differentiation. The chosen marker genes used for lineage identification (Rossant & Cross, 2001; Simmons & Cross, 2005) are also required for lineage specification.

4.5 | Chromatin immunoprecipitation

Twenty-five million (25×10^6) TSCs were grown in complete media (*expo*) or serum-deprived for 4 hr (*starved*), and fixed with 1% formaldehyde for 10 min at room temperature. Cell were lyzed with a Dounce homogenizer in 25 mM HEPES [pH 7.9], 1.5 mM $MgCl_2$, 10 mM KCl, 0.5% Nonidet P-40, 1 mM dithiothreitol. The nuclei were sonicated in sonication buffer (50 mM HEPES [pH 7.9], 140 mM NaCl, 1 mM EDTA, 1% Triton X–100, 0.1% deoxycholate, 1% SDS), and dialyzed in sonication buffer with 0.1% SDS. The extracts were precleared with protein-G beads, incubated overnight with anti-ERF antibody (S17S), and precipitated with protein-G beads for 2 hr at 4 °C. The beads were washed twice with each of the following buffers: sonication buffer with 0.1% SDS, wash buffer A (sonication buffer with 0.1% SDS and 500 mM NaCl), wash buffer B (20 mM Tris [pH 8.0], 1 mM EDTA, 250 mM LiCl, 0.5% Nonidet P-40, 0.5% deoxycholate), and 10 mM Tris with 1 mM EDTA [pH 7.5]. The cross-links were reversed overnight at 65 °C in 20 mM Tris [pH 8.0], 2 mM EDTA, 0.5% SDS, and 125 μg/ml proteinase K, and then treated with RNase. The DNA was phenol/chloroform-extracted and ethanol precipitated.

Quantitative PCR was performed as described above. All primer sets (Table 2) had comparable amplification efficiencies of

TABLE 1 List of primers for reverse-transcription PCR

Gene	Sequence
Cdx2	5′-TCTCCGAGAGGCAGGTTAAA
	5′-GCAAGGAGGTCACAGGACTC
Cx26	5′-GACCCGCTTCAGACCTGCTCCTTAC
	5′-GCCTGGAAATGAAGCAGTCCACTGT
Eomes	5′-AAAGGTCGTTCAAGGTGCTG
	5′-GTTAACTCAAGGTCCAACCC
Esrrb	5′-GGACACACTGCTTTGAAGCA
	5′-ACAGATGTCTCTCATCTGGC
Fgf2	5′-TTCTTCCTGCGCATCCATCC
	5′-CTGGAGTATTTCCGTGACCG
Gapdh	5′-CCAGTATGACTCCACTCACG
	5′-GACTCCACGACATACTCAGC
Gcm1	5′-ACGAAGAGATGGCATGCATG
	5′-CTTGTGACATTACACCTGGC
Pl1	5′-GGGCAGAAACCTTGTAATTC
	5′-ATGGATGTCCCTTTTAATGC
Tfeb	5′-AACAAAGGCACCATCCTCAA
	5′-CAGCTCGGCCATATTCACAC
Tpbpa (4311)	5′-CGGAAGGCTCCAACATAGAA
	5′-TTTCGCTCGTTGCCTAACTT

TABLE 2 List of primers for chromatin immunoprecipitation

Primer set name	Sequence
FGF2-promoter	5′-GGTGCAGACAATCTATTGGG
	5′-AGCGTGGGAAGATGAAAACC
FGF2-intron1	5′-CAGGCTGGATAACTTTGGAG
	5′-ACTGCCCAGTATTCCAGAGC
FGF2-intron2	5′-TCCTGGTGTTATCCATTGGC
	5′-CTGGAGTATTTCCGTGACCG
mouse CPH	5′-AGACCAGCAAGAAGATCACC
	5′-GGAAAATATGGAACCCAAAG

96.3–98.1%, as indicated by the 3-log standard curves established for each one.

4.6 | Animal care

Mice were maintained in specific, pathogen-free facilities at the Institute of Molecular Biology and Biotechnology, Heraklion, Greece. Protocols were approved through the General Directorate of Veterinary Services, Heraklion, Region of Crete. Experimental procedures were performed in accordance with the European Union DIRECTIVE 2010/63/EU on the protection of animals used for scientific purposes.

4.7 | Timed pregnancies, dissections, and histological analysis

Heterozygous male and female mice ($Erf^{dl1/+}$) were bred to obtain wild-type ($Erf^{+/+}$) and homozygous ($Erf^{dl1/dl1}$) mutant mouse embryos. Pregnant females were sacrificed at embryonic Day 9.5. Uteri were removed and immersed in phosphate-buffered saline (PBS). Placentas were dissected and fixed overnight at 4 °C in 4% paraformaldehyde in PBS; embryos or yolk sacs were kept for genotyping. Placentas for cryosections were incubated overnight after fixation with 30% sucrose in PBS, embedded in 7.5% Gelatin (Fluka), 1.5% Sucrose (Merck) in PBS, and snap-frozen in dry ice-cooled 2-methylbutane. Placentas were stored at −80 °C. Eight-micron sections were cut on a cryostat (Leica), adhered to superfrost slides, air dried, and stored at −80 °C until used.

4.8 | In situ hybridization

A 260-base pair (bp) *Fgf*2 probe that detects all *Fgf*2 splice variants was made. Total mRNA from embryonic Day 9.5 mouse placentas was extracted and reverse transcribed as described above, and then amplified with the primer pair 5′-TCTCGGCTTCAGGAAGAGTC and 5′-CAGCCGTCCATCTTCCTTCA, which amplifies all *Fgf2* transcript variants. The resulting 437-bp PCR product was digested with KpnI and SmaI to produce a 260-bp fragment corresponding to nucleotides 180–440 of the *Fgf*2 mRNA. This 260-bp fragment was cloned into the pBluescript-SK+ (Stratagene). Both sense and antisense *Fgf2* probes were prepared by labeling with digoxigenin-11-UTP. Synthesis of antisense dig-11-UTP-labeled RNA probe for ERF was described previously (Papadaki et al., 2007).

Frozen sections were air-dried for 30 min at room temperature, post-fixed for 10 min at room temperature in 4% paraformaldehyde in PBS, washed twice in PBS, incubated with 20 μg/ml proteinase K for 5 min at 37 °C, post-fixed in 4% paraformaldehyde, washed in PBS, and acetylated for 10 min in 0.1 M triethanolamine, 0.25% acetic anhydride. Hybridization was performed overnight at 55 °C in a solution containing 50% formamide, 5 × SSC (0.75 M NaCl, 0.075 M sodium citrate), 5 × Denhardt's solution, 0.25 mg/ml yeast RNA, with 3 ng/μl digoxigenin-labeled riboprobe. The sections were washed twice for 30 min at 55 °C in 2 × SSC (0.3 M NaCl, 0.03 M sodium citrate), incubated in 20 μg/ml RNase for 30 min at 37 °C, washed for 30 min at 55 °C in 1 × SSC (0.15 M NaCl, 0.015 M sodium citrate), and incubated for 1 hr at room temperature in 10% fetal calf serum in PBS. Sections were incubated for 2 hr at 37 °C with alkaline phosphatase-conjugated anti-digoxigenin (Roche). Probes were detected with NBT/BCIP solution (Roche).

4.9 | Statistical analysis

The appropriate statistical test was used for grouped data, combined with post-hoc significance tests. Specifically two-way ANOVA followed by the Newman–Kuels test (Figures 1, 3, and 4) or multiple *t*-tests corrected for multiple comparisons using the Holm-Sidak method (Figures 2 and 6) were used.

ACKNOWLEDGMENTS

We would like to thank Dr. Kourouniotis and the IMBB animal facility for their expert help with the mice. This work was supported by Greek Ministry of Education grants PYTHAGORAS II KA2092, PENED 03ED626, and SYNERGASIA 09SYN-11-902 to G.M., and HERAKLEITOS II KA 3396 to A.Z.

REFERENCES

Allegra, M., Zaragkoulias, A., Vorgia, E., Ioannou, M., Litos, G., Beug, H., & Mavrothalassitis, G. (2012). Semaphorin-7a reverses the ERF-induced inhibition of EMT in Ras-dependent mouse mammary epithelial cells. *Molecular Biology of the Cell*, *23*(19), 3873–3881.

Anson-Cartwright, L., Dawson, K., Holmyard, D., Fisher, S. J., Lazzarini, R. A., & Cross, J. C. (2000). The glial cells missing-1 protein is essential for branching morphogenesis in the chorioallantoic placenta. *Nature Genetics*, *25*(3), 311–314.

Arman, E., Haffner-Krausz, R., Chen, Y., Heath, J. K., & Lonai, P. (1998). Targeted disruption of fibroblast growth factor (FGF) receptor 2 suggests a role for FGF signaling in pregastrulation mammalian development. *Proceedings of the National Academy of Sciences of the United States of America*, *95*(9), 5082–5087.

Chlebova, K., Bryja, V., Dvorak, P., Kozubik, A., Wilcox, W. R., & Krejci, P. (2009). High molecular weight FGF2: The biology of a nuclear growth factor. *Cellular and Molecular Life Sciences*, *66*(2), 225–235.

Cross, J. C. (2005). How to make a placenta: Mechanisms of trophoblast cell differentiation in mice-a review. *Placenta*, *26*(Suppl A), S3–S9.

Cross, J. C., Baczyk, D., Dobric, N., Hemberger, M., Hughes, M., Simmons, D. G., . . . Kingdom, J. C. (2003). Genes, development and evolution of the placenta. *Placenta*, *24*(2-3), 123–130.

Daoud, G., Amyot, M., Rassart, E., Masse, A., Simoneau, L., & Lafond, J. (2005). ERK1/2 and p38 regulate trophoblasts differentiation in human term placenta. *The Journal of Physiology*, *566*(Pt 2), 409–423.

Douglas, G. C., VandeVoort, C. A., Kumar, P., Chang, T. C., & Golos, T. G. (2009). Trophoblast stem cells: Models for investigating trophectoderm differentiation and placental development. *Endocrine Reviews*, *30*(3), 228–240.

Erlebacher, A., Price, K. A., & Glimcher, L. H. (2004). Maintenance of mouse trophoblast stem cell proliferation by TGF-beta/activin. *Developmental Biology*, *275*(1), 158–169.

Georgiades, P., Ferguson-Smith, A. C., & Burton, G. J. (2002). Comparative developmental anatomy of the murine and human definitive placentae. *Placenta*, *23*(1) 3–19.

Himeno, E., Tanaka, S., & Kunath, T. (2008). Isolation and manipulation of mouse trophoblast stem cells. *Current Protocols in Stem Cell Biology*, *7*, 1E.4.1–1E.4.27.

Hu, D., & Cross, J. C. (2010). Development and function of trophoblast giant cells in the rodent placenta. *The International Journal of Developmental Biology*, *54*(2–3), 341–354.

Hughes, M., Dobric, N., Scott, I. C., Su, L., Starovic, M., St-Pierre, B., … Cross, J. C. (2004). The Hand1, Stra13 and Gcm1 transcription factors override FGF signaling to promote terminal differentiation of trophoblast stem cells. *Developmental Biology*, *271*(1) 26–37.

Kaitu'u-Lino, T. J., Hastie, R., Cannon, P., Binder, N. K., Lee, S., Stock, O., … Tong, S. (2014). Placental SEMA3B expression is not altered in severe early onset preeclampsia. *Placenta*, *35*(12), 1102–1105.

Kubaczka, C., Senner, C., Arauzo-Bravo, M. J, Sharma, N., Kuckenberg, P., Becker, A., … Schorle, H. (2014). Derivation and maintenance of murine trophoblast stem cells under defined conditions. *Stem Cell Reports*, *2*(2), 232–242.

Kunath, T., Strumpf, D., & Rossant, J. (2004). Early trophoblast determination and stem cell maintenance in the mouse-a review. *Placenta*, *25*(Suppl A), S32–S38.

Le Gallic, L., Sgouras, D., Beal, G., Jr., & Mavrothalassitis, G. (1999). Transcriptional repressor ERF is a Ras/mitogen-activated protein kinase target that regulates cellular proliferation. *Molecular and Cellular Biology*, *19*(6), 4121–4133.

Luo, J., Sladek, R., Bader, J. A., Matthyssen, A., Rossant, J., & Giguere, V. (1997). Placental abnormalities in mouse embryos lacking the orphan nuclear receptor ERR-beta. *Nature*, *388*(6644), 778–782.

Marzioni, D., Tamagnone, L., Capparuccia, L., Marchini, C., Amici, A., Todros, T., … Castellucci, M. (2004). Restricted innervation of uterus and placenta during pregnancy: Evidence for a role of the repelling signal Semaphorin 3A. *Developmental Dynamics: An Official Publication of the American Association of Anatomists*, *231*(4), 839–848.

Natale, D. R., Hemberger, M., Hughes, M., & Cross, J. C. (2009). Activin promotes differentiation of cultured mouse trophoblast stem cells towards a labyrinth cell fate. *Developmental Biology*, *335*(1), 120–131.

Ohinata, Y., & Tsukiyama, T. (2014). Establishment of trophoblast stem cells under defined culture conditions in mice. *PLoS ONE*, *9*(9) e107308.

Papadaki, C., Alexiou, M., Cecena, G., Verykokakis, M., Bilitou, A., Cross, J. C., … Mavrothalassitis, G. (2007). Transcriptional repressor erf determines extraembryonic ectoderm differentiation. *Molecular and Cellular Biology*, *27*(14), 5201–5213.

Pfarrer, C., Weise, S., Berisha, B., Schams, D., Leiser, R., Hoffmann, B., & Schuler, G. (2006). Fibroblast growth factor (FGF)-1, FGF2, FGF7 and FGF receptors are uniformly expressed in trophoblast giant cells during restricted trophoblast invasion in cows. *Placenta*, *27*(6–7), 758–770.

Polychronopoulos, S., Verykokakis, M., Yazicioglu, M. N., Sakarellos-Daitsiotis, M., Cobb, M. H., & Mavrothalassitis, G. (2006). The transcriptional ETS2 repressor factor associates with active and inactive Erks through distinct FXF motifs. *Journal of Biological Chemistry*, *281*(35), 25601–25611.

Prats, A. C., Vagner, S., Prats, H., & Amalric, F. (1992). Cis-acting elements involved in the alternative translation initiation process of human basic fibroblast growth factor mRNA. *Molecular and Cellular Biology*, *12*(10), 4796–4805.

Presta, M., Rusnati, M., Dell'Era, P., Tanghetti, E., Urbinati, C., Giuliani, R., & Leali, D. (2000). Examining new models for the study of autocrine and paracrine mechanisms of angiogenesis through FGF2-transfected endothelial and tumour cells. *Advances in Experimental Medicine and Biology*, *476*, 7–34.

Ralston, A., Cox, B. J., Nishioka, N., Sasaki, H., Chea, E., Rugg-Gunn, P., … Rossant, J. (2010). Gata3 regulates trophoblast development downstream of Tead4 and in parallel to Cdx2. *Development*, *137*(3), 395–403.

Rossant, J., & Cross, J. C. (2001). Placental development: Lessons from mouse mutants. *Nature Reviews Genetics*, *2*(7), 538–548.

Russ, A. P., Wattler, S., Colledge, W. H., Aparicio, S. A. J. R., Carlton, M. B. L., Pearce, J. J., … Evans, M. J. (2000). Eomesodermin is required for mouse trophoblast development and mesoderm formation. *Nature*, *404*(6773), 95–99.

Saben, J., Zhong, Y., McKelvey, S., Dajani, N. K., Andres, A., Badger, T. M., … Shankar, K. (2014). A comprehensive analysis of the human placenta transcriptome. *Placenta*, *35*(2), 125–131.

Schindelin, J., Arganda-Carreras, I., Frise, E., Kaynig, V., Longair, M., Pietzsch, T., … Cardona, A. (2012). Fiji: An open-source platform for biological-image analysis. *Nature Methods*, *9*(7), 676–682.

Senner, C. E., & Hemberger, M. (2010). Regulation of early trophoblast differentiation—lessons from the mouse. *Placenta*, *31*(11), 944–950.

Simmons, D. G., & Cross, J. C. (2005). Determinants of trophoblast lineage and cell subtype specification in the mouse placenta. *Developmental Biology*, *284*(1), 12–24.

Simmons, D. G., Fortier, A. L., & Cross, J. C. (2007). Diverse subtypes and developmental origins of trophoblast giant cells in the mouse placenta. *Developmental Biology*, *304*(2), 567–578.

Simmons, D. G., Natale, D. R., Begay, V., Hughes, M., Leutz, A., & Cross, J. C. (2008). Early patterning of the chorion leads to the trilaminar trophoblast cell structure in the placental labyrinth. *Development*, *135*(12), 2083–2091.

Soncin, F., Natale, D., & Parast, M. M. (2015). Signaling pathways in mouse and human trophoblast differentiation: A comparative review. *Cellular and Molecular Life Sciences: CMLS*, *72*(7), 1291–1302.

Strumpf, D., Mao, C. A., Yamanaka, Y., Ralston, A., Chawengsaksophak, K., Beck, F., & Rossant, J. (2005). Cdx2 is required for correct cell fate specification and differentiation of trophectoderm in the mouse blastocyst. *Development*, *132*(9), 2093–2102.

Sudheer, S., Bhushan, R., Fauler, B., Lehrach, H., & Adjaye, J. (2012). FGF inhibition directs BMP4-Mediated differentiation of human embryonic stem cells to syncytiotrophoblast. *Stem Cells and Development*, *21*(16), 2987–3000.

Tanaka, S., Kunath, T., Hadjantonakis, A. K., Nagy, A., & Rossant, J. (1998). Promotion of trophoblast stem cell proliferation by FGF4. *Science*, *282*(5396), 2072–2075.

Tarcic, G., Avraham, R., Pines, G., Amit, I., Shay, T., Lu, Y., … Yarden, Y. (2012). EGR1 and the ERK-ERF axis drive mammary cell migration in response to EGF. *FASEB Journal: Official Publication of the Federation of American Societies for Experimental Biology*, *26*(4), 1582–1592.

Touriol, C., Roussigne, M., Gensac, M. C., Prats, H., & Prats, A. C. (2000). Alternative translation initiation of human fibroblast growth factor 2 mRNA controlled by its 3'-untranslated region involves a Poly(A) switch and a translational enhancer. *The Journal of Biological Chemistry*, *275*(25), 19361–19367.

Tsang, M., & Dawid, I. B. (2004). Promotion and attenuation of FGF signaling through the Ras-MAPK pathway. *Science's STKE: Signal Transduction Knowledge Environment*, *2004*(228), pe17.

Twigg, S. R., Vorgia, E., McGowan, S. J., Peraki, I., Fenwick, A. L., Sharma, V. P., … Wilkie, A. O. (2013). Reduced dosage of ERF causes complex craniosynostosis in humans and mice and links ERK1/2 signaling to regulation of osteogenesis. *Nature Genetics*, *45*(3), 308–313.

Vandenheuvel, S., & Harlow, E. (1993). Distinct roles for cyclin-Dependent kinases in cell-Cycle control. *Science*, *262*(5142), 2050–2054.

Veazey, K. J., & Golding, M. C. (2011). Selection of stable reference genes for quantitative rt-PCR comparisons of mouse embryonic and extra-embryonic stem cells. *PLoS ONE*, *6*(11), e 27592.

Verykokakis, M., Papadaki, C., Vorgia, E., Le Gallic, L., & Mavrothalassitis, G. (2007). The RAS-dependent ERF control of cell proliferation and differentiation is mediated by c-Myc repression. *The Journal of Biological Chemistry*, *282*(41), 30285–30294.

Watson, E. D., & Cross, J. C. (2005). Development of structures and transport functions in the mouse placenta. *Physiology (Bethesda)*, *20*, 180–193.

Yang, W., Klaman, L. D., Chen, B., Araki, T., Harada, H., Thomas, S. M., … Neel, B. G. (2006). An Shp2/SFK/Ras/Erk signaling pathway controls trophoblast stem cell survival. *Developmental Cell*, *10*(3), 317–327.

Zhong, W., Wang, Q. T., Sun, T., Wang, F., Liu, J., Leach, R., … Rappolee, D. A. (2006). FGF ligand family mRNA expression profile for mouse preimplantation embryos, early gestation human placenta, and mouse trophoblast stem cells. *Molecular Reproduction and Development*, *73*(5), 540–550.

Zhou, Y., Gormley, M. J., Hunkapiller, N. M., Kapidzic, M., Stolyarov, Y., Feng, V., … Fisher, S. J. (2013). Reversal of gene dysregulation in cultured cytotrophoblasts reveals possible causes of preeclampsia. *The Journal of Clinical Investigation*, *123*(7), 2862–2872.

SUPPORTING INFORMATION

Additional Supporting information may be found online in the supporting information tab for this article.

How to cite this article: Vorgia E, Zaragkoulias A, Peraki I, Mavrothalassitis G. Suppression of *Fgf2* by ETS2 repressor factor (ERF) is required for chorionic trophoblast differentiation. *Mol Reprod Dev*. 2017;9999:1–10.